

MIXED POLYATOMIC CATIONS OF SULFUR,
SELENIUM AND TELLURIUM

By

MICHAEL JOSEPH COLLINS, B.Sc.

A Thesis

Submitted to the School of Graduate Studies,
in Partial Fulfilment of the Requirements

for the Degree

Doctor of Philosophy

©April, 1984

MIXED POLYATOMIC CATIONS OF SULFUR, SELENIUM AND TELLURIUM

DOCTOR OF PHILOSOPHY (1984)
(Chemistry)

McMASTER UNIVERSITY
Hamilton, Ontario

TITLE: Mixed Polyatomic Cations of Sulfur, Selenium,
and Tellurium.

AUTHOR: Michael Joseph Collins, B.Sc. (U. of Victoria)

SUPERVISOR: Professor R.J. Gillespie

NUMBER OF PAGES: xv, 254

To my wife and parents
and the amazing Leah.

ABSTRACT

The study of the behavior of the chalcogen elements sulfur, selenium and tellurium with the strong Lewis acids SbF_5 and AsF_5 in SO_2 solution has been continued. A large number of new salts of polyatomic cations of the chalcogens have been prepared and characterized by their X-ray crystal structures, namely $(\text{Te}_2\text{Se}_8)(\text{AsF}_6)_2$, $(\text{Te}_{4.5}\text{Se}_{5.5})(\text{AsF}_6)_2$, $(\text{Te}_2\text{Se}_6)(\text{Te}_2\text{Se}_8)(\text{AsF}_6)_4(\text{SO}_2)_2$, $(\text{Te}_6)(\text{Se}_8)(\text{AsF}_6)_6(\text{SO}_2)$, $(\text{Te}_2\text{Se}_4)(\text{SbF}_6)_2$, $(\text{Te}_{2.7}\text{Se}_{3.3})(\text{SbF}_6)_2$, $(\text{Te}_{3.4}\text{Se}_{2.6})(\text{SbF}_6)_2$, $(\text{Te}_2\text{Se}_4)(\text{Sb}_3\text{F}_{14})(\text{SbF}_6)$, $(\text{Te}_{2.1}\text{Se}_{3.9})(\text{SbF}_6)_2$ and $(\text{S}_{3.0}\text{Se}_{1.0})_2(\text{Sb}_4\text{F}_{17})(\text{SbF}_6)_3$. Many of the cations in these compounds, those with non-integral subscripts, possess occupational disorder with some or all of the cation sites partially occupied by two different chalcogen elements. The previously known, but incompletely characterized compounds $(\text{Te}_2\text{Se}_2)(\text{Sb}_3\text{F}_{14})(\text{SbF}_6)$ and $(\text{Te}_{3.0}\text{Se}_{1.0})(\text{Sb}_3\text{F}_{14})(\text{SbF}_6)$ were reprepared from stoichiometric reactions and their compositions confirmed by ^{77}Se and ^{125}Te NMR spectroscopy and X-ray crystallography. The new compounds $(\text{Te}_3\text{S}_3)(\text{SbF}_6)_2$, $(\text{Te}_2\text{Se}_8)(\text{SbF}_6)_2$ and $(\text{Te}_2\text{Se}_8)(\text{SbF}_6)_2(\text{SO}_2)$ were prepared and were found to be isomorphous with their hexafluoroarsenate analogues.

The new $\text{Te}_2\text{Se}_6^{2+}$ cation, which co-crystallizes with $\text{Te}_2\text{Se}_8^{2+}$ in the compound $(\text{Te}_2\text{Se}_6)(\text{Te}_2\text{Se}_8)(\text{AsF}_6)_4(\text{SO}_2)_2$, has

a novel cube-like structure, which is very different from that of S_8^{2+} and Se_8^{2+} , the known homopolyatomic cations of the same average oxidation state. The $Te_2Se_6^{2+}$ structure is compared with the structures of the other polyatomic cations and with the P_{11}^{3-} and As_{11}^{3-} anions. Selenium-77 and ^{125}Te NMR studies indicate that the $Te_2Se_6^{2+}$ and Se_8^{2+} cations retain their structures in solution. The spectra for a $Te_2Se_6^{2+}$ sample enriched to 77.3% in ^{125}Te are dominated by AA'X and AA'XX' satellite subspectra. The compound $(S_{3.0}Se_{1.0})_2(Sb_4F_{17})(SbF_6)_3$ provides the first example of a mixed Se-S cation as well as the only example of the mixed-valence, Sb(III)-Sb(V), $Sb_4F_{17}^-$ anion. The orientations of secondary bonds to Sb(III) atoms in the $Sb_4F_{17}^-$ and $Sb_3F_{14}^-$ anions and to divalent and trivalent chalcogen atoms of the cations are described. These secondary bonds form in directions that cap faces or bridge edges of polyhedra defined by the primary bonds and lone pairs of electrons. Unit cell volumes for the known structures of the polyatomic cations are compared to determine effective volumes for the AsF_6^- , SbF_6^- and $Sb_3F_{14}^-$ anions and the S, Se and Te atoms. These volumes have some predictive value in determining the composition of unknown compounds of known cell volume. Selenium-77 and ^{125}Te NMR data are presented for many of the cations, including spin-lattice relaxation time (T_1) measurements for the $S_xSe_{4-x}^{2+}$ cations.

Several new salts of MX_3^+ cations (M = S, Se, Te;

X = F, Cl, Br, I) were prepared and crystal structures were determined for the compounds $(\text{TeCl}_3)(\text{AlCl}_4)$ - triclinic, $(\text{TeCl}_3)(\text{AsF}_6)$, $(\text{TeCl}_3)(\text{SbF}_6)$ and $(\text{TeF}_3)_2(\text{SO}_4)$. The geometries of these and other MX_3^+ cations are compared with each other and with the isoelectronic neutral molecules. Trends are explained in terms of VSEPR arguments and the strengths of anion-cation interactions (secondary bonds). The ^{19}F , ^{77}Se and ^{125}Te NMR spectra of the SeF_3^+ and TeF_3^+ cations were recorded and the reduced density M-F coupling constants compared and related to the probable geometries of the cations in solution.

Solutions of the mixed F/OTeF₅ compounds

$\text{TeF}_x(\text{OTeF}_5)_{4-x}$ and $[\text{TeF}_x(\text{OTeF}_5)_{3-x}]^+[\text{AsF}_y(\text{OTeF}_5)_{6-y}]^-$ were prepared and characterized by ^{125}Te NMR spectroscopy. Trends in the ^{19}F - $^{125}\text{Te}(\text{IV})$, ^{19}F - $^{125}\text{Te}(\text{VI})$ and $^{125}\text{Te}(\text{IV})$ - $^{125}\text{Te}(\text{VI})$ scalar spin-spin coupling constants are explained in terms of the greater ionic character of the Te--F bond compared to the Te--OTeF₅ bond. The $\text{As}(\text{OTeF}_5)_6^-$ anion was of sufficiently high symmetry for ^{75}As NMR spectra to be recorded in CH_3CN and SO_2 solvents. The activation energy for Berry pseudorotation in $\text{Te}(\text{OTeF}_5)_4$ was determined from variable temperature ^{19}F and ^{125}Te NMR measurements.

ACKNOWLEDGEMENTS

I would like to thank Professor R.J. Gillespie for the opportunity and freedom that he has allowed me in delving into these intriguing problems, for his encouragement and support and for his example. I would especially like to thank Dr. J.F. Sawyer for solving most of the crystal structures presented here, for his many helpful suggestions and ideas and for providing several ORTEP drawings. I would also like to especially thank Dr. G.J. Schrobilgen for introducing me to multinuclear NMR spectroscopy, for his considerable guidance in this area and for his invaluable collaboration on the synthetic and spectroscopic work presented in chapter VIII. I gratefully acknowledge many helpful discussions with members of our research group, including Dr. J.E. Vekris, Dr. R.C. Burns, Dr. J.P. Kent, Dr. B.H. Christian and Dr. K.R. Morgan and I would like to thank Dr. U.R.K. Rao for simulating the ^{75}As NMR spectrum of the $\text{As}(\text{OTeF}_5)_6^-$ anion in chapter VIII. I would also like to thank Mr. J.I.A. Thompson, Mr. B.G. Sayer and Mr. R. Faggiani for their instruction and emergency assistance in the use of the spectrometers and X-ray equipment, and Ms. L. Gowers for running several of the Raman spectra presented here. Yet more thanks are due Dr. R. Lenkinski and Mr. B. MacDonald of the South Western Ontario NMR Center (Guelph) and Dr. C. Rodger of Bruker Spectrospin (Canada) for running some of the NMR spectra.

TABLE OF CONTENTS

	Page
CHAPTER I: INTRODUCTION.....	1
CHAPTER II: EXPERIMENTAL.....	6
II.1 Preparation and Purification of Materials.....	7
II.2 General Experimental Technique.....	9
II.3 Instrumentation.....	13
CHAPTER III: M_{10}^{2+} CATIONS.....	17
III.1 Introduction.....	18
III.2 Preparation of $Te_2Se_8(AsF_6)_2$	20
III.3 Preparation of $Te_{4.5}Se_{5.5}(AsF_6)_2$	20
III.4 Preparation of $Te_2Se_8(AsF_6)_2(SO_2)$ - Alternative Route.....	21
III.5 Preparation of $Te_2Se_8(SbF_6)_2$	22
III.6 Preparation of $Te_2Se_8(SbF_6)_2(SO_2)$	23
III.7 Selenium-77 NMR of the $Te_2Se_8^{2+}$ Cation.....	24
III.8 Selenium-77 NMR of the $S_xSe_{10-x}^{2+}$ Cation.....	24
III.9 Anion-Cation Interactions in M_{10}^{2+} Structures.....	26
III.10 Comparison of M_{10}^{2+} Structures.....	33
CHAPTER IV: M_8^{2+} CATIONS.....	37
IV.1 Introduction.....	38
IV.2 Preparation of $Te_6(Se_8)(AsF_6)_6(SO_2)$	38
IV.3 Preparation of $Te_2Se_6(Te_2Se_8)(AsF_6)_4(SO_2)_2$	40
IV.4 Selenium-77 NMR of Se_8^{2+}	44

IV.5	Selenium-77 and ^{125}Te NMR of $\text{Te}_2\text{Se}_6^{2+}$	50
IV.6	Anion-Cation Interactions in M_{10}^{2+} Structures.....	62
IV.7	Comparison of M_8^{2+} Structures.....	64
IV.8	The Te_6^{4+} Cation in $\text{Te}_6(\text{Se}_8)(\text{AsF}_6)_6(\text{SO}_2)$	72
CHAPTER V: M_6^{2+} CATIONS.....		76
V.1	Introduction.....	77
V.2	Preparation of $\text{Te}_2\text{Se}_4(\text{SbF}_6)_2$	80
V.3	Preparation of $\text{Te}_2\text{Se}_4(\text{Sb}_3\text{F}_{14})(\text{SbF}_6)$	81
V.4	Preparation of $\text{Te}_x\text{Se}_{6-x}(\text{SbF}_6)_2$	81
V.5	Preparation of $\text{Te}_{2.1}\text{S}_{3.9}(\text{SbF}_6)_2$	82
V.6	Preparation of $\text{Te}_3\text{S}_3(\text{SbF}_6)_2$	83
V.7	Anion-Cation Interactions in M_6^{2+} Structures.....	84
V.8	Comparison of M_6^{2+} Structures.....	85
CHAPTER VI: M_4^{2+} CATIONS.....		98
VI.1	Introduction.....	99
VI.2	Preparation of $\text{Te}_2\text{Se}_2(\text{Sb}_3\text{F}_{14})(\text{SbF}_6)$	100
VI.3	Preparation of $\text{Te}_{3.0}\text{Se}_{1.0}(\text{Sb}_3\text{F}_{14})(\text{SbF}_6)$	101
VI.4	Attempted Preparation of $\text{TeSe}_3(\text{Sb}_3\text{F}_{14})(\text{SbF}_6)$	102
VI.5	Preparation of $(\text{S}_{3.0}\text{Se}_{1.0})_2(\text{Sb}_4\text{F}_{17})(\text{SbF}_6)_3$	102
VI.6	Occupational Disorder in M_4^{2+} Structures.....	103
VI.7	Selenium-77 and ^{125}Te NMR of $\text{Te}_x\text{Se}_{4-x}^{2+}$	105
VI.8	Fluorine-19 NMR of $\text{Te}_2\text{Se}_2(\text{Sb}_3\text{F}_{14})(\text{SbF}_6)$	115
VI.9	Selenium-77 NMR of $\text{S}_x\text{Se}_{4-x}^{2+}$	116
VI.10	Raman Spectra.....	122
VI.11	Geometry About Sb(III) in $\text{Sb}_3\text{F}_{14}^-$ and $\text{Sb}_4\text{F}_{17}^-$	127

VI.12	Anion-Cation Interactions in M_4^{2+} Structures.....	135
CHAPTER VII: MX_3^+ CATIONS.....		141
VII.1	Introduction.....	142
VII.2	Preparation of $TeCl_3(AlCl_4)$ -triclinic.....	142
VII.3	Preparation of $TeCl_3(AsF_6)$	143
VII.4	Preparation of $TeCl_3(SbF_6)$	146
VII.5	Preparation of $TeCl_3(SbCl_6)$	147
VII.6	Preparation of $(TeF_3)_2(SO_4)$	147
VII.7	Discussion of Crystal Structures.....	148
VII.8	Geometry of the MX_3^+ Cation.....	162
VII.9	Anion-Cation Interactions in MX_3^+ Structures.....	167
VII.10	F-19, ^{77}Se and ^{125}Te NMR of SeF_3^+ and TeF_3^+	169
CHAPTER VIII: F-19, As-75 AND Te-125 NMR STUDY OF SOME $OTeF_5$ COMPOUNDS.....		175
VIII.1	Introduction.....	176
VIII.2	Preparation of $TeF_x(OTeF_5)_{4-x}$	178
VIII.3	Preparation of $[TeF_x(OTeF_5)_{3-x}][AsF_y(OTeF_5)_{6-y}]$	179
VIII.4	Preparation of $As(OTeF_5)_5$	179
VIII.5	Preparation of $Cs[As(OTeF_5)_6]$	180
VIII.6	Tellurium-125 NMR of $TeF_x(OTeF_5)_{4-x}$	180
VIII.7	Tellurium-125 NMR of $[TeF_x(OTeF_5)_{3-x}]^+$	185
VIII.8	Arsenic-75 NMR of the $As(OTeF_5)_6^-$ Anion.....	190
VIII.9	Berry Pseudorotation in $Te(OTeF_5)_4$ and $As(OTeF_5)_5$	198

CHAPTER IX: CONCLUSIONS.....	208
IX.1 Summary and Conclusions.....	209
IX.2 Discussion of Unit Cell Volumes.....	215
IX.3 Suggestions for Future Work.....	217
BIBLIOGRAPHY.....	225
APPENDIX.....	236
A.1 Unit Cell Dimensions and Space Groups.....	237
A.2 Final Atomic Positional and Thermal Parameters.....	238

LIST OF FIGURES

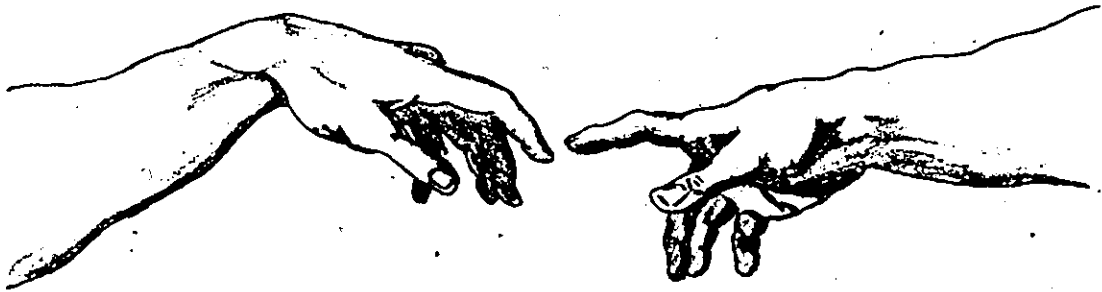
	Page
II.1 Typical reaction vessel.....	16
III.1 ORTEP views of the Se_{10}^{2+} and $\text{Te}_2\text{Se}_8^{2+}$ cations....	19
III.2 Selenium-77 NMR spectra of $\text{Te}_2\text{Se}_8^{2+}$	25
III.3 Selenium-77 NMR spectrum of a 2:1 Se-S mixture in 30% oleum.....	27
III.4 Anion-cation interactions in $\text{Te}_2\text{Se}_8(\text{AsF}_6)_2$ and $\text{Te}_{4.5}\text{Se}_{5.5}(\text{AsF}_6)_2$	29
III.5 The $\text{AX}_2\text{Y}_2\text{E}_2$ and $\text{AX}_3\text{Y}_3\text{E}$ geometries.....	31
III.6 Anion-cation interactions at Se(1) in $\text{Se}_{10}(\text{SO}_3\text{F})_2$	31
III.7 Anion-cation interactions at Te in $\text{Te}_2\text{Se}_6(\text{Te}_2\text{Se}_8)(\text{AsF}_6)_4(\text{SO}_2)_2$ and $\text{TeF}_3(\text{Sb}_2\text{F}_{11})$	32
III.8 Anion-cation interactions at Te(1) in $\text{Te}_{4.5}\text{Se}_{5.5}(\text{AsF}_6)_2$	36
IV.1 ORTEP views of the $\text{Te}_2\text{Se}_6^{2+}$ cation.....	42
IV.2 ORTEP views of the Te_6^{4+} and Se_8^{2+} cations in $\text{Te}_6(\text{Se}_8)(\text{AsF}_6)_6(\text{SO}_2)$	45
IV.3 Selenium-77 NMR spectrum of Se_8^{2+}	47
IV.4 Natural abundance ^{77}Se and ^{125}Te NMR spectra of the $\text{Te}_2\text{Se}_6^{2+}$ cation.....	52
IV.5 Tellurium-125 NMR spectrum of $\text{Te}_2\text{Se}_6^{2+}$, 77.3% enriched in Te-125.....	55
IV.6 Components used to simulate the spectrum in Figure IV.5.....	58
IV.7 Selenium-77 NMR spectrum of $\text{Te}_2\text{Se}_6^{2+}$, 77.3% enriched in Te-125.....	59
IV.8 Components used to simulate the spectrum in Figure IV.7.....	61

IV.9	Anion-cation interactions at $\text{Te}_2\text{Se}_6^{2+}$ in $\text{Te}_2\text{Se}_6(\text{Te}_2\text{Se}_8)(\text{AsF}_6)_4(\text{SO}_2)_2$	63
IV.10	Derivation of the Se_8^{2+} structure from the $\text{Se}_{10}(2+)$ structure.....	63
IV.11	Derivation of the $\text{Te}_2\text{Se}_6^{2+}$ structure from the $\text{Te}_2\text{Se}_8(2+)$ structure.....	66
IV.12	Effect of lone pairs of electrons on the $\text{Te}_2\text{Se}_6(2+)$ structure.....	70
IV.13	ORTEP view of the As_{11}^{3-} anion.....	70
V.1	The $\text{Te}_2\text{Se}_4^{2+}$ and $\text{Te}_3\text{S}_3^{2+}$ cations.....	78
V.2	Derivation of the $\text{Te}_2\text{Se}_4^{2+}$ structure.....	78
V.3	Anion-cation interactions at tellurium in $\text{Te}_2\text{Se}_4(2+)$ structures.....	86
V.4	Plots of (3)-(4) distance and cation volume as a function of mean Te percentage at sites (3) and (4) in the $\text{Te}_x\text{Se}_{6-x}(2+)$ cations.....	91
V.5	ORTEP views of the " $\text{Te}_2\text{S}_4^{2+}$ " cations in $\text{Te}_{2.1}\text{S}_{3.9}(\text{SbF}_6)_2$	94
VI.1	Te-125 NMR spectrum of $\text{Te}_{3.0}\text{Se}_{1.0}(\text{Sb}_3\text{F}_{14})(\text{SbF}_6)$ dissolved in 100% H_2SO_4	108
VI.2	Te-125 NMR spectrum of $\text{Te}_{3.0}\text{Se}_{1.0}(\text{Sb}_3\text{F}_{14})(\text{SbF}_6)$ dissolved in AsF_3	110
VI.3	Te-125 NMR spectrum of Te_4^{2+} in AsF_3	113
VI.4	Te-125 NMR spectrum of Te_4^{2+} in SO_2	114
VI.5	F-19 NMR spectrum of $\text{Te}_2\text{Se}_2(\text{Sb}_3\text{F}_{14})(\text{SbF}_6)$ in SO_2 at 200 K.....	114
VI.6	Se-77 NMR spectrum of $\text{S}_x\text{Se}_{4-x}^{2+}$ ($x = 0-3$).....	117
VI.7	Se-77 NMR spectrum resulting from a 2:2:3 S/Se/ AsF_5 mixture in SO_2	121
VI.8	Se-77 T_1 measurements for $\text{S}_x\text{Se}_{4-x}^{2+}$ ($x = 0-3$).....	123
VI.9	Raman spectrum of $\text{Te}_{3.0}\text{Se}_{1.0}(\text{Sb}_3\text{F}_{14})(\text{SbF}_6)$	124

VI.10	Raman spectra of $S_xSe_{4-x}^{2+}$ and $(S_{3.0}Se_{1.0})_2^-$ $(Sb_4F_{17})(SbF_6)_3 \dots x$	126
VI.11	ORTEP views of the $Sb_3F_{14}^-$ anion.....	128
VI.12	The AX_4Y_4E geometry.....	130
VI.13	Examples with the AX_4Y_4E geometry.....	131
VI.14	ORTEP view of the $Sb_4F_{17}^-$ anion.....	132
VI.15	Examples of the $AX_4Y_2Y'_3E$ geometry.....	134
VI.16	Anion-cation interactions in $Te_2Se_2(Sb_4F_{20})$ and $Te_{3.0}Se_{1.0}(Sb_4F_{20})$	138
VI.17	Anion-cation interactions in $(S_3Se)_2(Sb_7F_{35})$	139
VII.1	Raman spectra of some $TeCl_3^+$ salts.....	145
VII.2	ORTEP views of the $TeCl_3^+$ cations in $TeCl_3(AlCl_4)$ -triclinic.....	149
VII.3	The $TeCl_3^+$ cation in $TeCl_3(SbF_6)$ and $TeCl_3(AsF_6)$	157
VII.4	ORTEP drawing of $(TeF_3)_2(SO_4)$	161
VII.5	The geometry at Te(1) in $(TeF_3)_2(SO_4)$	163
VII.6	Te-125 NMR spectrum of the TeF_3^+ cation.....	172
VIII.1	ORTEP drawing of $B(OTeF_5)_3$	177
VIII.2	Te-125 NMR spectrum of a 3:2 mixture of TeF_4 and $B(OTeF_5)_3$ in SO_2ClF	182
VIII.3	Te-125 NMR spectrum for the reaction of $Te(OTeF_5)_4$ with excess AsF_5 in SO_2	182
VIII.4	Raman spectra of $As(OTeF_5)_5$, $Te(OTeF_5)_4$ and a 1:1 mixture of the above.....	187
VIII.5	Te-125 NMR spectrum of a 1:1 $As(OTeF_5)_5$ and $Te(OTeF_5)_4$ mixture in SO_2	187
VIII.6	As-75 NMR spectrum of the $As(OTeF_5)_6^-$ anion.....	193

VIII.7	Simulation of the ^{75}As NMR spectrum of $\text{As}(\text{OTeF}_5)_6$ for a range of y values.....	195
VIII.8	Te-125 NMR spectrum of $\text{Te}(\text{OTeF}_5)_4$ in SO_2ClF at 146 K.....	200
VIII.9	Variable temperature ^{19}F NMR spectra of $\text{Te}(\text{OTeF}_5)_4$ in SO_2ClF	201
VIII.10	Plot of $\log(\chi^{-1})$ against T^{-1} for the spectra in Figure VIII.9.....	201
VIII.11	F-19 NMR spectrum of $\text{As}(\text{OTeF}_5)_5$ in SO_2ClF	206
IX.1	Se-77 NMR spectrum of a 1:2 Te-Se mixture in 30% oleum.....	220

CHAPTER I
INTRODUCTION

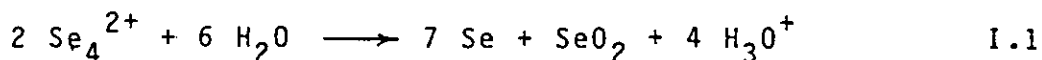


Tellurium was reported to produce a red solution with sulfuric acid as early as 1798 (1). Selenium and sulfur similarly were reported to produce colored solutions when dissolved in oleum (2, 3). The nature of the species producing these colors was unknown until fifteen years ago, however, when conductimetric and cryoscopic measurements performed in Professor Gillespie's laboratory at McMaster indicated that the colors were produced by positively-charged aggregates of chalcogen atoms, that is polyatomic cations such as Te_4^{2+} and Se_8^{2+} . At about the same time, Corbett and coworkers identified polyatomic cations of selenium and tellurium from phase diagram studies of the systems $\text{Se}-(\text{SeCl}_4-4\text{AlCl}_3)$ and $\text{Te}-(\text{TeCl}_4-4\text{AlCl}_3)$ (4) and Bjerrum and Smith concluded that polycations of tellurium were formed in reactions of tellurium with TeCl_4 in molten $\text{AlCl}_3\text{-NaCl}$ (5, 6). These early developments have been discussed in some detail in several review articles (7, 8, 9).

The fortunate crystallization of $\text{Se}_4(\text{HS}_2\text{O}_7)_2$ from a solution of selenium in oleum allowed for the first X-ray crystal structure determination of one of these polyatomic cations and confirmed the square-planar geometry of Se_4^{2+} (10, 11). A short time later several other crystalline compounds were isolated from AlCl_3 melts (12, 13), but the vast majority of compounds have been isolated as AsF_6^- or SbF_6^- salts from SO_2 solution. All of the salts of the polyatomic cations that have been characterized by X-ray

crystallography prior to the present work, or by other research groups during this work, are listed in Table I.1. A polyatomic cation of oxygen, O_2^+ , has also been isolated as PtF_6^- , AsF_6^- , SbF_6^- , PF_6^- and BF_4^- salts (7).

The polyatomic cations are highly electrophilic, hence the need for large anions such as SO_3F^- , $AlCl_4^-$ and SbF_6^- , which are the very weak conjugate bases of very strong acids, and solvents of very low basicity such as HSO_3F , SO_2 or AsF_3 . None of the cations are stable in aqueous media or even if exposed to moist air since disproportionation can occur, as in reaction I.1.



The structures of these polyatomic cations provide us with important basic information on the nature of the bonding in compounds of the main-group elements. Relationships between these structures and a few basic cluster shapes have been developed by Gillespie (9). Comparisons of these relatively electron-rich compounds with the transition metal clusters and the electron-deficient boranes have also been made (9).

The objective of the present work was to prepare new polyatomic cations of the chalcogen elements and to determine their structures so that a more comprehensive structural model with greater predictive value could be developed. The preparation of mixed, or heteropolyatomic cations was of

particular interest since the homopolyatomic cations had already been studied in great depth and it was clear that new structural types could result from the mixed systems. The $\text{Te}_2\text{Se}_4^{2+}$ cation, for example, has no isostructural homopolyatomic M_6^{2+} analogue. Selenium-77 and ^{125}Te NMR spectroscopy were used to examine the species in solution, while X-ray crystallography proved to be invaluable in determining the solid-state structures of the new compounds.

A few TeCl_3^+ and TeF_3^+ salts were isolated as byproducts in reactions designed to prepare new chalcogen polyatomic cations. Salts of these MX_3^+ cations ($\text{M} = \text{S}, \text{Se}, \text{Te}$; $\text{X} = \text{F}, \text{Cl}, \text{Br}, \text{I}$) were of interest in terms of both the cation geometry and the strong interactions between the anions and cations in the structures. Several additional salts were prepared to further investigate these features. The ^{19}F , ^{77}Se and ^{125}Te NMR spectra of the SeF_3^+ and TeF_3^+ cations were recorded to determine if trends in the cation geometry observed in the solid state could also be observed in solution. A number of Te(IV) F/OTeF_5 derivatives were also examined in solution utilizing ^{19}F and ^{125}Te NMR spectroscopy. These subjects are explored in more detail at the beginning of each chapter.

Table I.1 Salts of the Polyatomic Cations of the Chalcogens Characterized by X-Ray Crystallography.

	Compound	Ref.	
M_{19}^{2+}	$S_{19}(AsF_6)_2$	(14)	
	$S_{19}(SbF_6)_2$	(15)	
M_{10}^{2+}	$Se_{10}(AsF_6)_2$	(16)	
	$Se_{10}(SbF_6)_2$	(16)	
	$Te_2Se_8(AsF_6)_2(SO_2)$	(17)	
	$Te_{3.7}Se_{6.3}(AsF_6)_2$	(17)	
M_8^{2+}	$S_8(AsF_6)_2$	(18)	
	$S_8(Sb_3F_{14})(SbF_6)$	(19)	
	$Se_8(AlCl_4)_2$	(12)	
M_6^{2+}	$Te_3S_3(AsF_6)_2$	(20)	
	$Te_2Se_4(AsF_6)_2$	(21)	
	$Te_2Se_4(SbF_6)_2^a$	(20)	
M_4^{2+}	$S_4(AsF_6)_2(SO_2)_{0.6}$	(22)	
	$S_4(S_7Br)_4(AsF_6)_6$	(22)	
	$S_4(S_7I)_4(AsF_6)_6$	(22)	
	$Se_4(HS_2O_7)_2$	(10, 11)	
	$Se_4(AlCl_4)_2$	(23)	
	$Se_4(Sb_9F_{39})$	(23)	
	$Te_4(SbF_6)_2$	(23)	
	$Te_4(AlCl_4)_2$	(13)	
	$Te_4(Al_2Cl_7)_2$	(13)	
	$Te_2Se_2(Sb_3F_{14})(SbF_6)^b$	(24)	
	$Te_{3.3}Se_{0.7}(Sb_3F_{14})(SbF_6)^b$	(24)	
	M_6^{4+}	$Te_6(AsF_6)_4(AsF_3)_2$	(25, 26)
		$Te_6(AsF_6)_4(SO_2)_2$	(26)

(a) Composition suspect - see chapter V. (b) Incompletely characterized prior to present work.

CHAPTER II EXPERIMENTAL



II.1 Preparation and Purification of Materials.

Acetonitrile. CH_3CN (Caledon Laboratories) was triply distilled onto and then stored over P_4O_{10} .

Aluminum Trichloride. AlCl_3 (McArthur Chemical Co.) was vacuum sublimed (dynamic vacuum) at 380 K through a layer of aluminum pellets to remove any iron chlorides.

Antimony Pentachloride. SbCl_5 (J.T. Baker) was used directly from the bottle.

Antimony Pentafluoride. SbF_5 (Ozark-Mahoning) was distilled under vacuum and stored in an F.E.P. bottle in a dry box.

Arsenic. Arsenic metal powder (Alfa Inorganics, 99.5%) was heated to 470 K under vacuum to remove arsenic(III) oxide by sublimation.

Arsenic Trifluoride. AsF_3 was prepared by direct fluorination of the metal at 77K in a nickel can and the product was stored in a nickel can over sodium fluoride. An alternative route from As_2O_3 , CaF_2 and H_2SO_4 was also followed (27).

Arsenic Pentafluoride. After first preparing AsF_3 as described above, a 10% excess of fluorine (for the production of AsF_5) was added and the nickel can heated to 470 K overnight. The product was then cooled to 77 K and the excess fluorine pumped off through a soda lime trap. AsF_5 was stored in a nickel cylinder fitted with an Autoclave valve (Engineers Inc.).

Boron tris (Pentafluoroorthotellurate). $\text{B}(\text{OTeF}_5)_3$ was prepared from BCl_3 (Matheson) and HOTeF_5 as previously describ-

ed (28).

Bromine. Bromine (Fisher Scientific Co.) was kindly supplied by Dr. B.H. Christian. It was stored over anhydrous calcium chloride for 1 week and then distilled onto and stored over P_4O_{10} .

Chlorine. Chlorine (Canadian Liquid Air, 99.5%) was passed through sulfuric acid and P_4O_{10} suspended in glass wool before use.

Fluorine. Fluorine (Matheson, 98%) was passed through sodium fluoride before use.

Fluorosulfuric Acid. HSO_3F (J.T. Baker Co.) which had been purified by standard procedures (29) was kindly donated by Drs. J.E. Vekris and G.J. Schrobilgen.

Heptasulfurtellurium dichloride. S_7TeCl_2 was prepared in a scaled-down version of the published procedure (30).

Methylene Chloride. CH_2Cl_2 (Fisher Scientific Co.) was stored over anhydrous calcium chloride for one week and then distilled onto and stored over P_4O_{10} .

Pentafluoroorthotelluric Acid. $HOTeF_5$ was prepared from telluric acid (BDH) and HSO_3F by standard procedures (140).

Phosphorus Pentoxide. P_4O_{10} (British Drug House) was used directly from the bottle.

Sodium Fluoride. NaF (J.T. Baker) was dried under vacuum at 420 K for 48 h before use.

Sulfur, Selenium and Tellurium. Sulfur (BDH), selenium

(Koch-Light Laboratories Ltd., 99.95%) and tellurium (Koch-Light Laboratories Ltd., 99.7%) were dried under vacuum at room temperature overnight before use.

Sulfur Dioxide. SO_2 (Canadian Liquid Air) was stored over P_4O_{10} for at least 24 h before use.

Hexafluoroarsenate Salts of Sulfur Polyatomic Cations. $\text{S}_{19}(\text{AsF}_6)_2$, $\text{S}_8(\text{AsF}_6)_2$ and $\text{S}_4(\text{AsF}_6)_2$ were prepared using standard procedures (14, 18, 22). $\text{S}_4(\text{AsF}_6)_2$ was pumped under vacuum overnight at room temperature to remove SO_2 initially trapped in the lattice and stored in the dark at 250 K.

Sulfuric Acid. 100% H_2SO_4 was prepared from 96% H_2SO_4 and 30% oleum (Fisher Scientific Co.) following the previously established procedure (31).

Sulfuryl Chlorofluoride. SO_2ClF (Columbia Organic Chemicals Ltd.) was distilled onto crude SbF_5 to remove SO_2 impurity before distilling onto and storing over NaF.

Tellurium Tetrachloride. TeCl_4 was prepared by the reaction of chlorine gas with hot tellurium (33).

Tellurium Tetrafluoride. TeF_4 was prepared by the method of Lentz et al. (34) and kindly supplied by Dr. G.J. Schrobilgen.

II.2 General Experimental Technique.

Manipulation of Materials. Most of the compounds studied were moisture-sensitive and had to be handled in dry

nitrogen atmosphere or under vacuum. Solids were transferred inside a glove box equipped with an evacuable port (S. Blickman). When not in use the box was continuously flushed with nitrogen that originated as the boil-off of a liquid nitrogen tank and was subsequently passed through a dehumidifier (Lectrodryer). The moisture level was ca. 0.1 ppm H_2O or less. Gases and liquids of high vapor pressure were transferred using a calibrated Pyrex vacuum line fitted with Rotaflo valves and a mercury manometer. Reaction vessels and reagent storage vessels were attached to the line using 1/4" o.d. Teflon unions (Swagelok) and Teflon valves (32). Other liquids were transferred in a glove bag or in the glove box: 100% H_2SO_4 was transferred with Pasteur pipettes; $SbCl_5$ with a glass syringe equipped with a long stainless steel needle; and SbF_5 with an all-glass syringe with a 3 mm o.d. glass tube extension as the "needle". All glassware was dried before use in an oven set at 450 K for at least one half-hour and/or under vacuum overnight.

Reaction Vessels. A typical reaction vessel is shown in Figure II.1. Bulbs A and B were both equipped with 1/4" o.d. glass tubing for attachment to the vacuum line and were flame-sealed after all the reactants had been transferred into the vessel. Rotaflo valves D and E and sidearm C were optional depending on the complexity of the reaction.

Reactions were generally carried out in bulb A with mixing of reagents accomplished with the magnetic stirring bar and an external magnetic stirrer. After completion of the reaction the solution was filtered through a medium porosity glass frit into bulb B and the products allowed to crystallize. Crystallization was usually prompted by slow distillation of the solvent back into bulb A, accomplished by slowly dripping cold water onto bulb A. The remaining solution was then poured back into bulb A, residual solvent distilled off of the product by freezing bulb A in liquid N_2 and the product isolated by flame-sealing. Several crops of crystals could be obtained by repeated flame-sealing in segments of sidearm C. If a crystalline product was suspected to have SO_2 (solvent) molecules incorporated in the lattice, the solution in ampoule A was cooled to 245 K only in a dry ice / acetone bath so that a pressure in the vessel was maintained (just under 1 atmosphere) and the 1/4" tubing could still be flame-sealed. Rotaflo valve D was required for reactions involving SbF_5 . The SbF_5 was introduced into bulb B with valve D closed. The vessel was weighed before and after this addition and quantities of the other reagents were then based on the weight of SbF_5 and were transferred into bulb A. Valve E was required if the solvent or insoluble reaction products were to be recovered. Sidearm C could be replaced with an NMR tube to monitor the reaction solution.

NMR Samples. Samples were prepared in 5 mm and 10 mm o.d. precision glass, round bottom NMR tubes (Wilmad) joined to 1/4" o.d. standard wall tubing. The appropriate solvent was either pipetted (100% H_2SO_4 , oleum) or vacuum distilled (AsF_3 , CH_3CN , SO_2 , SO_2ClF) onto the solute before flame-sealing. Samples from reaction mixtures were obtained using the apparatus as described above. Reactions designed for NMR analysis only were performed using a scaled-down version of the apparatus in Figure II.1 with bulb B removed so that the solution was poured directly through the frit into an NMR tube.

Crystal Mounting. Samples to be examined by X-ray crystallography were handled in a dry box equipped with a stereoscopic microscope (Bausch and Lomb). The crystals were manipulated under the microscope using an iridium wire probe and cut to size, if required, with a stainless steel scalpel. With the aid of the probe they were placed inside 0.2 mm and 0.3 mm o.d. Lindemann glass capillaries (Wolfgang Mueller) that had previously been dried under vacuum at 470 K for at least three days. The crystals were pushed into the capillaries with thin glass fibres until wedged and the capillaries sealed inside the dry box with a stainless steel wire that was heated until red hot by passing an electric current through it. The capillaries were cut to size outside the dry box with a micro torch.

II.3 Instrumentation

Laser Raman Spectroscopy. The spectrometer was a Spex Industries Model 14018 double monochromator equipped with 1800-grooves/mm Holographic gratings. An RCA C31034 phototube detector in conjunction with a pulse count system consisting of pulse amplifier, analyzer and rate meter (Hamner NA-11, NC-11 and N-780A respectively) and a Texas Instruments Model FSOZWBA strip-chart recorder were used to record the spectra. Two choices of exciting radiation were available: the green 5145 Å argon ion laser (Spectra-Physics Model 164, adjustable to 900 mW, or a Coherent Model Innova 90, giving up to 3.5 W); and the red 6328 Å helium-neon laser (Spectra-Physics Model 125, with a fixed power of 65 mW). Samples were run in their reaction vessels (Pyrex glass) or in cylindrical Pyrex glass or F.E.P. tubes. The sample tubes were mounted vertically, at 45° to the incident laser beam and the Raman scattered radiation was observed at 45° to the laser beam or 90° to the sample tube direction. Low temperature spectra were recorded at 77 K by submerging the sample in an unsilvered Pyrex glass Dewar filled with liquid nitrogen. Sample tubes could be spun up to 1000 rpm by means of a Variac-controlled electric motor. Slit widths depended on the scattering efficiency of the sample, laser power, etc., with 150 μm being typical (spectral band pass: 5145 Å, 1.8 cm⁻¹; 6328 Å, 1.2 cm⁻¹). The scanning rate was

generally $0.5 \text{ cm}^{-1} \text{ s}^{-1}$. All spectra were referenced to the 169 cm^{-1} band of Hg_2Cl_2 (35) and Raman shifts quoted are estimated to be accurate to $\pm 2 \text{ cm}^{-1}$.

Nuclear Magnetic Resonance Spectroscopy. Spectra^o were recorded using a Bruker WH-90 Spectrometer equipped with a Nicolet 1080 computer and Bruker WM-250 and WM-400 Spectrometers equipped with Aspect 2000 computers. The 400 MHz spectra were recorded at the South Western Ontario NMR Center, Guelph. Acetone d-6 was used to tune the shim coils in all cases and as the low temperature lock substance with the WH-90. Deuterated water was the room temperature lock substance in the latter case. Spectra were recorded unlocked on the superconducting WM-250 and WM-400 instruments. Field drift was $< 0.1 \text{ Hz/h}$ on the WM-250 and somewhat larger on the WM-400. For variable temperature measurements, samples were allowed to equilibrate for at least 15 min after each temperature change and the temperature was monitored by placing a copper-constantan thermocouple within a genitron-filled NMR tube into the sampling region of the probe. Temperatures were considered to be accurate to within $\pm 1 \text{ K}$. Typical acquisition parameters are found in Table II.1. The pulse widths correspond to nuclide tip angles of approximately 90° . No relaxation delays were applied. Line broadening parameters used in exponential multiplication of the free induction decays were generally less than or equal to the data point resolutions. Fluorine-19 spectra were obtained

on the WM-250 in 5 mm o.d. sample tubes with a combination $^1\text{H}/^{19}\text{F}$ probe and a fixed frequency transmitter, or in 10 mm o.d. sample tubes using the ^1H decoupler coils of a broad band probe retuned to 235.361 MHz as the observe coils. All other nuclei were recorded in 10 mm o.d. sample tubes, with the exception of ^{125}Te on the WH-90. The ^{125}Te probe on this instrument was not equipped with an internal locking substance and ^{125}Te samples were run in 8 mm o.d. NMR tubes inside 10 mm o.d. NMR tubes with the space between the tubes filled with D_2O for room temperature spectra or acetone- d_6 for low temperature spectra.

X-Ray Crystallography. Preliminary ~~precession~~ precession photographs were used to check crystal quality and to obtain cell and symmetry information. X-ray measurements were made on a Syntex P2₁ or a Nicolet P3 diffractometer using graphite monochromatized Mo K α radiation ($\lambda = 0.71069 \text{ \AA}$). Accurate unit cell dimensions for each compound were obtained by a least-squares fit of 2θ , ω and χ for 15 high-angle reflections. The X-ray crystallographic analysis was performed in collaboration with Dr. J.F. Sawyer, who collected intensity data for twelve of the compounds reported here and solved thirteen of the structures (see Appendix). ORTEP drawings of the finished structures are to the 50% probability level unless otherwise indicated.

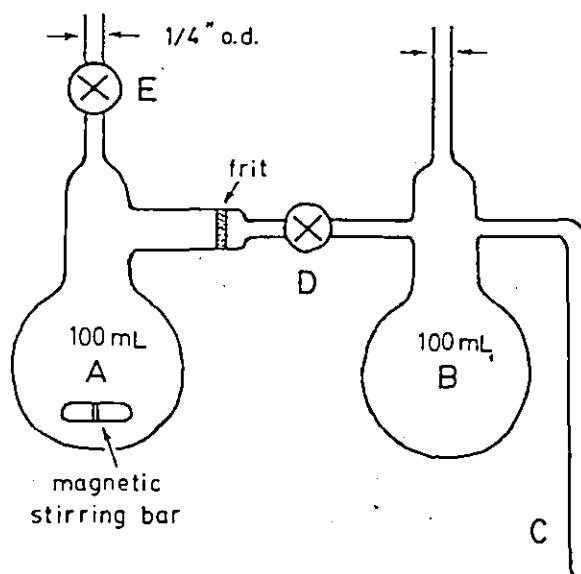


FIGURE II.1 A Typical reaction vessel.

Table II.1. Typical NMR Acquisition Parameters.

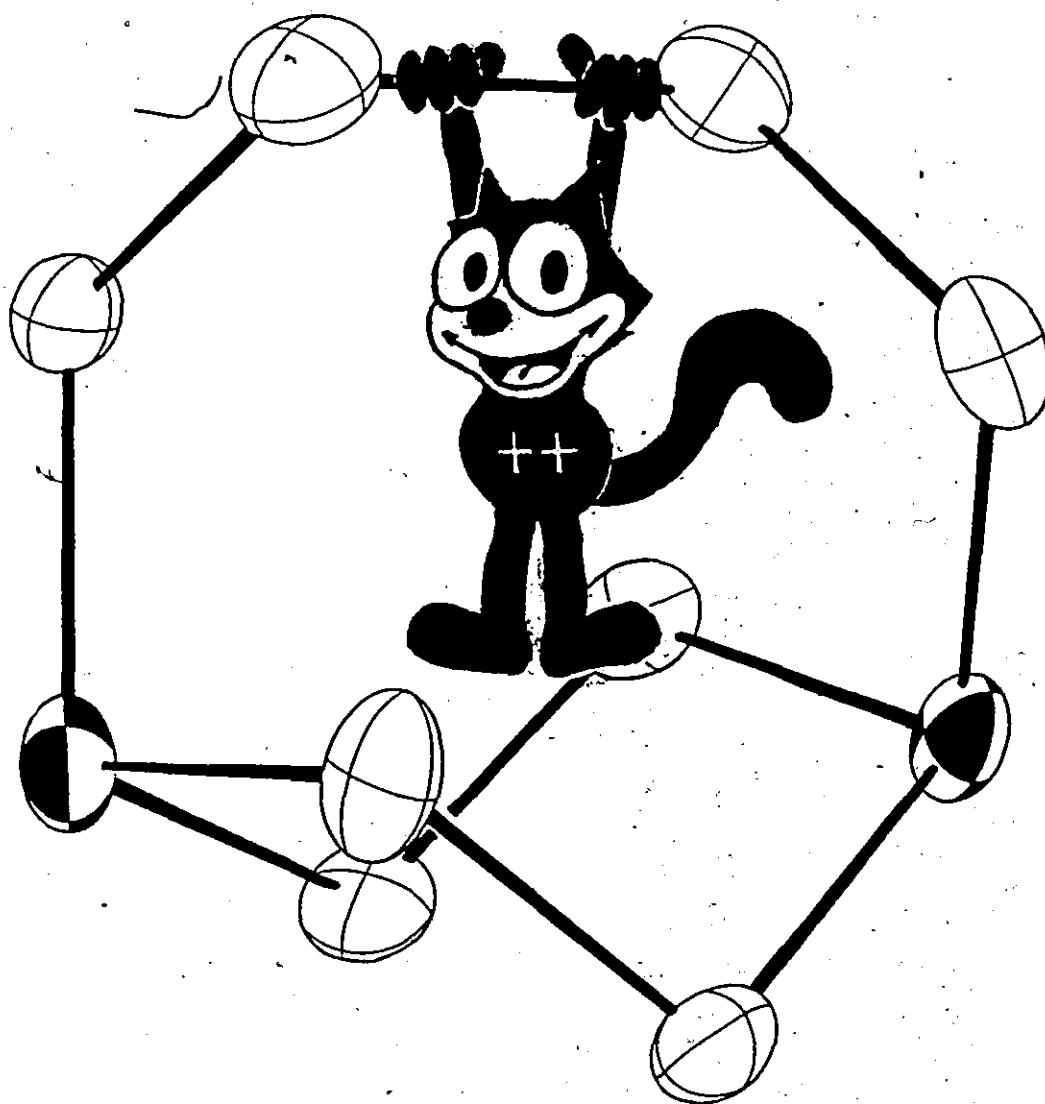
Nucleus	F-19		As-75		Se-77			Te-125		
	5.8719	5.8719	9.3950	2.1139	5.8719	9.3950	2.1139	5.8719	9.3950	
Field (T)	5.8719	5.8719	9.3950	2.1139	5.8719	9.3950	2.1139	5.8719	9.3950	
Frequency (MHz)	235.361	42.83	68.52	17.19	47.77	76.41	28.43	78.97	126.33	
Pulse width (μ s)	5	30	70	20	30	40	20	20	20	
Receiver gain	4	64	-	-	800	-	-	400	-	
Delay time (μ s)	5	2	8	150	5	5	150	5	2	
Spectral width (KHz)	50	100	31	50	50	50	50	50	100	
Memory (K)	32	32	8	16	32	16	16	16	16	
Resolution (Hz/pt)	3.0	6.1	7.6	6.1	3.0	6.1	6.1	6.1	12.2	
Number of scans (K)	2	30	20	300	100	10	300	20	20	
Reference (ext.)	CFCl_3	AsF_6^- ^a		sat'd aq	H_2SeO_3 ^b		sat'd aq.	Te(OH)_6 ^b		

(a) Saturated solution of NaAsF_6 in CH_3CN .

(b) Conversions to chemical shifts (ppm) with respect to neat Me_2Se and Me_2Te at 299 K are given by $\delta[\text{Me}_2\text{Se}] = \delta[\text{H}_2\text{SeO}_3] + 1302.6$ and $\delta[\text{Me}_2\text{Te}] = \delta[\text{Te(OH)}_6] + 710.9$.

CHAPTER III

M_{10}^{2+} CATIONS



III.1 Introduction.

Although no S_{10}^{2+} or Te_{10}^{2+} salts are known, Se_{10}^{2+} has been isolated as $Se_{10}(AlCl_4)_2$, $Se_{10}(AsF_6)_2$, $Se_{10}(SbF_6)_2$ (16) and $Se_{10}(SO_3F)_2$ (36). The mixed $Te_2Se_8^{2+}$ cation in $Te_2Se_8(AsF_6)_2(SO_2)$ is isostructural with Se_{10}^{2+} (17). Another compound, $Te_{3.7}Se_{6.3}(AsF_6)_2$ apparently contains a disordered mixture of $Te_xSe_{10-x}^{2+}$ cations (17). In all cases the cation has a bicyclo (4.2.2) decane structure (Fig. III.1). It can alternatively be thought of as a six-membered, boat-shaped ring linked across the middle by a four-atom chain. This structure can be derived from the basic cuneane or pentagonal prism clusters by adding bridging atoms across the edges and/or removing certain bonds (9, 16). As the two three-coordinate positions must carry a formal positive charge, it is not surprising that they are occupied by the more electropositive tellurium atoms in $Te_2Se_8^{2+}$ (Fig. III.1).

The sole example of a cation of lower average oxidation state than M_{10}^{2+} is S_{19}^{2+} (14). Attempts to produce the analogous Se_{19}^{2+} cation or salts of Se_x^{2+} ($x > 10$) have produced only Se_{10}^{2+} (16), although the results of a potentiometric and spectrophotometric study of selenium in $NaCl-AlCl_3$ melts have been interpreted as indicating the presence of the Se_{12}^{2+} and Se_{16}^{2+} cations (37). Selenium-77 NMR studies also indicate a Se_x^{2+} species where $x > 10$ (see section III.8). In many of the preparations described in

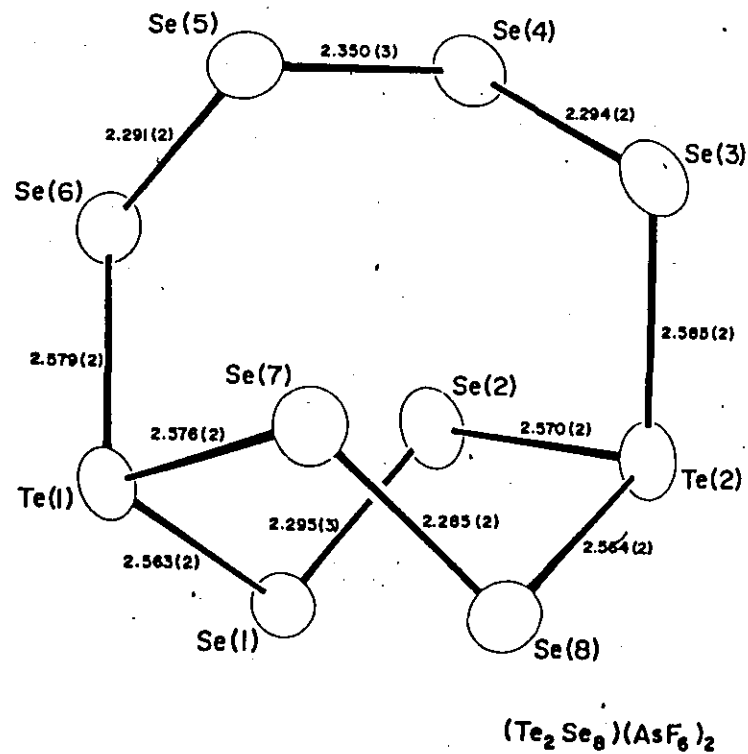
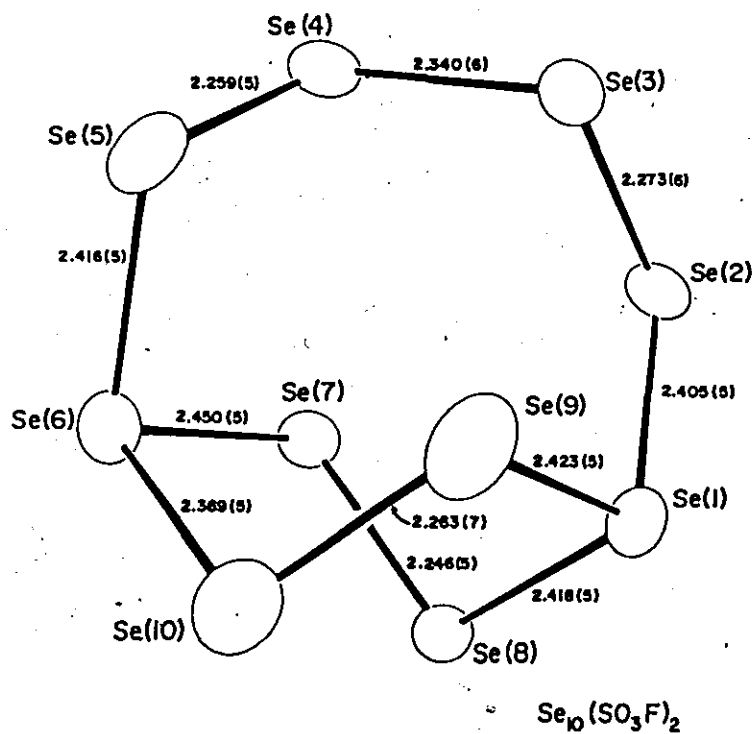


FIGURE III.1 ORTEP views of the Se_{10}^{2+} cation in $\text{Se}_{10}(\text{SO}_3\text{F})_2$ (taken from ref. (36)) and the $\text{Te}_2\text{Se}_8^{2+}$ cation in $\text{Te}_2\text{Se}_8(\text{AsF}_6)_2$.

the following sections the reagent stoichiometries were such that they could, in principle, have produced mixed cations of average oxidation state < 0.2 . In all cases, however, the resulting crystalline compounds contained only the M_{10}^{2+} cation.

III.2 Preparation of $(Te_2Se_8)(AsF_6)_2$.

Using the procedure outlined in chapter II, 0.5002 g (6.33 mmol) Se and 0.1148 g (0.900 mmol) Te were reacted with 0.243 g (1.43 mmol) AsF_5 in 25 mL of SO_2 . The initial green solution turned brown after 1 h. The mixture was stirred for 4 days and then filtered and left to stand for 1 week. The resulting shiny black needles were separated from the solution and a subsequent X-ray crystal structure determination identified the compound as $(Te_2Se_8)(AsF_6)_2$ (Fig. III.1).

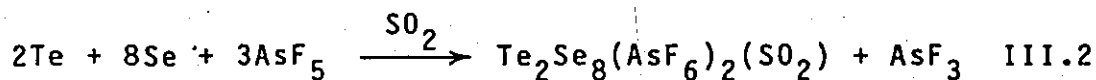
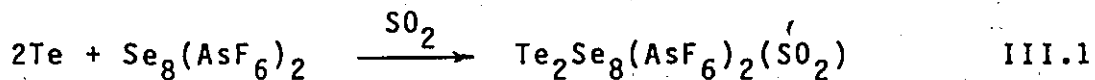
III.3 Preparation of $(Te_{4.5}Se_{5.5})(AsF_6)_2$.

Following the procedure outlined in chapter II, 0.4804 g (6.08 mmol) Se and 0.7786 g (6.10 mmol) Te were combined with 0.607 g (3.58 mmol) AsF_5 in 40 mL of SO_2 . The initial brown solution color persisted for the course of the reaction. After 24 h of stirring a large quantity of dark brown powder had precipitated. Since the solubility of many of the salts of the polyatomic cations in SO_2 increases at depressed temperatures, i.e. the heat of solution is posi-

tive, the reaction mixture was cooled in liquid N_2 to just above the freezing point of the solution before filtering. The solution bulb was placed in a dry ice/acetone bath, which was slowly warmed to 295 K over a period of 48 h. The resulting brown-black crystals and powder were then isolated and a subsequent X-ray crystal structure determination identified the crystals as $(Te_{4.5}Se_{5.5})(AsF_6)_2$. These crystals are isomorphous with $(Te_{3.7}Se_{6.3})(AsF_6)_2$ (17) and the atomic coordinates of this latter compound were used in the initial refinement of the structure. The cation of these compounds is occupationally disordered with several of the atomic sites occupied by both selenium and tellurium.

III.4 Preparation of $Te_2Se_8(AsF_6)_2(SO_2)$ - Alternative Route.

The published preparation of $(Te_2Se_8)(AsF_6)_2(SO_2)$ involves the reaction of elemental Te with $Se_8(AsF_6)_2$ (17). In the present preparation elemental Te and Se are reacted with AsF_5 (compare reactions III.1 and III.2).



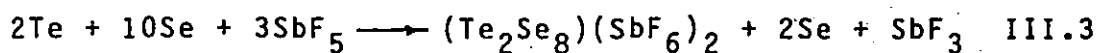
Following the procedure as outlined in chapter II, 0.5114 g (6.48 mmol) Se and 0.2080 g (1.63 mmol) Te were reacted with 0.415 g (2.44 mmol) AsF_5 in 30 mL of SO_2 . The initial green solution turned deep brown after several min. Stirring was continued for 96h before filtering the solution. Within 24h

a large number of dark brown, needle-like crystals had formed. After pouring off the solvent it was observed that the crystals turned a bright red color upon cooling in liquid N_2 , allowing a Raman spectrum to be recorded with the red, He-Ne laser. Raman spectrum (77 K, 6328 Å, spinning sample, values are cm^{-1} with relative intensities in parentheses): 80(22), 87(22), 106(32), 112(56), 122(16), 130(11), 141(11), 192(32), 197(26), 204(sh), 208(100), 217(13), 253(12), 280(37), 288(21), 340(6,br), 381(6). Precession photographs revealed that the crystals were $(Te_2Se_8)(AsF_6)_2(SO_2)$.

III.5 Preparation of $(Te_2Se_8)(SbF_6)_2$.

Following the procedure outlined in chapter II, 2.0256 g (25.65 mmol) Se and 0.6572 g (5.15 mmol) Te were reacted with 1.668 g (7.70 mmol) SbF_5 in 40 mL of SO_2 . The initial green solution turned brown during the first hour of stirring. After heating at 330 K for 12 h most of the product had precipitated leaving a pale green solution. The reaction mixture was then stirred at 295 K for a further 24 h, cooled in liquid N_2 until close to the freezing point of the solution and filtered. A large number of shiny black needles formed from this brown solution during the following 24 h. These crystals were allowed to grow for 1 week before isolating them from the solution. Precession photographs revealed that the crystals were isomorphous with

$(\text{Te}_2\text{Se}_8)(\text{AsF}_6)_2$ and their composition was then presumably $(\text{Te}_2\text{Se}_8)(\text{SbF}_6)_2$. Accurate cell dimensions were determined on a Syntex P2₁ diffractometer (Appendix). Reaction III.3 describes the reagent stoichiometry used to prepare this compound as described above. $(\text{Te}_2\text{Se}_8)(\text{SbF}_6)_2$ was also prepared in a room temperature reaction using considerably less selenium (reaction IV.5).



III.6 Preparation of $(\text{Te}_2\text{Se}_8)(\text{SbF}_6)_2(\text{SO}_2)$

Following the procedure as outlined in chapter II, Te (0.7515 g, 5.89 mmol), Se (1.3959 g, 17.68 mmol), and SbF₅ (1.916 g, 8.84 mmol) were combined in 45 mL of SO₂. The initial green solution turned dark brown within 1/2 h and large quantities of finely-divided brown precipitate formed. No further change was observed after 3 h of stirring. The solution was then cooled to near its freezing point, filtered and allowed to stand in a dry ice/acetone bath to slowly come to room temperature. After 48 h the solution was poured off leaving a large quantity of brown crystals. Precession photographs of these needles and plates revealed that they were isomorphous with $(\text{Te}_2\text{Se}_8)(\text{AsF}_6)_2(\text{SO}_2)$, but they were twinned and accurate cell parameters were not determined on a diffractometer. When some of the crystals were dissolved in 100% H₂SO₄ the

^{77}Se NMR spectrum identified the $\text{Te}_2\text{Se}_8^{2+}$ cation (section III.7) and therefore this compound was presumably $(\text{Te}_2\text{Se}_8)(\text{SbF}_6)_2(\text{SO}_2)$.

III.7 Selenium-77 NMR of the $\text{Te}_2\text{Se}_8^{2+}$ Cation

When $(\text{Te}_2\text{Se}_8)(\text{AsF}_6)_2$ is dissolved in 100% H_2SO_4 the resulting ^{77}Se NMR spectrum initially consists of four resonances of roughly equal intensity (Fig. III.2). Since there are four separate selenium environments in the solid-state structure, each containing two selenium atoms (Fig. III.1), it would appear that the same structure is retained in solution. There is a fifth, smaller resonance in the spectrum at -732.7 ppm. This resonance became relatively more intense with time and has been assigned to $\text{Te}_2\text{Se}_6^{2+}$ (section IV.5). Numerous additional resonances appeared with time as $\text{Te}_2\text{Se}_8^{2+}$ is slowly oxidized in 100% H_2SO_4 . Salts of the $\text{Te}_2\text{Se}_8^{2+}$ cation are not sufficiently soluble in SO_2 for a ^{77}Se NMR spectrum to be recorded and they appear to react with AsF_3 . The ^{77}Se NMR spectrum of the resulting solution in AsF_3 (Fig. III.2) contains numerous signals in the same region as those observed in the 100% H_2SO_4 solution, but of different intensities. This spectrum does not change with time and $\text{Te}_2\text{Se}_6^{2+}$ is again one of the major decomposition products (see section IV.5).

III.8 Selenium-77 NMR of the $\text{S}_x\text{Se}_{10-x}^{2+}$ Cation.

When a 2:1 Se-S mixture was dissolved in 30% oleum

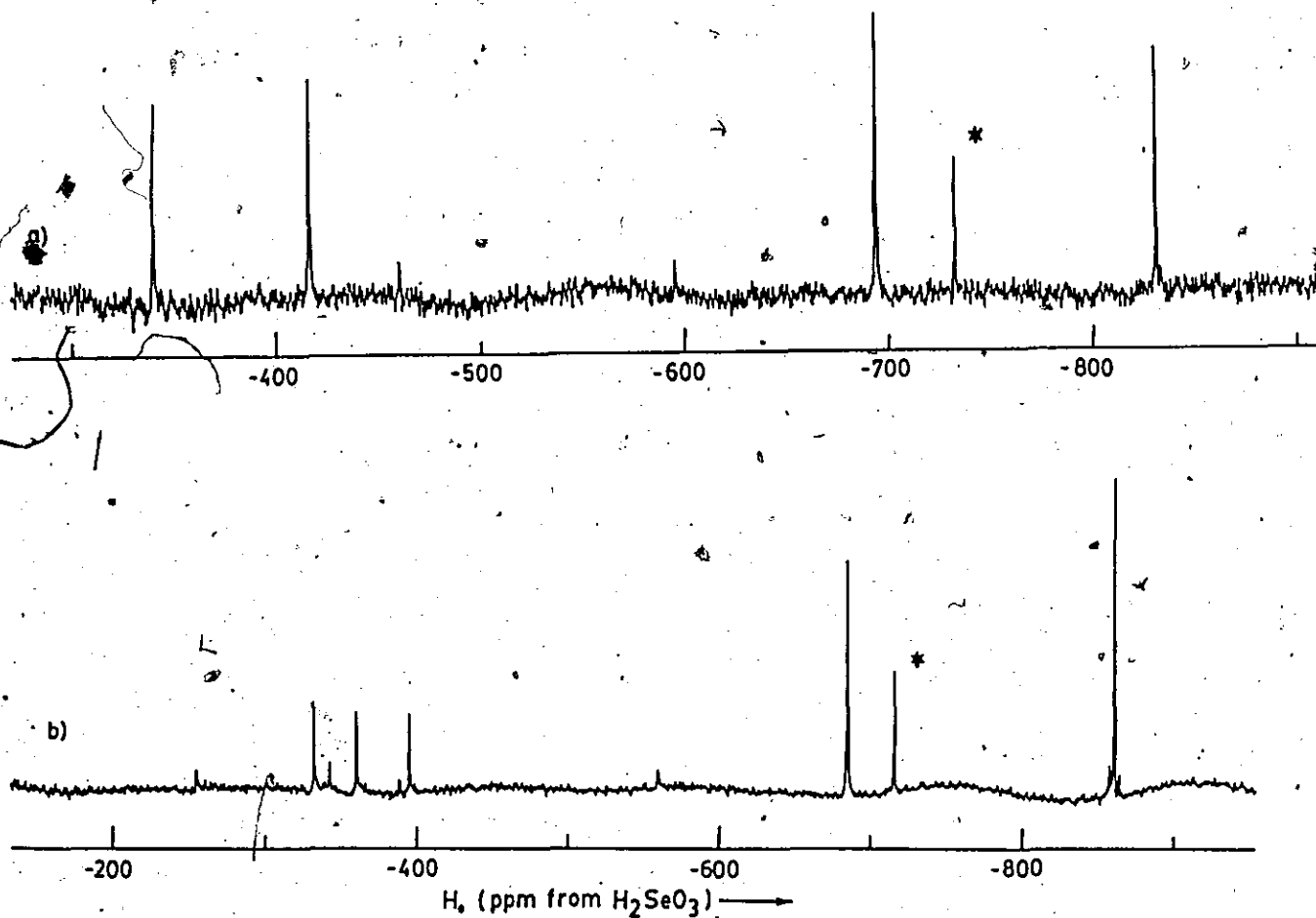


FIGURE III.2 ⁷⁷Se NMR spectra (47.77 MHz) of a) $\text{Te}_2\text{Se}_8(\text{AsF}_6)_2$ in 100% H_2SO_4 (0.1 m; 100,000 scans; 6.1 Hz/pt) and b) $\text{Te}_2\text{Se}_8(\text{AsF}_6)_2(\text{SO}_2)$ in AsF_3 (0.1 m; 400,000 scans; 6.1 Hz/pt). (*) indicates $\text{Te}_2\text{Se}_6^{2+}$.

the initial species observed was Se_4^{2+} but over a period of 5 weeks the Se_4^{2+} signal disappeared and the characteristic lines of Se_{10}^{2+} became dominant. The Se_{10}^{2+} spectrum consists of two signals of intensity 4:1 (38). At the same time a number of other resonances appeared in the same region of the spectrum (Fig. III.8). The Se_4^{2+} , Se_8^{2+} and Se_{10}^{2+} cations account for all of the resonances that are observed upon dissolving selenium alone in 30% oleum, except for a resonance at -511 ppm. This resonance is also observed as Se_{10}^{2+} disproportionates at low temperature in SO_2 solution to Se_8^{2+} and an unknown species of presumably lower average oxidation state (38). The positions of the present resonances do not correspond to any of these species. Since they are found in the same region as the Se_{10}^{2+} resonances, these new resonances probably result from mixed $\text{S}_x\text{Se}_{10-x}^{2+}$ cations.

III.9 Anion-Cation Interactions in M_{10}^{2+} Structures.

There are a number of anion-cation contacts in the structures noted above that are significantly shorter than the sum of the van der Waals radii of fluorine and tellurium or fluorine and selenium (39) ($F = 1.47$, $\text{Se} = 1.90$, $\text{Te} = 2.06 \text{ \AA}$). Interactions such as these have been called "secondary bonds" (40). They are common in compounds of the main-group elements where there are holes in the primary coordination sphere of a given atom resulting from lone

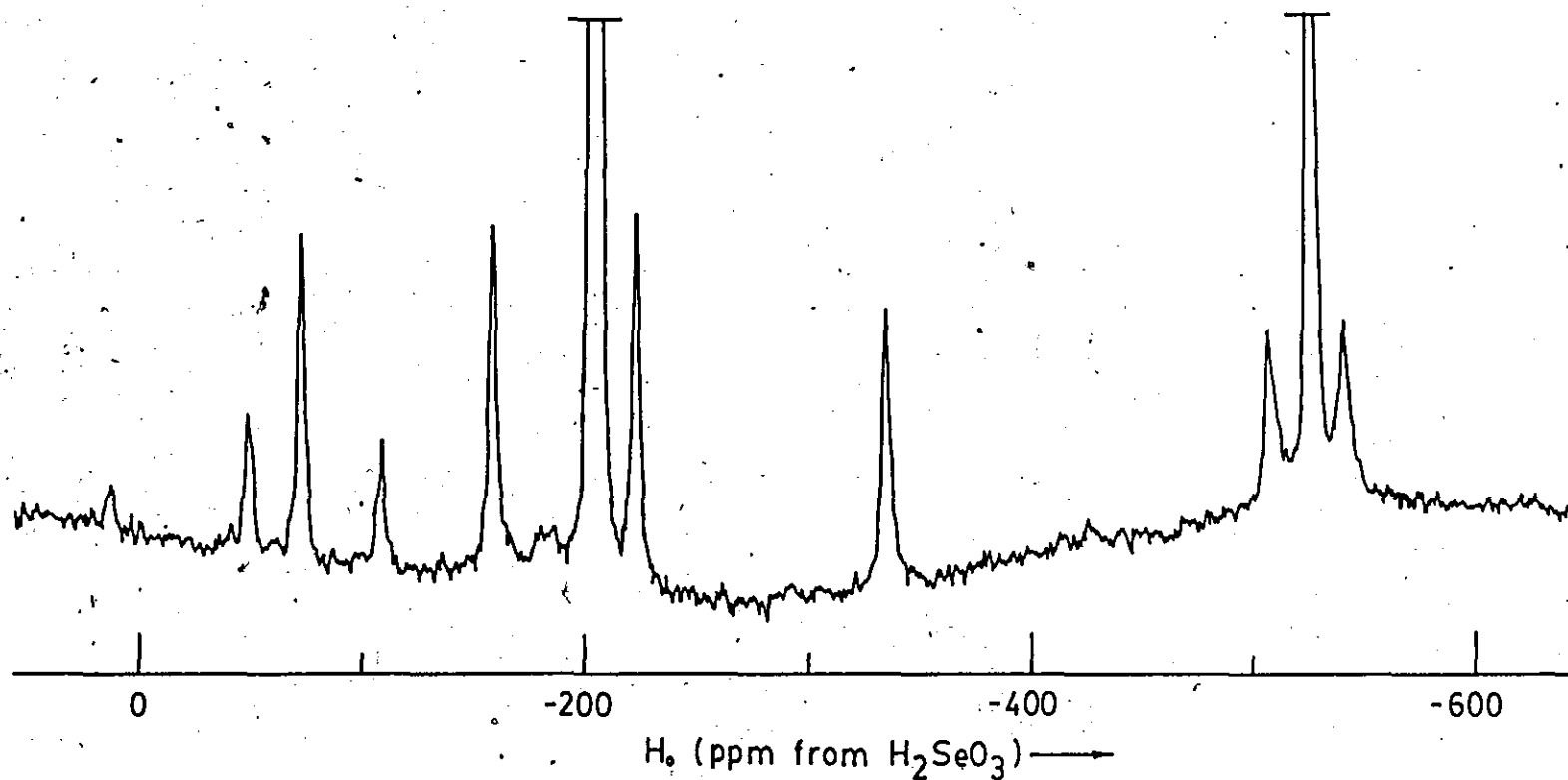


FIGURE III.3 Se-77 NMR spectrum of a 2:1 Se/S mixture in 30% oleum (1.4551 g Se; 0.2985 g S; 5 g oleum) run after 5 weeks at 295 K (17.19 MHz; 300,000 scans; 6.1 Hz/pt). Truncated peaks are Se₁₀²⁺.

pairs of electrons. Secondary bonds to this central atom, A, are assumed to be nucleophilic in nature with the remote atoms, Y, donating electron density into antibonding orbitals associated with the primary, A--X, bonds (40). In a recent high-resolution X-ray diffraction study of $(\text{CH}_3)_2\text{TeCl}_2$, the observed electron density distribution supports this donor-acceptor model for the bonding between tellurium and two chlorine atoms on adjacent molecules (41, 42).

The secondary bonds in the M_{10}^{2+} structures (Fig. III.4) are generally approximately collinear with the A--X bonds. For divalent selenium (or mixed Se/Te) atoms the primary geometry is a tetrahedron, AX_2E_2 , where E is a lone pair. The addition of two secondary bonds trans to the A--X bonds produces a bicapped tetrahedron $\text{AX}_2\text{Y}_2\text{E}_2$ (Fig. III.5). The arrangement of primary and secondary bonds is planar. Examples with this geometry are Se(1), Se(3) and Se(5) of $\text{Te}_2\text{Se}_8(\text{AsF}_6)_2$ and Te(2) of $\text{Te}_{4.5}\text{Se}_{5.5}(\text{AsF}_6)_2$ (Fig. III.4). Several of the divalent atoms in the M_{10}^{2+} structures have additional secondary bonds that are trans to neither the primary bonds nor the lone pairs. These are frequently in positions which bridge the E--E edge of the AX_2E_2 tetrahedron. Examples with this $\text{AX}_2\text{Y}_2\text{Y}'\text{E}_2$ geometry are Se(6) and Se(8) of $\text{Te}_2\text{Se}_8(\text{AsF}_6)_2$, Fig. III.4. The arrangement of weak contacts to divalent sulfur and selenium atoms has been dis-

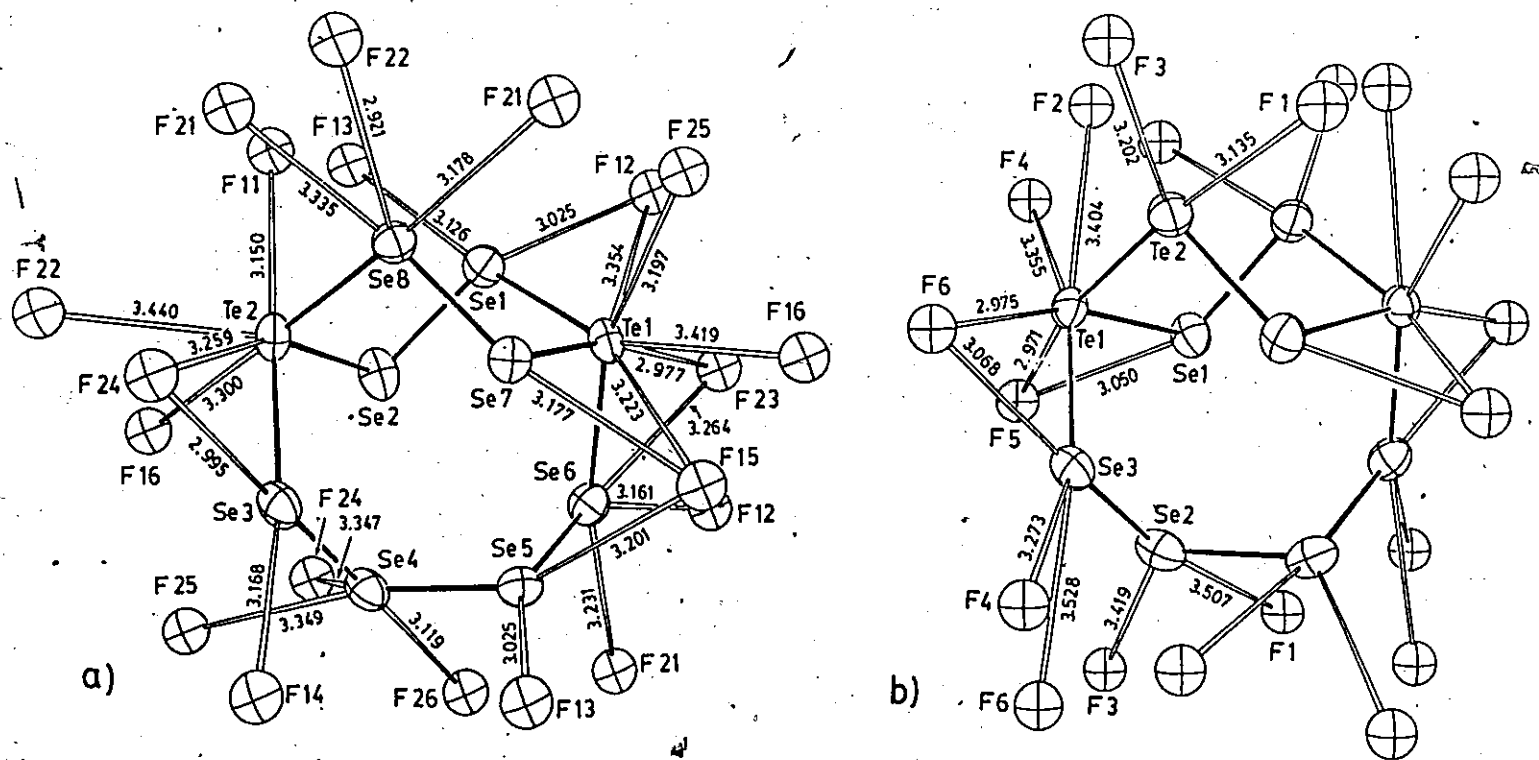


FIGURE III.4 Interionic contacts in a) $\text{Te}_2\text{Se}_8(\text{AsF}_6)_2$ and b) $\text{Te}_{4.5}\text{Se}_{5.5}(\text{AsF}_6)_2$.

cussed by Dunitz et al. (43) and Gillespie et al. (44, 45).

For trivalent atoms with one lone pair the formation of secondary bonds trans to each of the primary bonds results in an AX_3Y_3E monocapped octahedron (Fig. III.5). This geometry is frequently observed for the bridgehead atoms of the M_{10}^{2+} structures (see for example $Se_{10}(SO_3F)_2$, Fig. III.6). The same arrangement is observed for many of the M_8^{2+} (section IV.6) and M_6^{2+} salts (section V.7), and is very prominent in salts of the MX_3^+ cations (chapter VII). As was the case for the divalent atoms, however, secondary bonds are sometimes observed to these bridgehead atoms in addition to those trans to the primary bonds. Atom Te(1) of $(Te_2Se_6)(Te_2Se_8)(AsF_6)_4(SO_2)_2$ has six secondary bonds in an $AX_3Y_3Y'_3E$ arrangement where the primary bonds and two sets of secondary bonds are perfectly staggered and the coordinated atoms lie in three distinct planes (Fig. III.7). A similar arrangement is observed for Te in $(TeF_3)(Sb_2F_{11})$ (46) except that the upper and lowermost sets of bonds are eclipsed, resulting in a tricapped trigonal-prismatic arrangement of primary and secondary bonds about Te with the lone pair capping a triangular face of the trigonal prism (Fig. III.7). Another way of visualizing this is to consider the secondary bonds to be capping the faces and bridging the edges of the tetrahedron defined by the three primary bonds and the lone pair (Fig. III.5). Atoms F(4), F(5) and F(6) are face-capping while F(2)', F(8) and F(13) are edge-

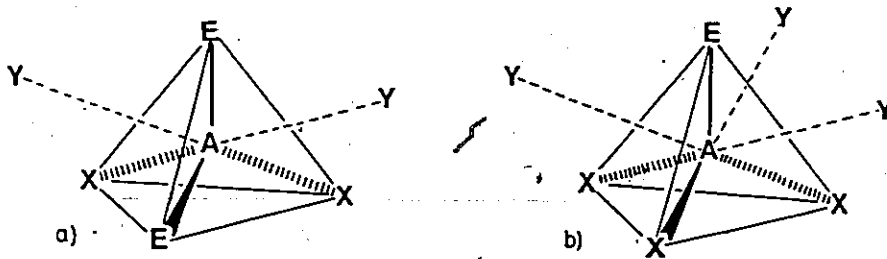


FIGURE III.5 The $AX_2Y_2E_2$ and AX_3Y_3E geometries.

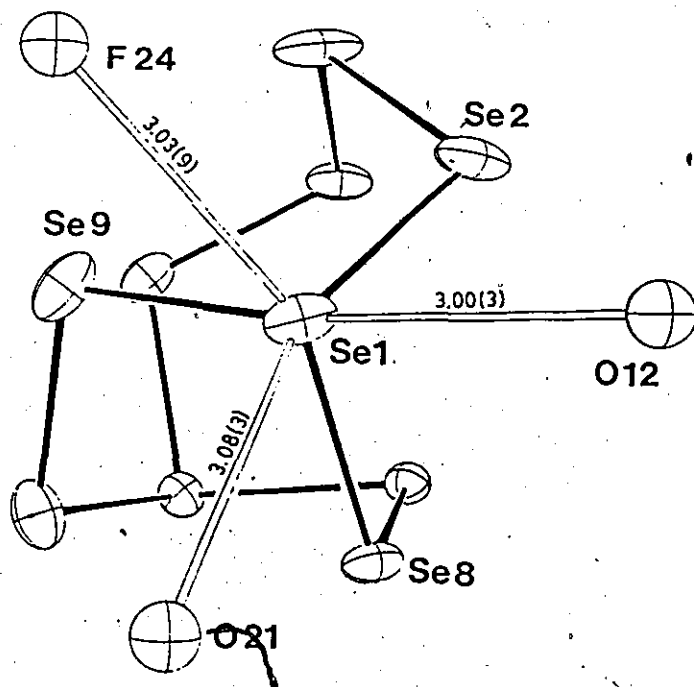


FIGURE III.6 Anion-cation interactions at Se(1) in $Se_{10}(SO_3F)_2$.

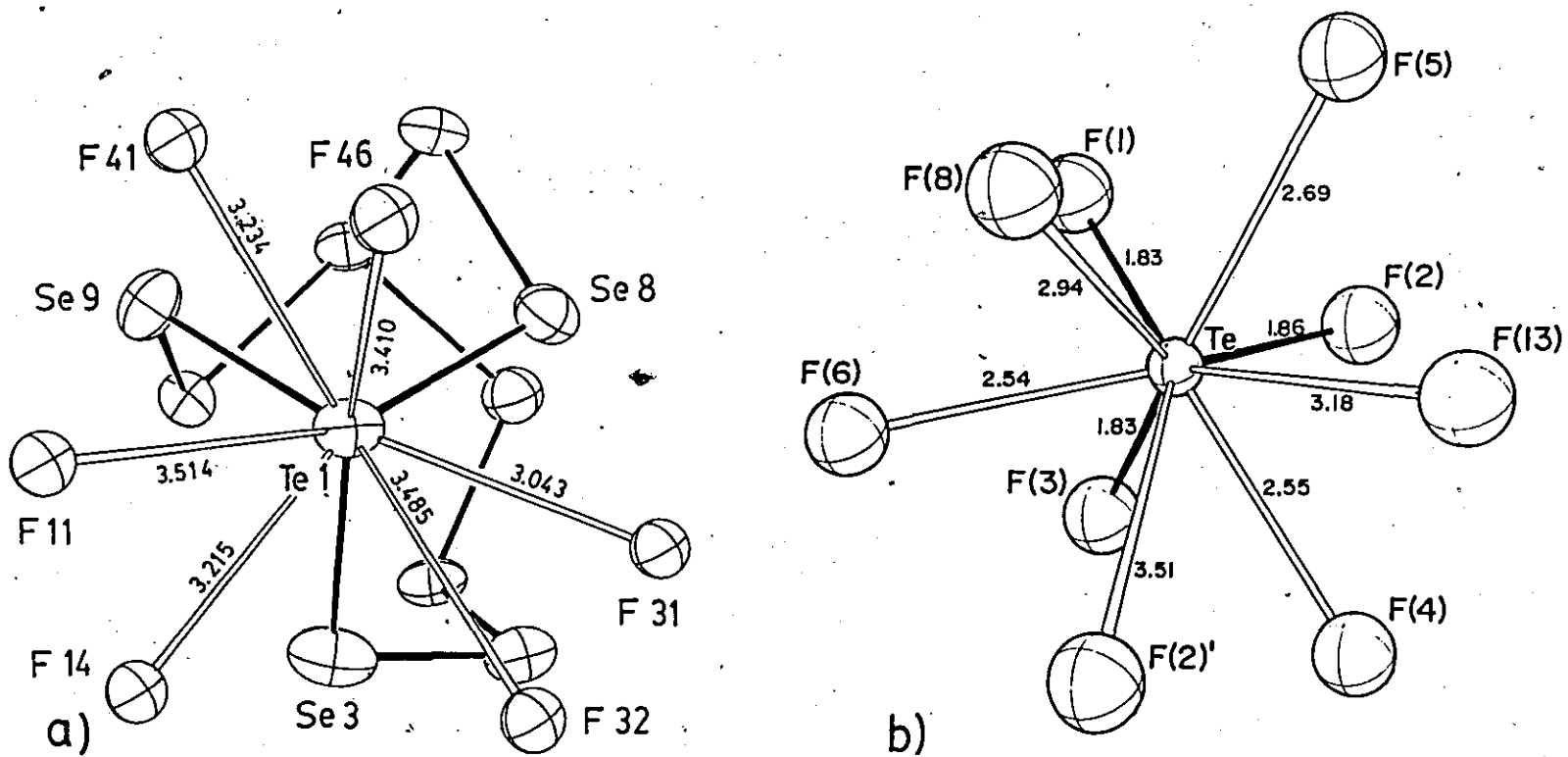


FIGURE III.7 Anion-cation interactions at Te in (a) $\text{Te}_2\text{Se}_6(\text{Te}_2\text{Se}_8)(\text{AsF}_6)_4(\text{SO}_2)_2$ (this work) and (b) $\text{TeF}_3(\text{Sb}_2\text{F}_{11})$, redrawn by Dr. J.F. Sawyer from coordinates in reference (46).

bridging in $(\text{TeF}_3)(\text{Sb}_2\text{F}_{11})$. For $\text{Te}(1)$ of $(\text{Te}_{4.5}\text{Se}_{5.5})(\text{AsF}_6)_2$, $\text{F}(2)$, $\text{F}(5)$ and $\text{F}(6)$ are face-capping while $\text{F}(4)$ is edge-bridging, giving an overall $\text{AX}_3\text{Y}_3\text{Y}'\text{E}$ geometry (Fig. III.4 and III.8). The geometries of primary and secondary bonds about analogous $\text{Sb}(\text{III})$ atoms have been discussed in some detail elsewhere (87).

Another general feature of the anion-cation contacts in the present structures is that there are more of them directed toward the three-coordinate, bridge-head positions of the cations where the positive charges are formally located. This is consistent with the nucleophilic nature of these interactions.

III.10 Comparison of M_{10}^{2+} Structures.

Bond lengths of the $\text{Te}_x\text{Se}_{10-x}^{2+}$ cation in the compounds $(\text{Te}_2\text{Se}_8)(\text{AsF}_6)_2$, $(\text{Te}_2\text{Se}_6)(\text{Te}_2\text{Se}_8)(\text{AsF}_6)_4(\text{SO}_2)_2$ and $(\text{Te}_{4.5}\text{Se}_{5.5})(\text{AsF}_6)_2$ are compared with those from the published structures of $(\text{Te}_2\text{Se}_8)(\text{AsF}_6)_2(\text{SO}_2)$ and $(\text{Te}_{3.7}\text{Se}_{6.3})(\text{AsF}_6)_2$ in Table III.1. The cation in $(\text{Te}_{4.5}\text{Se}_{5.5})(\text{AsF}_6)_2$ is a disordered mixture of $\text{Te}_x\text{Se}_{10-x}^{2+}$ cations. The distribution of the tellurium and selenium atoms in this cation is outlined in Table III.2. The bond lengths of this cation are significantly longer than those of $\text{Te}_2\text{Se}_8^{2+}$ in $(\text{Te}_2\text{Se}_8)(\text{AsF}_6)_2$ or $(\text{Te}_2\text{Se}_6)(\text{Te}_2\text{Se}_8)(\text{AsF}_6)_4(\text{SO}_2)_2$, as would be expected for partial substitution of tellurium at the selenium sites of $\text{Te}_2\text{Se}_8^{2+}$. The bond lengths of this cation

TABLE III.1 Bond Lengths in the $\text{Te}_x\text{Se}_{10-x}^{2+}$ Cation.

Bond Lengths (Å) ^a	I ^b	II ^c	III ^d	IV ^e	V ^f
Te(1)-Se(1)	2.563(2)	2.643(8)	2.572(6)	2.602(1)	2.61(1)
Te(1)-Se(6)	2.579(2)	2.579(8)	2.529(8)	2.614(1)	2.63(1)
Te(1)-Se(7)	2.576(2)	2.644(8)	2.584(8)	2.678(1)	2.66(5)
Te(2)-Se(2)	2.570(2)	2.613(8)	2.603(7)	2.678(1)	2.73(3)
Te(2)-Se(3)	2.585(2)	2.602(8)	2.562(7)	2.614(1)	2.63(1)
Te(2)-Se(8)	2.564(2)	2.583(8)	2.586(6)	2.602(1)	2.61(1)
Se(1)-Se(2)	2.295(3)	2.373(8)	2.323(7)	2.414(1)	2.53(4)
Se(3)-Se(4)	2.294(2)	2.328(8)	2.283(10)	2.434(1)	2.50(2)
Se(4)-Se(5)	2.350(3)	2.401(8)	2.376(9)	2.506(2)	2.54 ^g
Se(5)-Se(6)	2.291(2)	2.318(8)	2.316(10)	2.434(1)	2.43 ^g
Se(7)-Se(8)	2.285(2)	2.356(8)	2.313(8)	2.414(1)	2.31(5)
Reference	h	17	h	h	17

- (a) Atomic numbering corresponds to $(\text{Te}_2\text{Se}_8)(\text{AsF}_6)_2$, Fig. III.1.
 (b) $(\text{Te}_2\text{Se}_8)(\text{AsF}_6)_2$. (c) $(\text{Te}_2\text{Se}_8)(\text{AsF}_6)_2(\text{SO}_2)$.
 (d) $(\text{Te}_2\text{Se}_6)(\text{Te}_2\text{Se}_8)(\text{AsF}_6)_4(\text{SO}_2)_2$. (e) $(\text{Te}_{4.5}\text{Se}_{5.5})(\text{AsF}_6)_2$.
 (f) $(\text{Te}_{3.7}\text{Se}_{6.3})(\text{AsF}_6)_2$. (g) Standard error uncertain.
 (h) This work.

TABLE III.2 Occupation of the Sites in the $\text{Te}_x\text{Se}_{10-x}^{2+}$ Cation of $(\text{Te}_{4.5}\text{Se}_{5.5})(\text{AsF}_6)_2$.

SITE	POPULATION [*] PARAMETER	NO. OF ELECTRONS	% Te	% Se
Te(1)	0.998	51.90	100	0
Te(2)	0.844	43.89	55	45
Se(1)	1.064	36.18	12	88
Se(2)	1.230	41.82	43	57
Se(3)	1.068	36.31	13	87

Overall Composition: $\text{Te}_{4.46}\text{Se}_{5.54}^{2+}$

(*) From refinement in the program SHELX (48).

are, however, on average less than those of the mixed cation in $(\text{Te}_{3.7}\text{Se}_{6.3})(\text{AsF}_6)_2$ (17). Since the refinement of the structure of this latter compound terminated with an R-factor of 0.12 while a value of 0.03 was obtained for $(\text{Te}_{4.5}\text{Se}_{5.5})(\text{AsF}_6)_2$, the composition of the present compound is probably more reliable. The compound formulated as $(\text{Te}_{3.7}\text{Se}_{6.3})(\text{AsF}_6)_2$ probably contains a higher concentration of tellurium.

Many of the bond lengths in the published structure of $(\text{Te}_2\text{Se}_8)(\text{AsF}_6)_2(\text{SO}_2)$ (17) are also longer than analogous bonds in $(\text{Te}_2\text{Se}_8)(\text{AsF}_6)_2$. This suggests that there is partial tellurium substitution at the selenium positions of this former compound as well, or at least in the particular sample chosen for the X-ray crystal structure determination. Bonds to Se(1) and Se(7) show the greatest deviation (Table III.1), indicating significant tellurium substitution at these sites. The consistency of the Te--Se and Se--Se bond lengths in the $(\text{Te}_2\text{Se}_8)(\text{AsF}_6)_2$ structure suggests that there is little or no disorder in this cation. The central bond in the four-atom selenium chain is somewhat longer than the other Se--Se bond lengths, but a lengthening is also observed for this bond in the Se_{10}^{2+} structures (16, 36) and a similar effect has been observed in chains of four or more sulfur atoms (47). A large excess of selenium was used in the preparation of $(\text{Te}_2\text{Se}_8)(\text{AsF}_6)_2$ (section III.2), which

would also tend to limit the possibility of finding tellurium in the divalent positions. Occupational disorder is very common in mixed cations of the chalcogen elements, as will become clear in the following chapters.

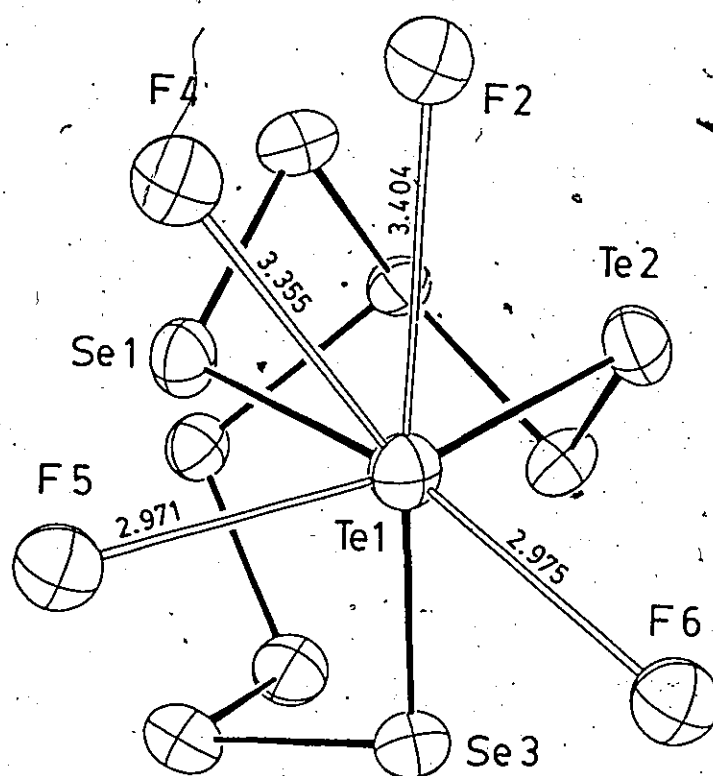
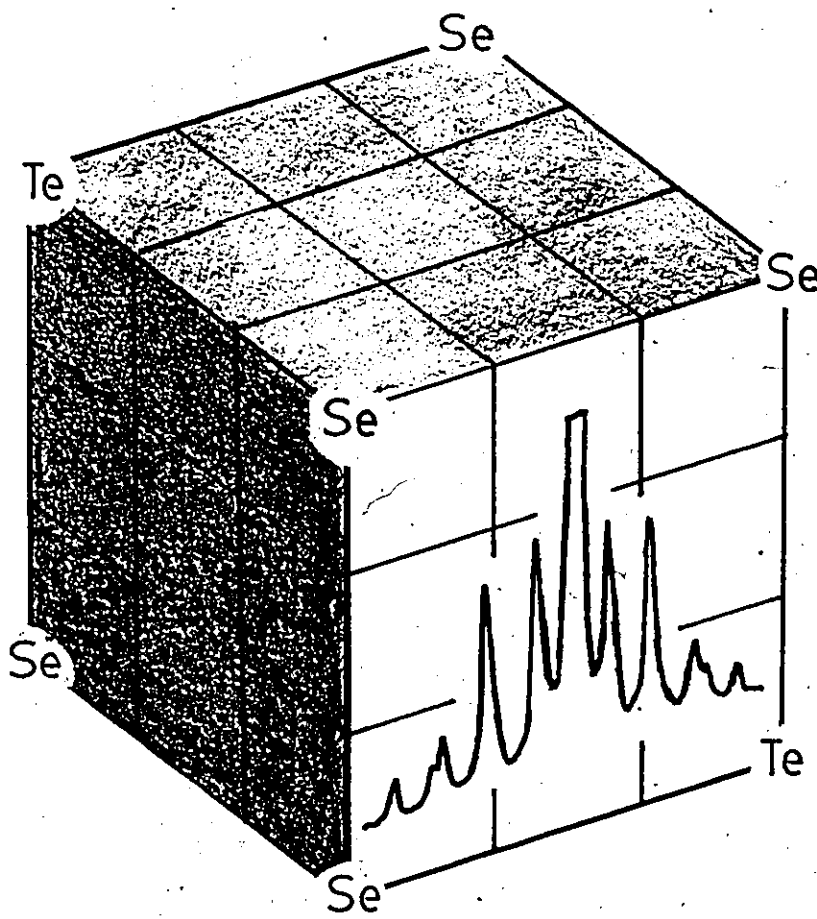


FIGURE III.8 Anion-cation interactions at Te(1) in $\text{Te}_{4.5}\text{Se}_{5.5}(\text{AsF}_6)_2$.

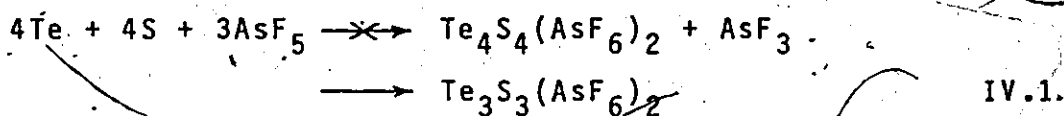


CHAPTER IV

M_8^{2+} CATIONS

IV.1 Introduction.

Although Se_8^{2+} was one of the first polyatomic cations identified by cryoscopy (49a) and $\text{Se}_8(\text{AlCl}_4)_2$ one of the first salts of the polyatomic cations to be characterized by X-ray crystallography (12), few compounds of Se_8^{2+} or related cations have been prepared. Two salts of the isostructural S_8^{2+} cation have been identified by X-ray crystallography, $\text{S}_8(\text{AsF}_6)_2$ and $\text{S}_8(\text{Sb}_3\text{F}_{14})(\text{SbF}_6)$ (18, 19). Compounds of the Te_8^{2+} cation are unknown although Bjerrum has found some evidence for this species in $\text{NaCl}/\text{AlCl}_3$ melts (49b). No mixed cations of this average oxidation state (+0.25) have been characterized other than $\text{Te}_2\text{Se}_6^{2+}$ which is reported here. Reactions designed to prepare such mixed species invariably result in compounds of higher oxidation state cations such as $(\text{Te}_3\text{S}_3)(\text{AsF}_6)_2$ (20) in reaction IV.1, or lower oxidation state species such as $(\text{Te}_2\text{Se}_8)(\text{SbF}_6)_2$ (see section IV.3).



IV.2 Preparation of $(\text{Te}_6)(\text{Se}_8)(\text{AsF}_6)_6(\text{SO}_2)$.

Anhydrous SO_2 (30 mL) and AsF_5 (2.37 g, 13.9 mmol) were condensed at 77 K onto a mixture of powdered Te (0.4447 g, 3.485 mmol) and Se (0.2756 g, 3.490 mmol) in a double-bulb reaction vessel following the method outlined in chap-

ter II. The initial green solution turned a deep blood-red after about 0.5 h. This color persisted for 48 h, at which point the reaction vessel was heated to 340 K. After a few hours the solution became yellow-brown in color and there was a large quantity of black crystalline material at the bottom of the vessel. Heating was continued for one week at 340 K with occasional stirring, but no further change was observed. On cooling to room temperature much of the black residue dissolved, producing a deep green solution. In order to recrystallize the black material the reaction mixture was cooled further and then filtered. After 24 h at room temperature a large number of black crystals had formed. The solution was then poured off and the crystals isolated under an atmosphere of SO_2 . Under a microscope the rhombic-shaped crystals were observed to be dark green in color. Since the crystals tend to readily lose SO_2 with a consequent loss of crystallinity, several crystals were studied before a suitable stable crystal was found from which an X-ray diffraction data set could be collected. The subsequent structure solution identified the compound as $(\text{Te}_6)(\text{Se}_8)(\text{AsF}_6)_6(\text{SO}_2)$. The structure contains the previously known trigonal prismatic Te_6^{4+} and cyclic Se_8^{2+} cations, but this is the first time that two different Group VI homopolyatomic cations have been found together in the same crystal lattice.

In a similar reaction using excess AsF_5 , but at room

temperature, precession photographs revealed that $(\text{Te}_2\text{Se}_4)(\text{AsF}_6)_2$ was the only crystalline product, although the ^{77}Se NMR spectrum of the mother liquor showed the presence of $\text{cis-Te}_2\text{Se}_2^{2+}$ (328 ppm) and TeSe_3^{2+} (547 and 453 ppm) as well as $\text{Te}_2\text{Se}_4^{2+}$ (-477 and -1181 ppm). The ^{77}Se chemical shifts of these species have been well-established in solution in oleum (50). Apparently mixed cations such as these are thermodynamically unstable with respect to the homopolyatomic cations and the long reaction time and high temperatures used in the present reaction led to the thermodynamically stable products.

When $(\text{Te}_6)(\text{Se}_8)(\text{AsF}_6)_6(\text{SO}_2)$ was redissolved in SO_2 , the Se_8^{2+} cation was initially observed in the ^{77}Se NMR spectrum (see section IV.4). After several weeks at room temperature, however, the ^{125}Te NMR spectrum showed the presence of $\text{Te}_2\text{Se}_4^{2+}$ (630.3 ppm) as well as Te_6^{4+} (-562.9 ppm). These chemical shifts correspond to those previously observed for these species in oleum (50). It would appear that although the Te_6^{4+} and Se_8^{2+} cations are compatible in the solid state, slow oxidation-reduction occurs in solution.

IV.3 Preparation of $(\text{Te}_2\text{Se}_6)(\text{Te}_2\text{Se}_8)(\text{AsF}_6)_4(\text{SO}_2)_2$.

Anhydrous SO_2 (30 mL) and AsF_5 (2.33 g, 13.7 mmol) were condensed at 77 K onto a mixture of powdered Te (1.82 g, 14.3 mmol), Se (1.13 g, 14.3 mmol) and S (0.458 g, 14.3

mmol). The initial green solution turned red within 5 min of stirring. After 1 h a large quantity of chocolate-brown powder had precipitated from the red-brown solution. No further change was observed after 8 h and the solution was filtered and allowed to stand. When no crystals were obtained after 48 h the solvent was slowly distilled off and 2 weeks later a large quantity of dark brown crystals had formed. These were isolated under an atmosphere of SO_2 and a subsequent X-ray crystal structure determination identified the compound as $(\text{Te}_2\text{Se}_6)(\text{Te}_2\text{Se}_8)(\text{AsF}_6)_4(\text{SO}_2)_2$. This compound is similar to $(\text{Te}_6)(\text{Se}_8)(\text{AsF}_6)_6(\text{SO}_2)$ in that two different polyatomic cations are found in the same structure. The new $\text{Te}_2\text{Se}_6^{2+}$ cation has a novel cube-like geometry (Fig. IV.1).

Attempts to prepare crystalline salts of the $\text{Te}_2\text{Se}_6^{2+}$ cation in the absence of sulfur have all failed (see reactions IV.2 to IV.5). The $\text{Te}_2\text{Se}_6^{2+}$ cation was observed (-717.0 ppm), however, along with $\text{Te}_2\text{Se}_4^{2+}$ (-478.2, -1185 ppm) (50) in the ^{77}Se NMR spectrum of the product mixture of reaction IV.2 redissolved in SO_2 . The peak intensities indicated that there was approximately twice as much $\text{Te}_2\text{Se}_4^{2+}$ as $\text{Te}_2\text{Se}_6^{2+}$ in solution. All reactions were carried out in SO_2 solution and the products of reactions IV.3 to IV.5 were identified from their precession photographs.

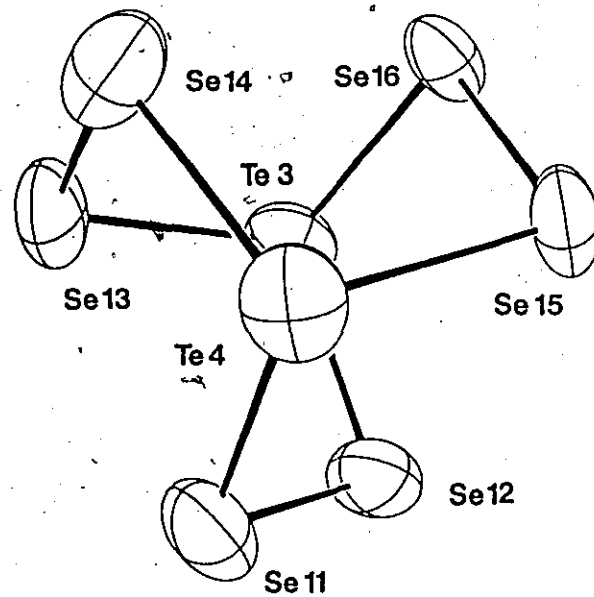
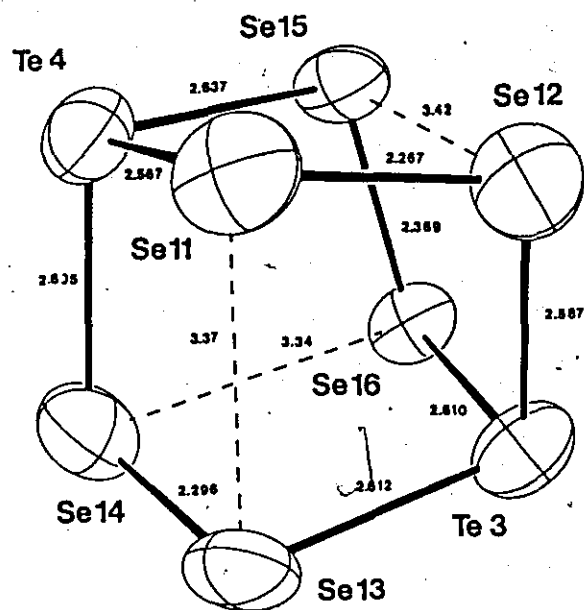
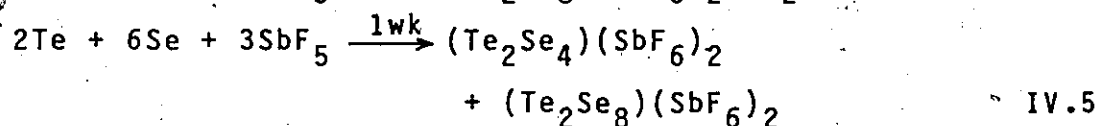
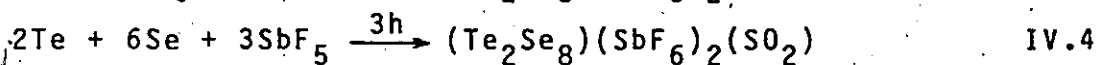
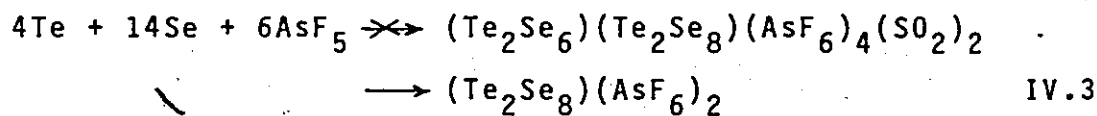


FIGURE IV.1 ORTEP views of the $\text{Te}_2\text{Se}_6^{2+}$ cation in $\text{Te}_2\text{Se}_6(\text{Te}_2\text{Se}_8)(\text{AsF}_6)_4(\text{SO}_2)_2$.



The $\text{Te}_2\text{Se}_6^{2+}$ cation can be prepared in the absence of sulfur (reaction IV.2), but no crystalline samples with this cation were prepared without this "magic" element. Even in reaction IV.3 where the stoichiometry is such as to allow for equal amounts of both $\text{Te}_2\text{Se}_6^{2+}$ and $\text{Te}_2\text{Se}_8^{2+}$, as found in the compound prepared from the Te-Se-S mixture, no crystalline product was obtained with the $\text{Te}_2\text{Se}_6^{2+}$ cation. This phenomenon has also been observed in the preparation of crystalline $\text{Te}_4(\text{SbF}_6)_2$ from a reaction involving sulfur (section V.7). This compound had proven to be too insoluble in SO_2 for good crystalline samples to be prepared from tellurium alone, although crystals of $\text{Te}_4(\text{SbF}_6)_2$ were isolated from a Ge/Te mixture (23). The importance of sulfur in the isolation of these crystalline compounds is probably related to their solubilities. The standard procedure in the preparation of salts of the polyatomic cations involves filtering a saturated SO_2 solution from which crystals slowly form (see chapter II). Compounds of low solubility would precipitate from the solution prior to filtration. The

polyatomic sulfur cations are all extremely soluble in SO_2 and the solubilities of $\text{Te}_2\text{Se}_6^{2+}$ and other relatively insoluble cations are apparently enhanced in the presence of these sulfur cations. With a significant concentration of $\text{Te}_2\text{Se}_6^{2+}$ (or Te_4^{2+}) present in the filtrate, crystalline samples can be produced.

IV.4 Selenium-77 NMR of Se_8^{2+} .

The natural abundance ^{77}Se NMR spectrum of Se_8^{2+} dissolved in SO_2 or oleum consists of five lines, with two of the lines one-half the intensity of the remaining three (38). This is consistent with the solid-state structure of this cation where there are five distinct selenium environments and for three of these there are two chemically equivalent nuclei (Fig. IV.2). There is no mirror plane in either of the crystal structures of this cation, but the slight deviations from C_s symmetry probably result from packing considerations in these compounds (see section IV.6) and the cation would be expected to have a mirror plane in solution. The ^{77}Se chemical shifts had previously been established and they were assigned on the basis of couplings observed for a sample enriched to 94.4% in ^{77}Se . The splittings in these spectra were very complex, however, and there was some ambiguity in the chemical shift assignments and in the values of the coupling constants (38). The present study was designed to obtain the ^{77}Se - ^{77}Se coupling con-

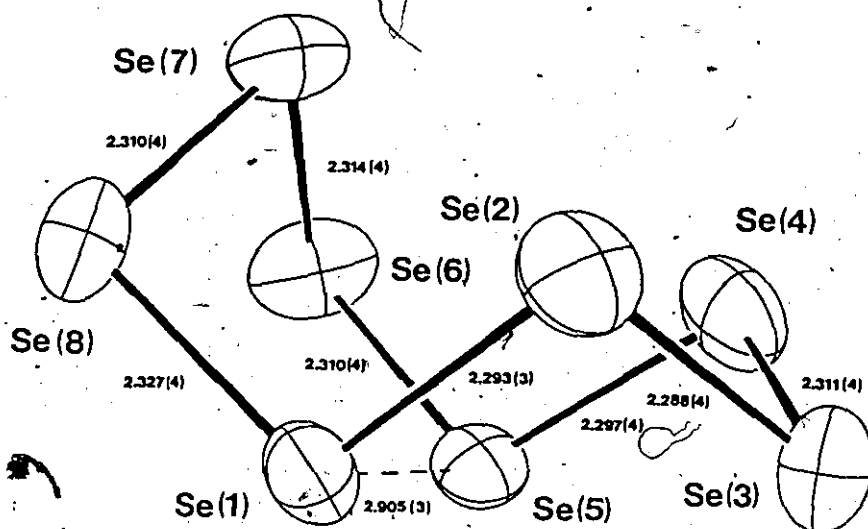
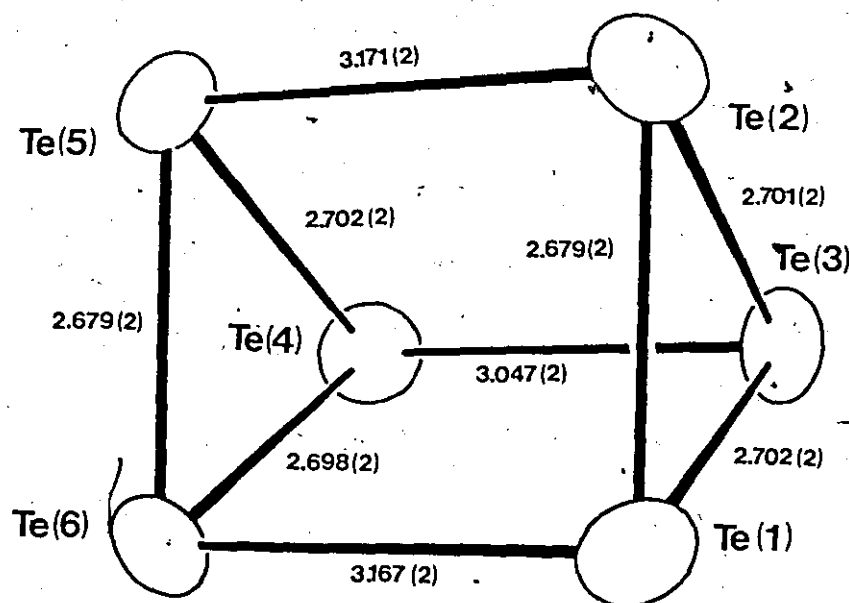


FIGURE IV.2 ORTEP views of the Te_6^{4+} and Se_8^{2+} cations in $(\text{Te}_6)(\text{Se}_8)(\text{AsF}_6)_6(\text{SO}_2)$.

starts from a natural abundance sample since the simplified spectrum could be easily interpreted.

The $\text{Se}_8(\text{AsF}_6)_2$ sample used in this study was prepared using methods as described in chapter II. A 5% excess of AsF_5 ensured that no $\text{Se}_{10}(\text{AsF}_6)_2$ would result. The Se_{10}^{2+} cation is known to disproportionate to Se_8^{2+} and an unknown species in SO_2 solution (38). This equilibrium would probably broaden the Se_8^{2+} resonances in the ^{77}Se NMR spectrum, with resulting loss of coupling information. The solubility of $\text{Se}_8(\text{AsF}_6)_2$ in SO_2 increases at lower temperatures so the solution was prepared (by Dr. R.C. Burns) and the spectrum run at 200 K. Cooling additionally served to separate most of the $\text{Se}_4(\text{AsF}_6)_2$ impurity that resulted from the excess AsF_5 used in the preparation, since $\text{Se}_4(\text{AsF}_6)_2$ has a very low solubility at 200 K and can be easily filtered off.

Resonance (A) in the ^{77}Se spectrum (Fig. IV.3) exhibits the largest couplings and the highest frequency chemical shift (Table IV.1), both of which are consistent with a large concentration of positive charge on the atoms producing this resonance. The short cross-ring distance between Se(1) and Se(5) (Fig. IV.2) indicates that these two atoms can be described as being essentially three-coordinate and much of the charge of the cation is then anticipated to reside on these atoms. A recent molecular orbital investigation of the S_8^{2+} cation (51) has revealed that S(1) and

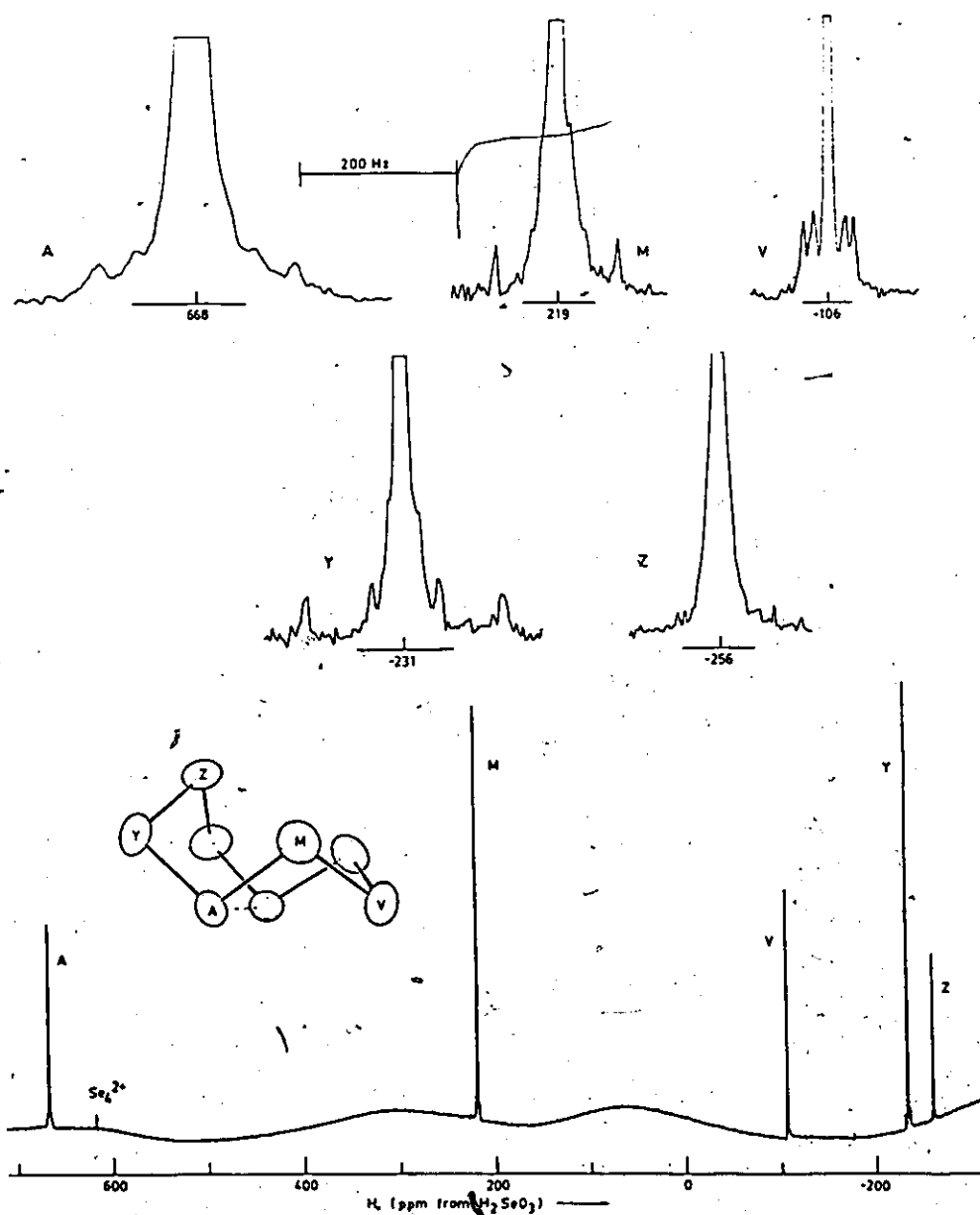


FIGURE IV.3 ^{77}Se NMR spectrum of the Se_8^{2+} cation (saturated SO_2 solution at 200 K; 47.77 MHz; 125,000 scans; 3.0 Hz/pt). ^{77}Se - ^{77}Se coupling is observed as satellite doublets about all resonances with the exception of resonance (Z).

TABLE IV.1 ^{77}Se NMR Parameters for Se_8^{2+} in SO_2 at 200 K.

Resonance	δ (ppm)	I^a	Coupling ^b	$J(\pm 6\text{Hz})$
A	668.0	1.9	(1)-(8)	246
M	219.3	2.1	(1)-(2)	152
V	-106.1	0.7	(1)-(6)	84
Y	-231.2	2.0	(1)-(3)	41
Z	-256.3	1.2	(1)-(4)	36
			(2)-(3)	65
			(7)-(8)	37

(a) Integration scaled to a total of 8.

(b) Numbering corresponds to Fig. IV.2.

TABLE IV.2 Charge Distribution in Se_8^{2+} .

Position ^a	Charge ^b
1, 5	+0.662
6, 8	+0.179
2, 4	+0.127
3	+0.037
7	+0.028

(a) Numbering corresponds to Se_8^{2+} , Fig. IV.2

(b) Data taken from reference (51).

S(5) carry 66% of the positive charge although there is considerable charge delocalization (see Table IV.2). The isostructural Se_8^{2+} cation presumably has a similar charge distribution and resonance (A) probably results from Se(1) and Se(5). The pair of atoms Se(8) and Se(6) are adjacent to Se(1) and Se(5) and they have the next largest concentration of positive charge (Table IV.2). Resonance (Y) can be assigned to these atoms then on the basis of the large couplings observed to Se(1) and Se(5), both directly-bonded (246 Hz) and across the ring (84 Hz), (see Table IV.1). Resonance (M) then results from Se(2) and Se(4), which are also adjacent to Se(1) and Se(5) but have less positive charge. The observed couplings to Se(1) and Se(5) are smaller (152 and 36 Hz for directly-bonded and cross-ring interactions respectively). Resonances for the two unique Se atoms, Se(3) and Se(7), have one half the integrated area of the others (Table IV.1) and they can be distinguished from each other on the basis of couplings to adjacent Se atoms. The largest coupling observed for resonance (V) is 64 Hz. This must be a directly-bonded coupling and resonance (V) can be assigned to Se(3) since the resonance for atoms Se(2) and Se(4), which are directly bonded to Se(3), also displays a coupling of this magnitude, 66 Hz. These values are equal within the data point resolution of 3 Hz/pt. The other coupling observed for Se(3), 41 Hz, must be a long-range coupling to Se(1) and Se(5). Resonance (Z)

can be assigned by default to the second unique selenium atom, Se(7). No couplings were large enough to be resolved for this resonance, but resonance (Y) for the two selenium atoms adjacent to Se(7) has a just-resolved coupling of 37 Hz which is probably the directly-bonded coupling to Se(7). The relatively small couplings to Se(3) and Se(7) are consistent with the small concentration of positive charge located at these sites (Table IV.2). These chemical shift assignments correspond to those of the enriched sample (38).

IV.5 Selenium-77 and Tellurium-125 NMR of $\text{Te}_2\text{Se}_6^{2+}$.

Numerous resonances were observed in the ^{77}Se NMR spectrum of a 100% H_2SO_4 solution of $(\text{Te}_2\text{Se}_6)(\text{Te}_2\text{Se}_8)(\text{AsF}_6)_4(\text{SO}_2)_2$, the intensities of which varied with time. A single resonance at -732 ppm grew and then diminished in intensity in a manner not mimicked by any of the other resonances, indicating that the species producing this resonance had only one selenium environment. A resonance at -732 ppm was also observed in the spectra of solutions of $(\text{Te}_2\text{Se}_8)(\text{AsF}_6)_2$ in 100% H_2SO_4 (see Table IV.3 and Fig. IV.4). It could not be attributed to $\text{Te}_2\text{Se}_8^{2+}$ (see section III.7) and was therefore assigned to $\text{Te}_2\text{Se}_6^{2+}$ produced by decomposition of $\text{Te}_2\text{Se}_8^{2+}$ since $\text{Te}_2\text{Se}_6^{2+}$ has only one selenium environment in the solid-state structure (Fig. IV.1).

Since $(\text{Te}_2\text{Se}_6)(\text{Te}_2\text{Se}_8)(\text{AsF}_6)_4(\text{SO}_2)_2$ is difficult to prepare while salts of the $\text{Te}_2\text{Se}_8^{2+}$ cation can be routinely

TABLE IV.3 ^{77}Se and ^{125}Te NMR Parameters for $\text{Te}_2\text{Se}_6^{2+}$.

Sample	Solvent	δ (ppm)		J (Hz)	
		^{77}Se	^{125}Te	^{77}Se - ^{125}Te	^{125}Te - ^{125}Te
a	AsF_3	-717.7	901.9	$355^g, 31^g$	120
b		-719.2	901.7	$355^g, 32^g$	
				354^h	
c	100% H_2SO_4	-732.9		317^h	
d		-733.1	963.9	322^g	
e		-732.4			
f	SO_2	-717.0	942.1		

- (a) 26.8 mg, 0.210 mmol Te (7.3% ^{125}Te) and 87.2 mg, 1.10 mmol Se were reacted with 0.32 mmol AsF_5 in AsF_3 for 16 h and the solution filtered into an NMR tube and sealed.
- (b) $(\text{Te}_2\text{Se}_8)(\text{AsF}_6)_2(\text{SO}_2)$ dissolved in AsF_3 (0.03 molal).
- (c) 0.2857 g, 2.24 mmol Te and 0.3567 g, 4.52 mmol Se were dissolved in 1.5 g 100% H_2SO_4 .
- (d) $(\text{Te}_2\text{Se}_8)(\text{SbF}_6)_2(\text{SO}_2)$ dissolved in 100% H_2SO_4 .
- (e) $(\text{Te}_2\text{Se}_6)(\text{Te}_2\text{Se}_8)(\text{AsF}_6)_4(\text{SO}_2)_2$ dissolved in 100% H_2SO_4 .
- (f) Brown powder produced from reaction IV.2 redissolved in SO_2 .
- (g) From ^{125}Te spectrum.
- (h) From ^{77}Se spectrum.

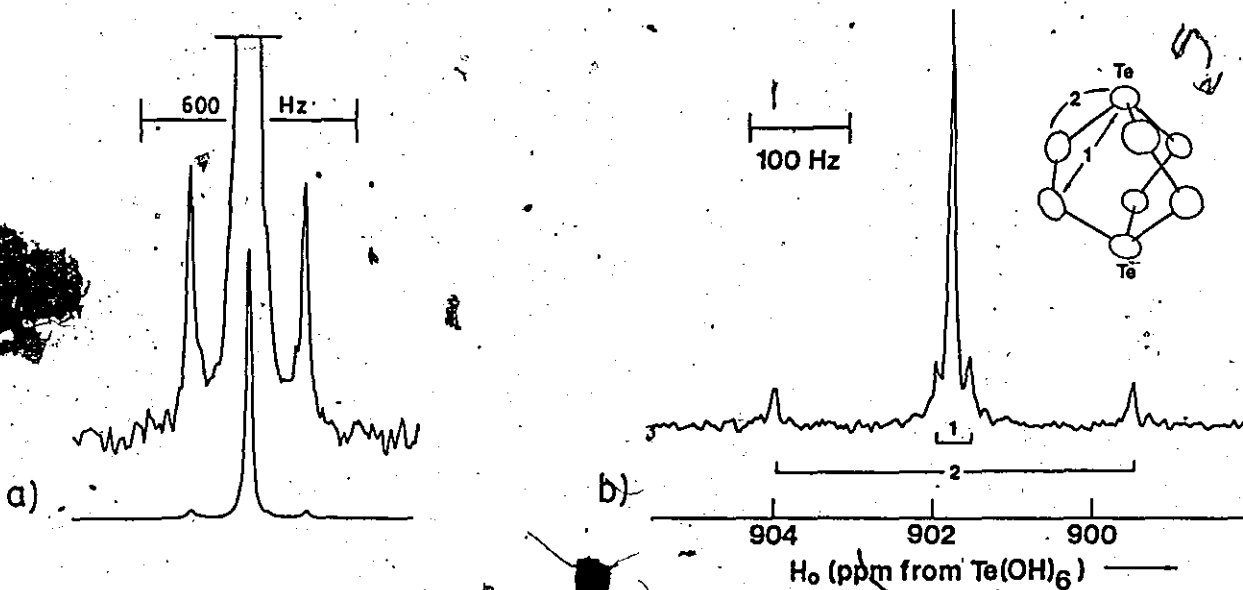


FIGURE IV.4 Natural abundance ^{77}Se and ^{125}Te NMR spectra of the $\text{Te}_2\text{Se}_6^{2+}$ cation. (a) ^{77}Se spectrum, sample c, Table IV.3 (76.41 MHz; 80,000 scans; 6.1 Hz/pt). Satellite doublet results from $J(^{77}\text{Se}-^{125}\text{Te})$. (b) ^{125}Te spectrum, sample b, Table IV.3 (78.97 MHz; 148,000 scans; 3.0 Hz/pt). Both $J(^{77}\text{Se}-^{125}\text{Te})$ and $2J(^{77}\text{Se}-^{125}\text{Te})$ are observed.

prepared, subsequent investigations of the $\text{Te}_2\text{Se}_6^{2+}$ cation were made on solutions of $\text{Te}_2\text{Se}_8^{2+}$ salts. Moreover, since AsF_3 solutions of $(\text{Te}_2\text{Se}_8)(\text{AsF}_6)_2$ produce a similar decomposition peak to that observed for the 100% H_2SO_4 solution (Table IV.3), but with considerable reduction in linewidth and a corresponding increase in the signal-to-noise ratio, solutions in AsF_3 rather than H_2SO_4 were studied.

The resonance assigned to $\text{Te}_2\text{Se}_6^{2+}$ from the ^{125}Te NMR spectrum of natural abundance $(\text{Te}_2\text{Se}_8)(\text{AsF}_6)_2(\text{SO}_2)$ dissolved in AsF_3 displays two clearly resolved doublets about the central, uncoupled peak (Fig. IV.4). The total intensity of the outer satellite peaks ($J = 355 \pm 6$ Hz) is 22% relative to the central line, while the inner satellites ($J = 32 \pm 6$ Hz) appear to be of comparable magnitude but are not as well resolved. This intensity is consistent with coupling of tellurium to three equivalent, natural abundance selenium nuclei (Table IV.4). The coupling constants indicate that one set of three selenium atoms is directly bonded to tellurium, while the second set is more remote. This is consistent with the solid-state structure of $\text{Te}_2\text{Se}_6^{2+}$ (Fig. IV.4). In the ^{77}Se spectrum of this same sample a resonance was observed with a satellite doublet of 7% intensity relative to the central line, and a coupling of 354 ± 12 Hz (Table IV.3). The 32 Hz coupling was not resolved. The doublet intensity indicates coupling to one natural abund-

TABLE IV.4 Satellite Intensities for Coupling to Natural Abundance Selenium-77, Tellurium-123 and Tellurium-125.

Nucleus	# ^b	Uncoupled	Intensity Doublet	Triplet	% ^c
⁷⁷ Se	1	92.42	7.58	-	8.2
	2	85.41	14.01	0.57	16.3
	3	78.94	19.42	1.59	24.4
¹²³ Te	1	99.13	0.87	-	0.9
	2	98.27	1.72	0.01	1.8
	3	97.41	2.56	0.02	2.6
¹²⁵ Te	1	93.01	6.99	-	7.5
	2	86.51	13.00	0.45	15.0
	3	80.46	18.14	1.36	22.4

(a) ⁷⁷Se = 7.58%; ¹²³Te = 0.87%; ¹²⁵Te = 6.99% (67).
 (b) Number of equivalent atoms. (c) Total intensity of doublet relative to central line (uncoupled peak plus contribution from triplet).

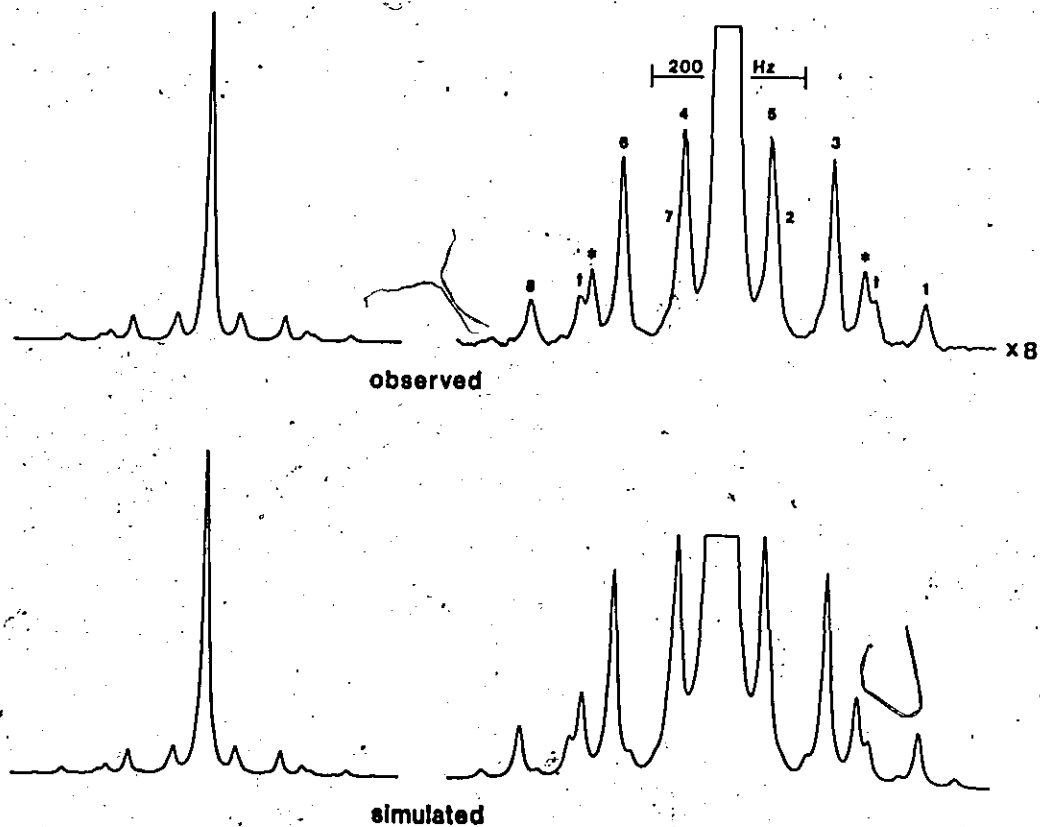


FIGURE IV.5 Observed and simulated ^{125}Te NMR spectrum of $\text{Te}_2\text{Se}_6^{2+}$, 77.3% enriched in ^{125}Te , sample a, Table IV.3 (116,000 scans; 2.4 Hz/pt; 78.97 MHz). (1-8) AA'X; (*) AX; (+) AA'XX'.

ance tellurium nucleus (Table IV.4) and is again consistent with the solid-state structure.

When the concentration of ^{125}Te in the sample was enriched to 77.3%, a large number of satellite peaks appeared in the ^{125}Te spectrum in addition to those observed in the natural abundance spectrum (Fig. IV.5). These peaks are too intense to result from ^{77}Se - ^{125}Te coupling and since the two tellurium atoms in the structure are chemically equivalent the additional lines in the spectrum must result from magnetic inequivalence. The most important satellite pattern for natural abundance selenium and 77.3% enrichment in ^{125}Te is an AA'X spectrum (ABX with $\delta_A = \delta_B$) arising from both tellurium atoms and one selenium atom (Table IV.5). This has eight lines in the AA' (^{125}Te) region and six lines in the X (^{77}Se) region (52). Six of the eight AA' lines can be clearly observed in the spectrum with the remaining two as shoulders on the two AA' lines closest to the central, uncoupled line (Fig. IV.5). Using previously established methods (52, 53) the two ^{77}Se - ^{125}Te couplings and the ^{125}Te - ^{125}Te coupling (Table IV.3) were extracted from the line separations in the AA'X multiplet (Table IV.6). The former two agree with those observed in the natural abundance ^{125}Te spectrum. Using the values of these coupling constants and the probabilities of the isotopic distribution for 7.50% ^{77}Se and 77.3% enrichment in ^{125}Te (Table IV.5) and assuming the solid-state structure of two tellurium atoms joined by

TABLE IV.5 Isotopic Distribution in $\text{Te}_2\text{Se}_6^{2+}$.

SPIN-1/2 NUCLEI ^a	COUPLING PATTERN	SPIN DISTRIBUTION				M^b	% ^c	NMR-ACTIVE%	
		Se		Te				77-Se	125-Te
		1/2	0	1/2	0				
None	-	-	6	-	2	1	3.23	-	-
1	X	1	5	-	2	6	1.57	4.20	-
1,2	X_2 (I)	2	4	-	2	3	0.06	0.17	-
1,3	X_2 (II)	2	4	-	2	6	0.13	0.35	-
1,4	X_2 (III)	2	4	-	2	6	0.13	0.35	-
7	A	-	6	1	1	2	21.98	-	23.17
7,8	A_2	-	6	2	-	1	37.43	-	39.46
1,8	AX(I)	1	5	1	1	6	5.35	14.32	5.64
1,7	AX(II)	1	5	1	1	6	5.35	14.32	5.64
1,7,8	AA'X	1	5	2	-	6	18.21	48.74	19.20
1,2,7	AXX'(I)	2	4	1	1	6	0.43	1.15	0.45
1,3,7	AXX'(II)	2	4	1	1	12	0.87	2.33	0.92
1,4,8	AX ₂	2	4	1	1	6	0.43	1.15	0.45
1,4,7	A'X ₂	2	4	1	1	6	0.43	1.15	0.45
1,3,7,8	AA'XX'(I)	2	4	2	-	6	1.48	3.96	1.56
1,2,7,8	AA'XX'(II)	2	4	2	-	3	0.74	1.98	0.78
1,4,7,8	AA'X ₂	2	4	2	-	6	1.48	3.96	1.56
TOTAL							99.3	98.13	99.28

(a) Numbering is as follows: 1=Se(11); 2=Se(12); 3=Se(13); 4=Se(14); 5=Se(15); 6=Se(16); 7=Te(3); 8=Te(4). (Fig. IV.1.)

(b) Multiplicity.

(c) Percentage of isotopic isomer for 7.50% ⁷⁷Se, 77.3% ¹²⁵Te.

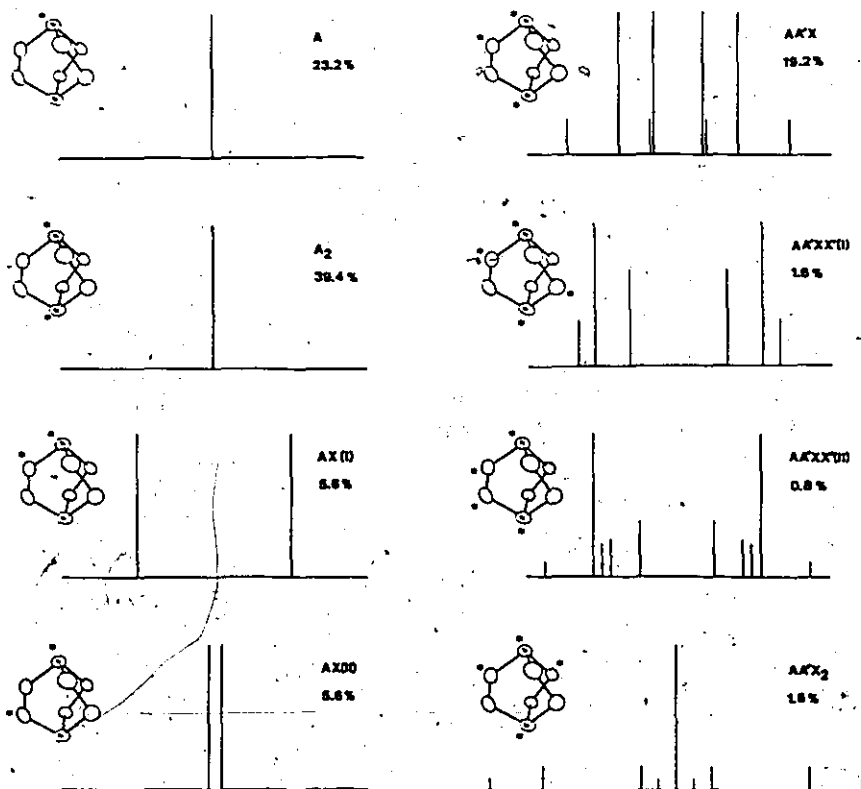


FIGURE IV.6 Components used to simulate the ^{125}Te NMR spectrum of $\text{Te}_2\text{Se}_6^{2+}$, 77.3% enriched in ^{125}Te .

TABLE IV.6 AA'X Assignments in $\text{Te}_2\text{Se}_6^{2+}$, AA' Region.

Line	Position/Hz ^a	
	Observed ^b	Simulated
1	-256	-257
2	-63 ^c	-64
3	-136	-137
4	57	56
5	-54	-56
6	138	137
7	66 ^c	64
8	258	257

(a) Relative to uncoupled line as zero. (b) Data point resolution is 2.4 Hz/pt. (c) Estimated from other line positions.

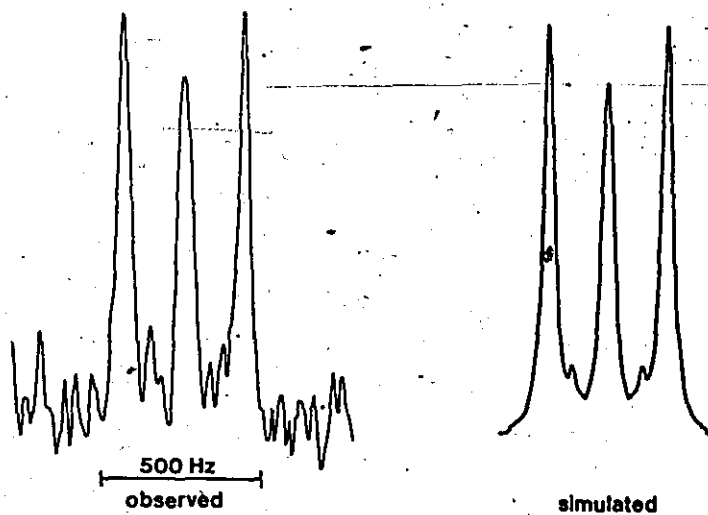


FIGURE IV.7 Observed and simulated ^{77}Se NMR spectrum of $\text{Te}_2\text{Se}_6^{2+}$, 77.3% enriched in ^{125}Te , natural abundance ^{77}Se (sample (a), Table IV.3). The observed spectrum was accumulated at 76.41 MHz in 48,000 scans, 6.1 Hz/pt. A line broadening of 12 Hz was applied to the exponential smoothing of the free-induction decay.

three, two-atom selenium chains, a series of spectra were simulated and summed (Fig. IV.5 and IV.6). The simulated AA'XX' multiplets required estimates of the ^{77}Se - ^{77}Se couplings. The three-bond ^{77}Se - ^{77}Se coupling in AA'XX'(I) was set to zero and the directly-bonded coupling in AA'XX'(II) set to 100 Hz. (The mean directly-bonded coupling in Se_8^{2+} is 108 Hz (section IV.4).) Since the two strongest peaks in these multiplets are insensitive to the magnitude of this coupling (compare AA'XX'(I) and AA'XX'(II) in Fig. IV.6) and the species producing these multiplets are of very low probability (Table IV.5), these estimates did not produce any significant error. The AA'X₂ splitting pattern is independent of the ^{77}Se - ^{77}Se coupling constant. The resulting simulation (including a linewidth of 12 Hz) fits the observed spectrum extremely well with all of the observed satellites accounted for (Fig. IV.5). The AA'X and AA'XX' systems have been reported, for example, in the ^1H spectrum of 2-furfurol (54) and the ^{19}F spectrum of 1,2-dichloro-3,4,5,6-tetrafluorobenzene (55) respectively, but to our knowledge this is the first report of such inequivalence involving heavy nuclei.

The ^{77}Se NMR spectrum of this same sample complements the above analysis (Fig. IV.7). The simulated spectrum incorporates the X portions of the coupling patterns described above as well as X, X₂, AXX' and AX₂ components.

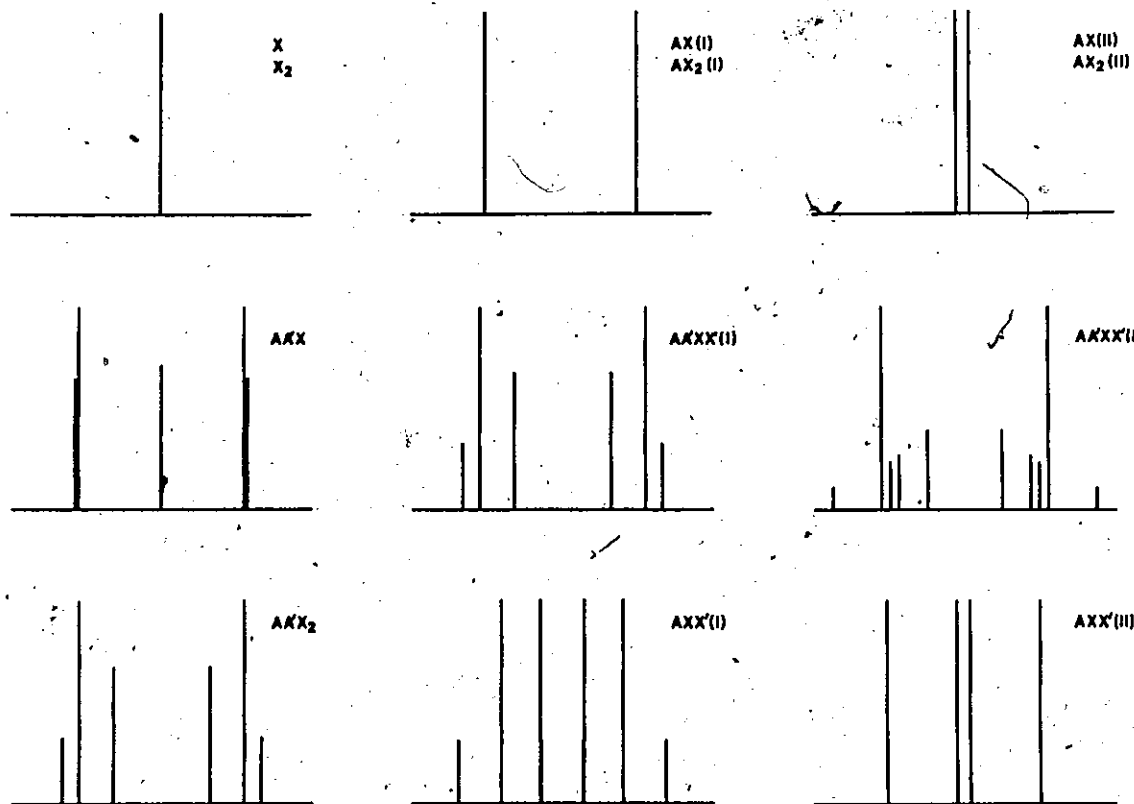


FIGURE IV.8 Components used to simulate the ^{77}Se NMR spectrum of $\text{Te}_2\text{Se}_6^{2+}$, 77.3% enriched in ^{125}Te , natural abundance ^{77}Se .

(Table IV.5). The individual components used in this simulation are given in Figure IV.8. The signal-to-noise ratio in the observed spectrum was not good enough to determine any ^{77}Se - ^{77}Se couplings and the estimates used in the ^{125}Te simulation were retained here. The simulated ^{77}Se spectrum matched the observed spectrum when a line width of 30 Hz was used in the simulation.

The results of this ^{77}Se and ^{125}Te NMR investigation of the $\text{Te}_2\text{Se}_6^{2+}$ cation are consistent with retention in solution of the solid-state arrangement of two tellurium atoms joined by three, two-atom selenium chains. An important feature of the solid-state structure, however, is the large Te-Se-Se-Te dihedral angle of 69° (section IV.7). Vicinal ^1H - ^1H couplings in HCCH fragments are dependent upon the H-C-C-H dihedral angle (56). The observed ^{125}Te - ^{125}Te coupling for $\text{Te}_2\text{Se}_6^{2+}$ could, in principle, be of significance in deducing the Te-Se-Se-Te dihedral angle in solution, but since no other couplings have been reported for similar geometries, no correlation between the coupling constant and the dihedral angle can be established at present.

IV.6 Anion-Cation Interactions in M_8^{2+} Structures.

The interionic contacts to $\text{Te}_2\text{Se}_6^{2+}$ in $(\text{Te}_2\text{Se}_6)(\text{Te}_2\text{Se}_8)(\text{AsF}_6)_4(\text{SO}_2)_2$ that are less than the sum of van der Waals radii are given in Figure IV.9. The direc-

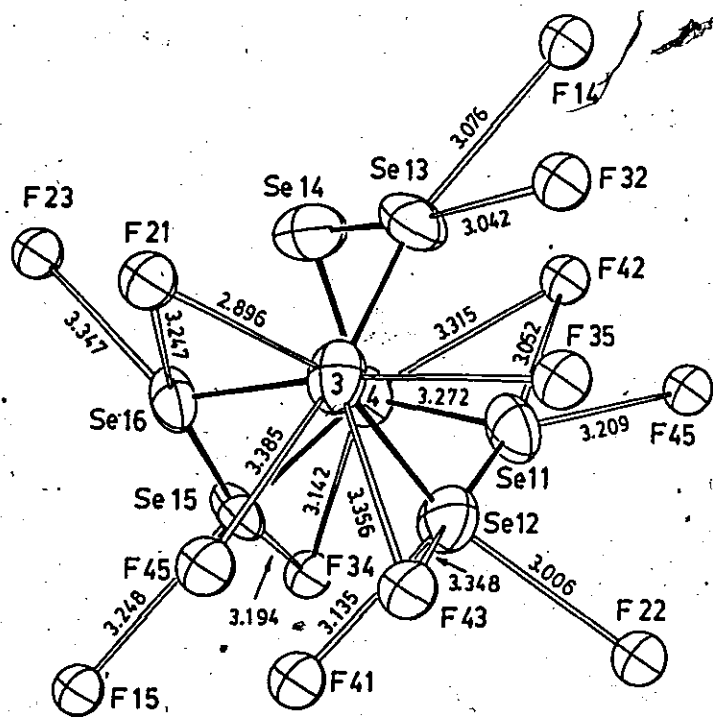


FIGURE IV.9 Anion-cation interactions at $\text{Te}_2\text{Se}_6^{2+}$ in $\text{Te}_2\text{Se}_6(\text{Te}_2\text{Se}_8)(\text{AsF}_6)_4(\text{SO}_2)_2$.

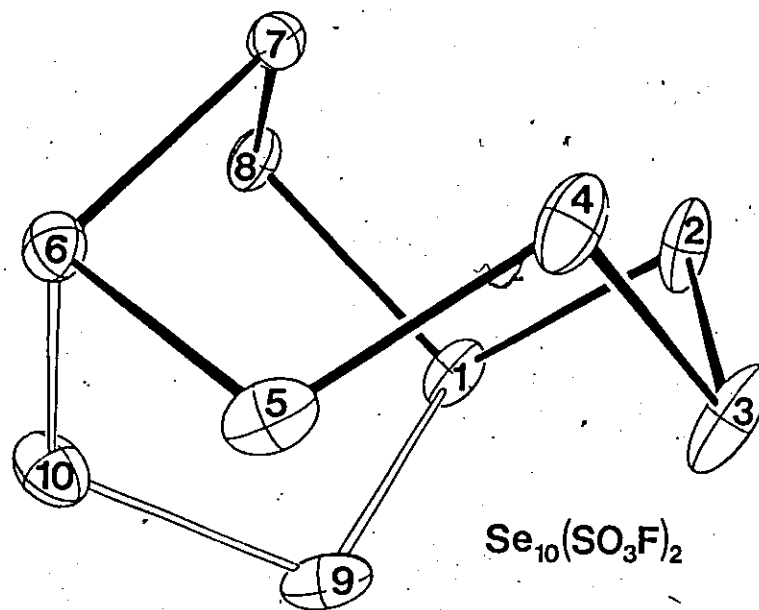


FIGURE IV.10 Derivation of the Se_8^{2+} structure (filled-in bonds) within the Se_{10}^{2+} structure (cf. Fig. IV.2). Thermal ellipsoids to 30% prob.

tions of these interactions are similar to those discussed above for the M_{10}^{2+} salts (section III.9). The geometry at Te(4) is AX_3Y_2E , with one of the Y components of the mono-capped octahedron missing. There are four secondary bonds to Te(3): F(21), F(35) and F(45) are approximately trans- to Te--Se bonds, or alternatively cap faces of the AX_3E tetrahedron, and F(43) bridges an edge of the tetrahedron. Similar $AX_3Y_3Y'E$ arrangements are observed for the M_{10}^{2+} salts (section III.9) and for $(TeCl_3)(SbF_6)$ (section VII.7). Contacts to the selenium atoms in $Te_2Se_6^{2+}$ are again mostly collinear with the primary bonds. Interionic contacts to $Te_2Se_8^{2+}$ in this compound were discussed in the previous chapter. The Se...F contacts to the Se_8^{2+} cation of $Te_6(Se_8)(AsF_6)_6(SO_2)$ are fewer in number and probably weaker than the analogous Se...Cl contacts in $Se_8(ATCl_4)_2$ (12), consistent with the greater polarizability of chlorine. The shortest of the Se...F and Se...Cl contacts are to the two atoms linked by the transannular interaction and which carry most of the positive charge.

IV.7 Comparison of M_8^{2+} Structures.

The mixed cations $Te_2Se_8^{2+}$ and $Te_xSe_{10-x}^{2+}$ are isostructural with the homopolyatomic cation Se_{10}^{2+} , which has the same average oxidation state (chapter III). The structure of $Te_2Se_6^{2+}$, however is very different from that of Se_8^{2+} , which again has the same average oxidation state as

the mixed $Te_2Se_6^{2+}$ cation. The Se_8^{2+} and S_8^{2+} cations are eight-membered rings with an exo-endo conformation and a long cross-ring bond (Figure IV.2). This structure has been described as being half-way between the crown-shaped ring of S_8 and Se_8 and the cuneane-like molecule S_4N_4 , which is isoelectronic with the unknown S_8^{4+} cation (9). The $Te_2Se_6^{2+}$ cation is a distorted cube with three of the edges (those not contained in the valence bond description) considerably longer than the other nine (Fig. IV.1). This structure is very similar to that of $Te_2Se_8^{2+}$ except that the unique four-atom selenium bridge of $Te_2Se_8^{2+}$ has been reduced to two selenium atoms, resulting in three identical two-atom bridges.

The $Te_2Se_6^{2+}$ and Se_8^{2+} structures can be related to each other by considering the structure of their parent species $Te_2Se_8^{2+}$ and Se_{10}^{2+} . Figure IV.10 demonstrates how the exo-endo eight-membered ring of Se_8^{2+} can be found within the Se_{10}^{2+} structure. Removal of atoms Se(9) and Se(10) along with forcing Se(1) and Se(5) closer together to form the long transannular bond results in Se_8^{2+} (compare Fig. IV.2 and IV.10). The Se_8^{2+} shape can similarly be found in $Te_2Se_8^{2+}$, as can the distorted cube of $Te_2Se_6^{2+}$ (Fig. IV.11). Formation of $Te_2Se_6^{2+}$ from $Te_2Se_8^{2+}$ in a similar fashion to Se_8^{2+} from Se_{10}^{2+} would, however, result in atoms Te(2) and Se(6) forming the transannular bond with Se(1) and Se(2) being eliminated and Te(1) becoming only

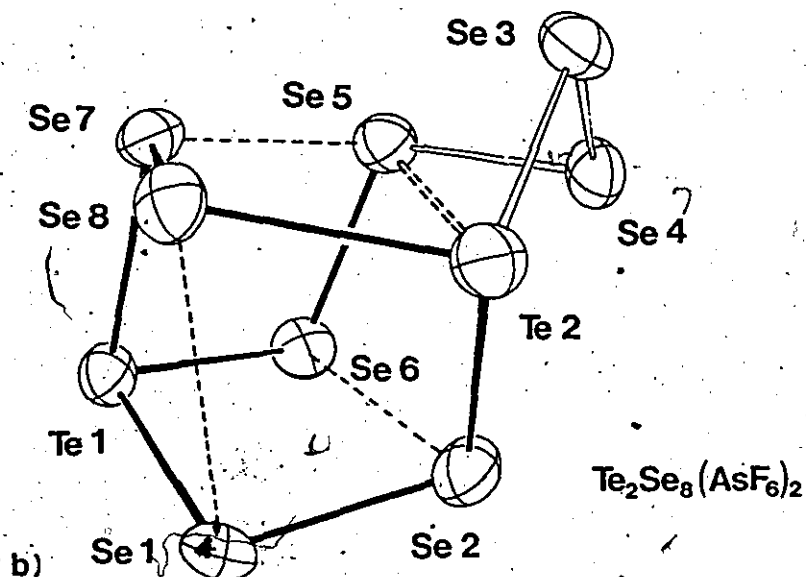
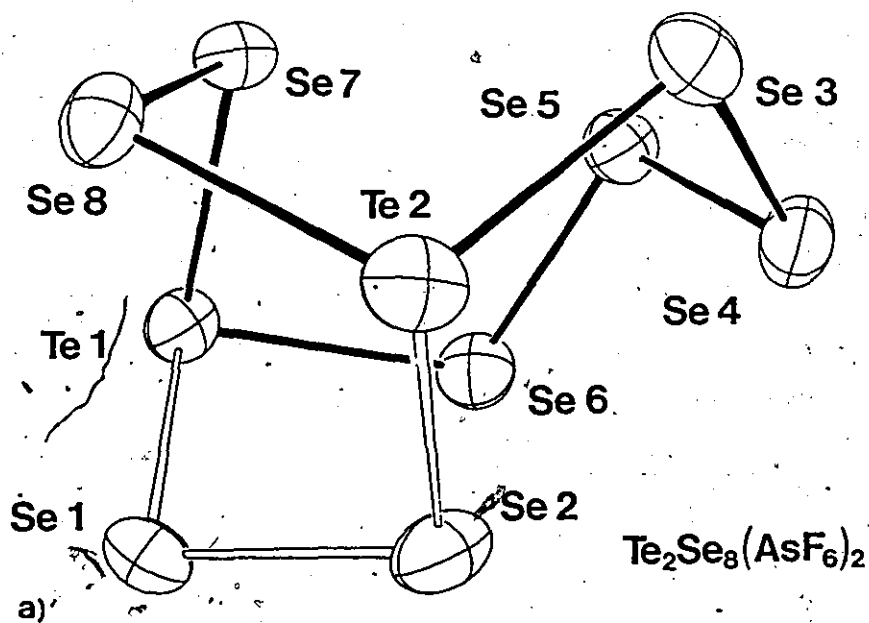


FIGURE IV.11 Derivation of a) the Se_8^{2+} -like structure and b) the $\text{Te}_2\text{Se}_6^{2+}$ structure (filled-in bonds) within the $\text{Te}_2\text{Se}_8^{2+}$ structure (cf. Fig. IV.1 and Fig. IV.2). Dotted lines indicate edges of the $\text{Te}_2\text{Se}_6^{2+}$ cube; double-dotted line indicates Te—Se bond to be formed.

two-coordinate. Since tellurium is more electropositive than selenium (57) a more favorable structure would have both tellurium atoms in three-coordinate positions, where the bulk of the positive charge is presumably located. The $\text{Te}_2\text{Se}_8^{2+}$ and $\text{Te}_2\text{Se}_4^{2+}$ cations exhibit this tendency with all of the three-coordinate positions in these cations occupied by tellurium. Formation of $\text{Te}_2\text{Se}_6^{2+}$ as in Figure IV.11b allows both tellurium atoms to remain three-coordinate and the resulting cube-like structure is apparently more favorable than the Se_8^{2+} -like structure.

Homoatomic cations and anions tend to adopt structures that allow for charge delocalization. The trigonal-prismatic Te_6^{4+} and square-planar S_4^{2+} , Se_4^{2+} , and Te_4^{2+} cations (26, 22, 10, 13) exhibit complete charge delocalization with all atoms equivalent. The P_6^{4-} anion is a regular hexagon (58) and the same structure has been proposed for the isovalent Te_6^{2+} cation (4, 51, 59). This charge-delocalized structure would presumably be more stable than a structure with localized bonding as observed in the related $\text{Te}_2\text{Se}_4^{2+}$ cation (see section V.1). There is considerable delocalization of charge in the S_8^{2+} and Se_8^{2+} structures (see section IV.4) and this is the most stable structure for these homoatomic cations. The large electronegativity difference between tellurium and selenium, however, is apparently of greater importance in determining the structures of

the mixed Te-Se cations, and $\text{Te}_2\text{Se}_6^{2+}$ is no exception. The $\text{Te}_2\text{Se}_4^{2+}$, $\text{Te}_2\text{Se}_6^{2+}$ and $\text{Te}_2\text{Se}_8^{2+}$ structures can be readily interpreted by electron-precise, localized bond descriptions. Since the electronegativity difference between selenium and sulfur is negligible (57) the hypothetical mixed $\text{S}_x\text{Se}_{8-x}^{2+}$ cations would be expected to adopt the Se_8^{2+} structure, while $\text{Te}_2\text{S}_6^{2+}$ should be isostructural with $\text{Te}_2\text{Se}_6^{2+}$.

In keeping with the above discussion, one would also expect the Se_{10}^{2+} cation to adopt a charge-delocalized structure, yet Se_{10}^{2+} has the same solid-state structure as $\text{Te}_2\text{Se}_8^{2+}$. Spectroscopic evidence suggests, however, that this structure may not be retained in solution. There is considerable difference between the solution and solid-state electronic spectra of the Se_{10}^{2+} cation and ^{77}Se NMR studies have provided evidence for intramolecular exchange in both SO_2 and 100% H_2SO_4 solution (16, 38). In contrast, the ^{77}Se NMR spectrum of $\text{Te}_2\text{Se}_8^{2+}$ in 100% H_2SO_4 shows no signs of exchange and is consistent with the solid-state structure (see sections III.7. and III.8).

There are three intramolecular Se...Se contact distances in $\text{Te}_2\text{Se}_6^{2+}$ (Fig. IV.1) that are considerably shorter than the van der Waals limit of 3.80 Å (39). Similar contacts are observed in $\text{Te}_2\text{Se}_8^{2+}$ and Se_{10}^{2+} (chapter III) and these have been described as weak bonds (16). These short contacts are in the positions of the three bonds that are

broken by the addition of electron pairs in deriving the structure of Se_{10}^{2+} and $\text{Te}_2\text{Se}_8^{2+}$ from the cuneane structure (9). Similarly, the short contacts in $\text{Te}_2\text{Se}_6^{2+}$ can result from breaking three edges of a cube by the addition of three electron pairs. Many of the main-group cages can be derived from a few basic cluster geometries in this fashion (9). Although these contacts in $\text{Te}_2\text{Se}_6^{2+}$ appear to be in stereochemically important positions, they may not indicate significant bonding interactions. This cube-like geometry and the resulting Se...Se contacts may be forced on the cation as a result of lone pair repulsions between adjacent selenium atoms in the bridges. The idealized bicapped trigonal prism (D_{3h}) geometry for $\text{Te}_2\text{Se}_6^{2+}$ would result in all of the lone pairs on selenium being eclipsed (Fig. IV.12). By increasing the Te-Se-Se-Te dihedral angle the lone pair repulsions can be reduced. A similar situation exists for cyclohexane where the twist-boat conformation, with all C--H bonds staggered, is 1.6 kcal lower in energy than the boat, where the C--H bonds are eclipsed along two of the C--C bonds (60). The $\text{Te}_2\text{Se}_6^{2+}$ cation can be viewed as consisting of three fused twist-boats. If the AX_2E_2 geometry about selenium was perfectly tetrahedral then the projected lone pair - lone pair angle in Figure IV.12b would be 120° and a dihedral angle of 60° would result in the favored staggered geometry of the lone pairs. Since lone pairs generally

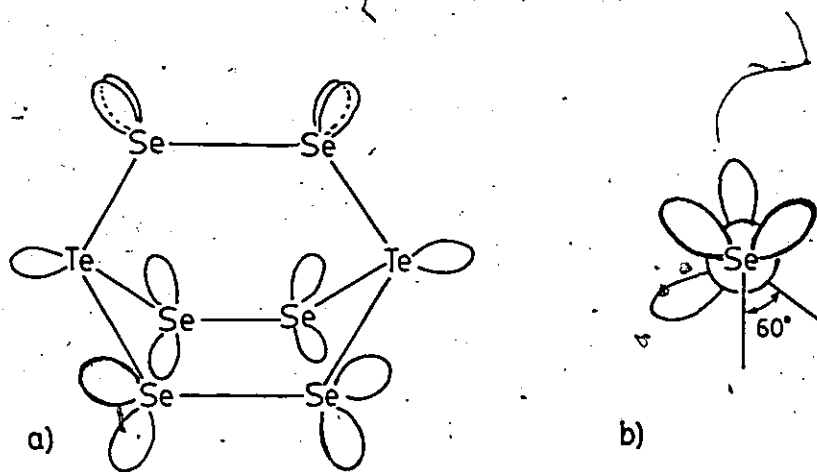


FIGURE IV.12 Orientation of lone pairs of electrons in $\text{Te}_2\text{Se}_6^{2+}$. a) Idealized D_{3h} geometry, all lone pairs eclipsed. b) View along Se-Te bond with Te-Se-Te dihedral angle of 60° , lone pairs are staggered.

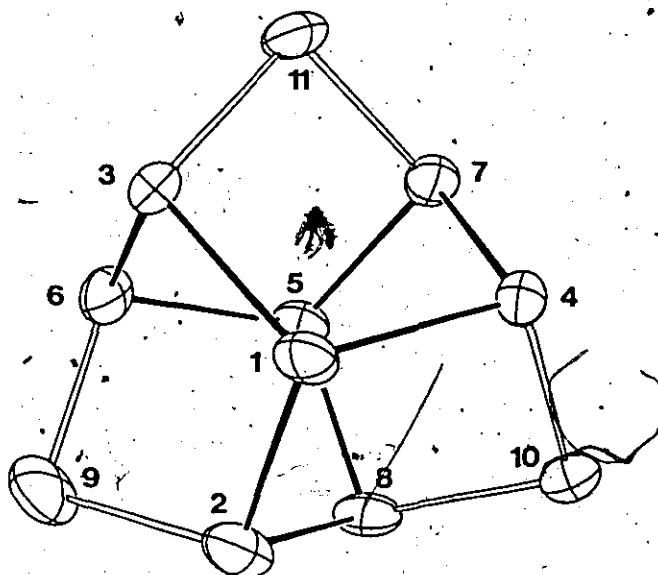


FIGURE IV.13 ORTEP view of the As_{11}^{3-} anion, redrawn from coordinates in ref. (63). Filled-in bonds indicate the $\text{Te}_2\text{Se}_6^{2+}$ -like core (cf. Fig. IV.1).

exert a greater repulsive effect than bond pairs, however (61), the projected lone pair - lone pair angle would be expected to be greater than 120° and the most favorable dihedral angle then somewhat greater than 60° . The observed dihedral angles in $(\text{Te}_2\text{Se}_6)(\text{Te}_2\text{Se}_8)(\text{AsF}_6)_4(\text{SO}_2)_2$ are 68.9 , 69.2 and 69.3° (mean 69.1°) which are very close to that expected for the most favorable lone pair geometry. The cubic structure of the cation therefore may result from lone pair repulsions or weak cross-ring bonds, or both.

The weak cross-ring bonding argument is supported by the structures of the P_{11}^{3-} and As_{11}^{3-} anions (62, 63). Like $\text{Te}_2\text{Se}_6^{2+}$, these species can be viewed as being derived from a cube (9) and P_{11}^{3-} has been suggested as a possible precursor to the as yet unprepared P_8 cubane (64). As described above, the $\text{Te}_2\text{Se}_6^{2+}$ structure results from the addition of electron pairs to three bonds of the cube related by a three-fold axis. In P_{11}^{3-} and As_{11}^{3-} these same bonds are broken, but by the addition of bridging atoms rather than by electron pairs (9). The resulting structures are remarkably similar (compare Figures IV.1 and IV.13). Removal of the three divalent arsenic atoms in As_{11}^{3-} leaves the $\text{Te}_2\text{Se}_6^{2+}$ structure. In an analogous fashion, removal of a sulfur or selenium atom from the bird-cage structure of P_4S_3 (65) or As_3Se_4^+ (66) results in the tent-shaped $\text{Te}_2\text{Se}_4^{2+}$ structure (see chapter V). Addition of the three bridging arsenic atoms to the eight-atom core of the As_{11}^{3-}

anion causes a somewhat greater distortion of the cubic geometry of this core than does the addition of three pairs of electrons in $\text{Te}_2\text{Se}_6^{2+}$. The mean Te-Se-Se-Te dihedral angle of 69.1° in $\text{Te}_2\text{Se}_6^{2+}$ is closer to the ideal cube value of 90° than is the related mean angle of 58.1° in As_{11}^{3-} .

IV.8 The Te_6^{4+} Cation in $(\text{Te}_6)(\text{Se}_8)(\text{AsF}_6)_6(\text{SO}_2)$.

The dimensions of the known Te_6^{4+} cations are compared in Table IV.7. All three examples have slightly distorted trigonal prismatic structures. In the present case, the Te_6^{4+} cation has no crystallographic symmetry and the end triangular faces are eclipsed with a small but significant angle of 3.00° between their planes (Fig. IV.2). This small angle between the end faces results in angles ranging from 88.50 to $91.48(5)^\circ$ in the "rectangular" faces. Although the cation in $(\text{Te}_6)(\text{AsF}_6)_4(\text{SO}_2)_2$ has no crystallographically imposed symmetry, it is the most regular example of this cation since the end triangular faces are parallel to within 0.60° and the atoms in the rectangular faces are within 0.006 \AA of their least-squares mean planes. In comparison, the cation in $(\text{Te}_6)(\text{AsF}_6)_4(\text{AsF}_3)_2$ has crystallographic symmetry $\underline{2}$ and an angle of 1.75° between the end triangular faces which are also twisted by 2.72° with respect to each other (26). There are also some significant variations in the Te-Te bond lengths in these cations (Table IV.7). In $(\text{Te}_6)(\text{AsF}_6)_4(\text{SO}_2)_2$ all the bonds in the

TABLE IV.7 Bond Lengths (Å) and Bond Angles (deg) in Te_6^{4+} Structures.

Bond Lengths ^a	I ^b	II ^c	III ^d
Te(1)--Te(2)	2.684(5)	2.662(3)	2.679(2)
--Te(3)	2.679(7)	2.673(2)	2.702(2)
--Te(6)	3.132(6)	3.132(2)	3.167(2)
Te(2)--Te(3)	2.694(5)	2.672(2)	2.701(2)
--Te(5)	3.148(6)	3.132(2)	3.171(2)
Te(3)--Te(4)	3.121(6)	3.062(2)	3.047(2)
Te(4)--Te(5)	2.677(5)	2.673(2)	2.702(2)
--Te(6)	2.675(7)	2.672(2)	2.698(2)
Te(5)--Te(6)	2.675(5)	2.662(3)	2.679(2)
Bond Angles			
triangular faces	59.8(1) to 60.3(1)	59.7(1) to 60.2(1)	59.47(5) to 60.32(5)
rectangular faces	88.9(2) to 91.4(2)	88.3(1) to 91.6(1)	88.51(6) to 91.48(6)

(a) The atomic numbering from ref. (26) has been modified to fit the present structure, i.e. for structure I, 1=4, 2=2, 3=6, 4=5, 5=1, 6=3, and for structure II, 1=3, 2=2, 3=1, 4=1', 5=3', 6=2'.

(b) $(\text{Te}_6)(\text{AsF}_6)_4(\text{SO}_2)_2$.

(c) $(\text{Te}_6)(\text{AsF}_6)_4(\text{AsF}_3)_2$.

(d) $(\text{Te}_6)(\text{Se}_8)(\text{AsF}_6)_6(\text{SO}_2)$.

end triangular faces have the same length and the bonds between these faces are also virtually equal in length. In the present cation the bonds between the triangular faces have lengths of 3.047(2), 3.167(2) and 3.172(2) Å. In each end triangular face the bonds which include the tellurium atoms involved in the short bond between these faces are significantly longer than the remaining bond (Table IV.7). A similar but less pronounced correlation is observed for the bond lengths in the cation in $(\text{Te}_6)(\text{AsF}_6)_4(\text{AsF}_3)_2$.

Variations in the dimensions of the Te_6^{4+} cation in these different structures can be attributed to differences in the anion-cation interactions. The interionic contacts to Te_6^{4+} in $(\text{Te}_6)(\text{Se}_8)(\text{AsF}_6)_6(\text{SO}_2)$ that are less than the van der Waals limits are included in Table IV.8. Atoms Te(3) and Te(4) which form the short bond in the rectangular faces (and the long bonds in the triangular faces) form several more (five to six) short Te...F contacts in the range 2.73 to 3.15 Å. The other tellurium atoms have only two to three contacts of similar length.

In a recent molecular orbital investigation of the Te_6^{4+} cation (51), it was calculated that the cation achieves its lowest energy when the two triangular faces are each folded back ca. 14° from the parallel positions of a regular trigonal prism, i.e. with one long bond and two short bonds between the triangular faces. In the present structure,

however, there is one short bond and two long bonds between these faces.

TABLE IV.8 Interionic Contacts (Å) to Te_6^{4+} in $\text{Te}_6(\text{Se}_8)(\text{AsF}_6)_6(\text{SO}_2)$.

Te(1)...F(13)	3.089(15)	Te(4)...F(12)	2.890(14)
...F(62)	3.453(15)	...F(52)	3.05(2)
...F(63)	3.148(15)	...F(55)	3.46(3)
...O(1)	3.284(16)	...F(41) ^e	3.090(12)
...F(11) ^a	3.011(14)	...F(42) ^e	3.292(15)
...F(21) ^a	3.199(18)	...F(43) ^e	3.123(13)
...F(231) ^a	3.21(3)	...F(31) ^c	3.030(13)
...F(262) ^a	3.43(4)		
Te(2)...F(36)	2.965(18)	Te(5)...F(34)	2.914(15)
...F(62)	3.471(14)	...F(42)	3.407(14)
...F(65)	3.146(16)	...F(45)	3.243(15)
...O(1)	3.357(15)	...O(1)	3.393(15)
...F(22) ^b	3.12(2)	...F(22) ^e	3.23(2)
...F(33) ^c	3.299(15)	...F(33) ^c	3.022(13)
...F(231) ^b	3.35(3)	...F(241) ^e	3.30(3)
...F(262) ^b	3.33(4)	...F(252) ^e	3.39(4)
Te(3)...F(14)	2.960(13)	Te(6)...F(13)	3.187(16)
...F(55)	2.73(3)	...F(42)	3.494(15)
...F(35) ^c	3.000(13)	...F(46)	3.118(19)
...F(61) ^d	3.135(15)	...O(1)	3.337(15)
...F(62) ^d	3.151(15)	...F(16) ^a	2.926(14)
...F(64) ^d	3.111(14)	...F(21)	3.16(2)
		...F(241)	3.25(3)

Symmetry Code

(a) 1-x, 1-y, -z

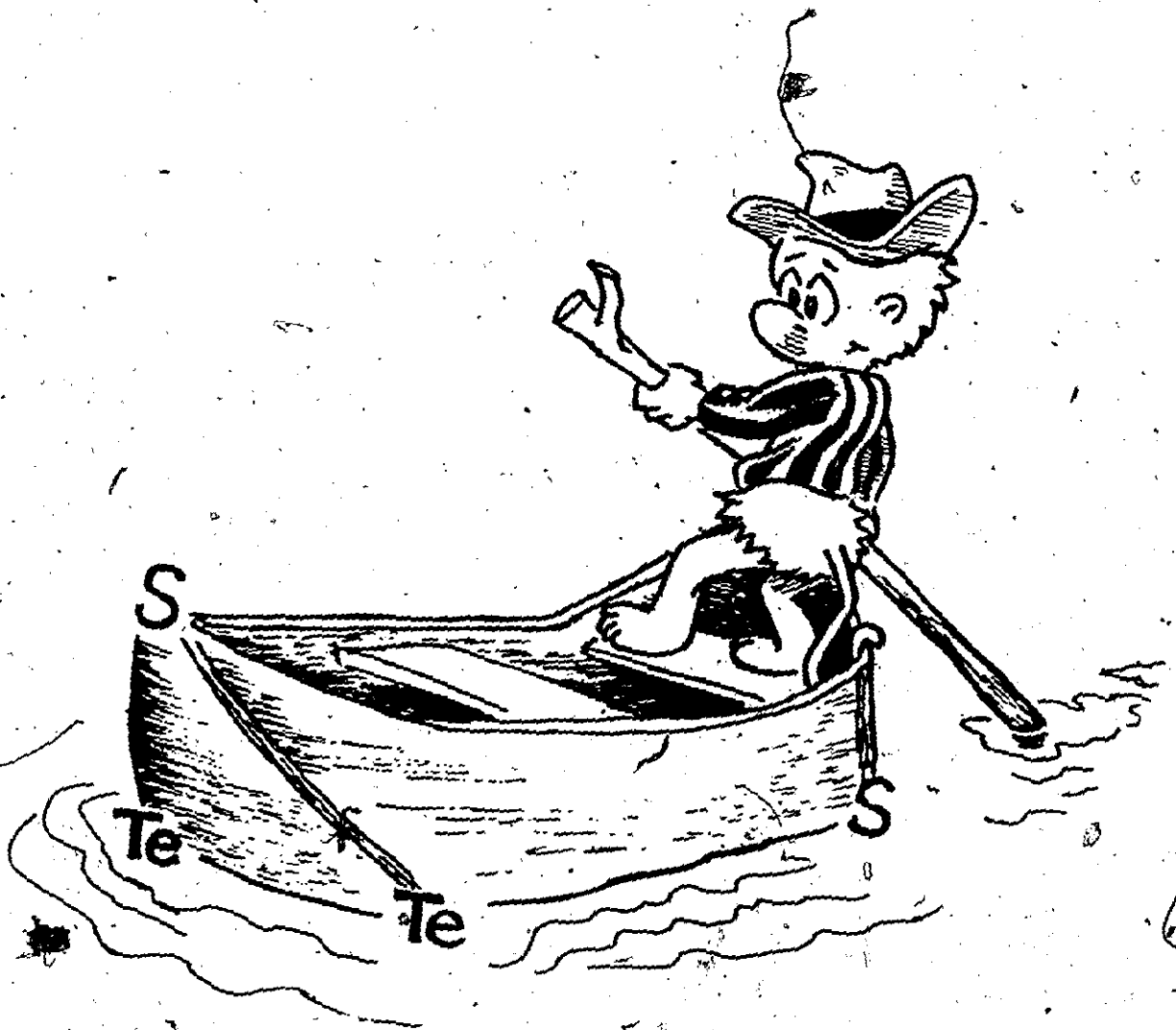
(b) -1+x, y, z

(c) -x, -y, -z

(d) -x, 1-y, -z

(e) 1-x, -y, -z

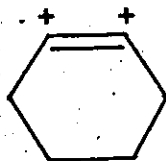
CHAPTER V
 M_6^{2+} CATIONS



V.1 Introduction.

There are three published X-ray crystal structures with chalcogen cations of average oxidation state +0.33. These are of the compounds $(\text{Te}_2\text{Se}_4)(\text{AsF}_6)_2$, $(\text{Te}_2\text{Se}_4)(\text{SbF}_6)_2$ and $(\text{Te}_3\text{S}_3)(\text{AsF}_6)_2$ (20). The crystal structure of $(\text{Te}_2\text{Se}_4)(\text{AsF}_6)_2$ has recently been redetermined (21). In all cases the cation is a six-membered ring in the boat conformation with one cross-ring bond (Fig. V.1). This cage structure can be visualized (9) as arising from the parent trigonal prism cluster structure by the addition of two pairs of electrons or from the "birdcage" structure of P_4S_3 (65) and related species such as Sb_7^{3-} (68) and As_3Se_4^+ (66) by removal of a bridging atom (Fig. V.2). The latter analogy is similar to the relationship between $\text{Te}_2\text{Se}_6^{2+}$ and P_{17}^{3-} (section IV.7).

The homoatomic species S_6^{2+} and Se_6^{2+} are unknown but the Te_6^{2+} cation has been isolated in the compounds $\text{Te}_6(\text{AlCl}_4)_2$ (54), $\text{Te}_6(\text{AsF}_6)_2$ (59) and $\text{Te}_6(\text{SbF}_6)_2$ (69). Good crystalline samples of these compounds have not been isolated, however, and the structure of the Te_6^{2+} cation is still uncertain. One possible structure is a planar six-membered ring, V.I (59).



V.I

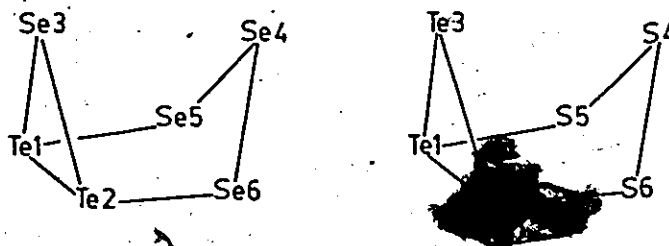


FIGURE V.1 The $\text{Te}_2\text{Se}_4^{2+}$ and $\text{Te}_3\text{S}_3^{2+}$ cations.

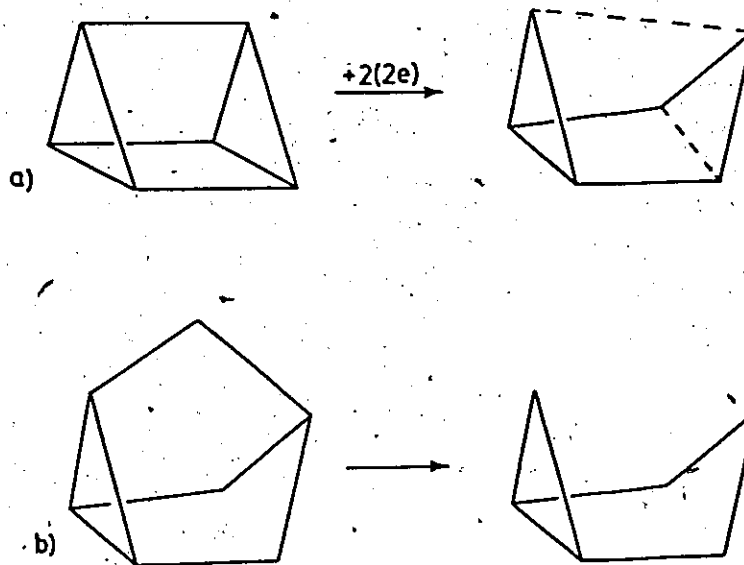


FIGURE V.2 Derivation of the $\text{Te}_2\text{Se}_4^{2+}$ structure from the trigonal prism and from the P_4S_3 (birdcage) structure.

If four of the Te atoms contribute one lone pair of electrons to the π system then this can be considered as a 10π aromatic system with a net of one π bond distributed over the six Te--Te bonds of the ring. This planar, delocalized structure is adopted by the isovalent P_6^{4-} and $1,3,5-S_3N_3^-$ anions (58, 70). In the isovalent $1,3-S_4N_2$ molecule the system is no longer completely delocalized and the structure is a half-chair (half-boat), with the central sulfur of the trisulfide unit out of the plane of the other five atoms (71). This structure is intermediate between the completely delocalized planar structure of P_6^{4-} (Te_6^{2+}) and the boat-shaped, bond-localized $Te_2Se_4^{2+}$ structure. A recent molecular orbital investigation of the structures of some polyatomic cations and anions of the main-group elements concludes that the planar ring is the most favorable structure for Te_6^{2+} (51). This hypothesis is supported by a ^{125}Te Mössbauer study of $Te_6(AlCl_4)_2$ which provided no evidence for more than one Te site in the compound, as expected for the planar structure, but not for a boat structure (72).

The $Te_2Se_4^{2+}$ cation has been characterized by ^{77}Se and ^{125}Te NMR spectroscopy in 100% H_2SO_4 and oleum solutions (50). Chemical shifts and coupling constants are consistent with the solid-state structure being retained in solution. The isostructural $Te_3Se_3^{2+}$ cation has also been identified in these solutions (50). The ^{77}Se - ^{77}Se and ^{77}Se - ^{125}Te coup-

lings indicate that the Te--Te cross-ring bond is retained in this cation and the third tellurium atom is located at the opposite end of the cation, at site (4) (Fig. V.1). In contrast, the crystal structure (20) of $(\text{Te}_3\text{S}_3)(\text{AsF}_6)_2$ demonstrates that the third tellurium atom of the $\text{Te}_3\text{S}_3^{2+}$ cation is located at site (3), forming a Te_3 ring (Fig.V.1).

V.2 Preparation of $(\text{Te}_2\text{Se}_4)(\text{SbF}_6)_2$.

Following the procedure outlined in chapter II, 1.0301 g (4.987 mmol) of a finely-powdered 1:1 mixture of tellurium and selenium was mixed with 1.627 g (7.505 mmol) of SbF_5 in 30 mL of SO_2 . The initial green solution color turned red-brown after several minutes. After one week of stirring the solution was filtered and after standing for a few days black crystals were deposited. These were filtered and any remaining volatile material was removed by pumping under vacuum. A subsequent X-ray crystal structure determination identified the crystals as $(\text{Te}_2\text{Se}_4)(\text{SbF}_6)_2$. A crystal structure of $(\text{Te}_2\text{Se}_4)(\text{SbF}_6)_2$ has already been reported (20), but the space group of the present compound is different and the exact composition of the cation in the former compound is somewhat uncertain (see section V.8). Ditellurium tetraselenium bis(hexafluoroantimonate) has also been obtained in other long term (1 week) reactions involving different stoichiometries of Te, Se and SbF_5 (see reaction IV.5 and section VI.3). The previously reported (20)

" $(\text{Te}_2\text{Se}_4)(\text{SbF}_6)_2$ " was obtained after a reaction time of only 0.5 h (20).

V.3 Preparation of $(\text{Te}_2\text{Se}_4)(\text{Sb}_3\text{F}_{14})(\text{SbF}_6)$.

Following the procedure of chapter II, Te (0.7209 g, 5.650 mmol) and Se (1.3377 g, 16.936 mmol) were mixed with SbF_5 (4.9036 g, 22.624 mmol) in 40 mL of SO_2 . The solution was initially green but rapidly turned a deep brown and after one week of stirring was an amber-brown color. The solution was filtered and the solvent slowly removed by distillation. After 48 h a large quantity of black crystals had formed from the residual brown oil. The oil was poured off, the crystals washed with SO_2 and any remaining volatile materials were removed by pumping under vacuum. The prism- and block-shaped crystals were shown to be $\text{Te}_2\text{Se}_4(\text{Sb}_4\text{F}_{20})$ by a subsequent X-ray crystal structure determination.

V.4 Preparation of $(\text{Te}_x\text{Se}_{6-x})(\text{SbF}_6)_2$.

Following the procedure outlined in chapter II, Te (1.0891 g, 8.535 mmol) and Se (0.6744g, 8.541 mmol) were mixed with SbF_5 (1.848 g, 8.527 mmol) in 45 mL of SO_2 . After 4 h of stirring the mixture was cooled to 195 K in a dry ice/acetone bath and the deep brown solution filtered while still cold and allowed to stand. After 48 h the solution was poured off revealing a large number of flat needles and plates. Precession photographs revealed that the crystals were isomorphous with " $(\text{Te}_2\text{Se}_4)(\text{SbF}_6)_2$ " (20) but the

unit cell was slightly larger. A subsequent X-ray crystal structure determination using the atomic positions of " $(\text{Te}_2\text{Se}_4)(\text{SbF}_6)_2$ " in the initial refinement identified the compound as $(\text{Te}_{2.7}\text{Se}_{3.3})(\text{SbF}_6)_2$. This compound possesses occupational disorder in that two of the cation sites are partially occupied by both Se and Te. A similar situation exists for $(\text{Te}_{4.5}\text{Se}_{5.5})(\text{AsF}_6)_2$ (section III.3).

When the above procedure was followed except with a larger Te:Se ratio, i.e. 1.6514 g (12.942 mmol) Te and 0.5123 g (6.488 mmol) Se were reacted with 2.1043 g (9.709 mmol) SbF_5 , the resulting crystals were again isomorphous with " $(\text{Te}_2\text{Se}_4)(\text{SbF}_6)_2$ ". The X-ray crystal structure determination revealed the composition of this second compound to be $(\text{Te}_{3.4}\text{Se}_{2.6})(\text{SbF}_6)_2$.

V.5 Preparation of $(\text{Te}_{2.1}\text{S}_{3.9})(\text{SbF}_6)_2$.

Following the general procedure as outlined in chapter II, Te (0.8584 g, 6.727 mmol) and S (0.6471g, 20.18mmol) were reacted with SbF_5 (2.181 g, 10.1 mmol) in 20 mL of a 4:1 SO_2 - SO_2ClF solvent mixture. The solution was initially amber-brown but turned amber-red after 15 min. After 24 h of stirring the reaction mixture was cooled in a dry ice/acetone bath to 195 K and the solution filtered while still cold. The filtrate was left to stand in the cold bath which slowly warmed to room temperature over 4 days and a large quantity of thick amber-brown needles and blocks were

deposited. Precession photographs of the needles demonstrated that they were isomorphous with $(\text{Te}_2\text{Se}_4)(\text{SbF}_6)_2$ (section V.2) and a subsequent X-ray crystal structure determination identified the compound as $(\text{Te}_{2.1}\text{S}_{3.9})(\text{SbF}_6)_2$. One of the sulfur sites in each of the two independent cations in the structure is partially occupied by tellurium. The atomic coordinates from $(\text{Te}_2\text{Se}_4)(\text{SbF}_6)_2$ were used in the initial refinement of the structure.

The blocks isolated from this reaction were similar in color to $(\text{Te}_{2.1}\text{S}_{3.9})(\text{SbF}_6)_2$, but the morphology was different and precession photographs revealed a cubic space group with $a = 8.35 \text{ \AA}$. A data set was collected on a Syntex P2₁ diffractometer, but the structure could not be solved. Many of the rare earth sulfides, M_2S_3 , are cubic with axes of 8.2 to 8.3 Å (73). Sb_2S_3 and Sb_2Te_3 are known in orthorhombic modifications with similar cell volumes to the present compound (74, 75). This compound may be a cubic form of antimony sulfide or telluride or mixed antimony sulfide-telluride.

V.6 Preparation of $(\text{Te}_3\text{S}_3)(\text{SbF}_6)_2$.

Following the procedure outlined in chapter II, Te (1.2060 g, 9.451 mmol) and S (0.3026 g, 9.437 mmol) were mixed with SbF_5 (1.534 g, 7.079 mmol) in 45 mL SO_2 . After 5 h of stirring the deep violet solution was cooled to 195 K before filtering cold and allowed to slowly warm to 295 K.

After 3 days of standing the solution was poured off revealing a large quantity of black crystals. The crystals appeared to be of two distinct types: (1) large multifaceted, almost spherical crystals and (2) flat needles and plates. The spheres were triclinic and were identified by Raman (76, 77) and ^{125}Te NMR spectroscopy (50, 78) to be $(\text{Te}_4)(\text{SbF}_6)_2$. This compound has previously been prepared in crystalline form from a Ge/Te mixture (23). Precession photographs revealed that the remaining crystals were isomorphous with $(\text{Te}_3\text{S}_3)(\text{AsF}_6)_2$, which has been prepared from a reaction of the same stoichiometry but using AsF_5 as the oxidant (20). The present compound is then probably $(\text{Te}_3\text{S}_3)(\text{SbF}_6)_2$, although a disordered compound of the type $(\text{Te}_x\text{S}_{6-x})(\text{SbF}_6)_2$ cannot be ruled out. The unit cell dimensions of an isomorphous crop of crystals isolated using the same procedure, but with the Te/S/ SbF_5 reagent stoichiometry of 6:6:3, were accurately determined on a Syntex P2₁ diffractometer (see Appendix).

V.7 Anion-Cation Interactions in M_6^{2+} Structures.

As was noted in the previous two chapters describing the M_{10}^{2+} and M_8^{2+} structures, there are several interionic contacts to the M_6^{2+} cations that are significantly shorter than the van der Waals limits and are in stereochemically meaningful positions. The contacts to the three-coordinate tellurium atoms are generally shorter and greater in number

than those to the selenium and sulfur atoms. These observations are consistent with the greater size (polarizability) of tellurium and with the positive charges being localized at the three-coordinate tellurium atoms. The arrangement of the primary and secondary bonds to Te(11) in $(\text{Te}_2\text{Se}_4)(\text{SbF}_6)_2$ (Fig. V.3) produces a tricapped trigonal prism, with the lone pair of electrons on tellurium presumably capping a triangular face of the prism. This can be compared with geometries observed about tellurium in $(\text{Te}_2\text{Se}_6)(\text{Te}_2\text{Se}_8)-(\text{AsF}_6)_4(\text{SO}_2)_2$ and $(\text{TeF}_3)(\text{Sb}_2\text{F}_{11})$ in Figure III.7.

The $\text{Sb}_3\text{F}_{14}^-$ anion in the compound $(\text{Te}_2\text{Se}_4)(\text{Sb}_3\text{F}_{14})-(\text{SbF}_6)$ contains an Sb(III) atom as well as two Sb(V) atoms. The stereoactive lone pair of electrons on Sb(III) is of interest when considering interionic contacts. The geometry of this anion is described along with other salts containing the $\text{Sb}_3\text{F}_{14}^-$ anion in chapter VI.

V.8 Comparison of M_6^{2+} Structures.

All of the M_6^{2+} cations described above adopt the boat conformation with two tellurium atoms forming a cross-ring bond. The cations in the compounds $(\text{Te}_{2.7}\text{Se}_{3.3})(\text{SbF}_6)_2$ and $(\text{Te}_{3.4}\text{Se}_{2.6})(\text{SbF}_6)_2$ are occupationally disordered with both of the apical selenium positions of the boat (Se(3) and Se(4) of Fig. V.1) partially occupied by tellurium. In both cases the tellurium concentration is higher at the apex opposite the basal Te--Te bond (Table V.1). The lengths of

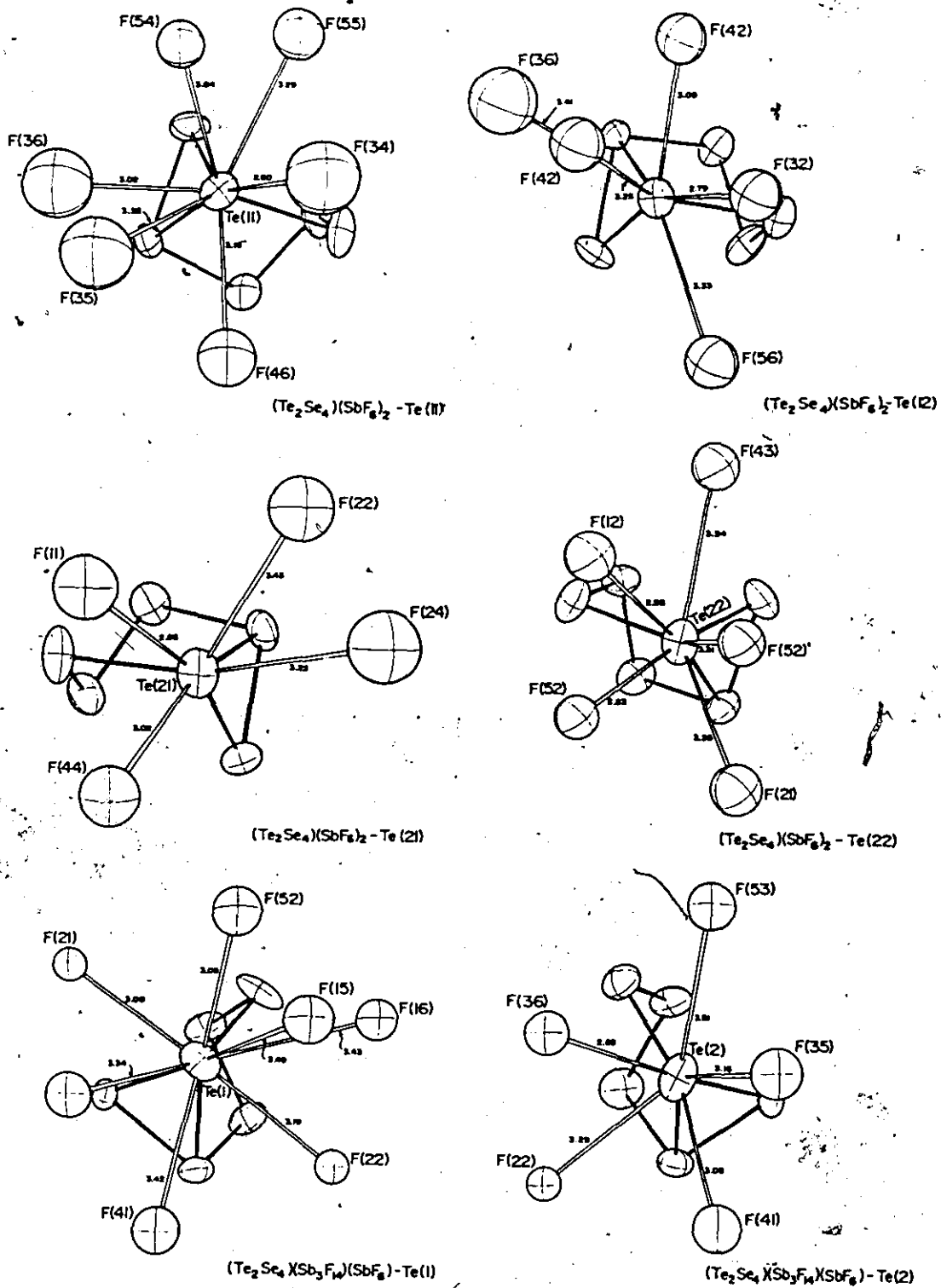


FIGURE V.3 Anion-cation interactions at Te in $\text{Te}_2\text{Se}_4^{2+}$ structures. All views toward assumed position of lone pair.

the bonds to the partially tellurium-substituted positions are significantly longer than the average Te--Se and Se--Se bonds in the structures with simple $\text{Te}_2\text{Se}_4^{2+}$ cations (Table V.2). Analogous bonds in different $\text{Te}_2\text{Se}_4^{2+}$ cations show some small variations as well, most probably as a result of differences in anion-cation interactions. The bond lengths to Se(3) and Se(4) in the published structures (20) of " $(\text{Te}_2\text{Se}_4)(\text{AsF}_6)_2$ " and " $(\text{Te}_2\text{Se}_4)(\text{SbF}_6)_2$ ", however, are significantly longer than the mean bond lengths to these positions in the other $\text{Te}_2\text{Se}_4^{2+}$ salts (Table V.2), indicating partial tellurium substitution in these structures as well.

The cross-ring Se(3)...Se(4) distances in the $\text{Te}_x\text{Se}_{6-x}^{2+}$ structures are comparable in magnitude to cross-ring distances in $\text{Te}_2\text{Se}_6^{2+}$, $\text{Te}_x\text{Se}_{10-x}^{2+}$ and Se_{10}^{2+} structures described earlier (chapters III and IV) and may all indicate weak bonding interactions. The observation that the Se(3) and Se(4) sites in the $\text{Te}_x\text{Se}_{6-x}^{2+}$ cation are preferentially occupied over the Se(5) and Se(6) sites by the larger, more polarizable tellurium atoms (see Table V.1) lends some support to this bonding argument. A plot of the Se(3)...Se(4) distance as a function of total tellurium content at these two positions for the mean $\text{Te}_2\text{Se}_4^{2+}$ cation (Te content = 0) and the mixed $(\text{Te}_{2.7}\text{Se}_{3.3})(\text{SbF}_6)_2$ and $(\text{Te}_{3.4}\text{Se}_{2.6})(\text{SbF}_6)_2$ structures gives a straight line with a correlation coefficient, $R = 0.99996$ (Fig. V.4). According

Table V.1 Occupation of the Sites in the $\text{Te}_x\text{Se}_{6-x}^{2+}$ Cation.

Site ^a	$(\text{Te}_{2.7}\text{Se}_{3.3})(\text{SbF}_6)_2$				$(\text{Te}_{3.4}\text{Se}_{2.6})(\text{SbF}_6)_2$			
	κ^b	# of electrons	%Te ^c	%Se ^c	κ^b	# of electrons	%Te ^c	%Se ^c
1	1.029(10)	53.5(5)	100	0	0.994(9)	51.7(5)	100	0
2	1.006(8)	52.3(4)	100	0	0.997(8)	51.8(4)	100	0
3	1.119(13) ^d	38.0(4)	22.5	77.5	0.874(8) ^e	45.4(4)	63.6	36.4
4	0.822(7) ^e	42.7(4)	48.6	51.4	0.936(7) ^e	48.7(4)	81.5	18.5
5	0.979(11)	33.3(4)	0	100	0.990(11)	33.7(4)	0	100
6	1.014(12)	34.5(4)	0	100	1.026(12)	34.9(4)	0	100

(a) Numbering as in Fig. V.1. (b) Population parameter from refinement in the program SHELX. (c) Sites where the number of electrons is within 3 standard deviations of 34 or 52 are considered to be 100% Se or Te respectively. (d) Refined as Se. (e) Refined as Te.

Table V.2 Bond Lengths in the $\text{Te}_2\text{Se}_4^{2+}$ and $\text{Te}_x\text{Se}_{6-x}^{2+}$ Cations.

Compound	Ref	Bond Length (Å) ^a								
		1 - 2	1 - 3	1 - 5	2 - 3	2 - 6	4 - 5	4 - 6	3...4	5...6
$\text{Te}_2\text{Se}_4(\text{AsF}_6)_2^b$	21	2.812(5)	2.547(6)	2.566(6)	2.530(6)	2.527(8)	2.284(9)	2.327(8)	3.350(8)	3.384(8)
		2.797(4)	2.563(5)	2.545(5)	2.568(5)	2.543(6)	2.324(7)	2.314(7)	3.390(7)	3.451(7)
$\text{Te}_2\text{Se}_4(\text{SbF}_6)_2^b$	c	2.800(3)	2.519(5)	2.558(5)	2.524(5)	2.554(5)	2.317(7)	2.335(7)	3.364(6)	3.469(6)
		2.809(4)	2.520(5)	2.553(5)	2.504(5)	2.551(6)	2.298(7)	2.305(6)	3.374(6)	3.429(6)
$\text{Te}_2\text{Se}_4(\text{Sb}_3\text{F}_{14})(\text{SbF}_6)$	c	2.770(4)	2.460(5)	2.522(6)	2.466(5)	2.494(5)	2.280(7)	2.268(7)	3.344(6)	3.372(7)
Mean $\text{Te}_2\text{Se}_4^{2+}$	-	2.798	2.522	2.549	2.518	2.534	2.301	2.310	3.364	3.421
$\text{Te}_{2.7}\text{Se}_{3.3}(\text{SbF}_6)_2$	c	2.793(2)	2.558(3)	2.552(3)	2.567(4)	2.546(3)	2.385(4)	2.400(4)	3.453(4)	3.491(4)
$\text{Te}_{3.4}\text{Se}_{2.6}(\text{SbF}_6)_2$	c	2.802(2)	2.646(3)	2.579(3)	2.646(3)	2.567(3)	2.445(3)	2.469(3)	3.543(3)	3.531(3)
$^*\text{Te}_2\text{Se}_4(\text{SbF}_6)_2^d$	20	2.786(7)	2.539(10)	2.532(9)	2.525(11)	2.539(9)	2.346(10)	2.346(11)	3.412(11)	3.445(10)
$^*\text{Te}_2\text{Se}_4(\text{AsF}_6)_2^e$	20	2.82(2)	2.59(2)	2.57(2)	2.56(2)	2.58(2)	2.33(2)	2.38(2)	3.49(2)	3.42(2)

(a) Numbering as in Fig. V.1. (b) Two independent cations in the structure. (c) This work. (d) Proposed composition based on 3...4 distance: $\text{Te}_{2.4}\text{Se}_{3.6}(\text{SbF}_6)_2$. (e) Proposed composition based on 3...4 distance: $\text{Te}_{3.0}\text{Se}_{3.0}(\text{AsF}_6)_2$.

to this plot, the Se(3)...Se(4) distances in the published structures of $(\text{Te}_2\text{Se}_4)(\text{AsF}_6)_2$ and $(\text{Te}_2\text{Se}_4)(\text{SbF}_6)_2$ indicate that these compounds would be better described as $(\text{Te}_{3.0}\text{Se}_{3.0})(\text{AsF}_6)_2$ and $(\text{Te}_{2.4}\text{Se}_{3.6})(\text{SbF}_6)_2$ respectively. These compounds were prepared from equimolar mixtures of tellurium and selenium and it would therefore not be surprising for the Te-Se ratio of the products to be greater than the value of 0.5 for $\text{Te}_2\text{Se}_4^{2+}$. The bond angles in the $\text{Te}_2\text{Se}_4^{2+}$ and $\text{Te}_x\text{Se}_{6-x}^{2+}$ cations (Table V.3) are sensitive to changes in the tellurium content of the cation as well. The Te(1)-Se(3)-Te(2) and Se(5)-Se(4)-Se(6) angles in the $\text{Te}_{3.4}\text{Se}_{2.6}^{2+}$ cation are nearly 4° smaller than in the mean $\text{Te}_2\text{Se}_4^{2+}$ cation. These angles in the published structures of $(\text{Te}_2\text{Se}_4)(\text{AsF}_6)_2$ and $(\text{Te}_2\text{Se}_4)(\text{SbF}_6)_2$ are smaller than those of the mean cation as well, again indicating partial tellurium substitution of the Se(3) and Se(4) sites in the compounds.

The unit cell volume of a compound is instructive in determining its composition. As outlined in section IX.2, the cell volume of a given compound can be accurately predicted from a summation of the average volumes occupied by its component parts. The AsF_6^- , SbF_6^- and $\text{Sb}_3\text{F}_{14}^-$ anions have average volumes of 101, 114 and 265 \AA^3 respectively, so that the mean volume of the $\text{Te}_2\text{Se}_4^{2+}$ cation, as determined by subtracting the appropriate anion volumes from the cell volumes of the compounds $(\text{Te}_2\text{Se}_4)(\text{AsF}_6)_2$ (redetermined struc-

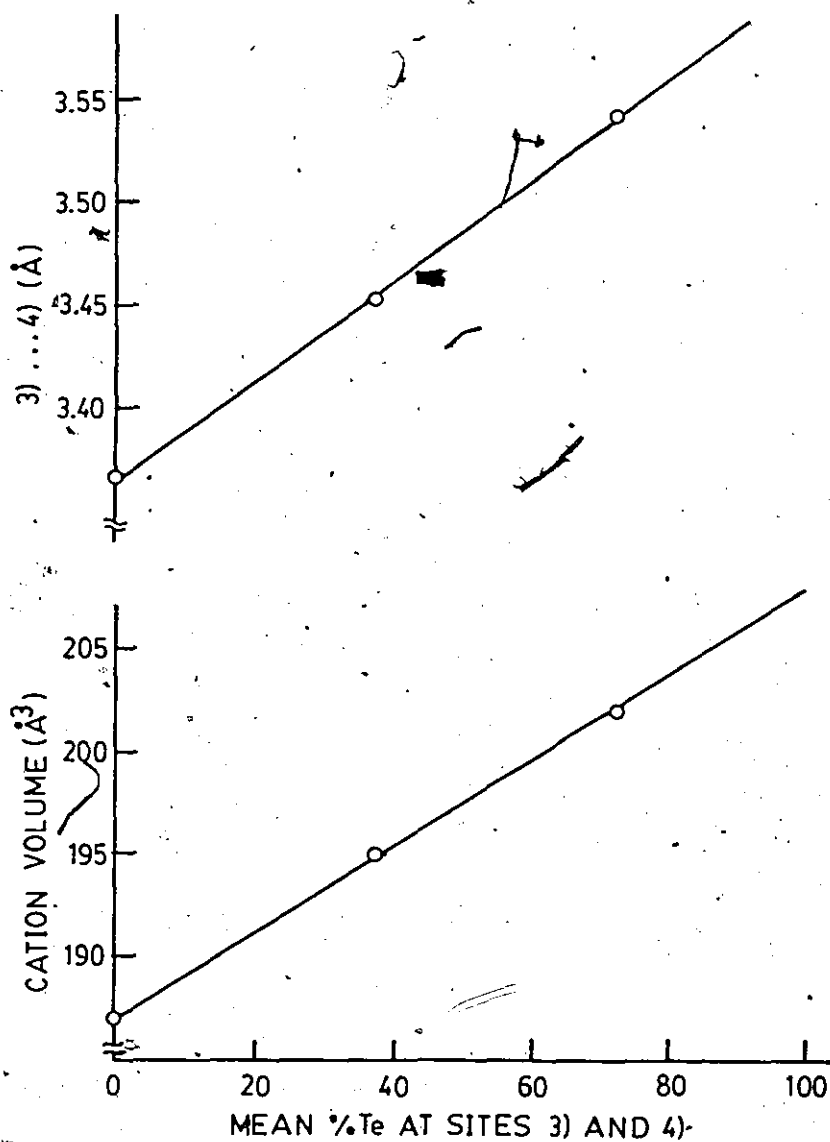


FIGURE V.4 Plots of site (3) - site (4) distance and cation volume as a function of mean Te percentage at sites (3) and (4) in $\text{Te}_x\text{Se}_{6-x}^{2+}$ cations.

Table V.3 Bond Angles in the $\text{Te}_2\text{Se}_4^{2+}$ and $\text{Te}_x\text{Se}_{6-x}^{2+}$ Cations.

Compound	Ref.	Bond Angle (deg) ^a									
		2-1-3	2-1-5	3-1-5	1-2-3	1-2-6	3-2-6	1-3-2	5-4-6	1-5-4	2-6-4
$\text{Te}_2\text{Se}_4(\text{AsF}_6)_2^b$	21	56.1(2)	96.9(2)	99.4(2)	56.7(2)	95.9(2)	101.0(2)	67.3(2)	94.4(3)	96.7(2)	97.2(3)
	b _E	57.1(1)	97.7(1)	99.7(2)	56.9(1)	97.0(2)	101.3(2)	66.1(1)	96.1(2)	97.4(2)	96.7(2)
$\text{Te}_2\text{Se}_4(\text{SbF}_6)_2^b$	c	56.4(1)	98.9(1)	99.7(2)	56.2(1)	96.0(1)	100.7(2)	67.4(1)	96.4(2)	96.6(2)	97.0(2)
	c	55.7(1)	97.4(1)	99.8(2)	56.3(1)	96.5(1)	101.0(2)	68.0(1)	96.3(2)	97.3(2)	97.0(2)
$\text{Te}_2\text{Se}_4(\text{Sb}_3\text{F}_{14})(\text{SbF}_6)$	c	55.9(1)	96.0(2)	100.5(2)	55.7(1)	97.8(2)	100.8(2)	68.4(1)	95.7(2)	97.8(2)	97.7(2)
Mean $\text{Te}_2\text{Se}_4^{2+}$	-	56.2	97.4	99.8	56.4	96.6	101.0	67.4	95.8	97.2	97.1
$\text{Te}_{2.7}\text{Se}_{3.3}(\text{SbF}_6)_2$	c	57.1(1)	96.9(1)	101.4(1)	56.8(1)	98.8(1)	100.0(1)	66.0(1)	93.7(1)	98.0(1)	98.3(1)
$\text{Te}_{3.4}\text{Se}_{2.6}(\text{SbF}_6)_2$	c	58.0(1)	97.0(1)	101.7(1)	58.0(1)	99.2(1)	100.9(1)	63.9(1)	91.9(1)	98.4(1)	98.4(1)
$^*\text{Te}_2\text{Se}_4(\text{SbF}_6)_2^d$	20	56.4(3)	96.8(2)	101.8(3)	56.9(2)	98.0(3)	99.9(3)	66.8(9)	94.3(4)	97.5(3)	98.1(3)
$^*\text{Te}_2\text{Se}_4(\text{AsF}_6)_2^e$	20	57(1)	99(1)	101(1)	59(1)	96(1)	99(1)	64(1)	94(1)	98(1)	99(1)

(a) Numbering as in Fig. V.1. (b) Two independent cations in the structure. (c) This work. (d) Proposed composition based on 3...4 distance: $\text{Te}_{2.4}\text{Se}_{3.6}(\text{SbF}_6)_2$. (e) Proposed composition based on 3...4 distance: $\text{Te}_{3.0}\text{Se}_{3.0}(\text{AsF}_6)_2$.

ture), $(\text{Te}_2\text{Se}_4)(\text{SbF}_6)_2$ (form reported here) and $(\text{Te}_2\text{Se}_4)-(\text{Sb}_3\text{F}_{14})(\text{SbF}_6)$, is 187 \AA^3 (Table V.4). This compares favorably with the value of 188 \AA^3 as calculated from the average Se and Te volumes of 28 and 38 \AA^3 respectively (Table IX.2). A plot of cation volume (Table V.4) as a function of the total %Te at the Se(3) and Se(4) sites (Table V.1) gives a linear plot for the mean $\text{Te}_2\text{Se}_4^{2+}$ cation and the $\text{Te}_{2.7}\text{Se}_{3.3}^{2+}$ and $\text{Te}_{3.4}\text{Se}_{2.6}^{2+}$ cations ($R = 0.9987$, see Fig. V.4). The published structures of " $(\text{Te}_2\text{Se}_4)(\text{AsF}_6)_2$ " and " $(\text{Te}_2\text{Se}_4)(\text{SbF}_6)_2$ " have cation volumes of 194 and 192 \AA^3 respectively, significantly larger than that of the mean $\text{Te}_2\text{Se}_4^{2+}$ cation, which again indicates some tellurium substitution at the presumed selenium sites in these compounds. The use of the cation volume as a measure of its composition is probably more useful than the bond length and bond angle comparisons described earlier since a complete structure determination is not required for the former comparison.

The $\text{Te}_2\text{S}_4^{2+}$ cation in $(\text{Te}_{2.1}\text{S}_{3.9})(\text{SbF}_6)_2$ is only the second Te-S cation to be characterized. This cation is isostructural with $\text{Te}_2\text{Se}_4^{2+}$, with the two tellurium atoms forming a cross-ring bond (Fig. V.5). Like the $\text{Te}_x\text{Se}_{6-x}^{2+}$ salts, there is some occupational disorder in this compound with S(13) and S(23) (Fig. V.5) partially substituted by tellurium in the two independent cations of the structure (Table V.5). As was observed for " $(\text{Te}_2\text{Se}_4)(\text{AsF}_6)_2$ " and

Table V.4 Cation Volumes in $\text{Te}_2\text{Se}_4^{2+}$ and $\text{Te}_x\text{Se}_{6-4x}^{2+}$ Structures.

Compound	Ref.	Unit Cell Volume	Z	Molec. Volume	Cation Volume (\AA^3)
$\text{Te}_2\text{Se}_4(\text{AsF}_6)_2$	21	3124	8	390	188
$\text{Te}_2\text{Se}_4(\text{SbF}_6)_2$	a	6614	16	413	185
$\text{Te}_2\text{Se}_4(\text{Sb}_3\text{F}_{14})(\text{SbF}_6)$	a	4546	8	568	189
Mean $\text{Te}_2\text{Se}_4^{2+}$	-	--	-	-	187
$\text{Te}_{2.7}\text{Se}_{3.3}(\text{SbF}_6)_2$	a	1691	4	423	195
$\text{Te}_{3.4}\text{Se}_{2.6}(\text{SbF}_6)_2$	a	1720	4	430	202
$^a\text{Te}_2\text{Se}_4(\text{SbF}_6)_2$	20	1679	4	420	192
$^c\text{Te}_2\text{Se}_4(\text{AsF}_6)_2$	20 ^p	1585	4	396	194

(a) This work. (b) Proposed composition based on 3...4 distance: $\text{Te}_{2.4}\text{Se}_{3.6}(\text{SbF}_6)_2$. (c) Proposed composition based on 3...4 distance: $\text{Te}_{3.0}\text{Se}_{3.0}(\text{AsF}_6)_2$.

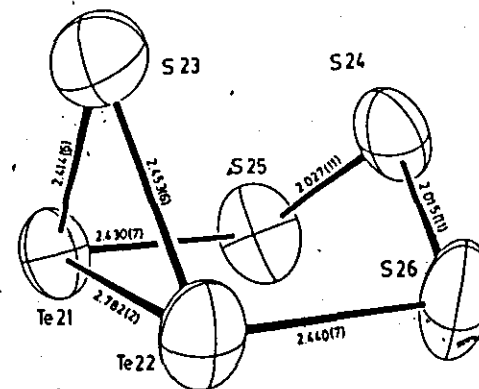
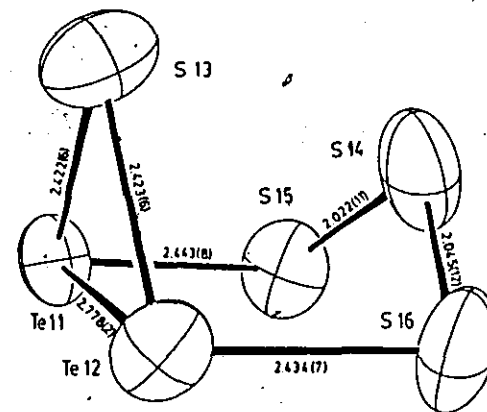


FIGURE V.5 ORTEP views of the $^a\text{Te}_2\text{Se}_4^{2+}$ cations in $(\text{Te}_{2.1}\text{S}_{3.9})(\text{SbF}_6)_2$.

"(Te₂Se₄)(SbF₆)₂", the bond lengths to S(4) in the published structure (20) of (Te₃S₃)(AsF₆)₂ (Fig. V.1) are significantly longer than to the analogous S(14) and S(24) atoms in (Te_{2.1}S_{3.9})(SbF₆)₂, indicating that there is probably some tellurium substitution at S(4) of (Te₃S₃)(AsF₆)₂ as well (Table V.6). The slight decrease in the S(5)-S(4)-S(6) bond angle in the (Te₃S₃)(AsF₆)₂ structure compared to (Te_{2.1}S_{3.9})(SbF₆)₂ (Table V.7) is again consistent with this supposition. The Te--S bonds of the Te₂S₃ ring are essentially the same length in both structures. The analogous Te--Se bonds of the Te_xSe_{6-x}²⁺ cations are of essentially equal length in all of the known compounds as well (Table V.3). It is a common feature in these structures that the two three-coordinate positions are essentially entirely occupied by tellurium while the remaining two atoms in the plane are either selenium or sulfur. If the composition is more tellurium-rich, then only the two apical positions become partially occupied by tellurium (see Tables V.1 and V.5).

An obvious difference of the Te_xS_{6-x}²⁺ and the Te_xSe_{6-x}²⁺ cations is the preference for tellurium occupation of site (3) in the Te-S cations and site (4) in the Te-Se cations. This behaviour may be related to the large difference in Te--S and Te--Se bond lengths. The (1)-(2)-(3) and (2)-(1)-(3) bond angles are particularly acute in all of these structures as a result of the cross-ring Te(1)--Te(2)

Table V.5 Occupation of Cation Sites in $(\text{Te}_{2.1}\text{S}_{3.9})(\text{SbF}_6)_2$

Site ^a	K ^b	Cation 1			Cation 2			
		# of electrons	%Te ^c	%S ^c	K ^b	# of electrons	%Te ^c	%S ^c
1	0.982(6)	51.1(3)	100	0	0.982(6)	51.0(3)	97.4	2.6
2	1.003(6)	52.2(3)	100	0	0.999(6)	51.9(3)	100	0
3	1.199(21)	19.2(4)	8.8	91.2	1.297(21)	20.8(4)	13.2	86.8
4	1.022(22)	16.4(4)	0	100	1.001(21)	16.0(4)	0	100
5	1.024(24)	16.4(4)	0	100	1.092(24)	17.5(4)	4.1	95.9
6	0.948(23)	15.2(4)	0	100	1.030(23)	16.5(4)	0	100

(a) Numbering as in Fig. V.1. (b) Population parameter from refinement in the program SHELX. (c) Sites where the number of electrons is within 3 standard deviations of 16 or 52 are considered to be 100% S or Te respectively.

Table V.6 Bond Lengths (Å) in the $\text{Te}_3\text{S}_3^{2+}$ and $\text{Te}_{2.1}\text{S}_{3.9}^{2+}$ Cations.

	$\text{Te}_3\text{S}_3(\text{AsF}_6)_2^a$		$\text{Te}_{2.1}\text{S}_{3.9}(\text{SbF}_6)_2$	
		Cation 1	Cation 2	
1 - 2 ^b	2.787(4)	2.778(2)	2.782(2)	
1 - 3	2.684(4)	2.422(6)	2.414(6)	
1 - 5	2.443(12)	2.443(8)	2.430(7)	
2 - 3	2.665(16)	2.423(6)	2.453(6)	
2 - 6	2.468(10)	2.434(7)	2.440(7)	
4 - 5	2.098(15)	2.022(11)	2.027(11)	
4 - 6	2.105(16)	2.045(12)	2.015(11)	
3...4	3.391(12)	3.181(11)	3.208(11)	
5...6	3.213(16)	3.137(11)	3.129(11)	

(a) From ref. (20). (b) Numbering as in Fig. V.1.

bond (Tables V.3 and V.7). These angles are most acute when site (3) is occupied by sulfur since Te--S bonds are shorter than Te--Se or Te--Te bonds. Site (4) is apparently slightly more favorable for tellurium occupation in the Te-Se cations, but in the Te-S case site (3) may be preferentially occupied to minimize the (1)-(2)-(3) and (2)-(1)-(3) angle strain.

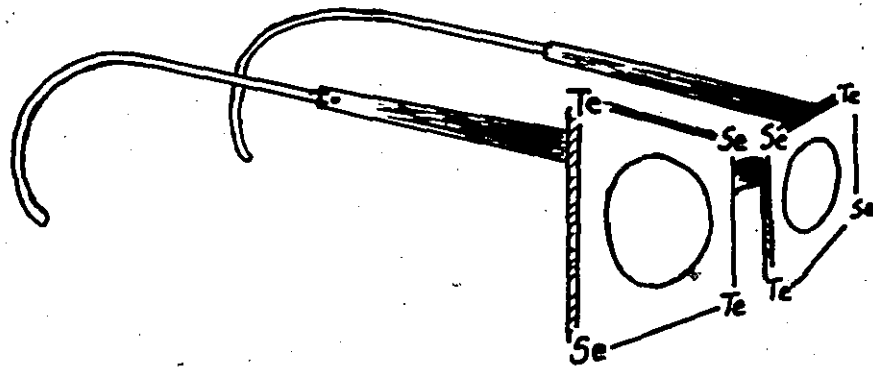
Table V.7 Bond Angles ($^{\circ}$) in the $\text{Te}_3\text{S}_3^{2+}$ and $\text{Te}_{2.1}\text{S}_{3.9}^{2+}$ Cations.

	$\text{Te}_3\text{S}_3(\text{AsF}_6)_2^a$	$\text{Te}_{2.1}\text{S}_{3.9}(\text{SbF}_6)_2$	
		Cation 1	Cation 2
2-1-3 ^b	58.3(1)	55.0(2)	55.8(2)
2-1-5	94.6(3)	93.2(2)	93.8(2)
3-1-5	100.3(3)	98.7(2)	99.0(2)
1-2-3	58.9(1)	55.0(2)	54.5(1)
1-2-6	95.4(3)	95.2(2)	94.3(2)
3-2-6	99.5(3)	97.2(3)	97.1(3)
1-3-2	62.8(1)	70.0(2)	69.7(2)
5-4-6	99.7(6)	101.0(5)	101.4(5)
1-5-4	98.7(4)	98.5(4)	98.9(4)
2-6-4	98.2(5)	98.9(4)	99.8(3)

(a) From ref. (20). (b) Numbering as in Fig. V.1

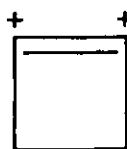
CHAPTER VI

M_4^{2+} CATIONS

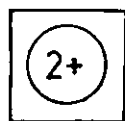


VI.1 Introduction.

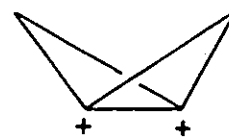
A large number of salts of the M_4^{2+} cation have been prepared where $M = S, Se, \text{ or } Te$ (see Table I.1). In all cases the cation has a very nearly square-planar (D_{4h}) structure. Small bond length differences and deviations of the bond angles from 90° have been attributed to charge-transfer interactions of the M_4^{2+} cations with the accompanying anions (23). The bond lengths in these cations are slightly shorter than the normally accepted values for the corresponding single bonds (40). This is consistent with a valence-bond description in terms of four equivalent resonance structures such as (VI.I), or alternatively in terms of molecular orbital theory (10) with delocalization of six π -electrons to give an aromatic system (VI.II). The isoelectronic species S_2N_2 and Bi_4^{2-} (both with 22 valence electrons) also have square-planar structures (79, 80). The Si_4^{6-} anion, however, has a butterfly structure (VI.III), and has been described as an opened Si_4^{4-} , which is a tetrahedron (64, 81). This Si_4^{6-} anion appears to have a localized bonding system in contrast to the π delocalization observed for S_2N_2 , Bi_4^{2-} and the M_4^{2+} cations.



VI.I



VI.II



VI.III

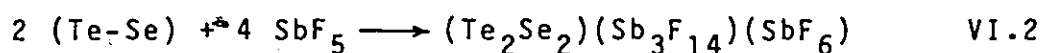
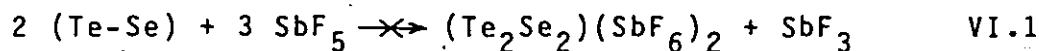
The complete series of $\text{Te}_x\text{Se}_{4-x}^{2+}$ cations have been observed in solution by NMR methods (50, 78) and the two fluoroantimonate salts $(\text{Te}_2\text{Se}_2)(\text{Sb}_3\text{F}_{14})(\text{SbF}_6)$ and $(\text{Te}_{3.3}\text{Se}_{0.7})(\text{Sb}_3\text{F}_{14})(\text{SbF}_6)$, the latter containing a disordered mixture of M_4^{2+} cations, had been incompletely characterized in our laboratory prior to the present work.

VI.2 Preparation of $(\text{Te}_2\text{Se}_2)(\text{Sb}_3\text{F}_{14})(\text{SbF}_6)$.

This compound was prepared using both a 1:1 mixture of selenium and tellurium powders and a 1:1 alloy (kindly provided by Dr. J.E. Vekris) finely-powdered in a mortar. In a typical experiment 1.033 g (5 mmol) of the 1:1 Te-Se alloy was reacted with 2.167 g (10 mmol) of SbF_5 in 30 mL of SO_2 solvent following the procedure outlined in chapter II. There was an immediate reaction producing a red solution, the color of which intensified very considerably on stirring for several hours. The reaction was allowed to proceed, with stirring, for one week. After filtering off a brown mixture of insoluble reaction products the deep blood-red solution was allowed to stand for 48 h at room temperature and a large quantity of black crystals was deposited. These crystals were shown to be $(\text{trans-Te}_2\text{Se}_2)(\text{Sb}_3\text{F}_{14})(\text{SbF}_6)$ by an X-ray crystal structure determination.

When the same procedure was used with the mixture of selenium and tellurium powders a green solution was initially obtained, indicating the formation of Se_8^{2+} . The color

of this solution changed to a blood-red after about 0.5 h. Precession photographs revealed that the resulting crystals were again $(\text{Te}_2\text{Se}_2)(\text{Sb}_3\text{F}_{14})(\text{SbF}_6)$, although the solution colors indicate that the compound was formed by a different route. When less oxidant was used, for example the amount required for reaction VI.1 rather than the stoichiometry used in the present case, reaction VI.2, the crystalline product was $(\text{Te}_2\text{Se}_4)(\text{SbF}_6)_2$ (see section V.2).



VI.3 Preparation of $(\text{Te}_{3.0}\text{Se}_{1.0})(\text{Sb}_3\text{F}_{14})(\text{SbF}_6)$.

Tellurium (1.8163 g, 14.23 mmol) and selenium (0.3747 g, 4.745 mmol) were reacted with SbF_5 (4.108 g, 18.95 mmol) in 30 mL of SO_2 using the procedure described above. A green solution was initially obtained which turned red within a few minutes. After stirring for 3.5 h the solution was filtered and allowed to stand for 24 h. the resulting black crystals were then isolated and their composition was shown to be $(\text{Te}_{3.0}\text{Se}_{1.0})(\text{Sb}_3\text{F}_{14})(\text{SbF}_6)$ by a subsequent X-ray crystal structure determination. The cation in this structure is occupationally disordered as described below. If the same procedure was followed except that a reaction time of one week was allowed, as for $\text{Te}_2\text{Se}_2(\text{Sb}_4\text{F}_{20})$, the crystalline product was $\text{Te}_2\text{Se}_4(\text{SbF}_6)_2$. Insoluble $\text{Te}_6(\text{SbF}_6)_4$ was presumably another major product in the one

week reaction.

VI.4 Attempted Preparation of $(\text{TeSe}_3)(\text{Sb}_3\text{F}_{14})(\text{SbF}_6)$.

When the procedure outlined above was employed except with a Te-Se ratio of 1:3, a deep amber oil resulted for reaction times of both 3.5 h and one week. Only in the latter case were crystals formed from the oil and these proved to be $(\text{Te}_2\text{Se}_4)(\text{Sb}_3\text{F}_{14})(\text{SbF}_6)$ as outlined in section V.3. A subsequent ^{77}Se NMR investigation of the oil, however, demonstrated that the major products were TeSe_3^{2+} (547.2 and 453.4 ppm) and Se_4^{2+} (627.7 ppm) with significant amounts of *cis*- $\text{Te}_2\text{Se}_2^{2+}$ (327.8 ppm) and $\text{Te}_2\text{Se}_4^{2+}$ (-473.6 and -1157.8 ppm) also observed. The ^{77}Se chemical shifts of these species have been well established in oleum (50).

VI.5 Preparation of $(\text{S}_{3.0}\text{Se}_{1.0})_2(\text{Sb}_4\text{F}_{17})(\text{SbF}_6)_3$.

Antimony pentafluoride will oxidize sulfur to S_4^{2+} only under extreme conditions (82, 83). Passmore and coworkers have shown, however, that in the presence of Br_2 or I_2 even the weaker oxidant AsF_5 will readily oxidize S_8 to S_4^{2+} (22). This method of halogen-assisted oxidation was used in the present preparation of a mixed S-Se cation. A trace of Br_2 (0.02 g, 0.1 mmol) was distilled onto a frozen mixture of SbF_5 (6.11 g, 28.2 mmol) and SO_2 (40 mL). Upon thawing, the cold solution was poured onto a mixture of selenium (0.5564 g, 7.047 mmol) and sulfur (0.6799 g, 21.20 mmol) powders. The pale orange solution color of Br_2 was immed-

ately replaced by a deep green and then a deep blue-green color after about 0.25 h. After stirring for 12 h the solution was filtered and allowed to stand for 48 h when a few canary-yellow crystals were observed under the deep blue solution. After 30 days the solution was poured off, leaving a large quantity of pale yellow crystals as well as the few canary-yellow crystals. Precession photographs revealed that the latter crystals were $(\text{Se}_4)(\text{Sb}_9\text{F}_{39})$ (23) while the former were a different compound but most of these crystals were twinned. After photographing about twenty of these crystals one was eventually found with only negligible twinning. A subsequent X-ray crystal structure determination revealed the composition of the pale yellow compound to be $(\text{S}_{3.0}\text{Se}_{1.0})_2(\text{Sb}_4\text{F}_{17})(\text{SbF}_6)_3$. This is the only crystalline compound as yet prepared with a mixed S-Se cation and additionally provides the only example of the $\text{Sb}_4\text{F}_{17}^-$ anion. The cation is occupationally disordered in a similar fashion to $(\text{Te}_{3.0}\text{Se}_{1.0})(\text{Sb}_3\text{F}_{14})(\text{SbF}_6)$, as described below.

VI.6 Occupational Disorder.

$(\text{Te}_{3.0}\text{Se}_{1.0})(\text{Sb}_3\text{F}_{14})(\text{SbF}_6)$: The cation in this structure possesses occupational disorder in that each of the four sites is partially occupied by both tellurium and selenium (see Table VI.1) and the average composition is $\text{Te}_{3.0}\text{Se}_{1.0}^{2+}$, which matches the stoichiometry of the reaction. The population parameters are consistent with a dis-

TABLE VI.1 Occupation of the Four Sites in
the $\text{Te}_{3.0}\text{Se}_{1.0}^{2+}$ and $\text{S}_{3.0}\text{Se}_{1.0}^{2+}$ Cations.^a

Site	$\text{Te}_{3.0}\text{Se}_{1.0}^{2+}$		$\text{S}_{3.0}\text{Se}_{1.0}^{2+}$	
	Te	Se	S	Se
1	0.66	0.34	0.60	0.40
2	0.91	0.09	0.85 [†]	0.15
3	0.60	0.40	0.68	0.32
4	0.85	0.15	0.87	0.13
Total	3.02	0.98	3.00	1.00

(a) Determined by refining the population parameters in the program SHELX (48).

ordered $\text{Te}_3\text{Se}^{2+}$ cation, although the crystallographic evidence does not exclude the possibility that the crystal contains a mixture of some or all of the cations $\text{Te}_x\text{Se}_{4-x}^{2+}$, $x = 0-4$, with the average composition of the mixture being $\text{Te}_{3.0}\text{Se}_{1.0}^{2+}$.

$(\text{S}_{3.0}\text{Se}_{1.0})_2(\text{Sb}_4\text{F}_{17})(\text{SbF}_6)_3$: There are two independent M_4^{2+} cations in this structure but both are situated at inversion centers so that there are only four independent sites. Each site is partially occupied by both sulfur and selenium as outlined in Table VI.1. As was the case for

$(\text{Te}_{3.0}\text{Se}_{1.0})(\text{Sb}_3\text{F}_{14})(\text{SbF}_6)$, the resulting $\text{S}_{3.0}\text{Se}_{1.0}^{2+}$ cation fits the stoichiometry of the reagents used in its preparation and could result from either a disordered S_3Se^{2+} cation or a mixture of different cations. Subsequent ^{77}Se and ^{125}Te NMR investigations, however, indicated that the latter hypothesis is true in both cases (sections VI.7 and VI.9).

VI.7 Selenium-77 AND ^{125}Te NMR OF $\text{Te}_x\text{Se}_{4-x}^{2+}$.

$(\text{Te}_2\text{Se}_2)(\text{Sb}_3\text{F}_{14})(\text{SbF}_6)$: When dissolved in 30% oleum this compound gave a ^{77}Se NMR spectrum consisting of one major resonance surrounded by a satellite doublet of total relative intensity 12%. This corresponds to coupling to two equivalent, naturally abundant tellurium atoms (see Table IV.4), as would be expected for trans- $\text{Te}_2\text{Se}_2^{2+}$. The chemical shift (356.8 ppm) and coupling constant (545 Hz) are consistent with those previously assigned for trans- $\text{Te}_2\text{Se}_2^{2+}$.

(see Table VI.2).

$(\text{Te}_{3.0}\text{Se}_{1.0})(\text{Sb}_3\text{F}_{14})(\text{SbF}_6)$: The ^{125}Te NMR spectrum of $(\text{Te}_{3.0}\text{Se}_{1.0})(\text{Sb}_3\text{F}_{14})(\text{SbF}_6)$ dissolved in 100% H_2SO_4 is presented in Figure VI.1. As described in section VI.6 above, the composition of this compound remained uncertain after the X-ray crystal structure analysis. It could not be determined whether the cation consisted of a disordered $\text{Te}_3\text{Se}^{2+}$ cation or a disordered mixture of $\text{Te}_x\text{Se}_{4-x}^{2+}$ cations of average composition $\text{Te}_{3.0}\text{Se}_{1.0}^{2+}$. Figure VI.1 indicates that the latter hypothesis is in fact the correct one as the cations $\text{trans-Te}_2\text{Se}_2^{2+}$, $\text{Te}_3\text{Se}^{2+}$ and Te_4^{2+} are identified by their chemical shift values (see Table VI.2). The intensity of the $\text{Te}_2\text{Se}_2^{2+}$ resonance is roughly half that of the Te_4^{2+} resonance indicating that since there are twice as many tellurium atoms in Te_4^{2+} , the two species are present in roughly equal concentrations. No other tellurium containing $\text{Te}_x\text{Se}_{4-x}^{2+}$ cations were observed and a ^{77}Se NMR investigation revealed no Se_4^{2+} . The average composition of the mixture of the cations is then $\text{Te}_{3.0}\text{Se}_{1.0}^{2+}$, in good agreement with the structure determination.

To confirm that the product was not a mixture of crystals of separate fluoroantimonate salts of Te_4^{2+} , $\text{Te}_2\text{Se}_2^{2+}$ and $\text{Te}_3\text{Se}^{2+}$ (disordered), the ^{125}Te NMR spectrum of a 100% H_2SO_4 solution of a single crystal from the same sample was obtained. The signal-to-noise ratio (S/N) was

TABLE VI.2 Chemical Shifts and Coupling Constants for the $\text{Te}_x\text{Se}_{4-x}^{2+}$ Cations in Various Solvents:

CATION	SOLVENT	δ (ppm) ^a		J (Hz)			REF
		¹²⁵ Te	⁷⁷ Se	⁷⁷ Se- ⁷⁷ Se	⁷⁷ Se- ¹²⁵ Te	¹²³ Te- ¹²⁵ Te	
Se_4^{2+}	68% oleum		636.7 ^b				50
	30% oleum		645.7				50
	SO_2		633.3				c
TeSe_3^{2+}	68% oleum	2641	455.2, 566.3 (1) : (2)		757 ^d		50
	65% oleum	2642 ^b			764 ^d , 581 ^e		78
	30% oleum	2632	444.8, 592.2	188	750 ^d , 597 ^e		50
	SO_2		453.4, 547.2				c
cis- $\text{Te}_2\text{Se}_2^{2+}$	68% oleum	2538 ^b	338.2 ^b		470 ^d , 195 ^e		50
	65% oleum	2552			457 ^d , 200 ^e		78
	AsF_3	2541					c
	SO_2		327.8				c
trans- $\text{Te}_2\text{Se}_2^{2+}$	68% oleum	2413 ^b	362.2		531		50
	65% oleum	2418 ^b			330		78
	30% oleum	2391	360.9		550		50
		2399	356.8		545		c
	100% H_2SO_4	2376	391.1		554		50
		2380			541		c
	AsF_3	2459	312.5		484		c
$\text{Te}_3\text{Se}^{2+}$	68% oleum	2196, 2292 (1) : (2)	129.6		207 ^d		50
	30% oleum	2197, 2293					c
	100% H_2SO_4	2221, 2292					c
	AsF_3	2161, 2314	111.2		165 ^d		c
	SO_2	2186, 2296				1347 930	78
Te_4^{2+}	68% oleum	1912					50
	65% oleum	1934 ^b				676 ^d , 602 ^e	78
	30% oleum	2100					50
		1926 ^b					c
	100% H_2SO_4	1971 ^b				680 ^{d,g} , 604 ^e	50
		1948					c
	AsF_3	1912				534 ^d , 743 ^e	c
	SO_2	1897					c
		1882 ^h				680 ^{h,i}	c

- (a) With respect to saturated aqueous $(\text{HO})_6\text{Te}$ and H_2SeO_3 . All samples run at ambient temp. unless otherwise noted.
 (b) Mean value. (c) This work. (d) cis-. (e) trans-. (f) Calculated value based on observed ^{123}Te - ^{125}Te coupling.
 (g) Misprinted in reference. (h) 200 K. (i) cis- and trans- not resolved.

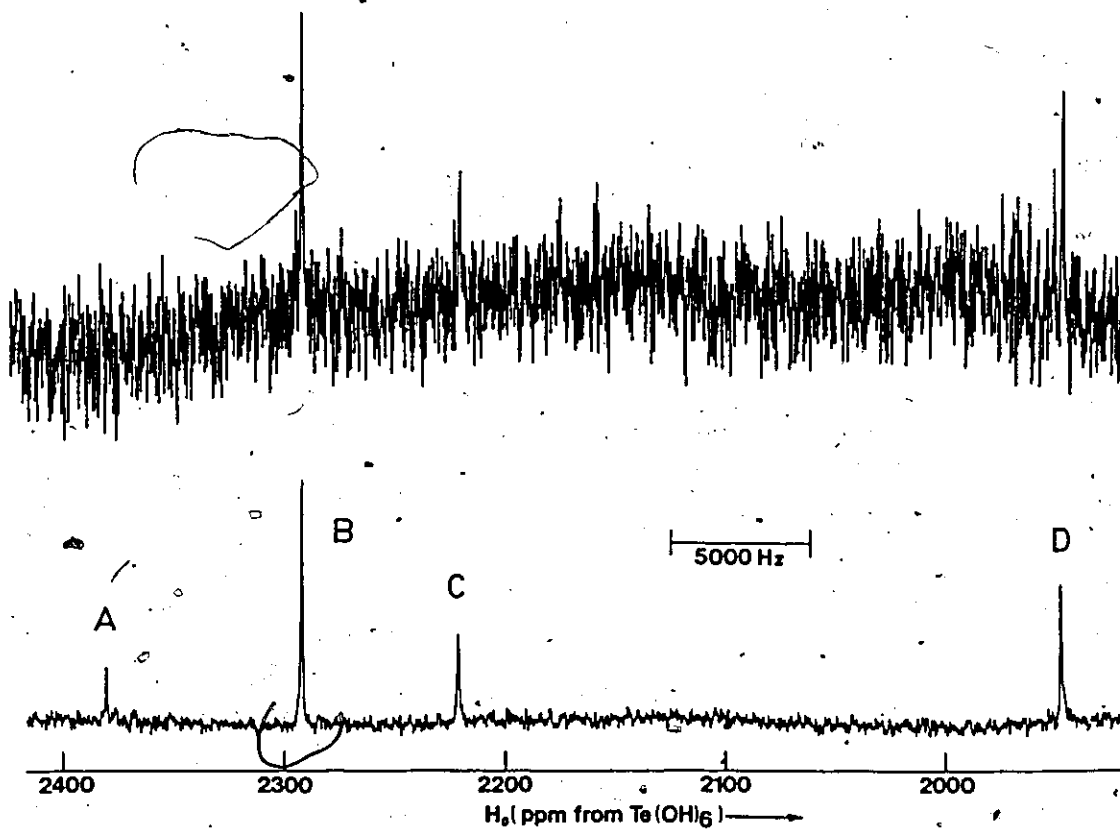


FIGURE VI.1 ^{125}Te NMR spectrum of $\text{Te}_{3.0}\text{Se}_{1.0}(\text{Sb}_4\text{F}_{20})$ dissolved in 100% H_2SO_4 . Lower trace; bulk crystalline sample, 78.97 MHz; 0.02 m; 20,000 scans; 7.6 Hz/pt. (A) $\text{trans-Te}_2\text{Se}_2^{2+}$, (B) and (C) $\text{Te}_3\text{Se}^{2+}$, (D) Te_4^{2+} . Upper trace; a single crystal, $7. \times 10^{-4}$ m, 390,000 scans.

understandably poor as the concentration was only 7×10^{-4} M and the natural abundance sensitivity of ^{125}Te relative to ^1H is 2.20×10^{-3} . After an accumulation of 390,000 scans (acquisition time = 12.5 h) the resonance due to trans- $\text{Te}_2\text{Se}_2^{2+}$, the weakest resonance observed for the bulk sample, could not be discerned with certainty over the noise level, but resonances for the species $\text{Te}_3\text{Se}^{2+}$ and Te_4^{2+} were clearly observed and in approximately the same ratio as in the bulk sample (Fig. VI.1). It appears clear then that the cation of this compound consists of a mixture of $\text{Te}_x\text{Se}_{4-x}^{2+}$ cations, with $\text{Te}_3\text{Se}^{2+}$, Te_4^{2+} and trans- $\text{Te}_2\text{Se}_2^{2+}$ being the major constituents.

The ^{125}Te NMR spectrum of $(\text{Te}_{3.0}\text{Se}_{1.0})(\text{Sb}_3\text{F}_{14})(\text{SbF}_6)$ dissolved in AsF_3 is presented in Figure VI.2. The spectrum is similar to that observed in 100% H_2SO_4 but the smaller half-width of the resonances in AsF_3 (30 Hz v.s. 50-55 Hz in 100% H_2SO_4) gives a better S/N and the satellite resonances from natural abundance couplings are observed. These couplings are of interest because their magnitudes are substantially different from those previously recorded in H_2SO_4 or oleum (see Table VI.2). The ^{77}Se - ^{125}Te coupling in trans- $\text{Te}_2\text{Se}_2^{2+}$ (484 Hz) is 61 Hz less than that in 30% oleum. The related ^{77}Se - ^{125}Te coupling in $\text{Te}_3\text{Se}^{2+}$ is only 165 Hz, substantially less than that observed in oleum, (207 Hz) and roughly one third the magnitude of the ^{77}Se - ^{125}Te coupling in trans- $\text{Te}_2\text{Se}_2^{2+}$. The ^{125}Te - ^{125}Te coupling in $\text{Te}_3\text{Se}^{2+}$ is

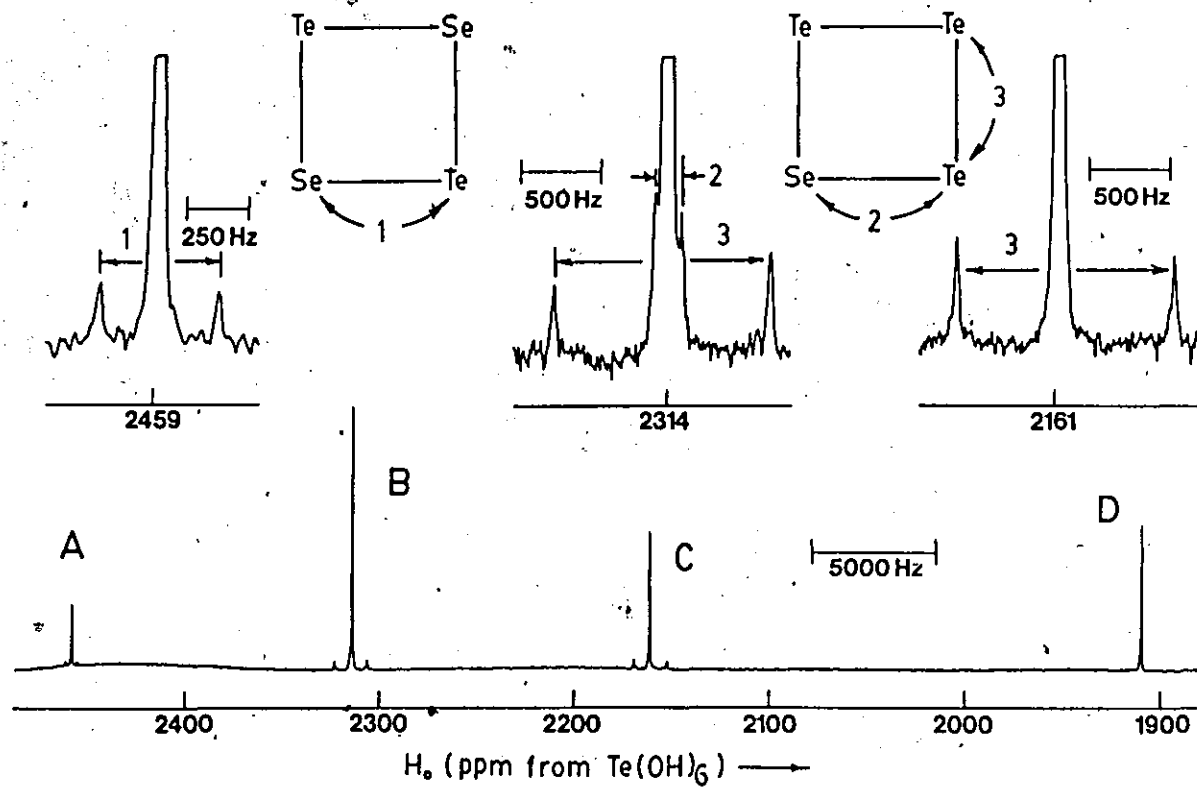


FIGURE VI. 2 ^{125}Te NMR spectrum of $\text{Te}_{3.0}\text{Se}_{1.0}(\text{Sb}_4\text{F}_{20})$ dissolved in AsF_3 (0.01 m; 120,000 scans; 10.2 Hz/pt; 78.97 MHz). (A)-(D) as in Fig. VI.1. Expanded spectra (130,000 scans; 5.5 Hz/pt) indicate ^{77}Se - ^{125}Te (1) and (2), and ^{125}Te - ^{125}Te (3) couplings.

1347 Hz, which is conversely very large with respect to that observed in SO_2 and the related ^{125}Te - ^{125}Te coupling (calculated from the observed ^{123}Te - ^{125}Te satellites) for Te_4^{2+} in AsF_3 (see Table VI.2). This coupling in $\text{Te}_3\text{Se}^{2+}$ is so large that a second order effect is observed. The satellite doublets are not symmetrical about the central uncoupled resonances and the inner lines of the doublets are more intense than the outer lines (Fig. VI.2). The large variations in these coupling constants in different solvents may be related to the electron donor properties of the solvents. Donation of electron density from the solvent to the cation presumably has some effect on the electronic configuration of the cation and therefore also affects the spin-spin couplings. A similar effect is observed in the solid state, where the dimensions of the M_4^{2+} cations are very much dependent upon the nature of their counter anions and this has been related to the electron donor properties of the counter anions (section VI.12).

The better S/N in AsF_3 additionally allows for a more rigorous check on the presence of small amounts of other $\text{Te}_x\text{Se}_{4-x}^{2+}$ cations in the structure. A small quantity of cis- $\text{Te}_2\text{Se}_2^{2+}$ was observed (2541 ppm), with the intensity of this peak on the order of one of the satellite peaks of trans- $\text{Te}_2\text{Se}_2^{2+}$. No TeSe_3^{2+} was observed in the ^{125}Te NMR spectrum, however, and a subsequent ^{77}Se NMR investigation

revealed only the expected resonances for $\text{Te}_3\text{Se}^{2+}$ and trans- $\text{Te}_2\text{Se}_2^{2+}$ (Table VI.2).

$\text{Te}_4(\text{SbF}_6)_2$: This compound formed as large black crystals from a reaction of a Te-S mixture with SbF_5 in SO_2 as described in section V.6, and proved extremely soluble in AsF_3 , allowing for a S/N good enough to distinguish the weak natural abundance ^{123}Te - ^{125}Te couplings in the ^{125}Te NMR spectrum (Fig. VI.3). Tellurium-123 has a natural abundance of only 0.87% and one would expect satellites of 1.8% and 0.9% total relative intensity to the central peak for the cis- and trans- couplings respectively (see Table IV.4). The observed satellites are 1.6% and 0.8% and demonstrate that the cis- (directly bonded) coupling of 534 Hz is actually less than the trans- (long range) coupling of 743 Hz. The opposite is observed in 100% H_2SO_4 (Table VI.2) where the cis- coupling is approximately 150 Hz larger than that observed here and the trans- coupling is 150 Hz less. The cis- and trans- couplings were not resolved in SO_2 (Fig. VI.4). Shoulders were observed, however, on the inner sides of the broad satellite resonances. These shoulders probably result from the trans- coupling since the intensity of this satellite doublet should be half that of the cis- doublet. The trans- coupling constant is apparently slightly smaller than the cis- coupling constant in SO_2 , as was observed in 100% H_2SO_4 . In all cases the two-bond trans- coupling seems unusually large compared to the cis- coupling. A large

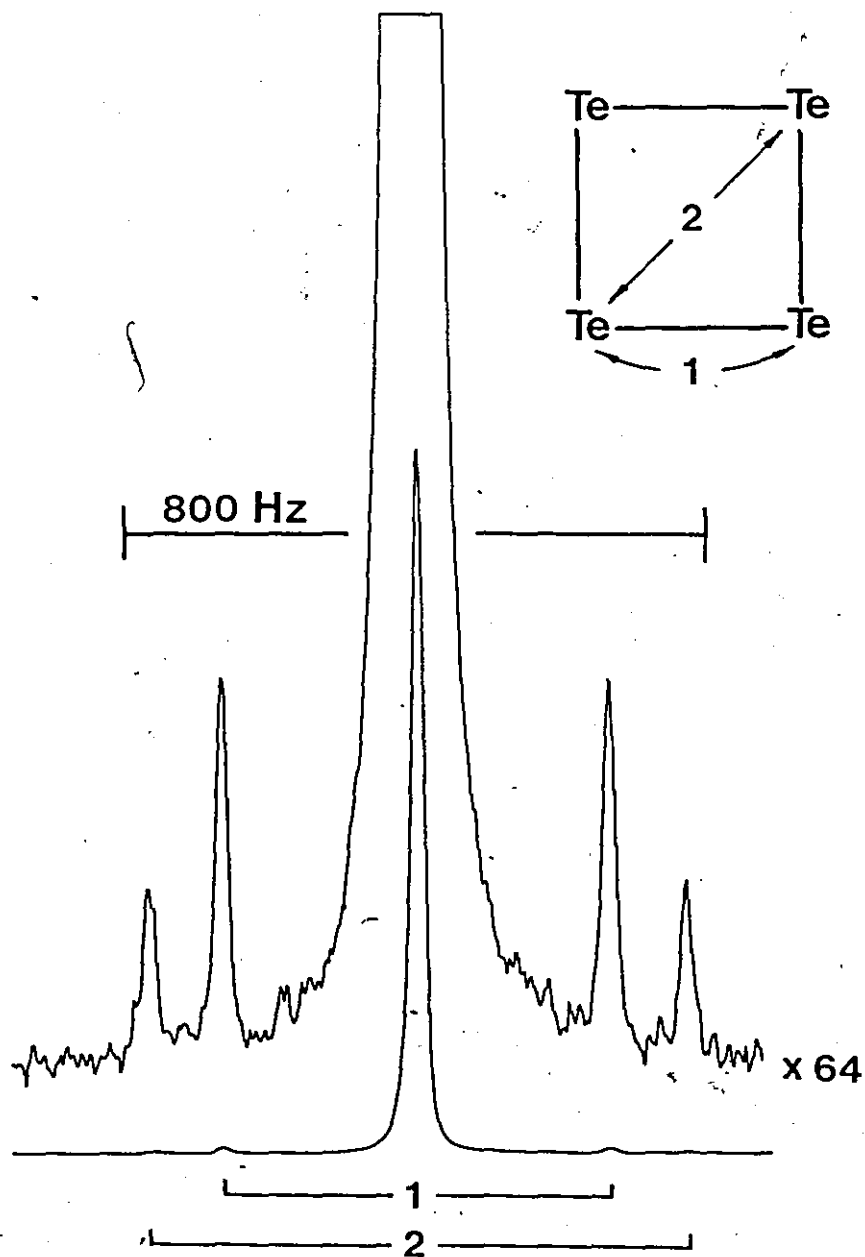


FIGURE VI.3 ^{125}Te NMR spectrum of $\text{Te}_4(\text{SbF}_6)_2$ dissolved in AsF_3 (78.97 MHz; 0.02 m; 160,000 scans; 3.0 Hz/pt).

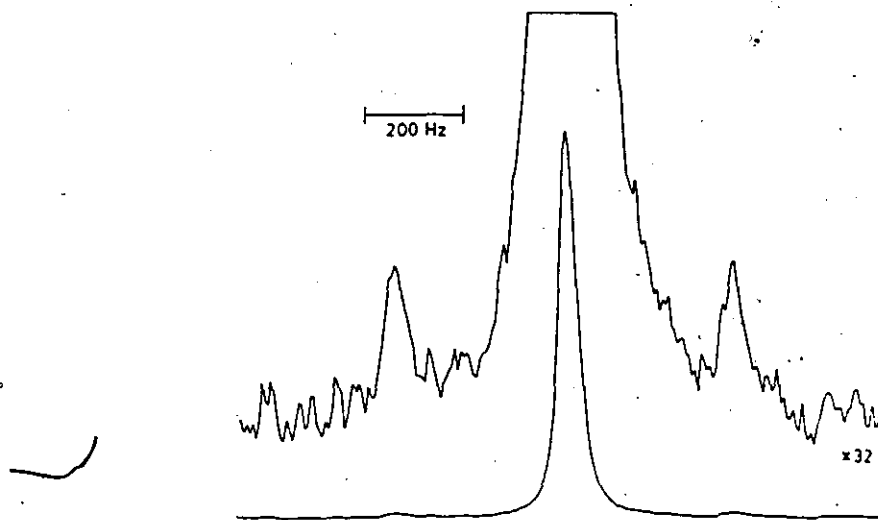


FIGURE VI.4 ^{125}Te NMR spectrum of $\text{Te}_4(\text{SbF}_6)_2$ dissolved in SO_2 at 200 K (sat'd sol'n; 49,000 scans; 6.1 Hz/pt; 78.97 MHz). cis- and trans- ^{123}Te - ^{125}Te couplings are not resolved.

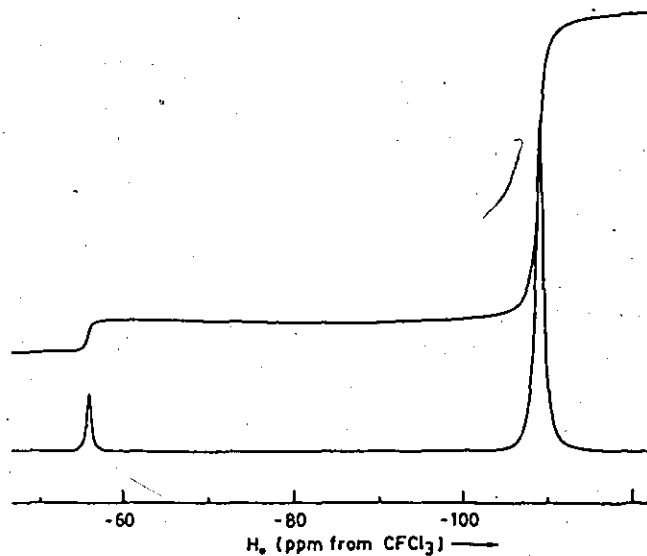


FIGURE VI.5 ^{19}F NMR spectrum of $\text{Te}_2\text{Se}_2(\text{Sb}_3\text{F}_{14})(\text{SbF}_6)$ dissolved in SO_2 at 200 K (235.36 MHz; 4800 scans; 3.0 Hz/pt).

trans-coupling has also been observed for Te_6^{4+} in 30% oleum (50) where the coupling across a rectangular face of the trigonal prism is of roughly the same magnitude as the coupling along a triangular face.

VI.8 Fluorine-19 NMR of $(\text{Te}_2\text{Se}_2)(\text{Sb}_3\text{F}_{14})(\text{SbF}_6)$.

A crystalline sample of $(\text{Te}_2\text{Se}_2)(\text{Sb}_3\text{F}_{14})(\text{SbF}_6)$ was ground with a mortar and pestle to a fine powder and dissolved in SO_2 close to the freezing point of the solvent. The sample was then placed in the probe of the spectrometer which had previously been cooled to 200 K. After allowing 15 min for the sample to thermally equilibrate the ^{19}F NMR spectrum was run (Fig. VI.5). Fluorine exchange was essentially stopped at this low temperature and two distinct fluorine resonances were observed at -56 and -109 ppm with respect to external CFCl_3 . The ratio of the integrals of these two resonances is 1:10. If the $\text{Sb}_3\text{F}_{14}^-$ anion dissociates to SbF_2^+ and two SbF_6^- ions in solution, the additional SbF_6^- ion in the $(\text{Te}_2\text{Se}_2)(\text{Sb}_3\text{F}_{14})(\text{SbF}_6)$ structure then gives a total of eighteen fluorine atoms on Sb(V) compared to the two fluorine atoms on Sb(III), or a 1:9 ratio, very close to that observed. If the $\text{Sb}_3\text{F}_{14}^-$ anion were retained in solution a larger number of fluorine resonances would be expected as well as substantial ^{19}F - ^{19}F coupling. The anion could dissociate into SbF_3 , SbF_5 and SbF_6^- fragments, but if this were the case separate SbF_5 and

SbF_6^- resonances would be expected at this temperature, since fluorine exchange is virtually stopped, and the relative intensity of the Sb(III) peak would be larger. It would appear then that distinct SbF_2^+ and SbF_6^- ions are present in solution and only form the $\text{Sb}_3\text{F}_{14}^-$ anion in the solid state.

VI.9 Selenium-77 NMR of $\text{S}_x\text{Se}_{4-x}^{2+}$.

Unlike $(\text{Te}_{3.0}\text{Se}_{1.0})(\text{Sb}_3\text{F}_{14})(\text{SbF}_6)$, the mixed S-Se compound $(\text{S}_{3.0}\text{Se}_{1.0})_2(\text{Sb}_4\text{F}_{17})(\text{SbF}_6)_3$ proved to be only sparingly soluble in AsF_3 , almost totally insoluble in SO_2 , and reacted with 100% H_2SO_4 . No detailed investigation of the nature of the cation could be carried out using ^{77}Se NMR, although the ^{77}Se NMR spectrum in AsF_3 after 250,000 scans consisted of five distinct resonances (635.7, 646.4, 671.3, 726.4, and 728.2 ppm with relative intensities 1:2:1:4:1 respectively) indicating that several of the $\text{S}_x\text{Se}_{4-x}^{2+}$ species were present. The S/N was too poor for any ^{77}Se - ^{77}Se couplings to be observed.

A series of mixtures of $\text{S}_x\text{Se}_{4-x}^{2+}$ cations were prepared in SO_2 by reacting AsF_5 and a trace of bromine (see section VI.5) with various stoichiometries of sulfur and selenium powders. The ^{77}Se NMR spectrum of a 1:1 mixture is given in Figure VI.6. The chemical shifts and intensities for this and other mixtures are listed in Table VI.3. The observed resonances are in the same region as those observed

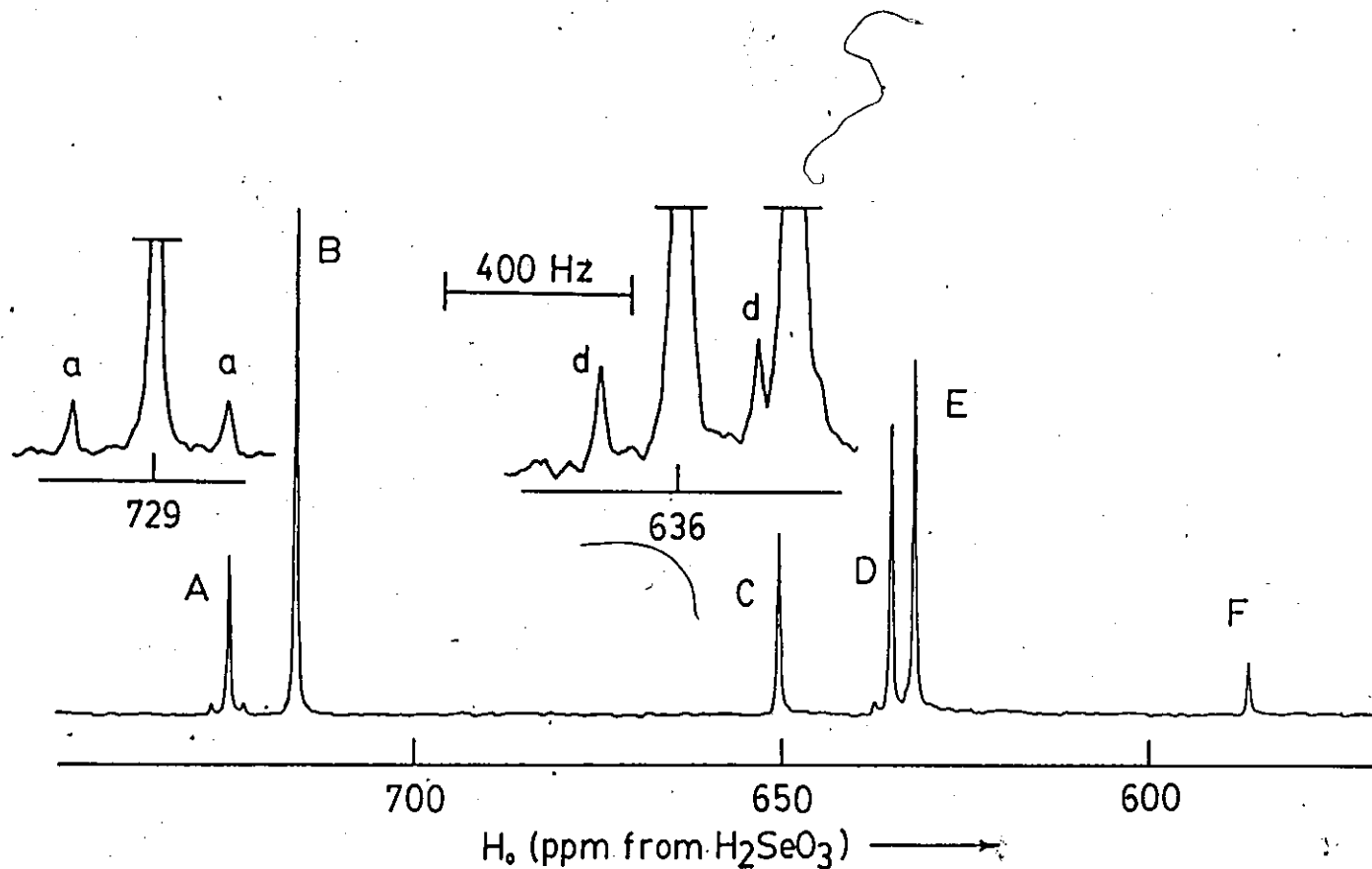


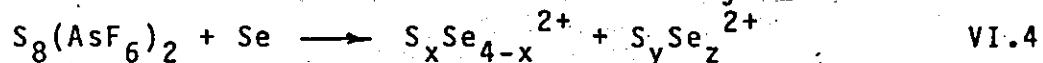
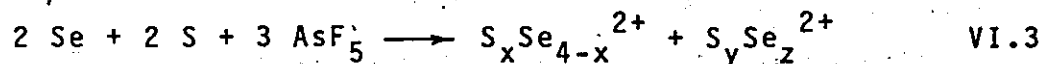
FIGURE VI.6 ^{77}Se NMR spectrum for the reaction of a 1:1 Se-S mixture with AsF_5 and a trace of bromine in SO_2 (0.0542 g S; 0.1325 g Se; 0.57 g AsF_5 ; 3 mL SO_2 ; 76.41 MHz; 5000 scans; 6.1 Hz/pt). (A) and (D) SSe_3^{2+} , (B) $\text{cis-S}_2\text{Se}_2^{2+}$, (C) S_3Se^{2+} , (E) Se_4^{2+} , (F) $\text{trans-S}_2\text{Se}_2^{2+}$. Expanded spectra show ^{77}Se - ^{77}Se coupling in SSe_3^{2+} .

for $(S_{3.0}Se_{1.0})_2(Sb_4F_{17})(SbF_6)_3$ dissolved in AsF_3 and the Raman spectra of the solutions are consistent with the formation of $S_xSe_{4-x}^{2+}$ cations (section VI.10). The ^{125}Te and ^{77}Se chemical shifts of the $Te_xSe_{4-x}^{2+}$ cations follow a simple trend based on their percentage composition of tellurium or selenium. Since selenium is more electronegative than tellurium (57), the greater the selenium content of the cation the more deshielded the tellurium or selenium environments are, and this is reflected in a gradual shift of both the ^{77}Se and ^{125}Te resonances to higher frequency (Table VI.2). Sulfur and selenium have roughly the same electronegativity, however (57), and not all of the $S_xSe_{4-x}^{2+}$ resonances can be assigned unambiguously. The resonance at 633 ppm is also observed when $Se_4(AsF_6)_2$ alone is dissolved in SO_2 and can be assigned to Se_4^{2+} . Published chemical shifts for Se_4^{2+} in oleum range from 636 to 646 ppm (50). Two resonances, at 636 and 729 ppm, are observed in a ratio of 2:1 with satellite doublets about each of them. The only $S_xSe_{4-x}^{2+}$ cation expected to display coupling is SSe_3^{2+} , which would also be expected to give two resonances in a ratio of 2:1, as observed. The satellite doublets are of 8.8% and 17.5% relative intensity for the large and the small resonance respectively. The expected relative intensities for coupling to one and two equivalent, natural abundance selenium nuclei, as in SSe_3^{2+} , are 8.2 and 16.3%

respectively (Table IV.4). The two resonances at 636 and 729 ppm can then be assigned to $S\text{Se}_3^{2+}$. The ^{77}Se - ^{77}Se coupling (336 Hz) is considerably larger than that observed for TeSe_3^{2+} in 30% oleum (188 Hz, see Table VI.2). The resonance at 651 ppm grows the most dramatically upon increasing the S:Se ratio of the reactants (Table VI.3) and is presumably therefore due to the sulfur-rich $S_3\text{Se}^{2+}$ cation. The relative intensity of the remaining two resonances is fairly constant for all of the mixtures, as would be expected for the two $S_2\text{Se}_2^{2+}$ cations. In the case of $\text{Te}_2\text{Se}_2^{2+}$ the cis-cation is usually observed in higher concentration than the trans- (see for example sections IV.2 and VI.4, and ref. (78)). For this reason the more intense resonance at 720 ppm can be tentatively assigned to cis- $S_2\text{Se}_2^{2+}$ and the resonance at 587 ppm to trans- $S_2\text{Se}_2^{2+}$. Using the assignments as described above one observes that the three highest frequency resonances (729, 720 and 651 ppm) have sulfur trans- to the selenium nucleus being observed; while for the three lower frequency resonances (636, 633 and 587 ppm) the trans- atom is selenium. In both of these groups of three resonances one of the three is of substantially lower frequency than the remaining two and the selenium environment corresponding to this resonance is cis- to two sulfur atoms. The remaining two resonances in each group have approximately equal chemical shifts. These selenium environments are cis- to one selenium and to one sulfur atom. These consist-

encies in the selenium environments lend some support to the above chemical shift assignments.

Although AsF_5 apparently does not oxidize sulfur to S_4^{2+} in the absence of halogen "catalysts" (see section VI.5 and ref. (22, 83)), mixed $\text{S}_x\text{Se}_{4-x}^{2+}$ cations were observed in the ^{77}Se NMR spectrum of the solution resulting from reaction VI.3, where no halogen was added to assist the reaction. Additional resonances were observed (Fig. VI.7) which probably resulted from other mixed Se-S cations since the resonances do not correspond to any of the known selenium homopolyatomic cations. Essentially the same product distribution was obtained in the reaction of S_8^{2+} with selenium (reaction VI.4).



It has been reported that Te_4^{2+} and Se_4^{2+} do not scramble to give mixed, square-planar species in solution (50). When $\text{Se}_4(\text{AsF}_6)_2$ and $\text{S}_4(\text{AsF}_6)_2$ were mixed in equal proportions in SO_2 solution, the ^{77}Se NMR spectrum revealed only Se_4^{2+} after 2 h at room temperature. After two weeks, however, the complete range of $\text{S}_4\text{Se}_{4-x}^{2+}$ cations was observed, with approximately the same product distribution as in Figure VI.6. The different behaviour of these pairs of cations is related to the electropositive nature of tellurium. The Se_4^{2+} cation can readily oxidize Te_4^{2+} to Te_6^{4+} and

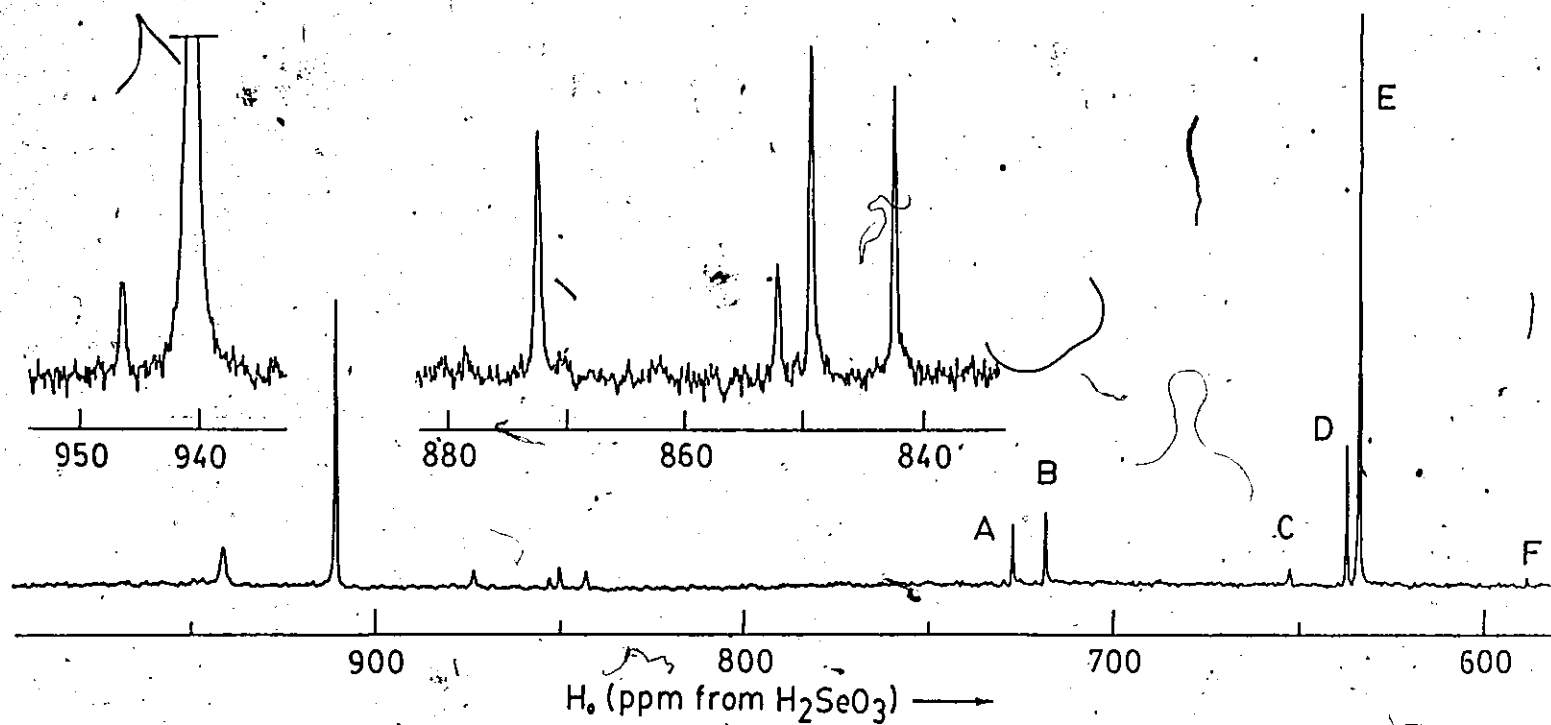


FIGURE VI.7 ^{77}Se NMR spectrum of the solution resulting from reaction VI.3 (0.2213 g Se; 0.0914 g S; 0.715 g AsF_5 ; 3 mL SO_2 ; 76.41 MHz; 7100 scans; 6.1 Hz/pt). (A)-(F) as in Fig. VI.6. Expanded spectra, 150,000 scans.

oxidation-reduction occurs rather than scrambling. Although S_4^{2+} is similarly a stronger oxidant than Se_4^{2+} , no polyatomic cation of selenium is known with a higher oxidation state than in Se_4^{2+} and oxidation-reduction is therefore unlikely in this mixture.

Spin-lattice relaxation time (T_1) measurements were carried out for the five most intense lines in Figure VI.6 and the results are presented in Figure VI.8. The average T_1 value is 0.38 s with the unique selenium atom of SSe_3^{2+} having the lowest observed value, 0.34 s, and the other selenium environment of this cation having the highest value, 0.43 s. Previous ^{77}Se T_1 values of 5-10 s for aqueous solutions of Na_2SeO_3 and Na_2SeO_4 , and 0.3-1.4 s for aqueous solutions of $NaHSeO_3$ and H_2SeO_3 have been reported (84). The selenium atoms in the M_4^{2+} ions are comparatively naked with respect to those buried in SeO_3^{2-} or SeO_4^{2-} ions and the T_1 's are then relatively short, which allows for rapid pulsing and accumulation of data. Another recent ^{77}Se relaxation time study reports T_1 values ranging from 0.7 s for H_2Se to 31 s for $(C_6H_5CH_2Se)_2$ and discusses the likely relaxation mechanisms (85).

VI.10 Raman Spectra.

$(Te_{3.0}Se_{1.0})(Sb_3F_{14})(SbF_6)$: The Raman spectra of this compound as a solid and in AsF_3 solution are presented in Figure VI.9. The pairs of peaks at 268 and 135 cm^{-1} and 217

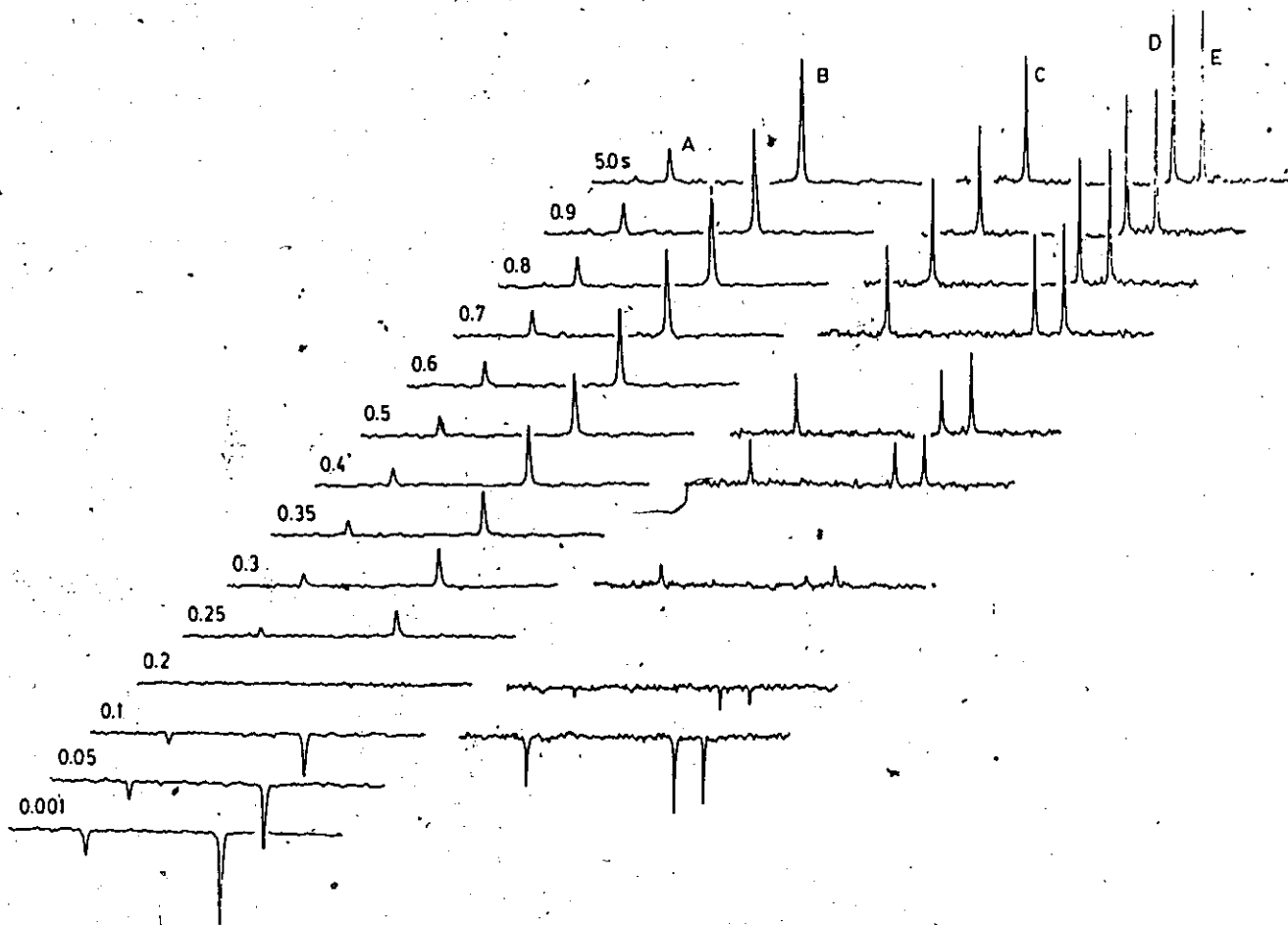


FIGURE VI.8 ^{77}Se T_1 measurements for the $\text{S}_x\text{Se}_{4-x}^{2+}$ cations ($x = 0-3$).
 (A)-(E) as in Fig. VI.6: (A) 0.34 s, (B) 0.39 s, (C) 0.36 s, (D) 0.43 s,
 (E) 0.39 s.

TABLE VI.3 Intensity in ^{77}Se NMR Spectra of $\text{S}_x\text{Se}_{4-x}^{2+}$ as a Function of Reactants Ratio.

RATIO ^a		CHEMICAL SHIFT (ppm)						I N T E N S I T Y
x	y	729 ^b	720	651	636 ^b	633 ^c	587	
1	: 3	9	22	9	19	40	2	
2	: 2	10	32	12	19	24	3	
3	: 1	5	34	41	6	10	3	
3.7	: 0.3	-	11	82	-	7	-	

(a) All reactions are $x \text{S} + y \text{Se} + 4 \text{AsF}_5 + \text{Br}_2$ (trace) in SO_2 . (b) SSe_3^{2+} . (c) Se_4^{2+} .

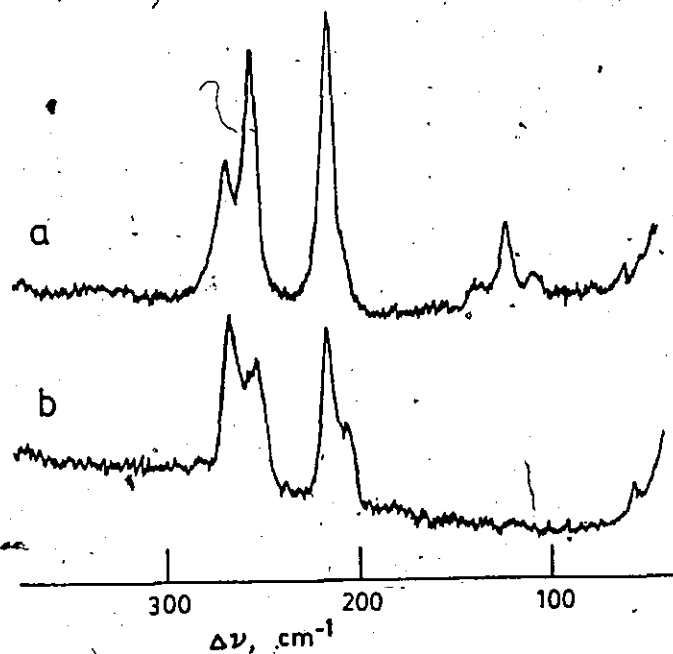


FIGURE VI.9 Raman spectrum (6328 Å) of $\text{Te}_{3.0}\text{Se}_{1.0}(\text{Sb}_3\text{F}_{14})(\text{SbF}_6)$. a) AsF_3 solution (sample described in Fig. VI.2); b) solid, 77 K.

and 105 cm^{-1} have been identified as belonging to $\text{trans-Te}_2\text{Se}_2^{2+}$ and Te_4^{2+} respectively (76, 77). These species are observed in the ^{125}Te NMR spectra of the same sample (section VI.7). The remaining peaks at 254, 209 and 120 cm^{-1} then presumably result from the $\text{Te}_3\text{Se}^{2+}$ cation, which has C_{2v} symmetry and six vibrational modes ($3A_1$, B_1 and $2B_2$), all of which are Raman and infrared active. Some of these modes are probably very close in energy and the Raman bands presumably overlap with each other or with the $\text{Te}_2\text{Se}_2^{2+}$ and Te_4^{2+} bands.

$S_x\text{Se}_{4-x}^{2+}$: The Raman spectra for compounds of nominal composition $(S_{2.0}\text{Se}_{2.0})(\text{AsF}_6)_2$ and $(S_{3.0}\text{Se}_{1.0})(\text{AsF}_6)_2$ in SO_2 solution and as the solid respectively are given in Figure VI.10. The signal-to-noise ratio is better for the solution spectrum as the solid decomposed markedly in the laser beam even at 77 K. Three regions can be distinguished: 1) S-S stretches at $610\text{-}500 \text{ cm}^{-1}$, 2) S-Se stretches at $490\text{-}400 \text{ cm}^{-1}$ and 3) Se-Se stretches at $350\text{-}300 \text{ cm}^{-1}$. As expected, the intensities of the bands in the Se-Se region increase relative to those in the S-S region as the Se:S ratio increases from 1:3 (Figure VI.10b) to 1:1 (Figure VI.10a). Three similar divisions are observed in the Raman spectra of disordered $S_x\text{Se}_{8-x}$ rings, although the peaks are all shifted to lower frequency for $S_x\text{Se}_{8-x}$, reflecting the lower bond order (86). The Raman spectrum of $(S_{3.0}\text{Se}_{1.0})_2(\text{Sb}_7\text{F}_{35})$ is very complex since the $\text{Sb}_4\text{F}_{17}^-$ anion has numerous bands in

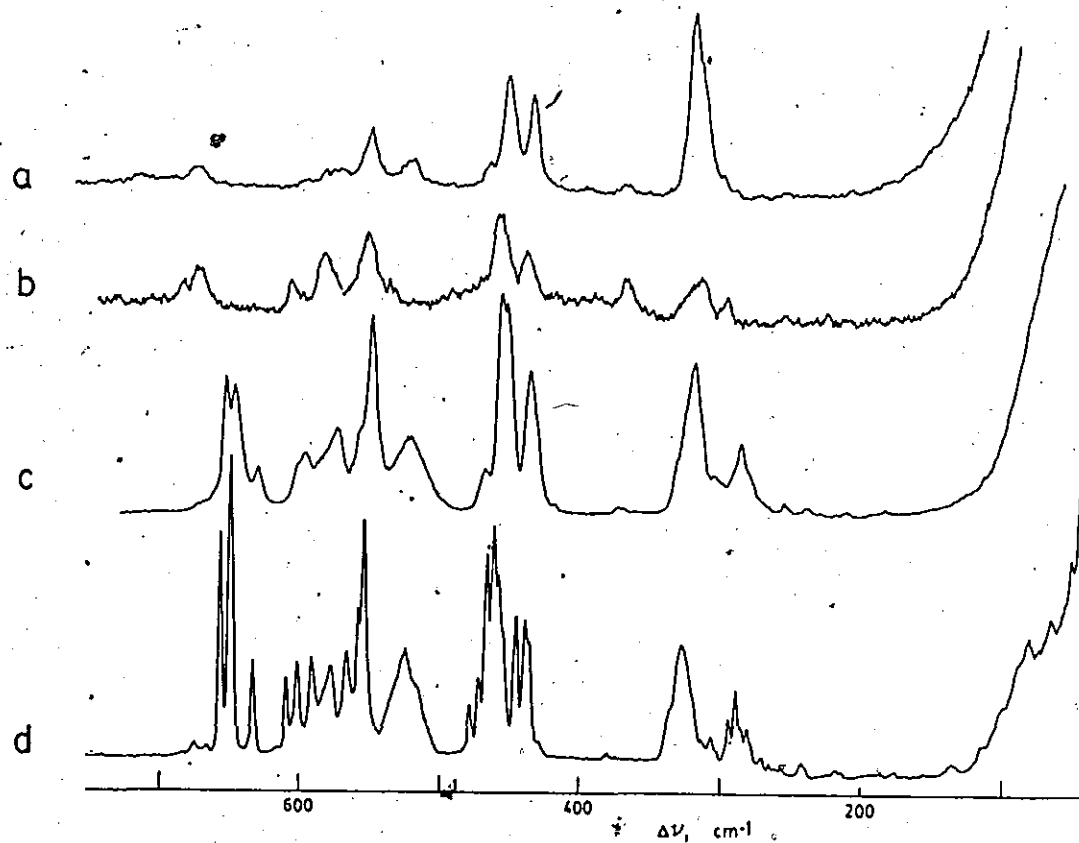


FIGURE VI.10 Raman spectra (5145 Å) of (a) the $(S_{2.0}Se_{2.0})(AsF_6)_2$ solution of Fig. VI.6, (b) solid $(S_{3.0}Se_{1.0})(AsF_6)_2$, spinning sample, 77 K, (c) and (d) powdered crystals of $(S_{3.0}Se_{1.0})_2(Sb_4F_{17})(SbF_6)_3$ at 295 K and 77 K.

the same region as those of $S_xSe_{4-x}^{2+}$ (Fig. VI.10c). The anion bands sharpen considerably upon cooling (Fig. VI.10d), however, allowing many of them to be distinguished.

VI.11 Geometry About Sb(III) in $Sb_3F_{14}^-$ and $Sb_4F_{17}^-$.

The $Sb_3F_{14}^-$ anion (Fig. VI.11) has one Sb(III) and two Sb(V) atoms and can alternatively be viewed as one SbF_2^+ and two SbF_6^- ions (see section VI.8). The primary geometry of the Sb(III) atom can be described as trigonal-bipyramidal, AX_4E , where the lone pair and the two terminal fluorine atoms occupy the equatorial plane and the bridging fluorine atoms are axial (61). Secondary bonding is frequently apparent in structures like this where there is a "hole" in the primary coordination sphere which corresponds to the approximate space occupied by the lone pair. These secondary bonds are presumed to be nucleophilic in nature and since the lone pair is less effective in screening the nucleus than is a coordinated atom the secondary bonds tend to form in the general direction of the space occupied by the lone pair while avoiding the direction of its maximum electron density and hence serve to further delineate its position. The directions of these contacts can be further described as either capping the faces or bridging the edges of the polyhedron describing the primary bonds and the lone pair, and preferentially those faces that contain the lone pair as a vertex (87). For three primary bonds the result-

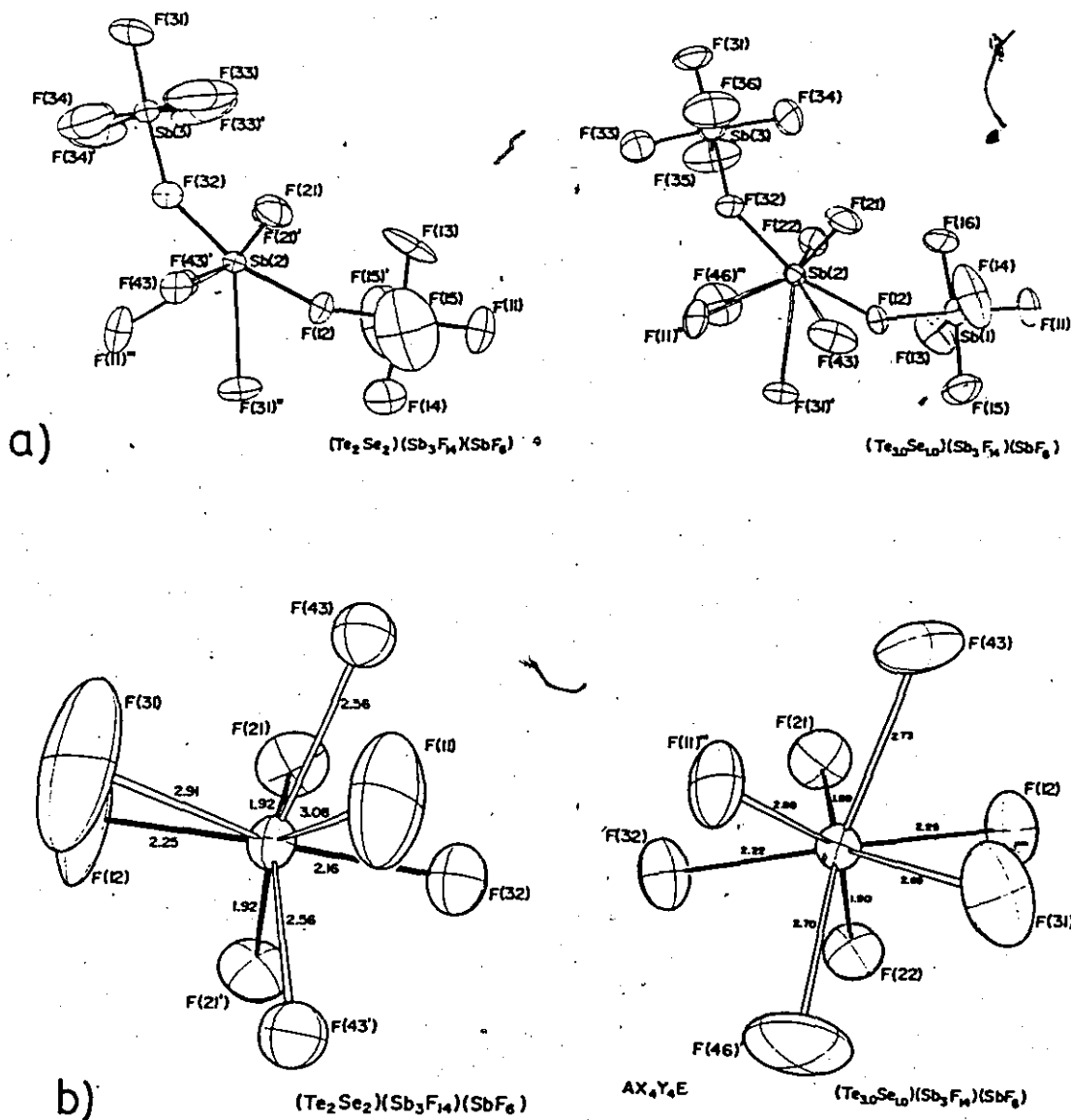


FIGURE VI.11 ORTEP views of the $Sb_3F_{14}^-$ anions in $Te_2Se_2(Sb_3F_{14})(SbF_6)$ and $Te_{3.0}Se_{1.0}(Sb_3F_{14})(SbF_6)$. (a) The complete anion, including interionic contacts to Sb(III). (b) Views directed toward the assumed positions of the lone pairs of electrons showing edge-bridging ($Te_2Se_2^{2+}$ salt) and face-capping ($Te_{3.0}Se_{1.0}^{2+}$ salt) secondary bonds (unfilled bonds).

ing geometry with face-capping secondary bonds is described by a monocapped octahedron (Fig. III.5). Four contacts capping the faces of the trigonal bipyramid in $\text{Sb}_3\text{F}_{14}^-$ produce a monocapped square antiprism about Sb(III) with the lone pair as the cap (Fig. VI.12). The $\text{Sb}_3\text{F}_{14}^-$ anion of $(\text{Te}_{3.0}\text{Se}_{1.0})(\text{Sb}_3\text{F}_{14})(\text{SbF}_6)$ provides a good example of this $\text{AX}_4\text{Y}_4\text{E}$ arrangement (Fig. VI.11). Other examples are Sb(III) of $\text{Na}_2(\text{SbF}_3)(\text{C}_2\text{O}_4)$ and $\text{Br}_3(\text{Sb}_2\text{F}_{11})(\text{Sb}_{10}\text{F}_{42})$, Sn(II) of $\text{SnF}_2(\text{AsF}_5)$ and $\text{Sn}(\text{NCS})\text{F}$, Te(IV) of diphenyl tellurium dinitrate (Fig. VI.13) and Pb(II) of $\text{Pb}(\text{L})(\text{NO}_3)_2$, where L is a tetra-aza macrocycle (87-93). Four contacts bridging the edges of the polyhedron, an $\text{AX}_4\text{Y}'_4\text{E}$ geometry, are observed for Sb(III) in $(\text{Te}_2\text{Se}_2)(\text{Sb}_3\text{F}_{14})(\text{SbF}_6)$ (Figure VI.11b) and for the I(V) atom in $\text{IF}_4(\text{Sb}_2\text{F}_{11})$ (94).

The compound $(\text{Se}_{3.0}\text{Se}_{1.0})_2(\text{Sb}_4\text{F}_{17})(\text{SbF}_6)_3$ provides the only crystallographic evidence of a mixed S-Se cation as well as the only example of the $\text{Sb}_4\text{F}_{17}^-$ anion, in which there are two Sb(III) atoms (Fig. VI.14). The $\text{Sb}_4\text{F}_{17}^-$ anion can be broken into an Sb_2F_5^+ and two SbF_6^- units. The central fluorine atom of Sb_2F_5^+ lies on a center of symmetry so that the Sb(III)--F--Sb(III) bond angle is 180° and the lone pairs on Sb(III) are perfectly staggered. The Sb(III)--F--Sb(III) bond angles in previously observed Sb_2F_5^+ units range from 149.8° in $(\text{SbF}_3)_3(\text{SbF}_5)$ (95) to 180° observed here, for $(\text{SbF}_3)_6(\text{SbF}_5)_5$ (96) and for one of the

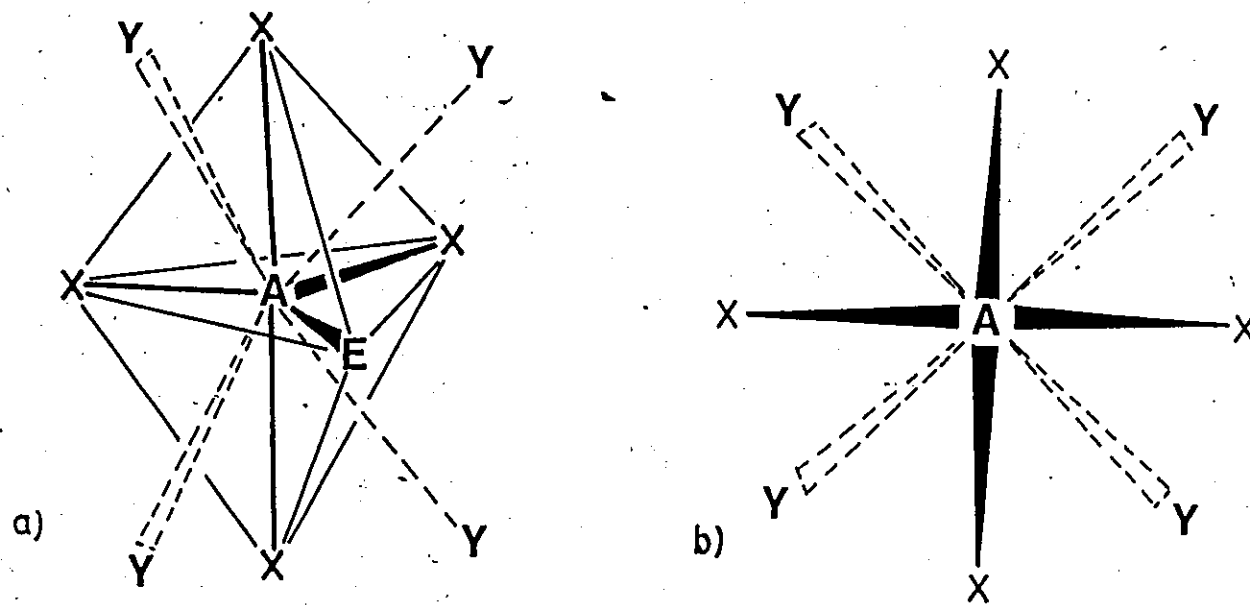


FIGURE VI.12 The AX_4Y_4E geometry. (a) Four contacts, Y, capping faces of the AX_4E polyhedron. (b) View directed toward the lone pair, E.

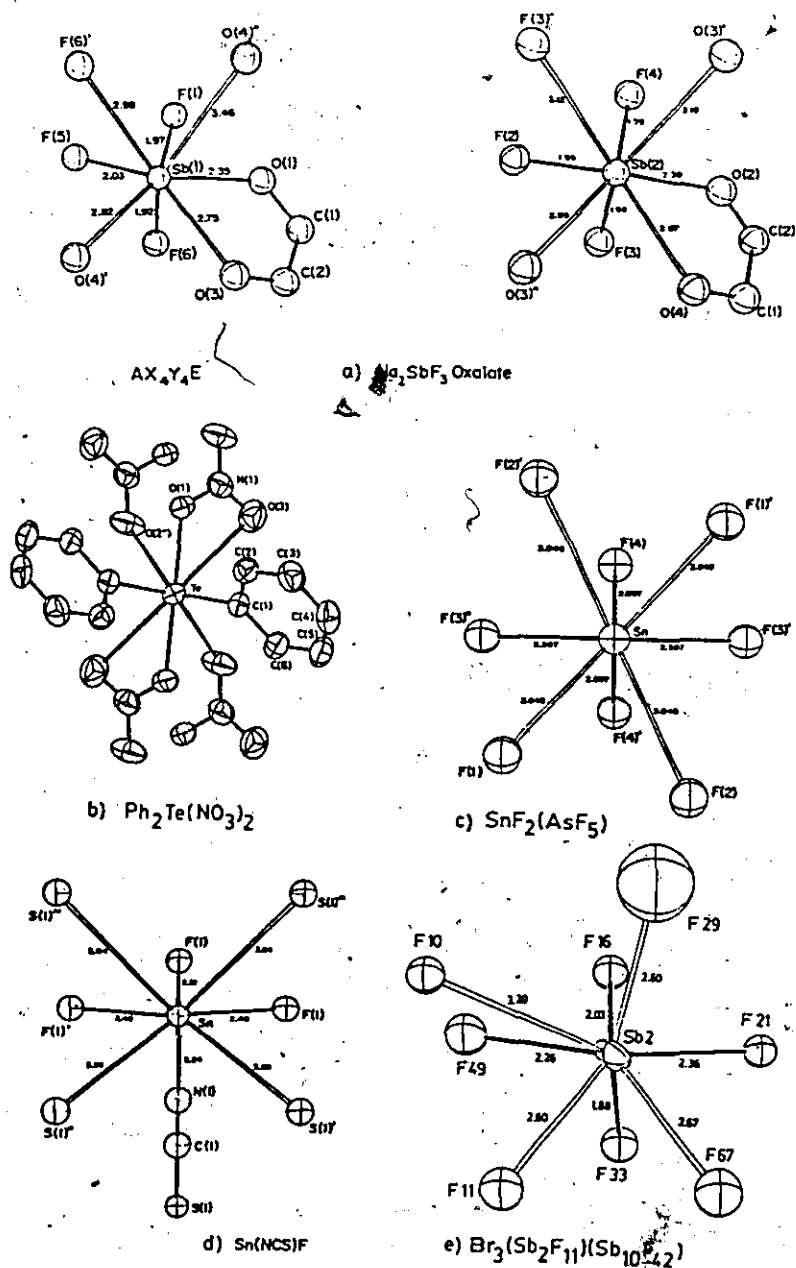


FIGURE VI.13 Examples of the AX₄Y₄E geometry. (a), (c) and (d) redrawn from coordinates in ref. (88), (90) and (91) by Dr. J.F. Sawyer; (b) reproduced from ref. (92); (e) ref. (89). All views are toward the assumed direction of the lone pair of electrons on the central atom, except (b), which is viewed from the opposite side.

TABLE VI.4 Bond Valence Calculations for
Sb(III) of $\text{Sb}_3\text{F}_{14}^-$ and $\text{Sb}_4\text{F}_{17}^-$.

COMPOUND	BOND VALENCE	
	1 ^a	2 ^b
$(\text{Te}_2\text{Se}_2)(\text{Sb}_3\text{F}_{14})(\text{SbF}_6)$	2.38	3.18
$(\text{Te}_{3.0}\text{Se}_{1.0})(\text{Sb}_3\text{F}_{14})(\text{SbF}_6)$	2.41	3.15
$(\text{Te}_2\text{Se}_4)(\text{Sb}_3\text{F}_{14})(\text{SbF}_6)$	2.41	3.14
$(\text{S}_{3.0}\text{Se}_{1.0})_2(\text{Sb}_4\text{F}_{17})(\text{SbF}_6)_3$	2.33	3.10

(a) Primary bonds only ($\text{Sb}-\text{F} \leq 2.33 \text{ \AA}$).
(b) All contacts to 3.52 \AA .

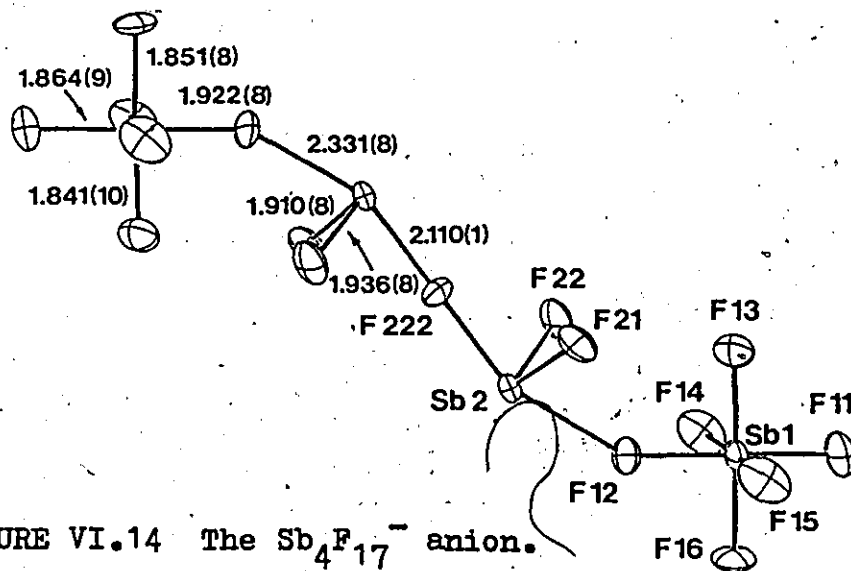


FIGURE VI.14 The $\text{Sb}_4\text{F}_{17}^-$ anion.

four Sb_2F_5^+ groups in $(\text{SbF}_3)_5(\text{SbF}_5)_3$ (97). The analogous angle in the isoelectronic Sn_2F_5^- anion has a value of 134° (98).

In all of these examples involving polymeric Sb(III)-Sb(V) anions and $\text{SbF}_3/\text{SbF}_5$ adducts it is difficult to clearly differentiate the primary and secondary bonds. For the $\text{Sb}_3\text{F}_{14}^-$ anion of $(\text{Te}_2\text{Se}_2)(\text{Sb}_3\text{F}_{14})(\text{SbF}_6)$ the longest distance between Sb(III) and a bridging fluorine of Sb(V) is 2.25 Å while the closest secondary bonds to Sb(III) are only 2.56 Å in length. The $\text{Sb}_4\text{F}_{17}^-$ anion has bridging distances of 2.33 Å and contact distances as short as 2.76 Å. In $(\text{Se}_4)(\text{Sb}_2\text{F}_4)(\text{Sb}_2\text{F}_5)(\text{SbF}_6)_5$ the difference is even less distinct with the longest primary bond being 2.15 Å and the shortest secondary 2.33 Å (23). This secondary bond is equal in length to one considered in the primary geometry of $\text{Sb}_4\text{F}_{17}^-$, emphasizing the somewhat arbitrary nature of the ionic units into which these complex anions can be divided.

The primary geometry about Sb(III) in $\text{Sb}_4\text{F}_{17}^-$ is also AX_4E and the geometry of the secondary bonds is similar to that observed above for $\text{Sb}_3\text{F}_{14}^-$ except that there is a fifth contact, to F(32)', of 3.37 Å which is only marginally less than the sum of van der Waals radii of 3.52 Å (39). This fluorine atom is capping a face of the AX_4E polyhedron, as is F(33)', while the other three contacts appear to be bridging edges, giving an overall $\text{AX}_4\text{Y}_2\text{Y}'_3\text{E}$ arrangement (Fig. VI.15a). The Sb(III) atom of $(\text{Te}_2\text{Se}_4)(\text{Sb}_3\text{F}_{14})(\text{SbF}_6)$

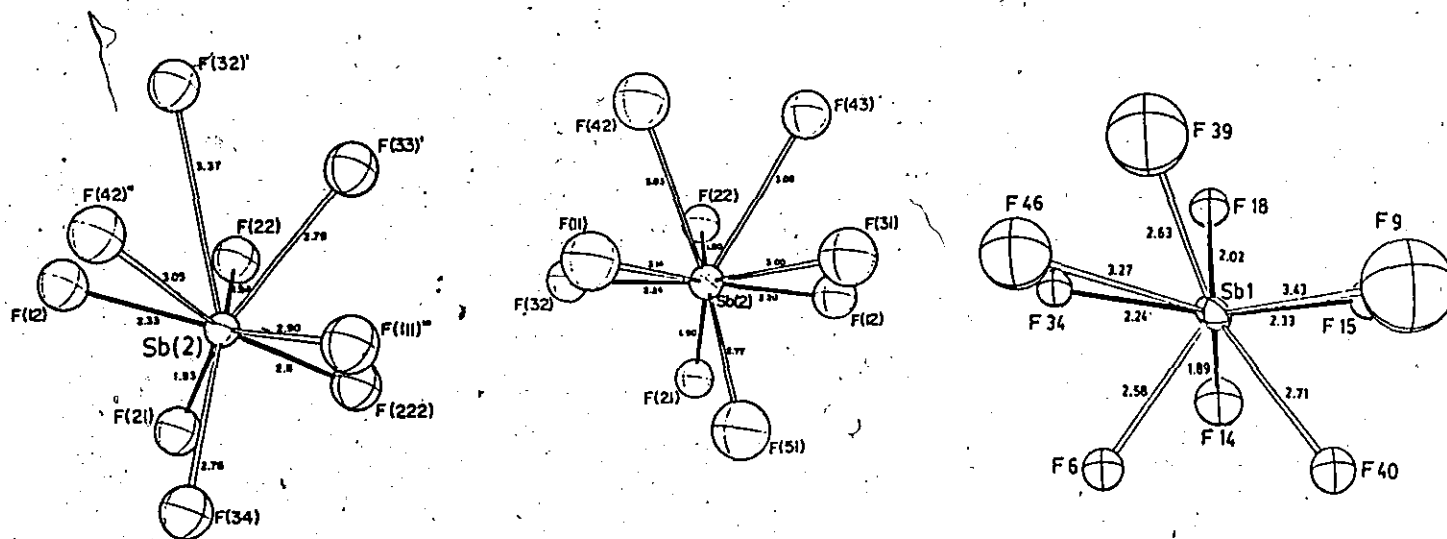


FIGURE VI.15 Views of the secondary bonding (unfilled bonds) to Sb(III) atoms of (a) $(S_{3.0}Se_{1.0})_2(Sb_4F_{17})(SbF_6)_3$, (b) $Te_2Se_4(Sb_3F_{14})(SbF_6)$ and (c) $Br_3(Sb_2F_{11})(Sb_{10}F_{42})$, ref. (89). All views are toward the assumed position of the lone pair of electrons on Sb(III).

(section V.3) has an identical geometry to that of Sb(III) in $\text{Sb}_4\text{F}_{17}^-$ (Fig. VI.15b). One of the Sb(III) atoms of $(\text{Br}_3)(\text{Sb}_2\text{F}_{11})(\text{Sb}_{10}\text{F}_{42})$, Sb(1), also has five contacts about a trigonal-bipyramidal primary geometry (89). In this case the three shorter contacts (2.58-2.71 Å) appear to be face-capping; the two longer contacts (3.27 and 3.43 Å) edge-bridging (Fig. VI.15c).

The significance of these secondary interactions to the overall bonding scheme in $\text{Sb}_3\text{F}_{14}^-$ and $\text{Sb}_4\text{F}_{17}^-$ is emphasized in Table VI.4. If only the primary bonds are considered ($\text{Sb}-\text{F} \leq 2.33$ Å) the valence about Sb using Brown's method of determining bond valence (99) ranges from 2.33 to 2.41. If, however, all interatomic distances less than the van der Waals limit are considered, the results range from 3.10 to 3.18, which is much closer to the anticipated value of 3.0. Several additional examples are provided by Sawyer and Gillespie (87) and Passmore et al. (97).

VI.12 Anion-Cation Interactions in M_4^{2+} Structures.

As described elsewhere (23), the slight deviations of the square-planar M_4^{2+} cations from perfect squares and the variations of bond lengths for a given cation from one structure to another may be attributed in part to the charge-transfer interactions of the M_4^{2+} cations with their accompanying anions. In an SCF-MO study of Te_4^{2+} (100) the calculated bond length was 0.054 Å shorter than that observed in

$\text{Te}_4(\text{AlCl}_4)_2$ and $\text{Te}_4(\text{Al}_2\text{Cl}_7)_2$ (13), but when the calculation was repeated simulating the chlorine atoms that are closest to the cation in the crystal structures by point charges of $-1/4 e^-$ (i.e. the four Cl atoms of the anion share the single negative charge equally) the bond length in the Te_4^{2+} ion increased by 0.06 Å to a value very close to the experimental value.

In all known cases of M_4^{2+} cations each edge of the square is bridged by at least one atom and there are generally several additional contacts along the extensions of the diagonals. These directions are presumably minima in the electron density about the cation and they may be correlated with the symmetries of the available lowest unoccupied molecular orbitals of the M_4^{2+} cations (23). The in-plane interactions are probably with the LUMO of σ symmetry while the out-of-plane interactions are with the LUMO of π symmetry. These molecular orbitals are relatively close in energy (13, 51, 100). The degree of this interaction of course depends upon the nature of the donor atoms. A more polarizable anion tends to donate more electron density into the antibonding orbitals of the cation, increasing the M--M bond length and thereby decreasing the HOMO-LUMO gap and the energy of transitions in the electronic absorption and diffuse-reflectance spectra. Such a trend is observed for Se_4^{2+} where the $\pi-\pi^*$ transition is observed to vary from

413 nm in $\text{Se}_4(\text{Sb}_2\text{F}_4)(\text{Sb}_2\text{F}_5)(\text{SbF}_6)_2$ to 524 nm in $\text{Se}_4(\text{HS}_2\text{O}_7)_2$ (77). Similarly, ^{77}Se - ^{125}Te and ^{125}Te - ^{125}Te coupling constants in ^{77}Se and ^{125}Te NMR spectra of $\text{Te}_x\text{Se}_{4-x}^{2+}$ cations are strongly dependent upon the solvent (see section VI.7).

Recent molecular orbital calculations indicate that there are differences in the σ bonding in the M_4^{2+} cations. In particular, the s-orbitals make a smaller contribution to the σ -bonds in Te_4^{2+} than in Se_4^{2+} and S_4^{2+} and the HOMO-LUMO gap decreases in the order $\text{S}_4^{2+} > \text{Se}_4^{2+} > \text{Te}_4^{2+}$ (101). This is reflected in both a reduction of the stereospecificity and an increase in the number of the contacts to Te_4^{2+} in salts of this cation (23) and to $\text{Te}_{3.0}\text{Se}_{1.0}^{2+}$ in $(\text{Te}_{3.0}\text{Se}_{1.0})(\text{Sb}_3\text{F}_{14})(\text{SbF}_6)$ (Fig. VI.16). The geometry about $\text{Te}_2\text{Se}_2^{2+}$, however, is well-defined in $(\text{Te}_2\text{Se}_2)(\text{Sb}_3\text{F}_{14})(\text{SbF}_6)$ (Fig. VI.16). It is noteworthy that the three shortest contacts (2.80, 2.93, and 2.99 Å) are all to tellurium and that tellurium has one more contact than does selenium (two contacts of lengths 3.10 and 3.12 Å). Since these contacts are assumed to be nucleophilic in nature the arrangement about $\text{Te}_2\text{Se}_2^{2+}$ is indicative of a build-up of positive charge on tellurium relative to selenium. This is reasonable in terms of the relative electronegativities of these two elements as described earlier (section IV.7). In the other mixed Te-Se cation, $\text{Te}_{3.0}\text{Se}_{1.0}^{2+}$ in $\text{Te}_{3.0}\text{Se}_{1.0}(\text{Sb}_4\text{F}_{20})$, Te(2) has the highest percentage of tellurium as well as the greatest number of contacts in the structure. The remaining

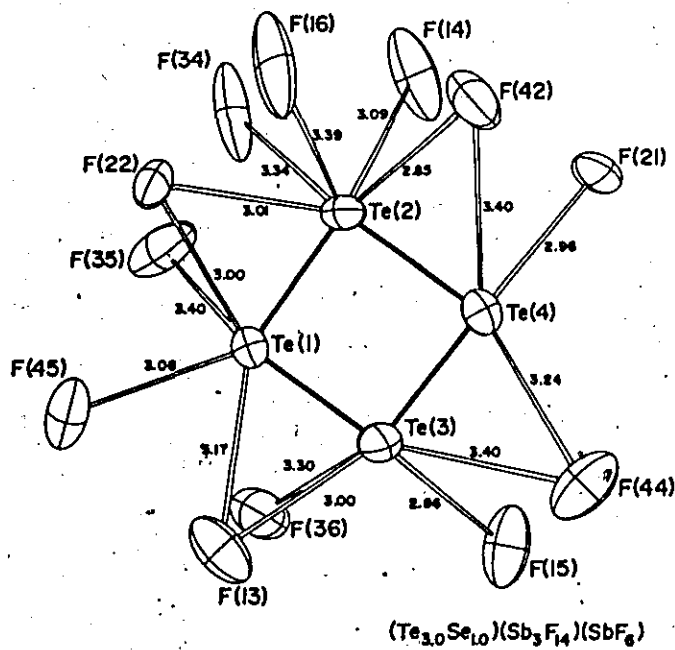
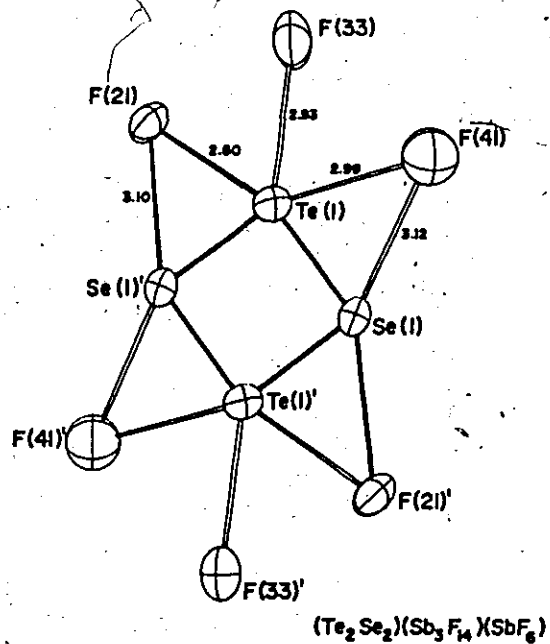


FIGURE VI.16 Anion-cation interactions in $\text{Te}_2\text{Se}_2(\text{Sb}_3\text{F}_{14})(\text{SbF}_6)$ and $\text{Te}_{3.0}\text{Se}_{1.0}(\text{Sb}_3\text{F}_{14})(\text{SbF}_6)$.

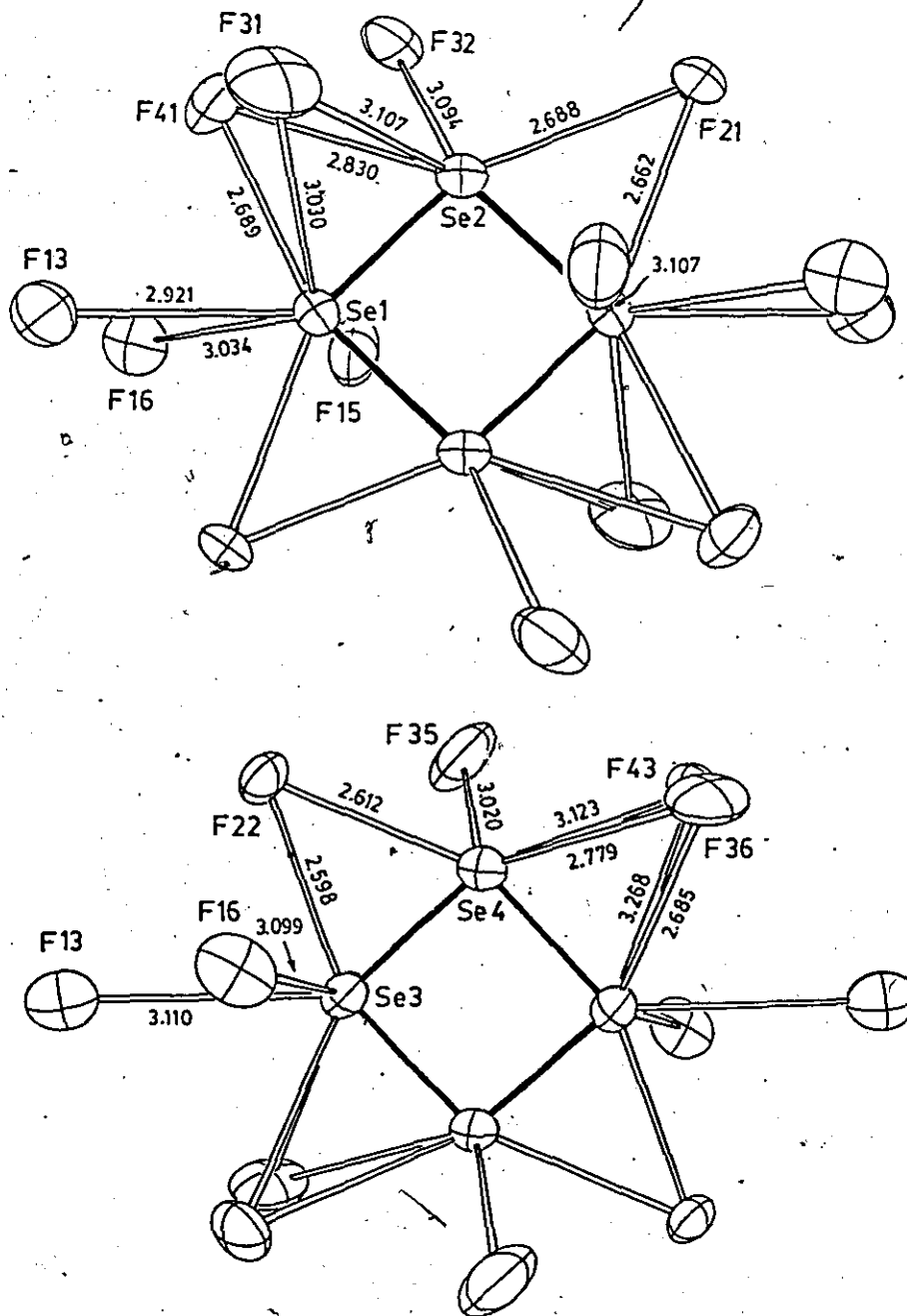
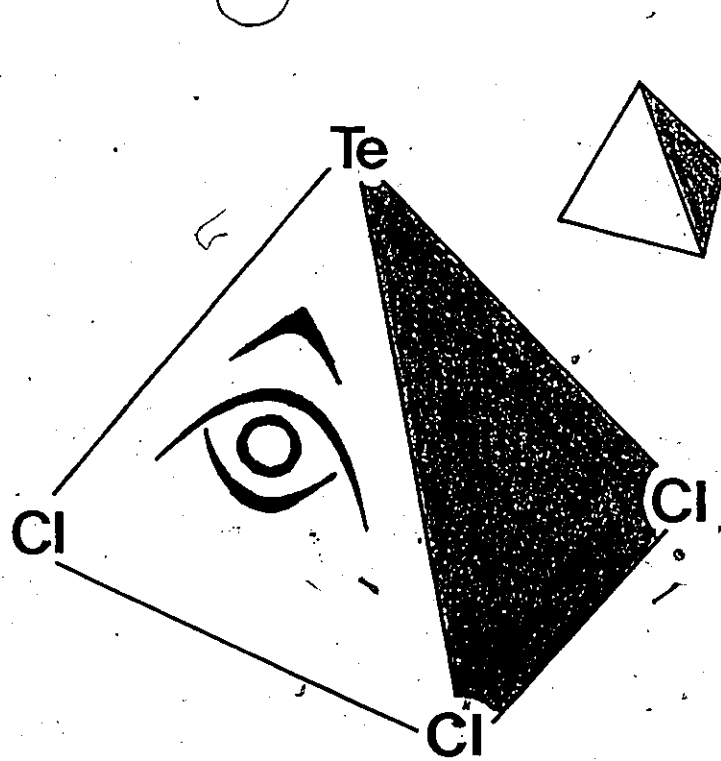


FIGURE VI.17 Anion-cation interactions in
 $(S_{3.0}Se_{1.0})_2(Sb_4F_{17})(SbF_6)_3$.

three sites, however, do not appear to reflect this trend.

Contacts to the $S_{3.0}Se_{1.0}^{2+}$ cations of $(S_{3.0}Se_{1.0})_2(Sb_4F_{17})(SbF_6)_3$ (Fig. VI.17) exhibit typical arrangements as described above. In each case the four shortest contacts (ranging from 2.598 to 2.830 Å) bridge the edges of the cation. The largest number of contacts occur at the sites relatively rich in selenium. There are six contacts to Se(1) and five contacts to Se(3) which are 40.2 and 32.1% selenium respectively, while Se(2) and Se(4) with 15.3 and 12.8% selenium have only four contacts.

CHAPTER VII
 MX_3^+ CATIONS



VII.1 Introduction.

A large number of salts of the MX_3^+ cation ($M = \text{S}, \text{Se}, \text{Te}; X = \text{F}, \text{Cl}, \text{Br}, \text{I}$) have been characterized by X-ray crystallography. Many of these structures have recently been summarized by Passmore et al. (102). In all cases the cation has essentially trigonal pyramidal, C_{3v} symmetry, as expected from VSEPR considerations (61). Interionic contacts are significant in all of these structures as well and generally form in directions around the lone pair of electrons and opposite the primary $M-X$ bonds to complete a distorted monocapped octahedron, $\text{AX}_3\text{Y}_3\text{E}$, around the central Group VI atom. Similar geometries are observed for bridgehead positions in M_{10}^{2+} , M_8^{2+} and M_6^{2+} cations as described above (see Fig. III.5 and III.6). It was of interest to characterize more salts of the MX_3^+ cation so that the secondary bonding interactions could be further studied and trends in the geometry of the cation with variations in M and/or X could be established.

VII.2 Preparation of $(\text{TeCl}_3)(\text{AlCl}_4)$ -triclinic.

Aluminum trichloride (0.533 g, 4.00 mmol) was added to S_7TeCl_2 (0.846 g, 2.00 mmol) (103) and 30 mL of CH_2Cl_2 was distilled onto this mixture in a double-bulb vessel at 77 K. Upon warming to 295 K the solution had the characteristic orange color of S_7TeCl_2 but after stirring for 24 h the color changed to a bright yellow and a large quantity of

white powder precipitated. The powder was filtered off and recrystallized in CH_2Cl_2 , producing thin white plates. The Raman spectrum of these crystals (Table VII.1 and Fig. VII.1) was consistent with $(\text{TeCl}_3)(\text{AlCl}_4)$ but the space group and unit cell parameters were inconsistent with the previously reported structure of this compound (104) and a structure determination was carried out. Yellow, block-like crystals also formed from the original reaction mixture and these were identified as S_8 (orthorhombic, $Fddd$) from precession photographs.

VII.3 Preparation of $(\text{TeCl}_3)(\text{AsF}_6)$.

The synthetic route followed here (reaction VII.1) is analogous to the reported preparation of $(\text{TeBr}_3)(\text{AsF}_6)$ (105). Arsenic pentafluoride (0.226 g, 1.33 mmol) and SO_2 (20 mL) were distilled onto TeCl_4 (0.2383 g, 0.8845 mmol) in a double-bulb vessel at 77 K. The mixture was warmed to room temperature and after 24 h of stirring the solution was a very pale yellow color, presumably as a result of Cl_2 produced in the reaction. Stirring was continued for one week with no apparent change. An oil was formed upon slow removal of the solvent, which deposited a large quantity of white powder upon cooling the other bulb of the vessel to 255 K to remove all of the solvent. The powder was transferred to another vessel and recrystallized from a 1:4 $\text{CH}_2\text{Cl}_2/\text{SO}_2$ mixed solvent, producing thin colorless plates.

Table VII.1 Raman Spectra of the TeCl_3^+ Salts Produced in Sections VII.2 through VII.5.

AlCl_4^-	SbCl_6^-	SbF_6^-	AsF_6^-
	77 K	295 K	in SO_2
			708(5) ^e
		667(10) ^d	671(8) ^e
		640(20) ^d	649(1) ^e
467(4) ^a			578(3) ^e
458(4) ^a			543(3) ^e
			442(2)
391(100)	399(76)	398(100)	399(96)
	386(31)	384(48)	406(100)
			388(48)
378(26)	370(10)	366(16)	376(40)
368(56)	360(20)	358(26)	355(32)
347(27) ^a	340(6) ^c	344(10) ^c	333(100) ^b
	313(100) ^b	312(78) ^b	
	265(11) ^b		285(9) ^b
	256(18) ^b		263(4) ^b
	257(23) ^b		284(14) ^d
193(4) ^a	195(8)		
	191(14)	188(17)	
	181(24)	179(27)	
	174(18)	172(38)	
168(14)	171(17)		169(8)
	165(19)	166(37)	173(16)
	152(10)		
148(21)	149(11)	149(22)	159(29)
144(18)	142(2)		146(38)
131(13)	133(3) ^c	130(5)	
	124(4)		
121(7) ^a	121(4)	121(8)	
	118(3)		
	93(1) ^c		
	84(2)	76(8)	82(8)
	73(5)		
	62(10)		
	54(5)	58(32)	
	48(9)		
	44(8)		
	38(18)		
	35(17)	34(79)	
	31(16)	28(57)	
			67(12)

(a) AlCl_4^- , ref. (160). (b) SbCl_6^- , ref. (128). (c) SbCl_3 , ref. (161). (d) SbF_6^- , ref. (162). (e) AsF_6^- , ref. (163).

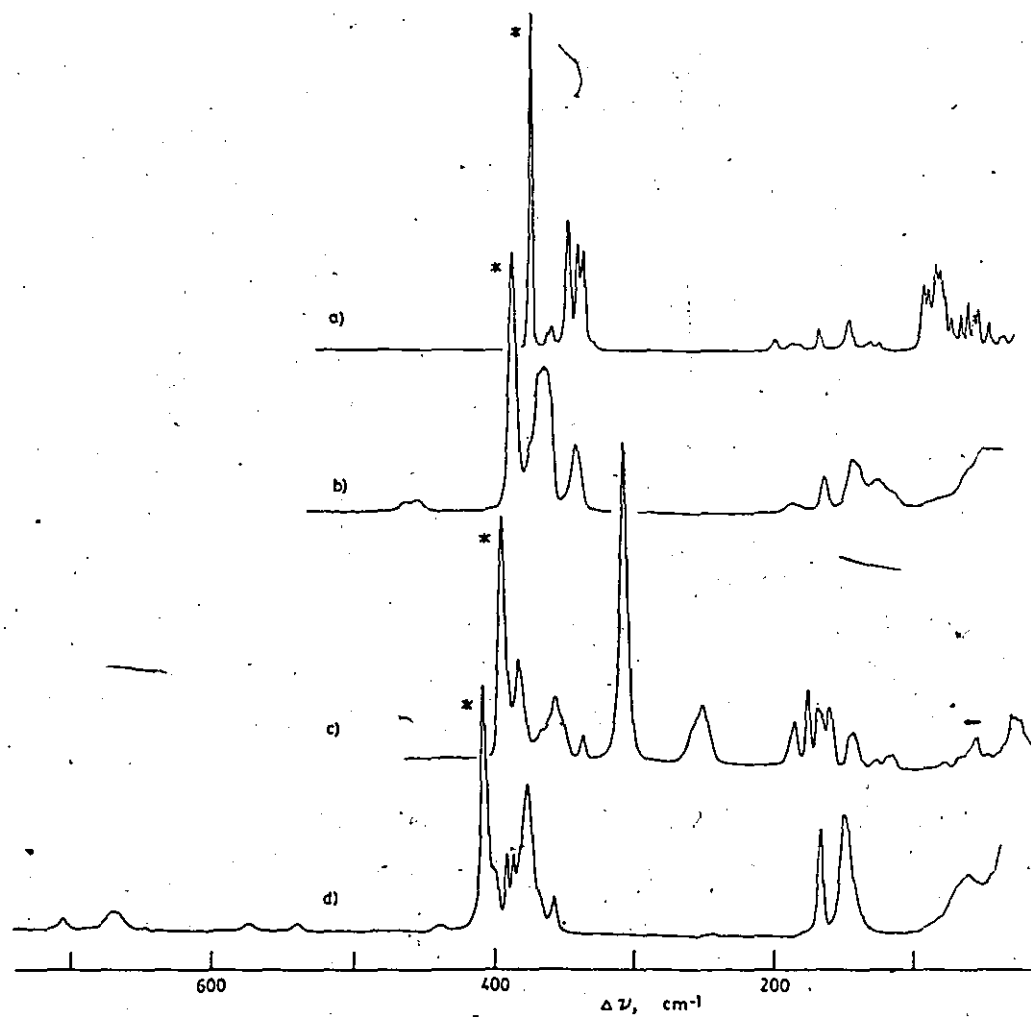
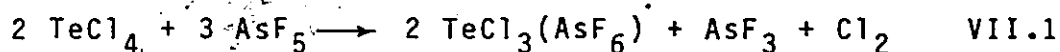


FIGURE VII.1 Raman spectra (5145 \AA) of a) TeCl_4 ; recrystallized from SO_2 , 77 K, b) $\text{TeCl}_3(\text{AlCl}_4)^-$, 295 K, c) $\text{TeCl}_3(\text{SbCl}_6)^-$, 77 K, d) $\text{TeCl}_3(\text{AsF}_6)^-$, 295 K. (*) indicates ν_1 of TeCl_3^+ .

The Raman spectrum of these crystals (Table VII.1 and Fig. VII.1) was significantly different from that previously reported for this compound (106), but a subsequent X-ray crystal structure determination confirmed the composition to be $(\text{TeCl}_3)(\text{AsF}_6)$.



VII.4 Preparation of $(\text{TeCl}_3)(\text{SbF}_6)$ - Attempted Recrystallization of $\text{TeF}_4(\text{SbF}_5)$.

Tellurium tetrafluoride (0.4714 g, 2.315 mmol) was combined with SbF_5 (0.4970 g, 2.293 mmol) and 30 mL of SO_2 in a double-bulb vessel and the reaction mixture stirred for 2 h before the SO_2 was slowly distilled off of the colorless solution leaving a white powder. This product, presumably $\text{TeF}_4(\text{SbF}_5)$ (107), proved to be too soluble in SO_2 to obtain good crystals so a portion of the product (0.4842 g, 1.152 mmol $\text{TeF}_4(\text{SbF}_5)$) was transferred into another double-bulb vessel, along with 15 mL SO_2 and 20 mL CH_2Cl_2 , producing a colorless solution free of residue. A large quantity of white powder precipitated after half of the solvent had been slowly removed by distillation. The remaining solvent, presumably mostly composed of the less-volatile CH_2Cl_2 , was left over the powder to encourage crystal growth. After two weeks the solution was a pale pink color and thin, colorless plate- and needle-shaped crystals had formed at the vapor-liquid interface. The Raman spectrum of these crystals (Table VII.1) was consistent with $(\text{TeCl}_3)(\text{SbF}_6)$ and

the X-ray crystal structure determination confirmed this composition.

VII.5 Preparation of $(\text{TeCl}_3)(\text{SbCl}_6)$.

Tellurium (0.4016 g, 3.147 mmol) was weighed into one bulb of a double-bulb vessel and an excess of SbCl_5 (4.67 g, 15.6 mmol) was added with a syringe to the other bulb in a dry-box. Thirty mL of SO_2 was condensed into the ampoule with the SbCl_5 at 77 K and after sealing the vessel and allowing the solvent to melt this yellow solution was poured onto the tellurium and the mixture stirred at room temperature. A pale magenta solution color was observed, indicating initial formation of Te_4^{2+} . After 2 h all the Te had reacted, producing a yellow solution free of residue. The vessel was heated at 340 K for 24 h with no apparent change. After slowly distilling some of the solvent to the other ampoule large yellow crystals were deposited. The Raman spectrum of these crystals indicated that they were $(\text{TeCl}_3)(\text{SbCl}_6)$ (see Table VII.1, Fig. VII.1). A subsequent X-ray crystallographic analysis revealed that the chlorine atoms were disordered and the structure was not completed. Space group and unit cell data are included in the Appendix.

VII.6 Preparation of $(\text{TeF}_3)_2(\text{SO}_4)$.

Thirty mL SO_2 and AsF_5 (2.187 g, 12.87 mmol) and a trace of Br_2 (20 mg) were condensed onto a mixture of Te

(0.8115 g, 6.360 mmol) and Se (0.5082 g, 6.436 mmol) at 77 K in a double-bulb vessel. After allowing the solvent to melt the reaction mixture was stirred producing first green, then brown and blood-red solution colors, returning to green after 2 h of mixing. These colors are consistent with the initial formation of Se_8^{2+} and/or Se_{10}^{2+} (both green) followed by the production of mixed Te-Se cations (red or brown in color), which react further to produce colorless TeF_3^+ and Se_8^{2+} and/or Se_{10}^{2+} . After 24 h a large quantity of finely-divided black powder had precipitated. The green solution was filtered and the solvent slowly distilled off, leaving a deep green oil. A few mL of SO_2 were distilled onto this oil in an NMR tube and the ^{77}Se NMR spectrum of this solution identified the Se_{10}^{2+} cation (see section III.7). No other species were observed. After several weeks a few colorless crystals formed in the NMR tube. These were isolated and were shown by X-ray crystallography to be $(\text{TeF}_3)_2(\text{SO}_4)$.

VII.6 Discussion of Crystal Structures.

$(\text{TeCl}_3)(\text{AlCl}_4)$ -triclinic: The geometries of the two independent TeCl_3^+ cations in this new modification of $(\text{TeCl}_3)(\text{AlCl}_4)$ (a monoclinic form has been reported (104)), are given in Figure VII.2, complete with secondary Te...Cl interactions. Both cations have a tetrahedral AX_3E primary bond geometry, which is consistent with VSEPR theory. Three

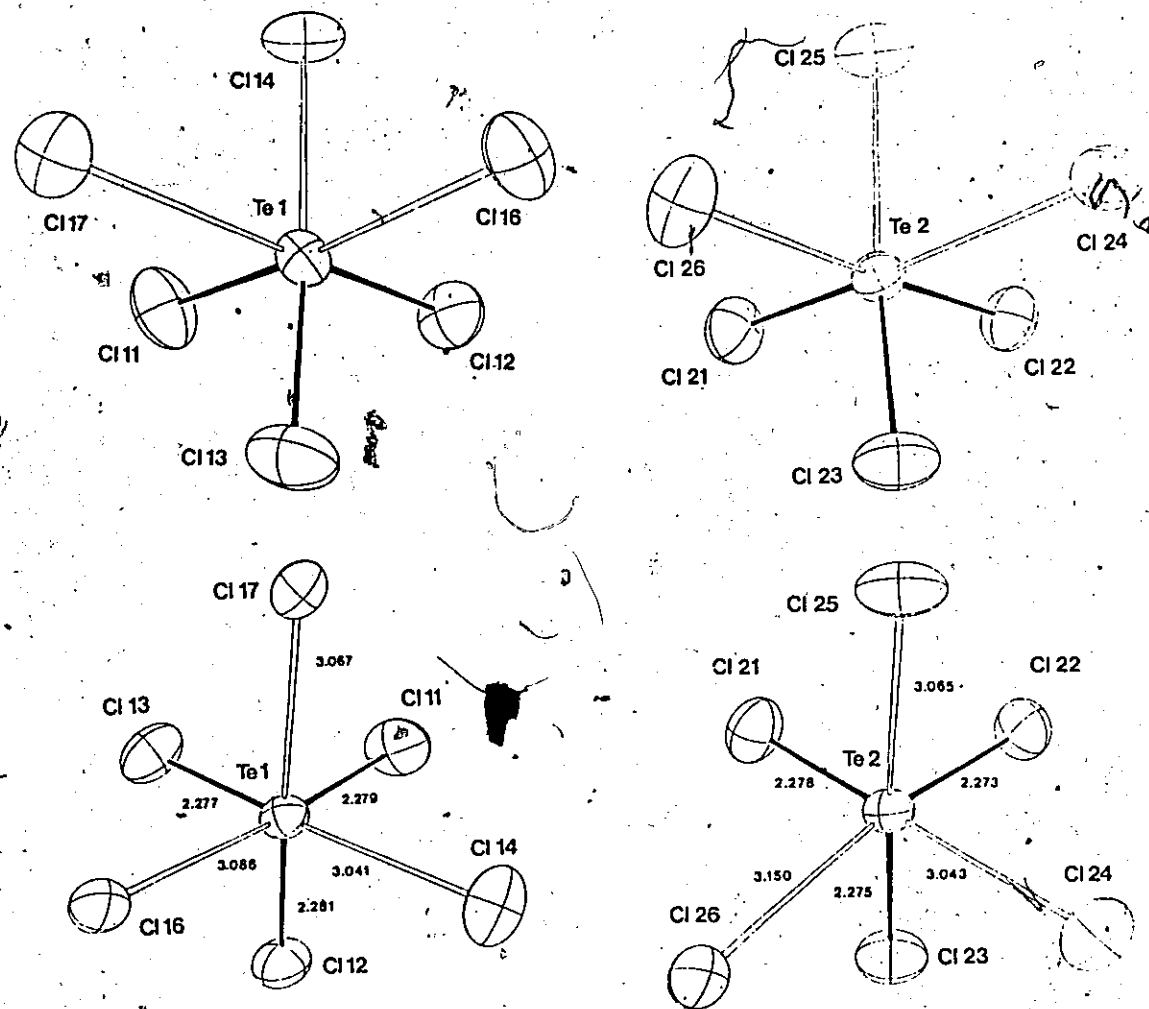


FIGURE VII.2 ORTEP views of the two TeCl_3^+ cations in $\text{TeCl}_3(\text{AlCl}_4)$ -triclinic, examples of the $\text{AX}_3\text{Y}_3\text{E}$ geometry. Lower views are toward the assumed position of the lone pair of electrons.

secondary bonds opposite the primary bonds complete a distorted monapped AX_3Y_3E octahedron (cf. Fig. III.5). The $TeCl_3^+$ cation in $TeCl_4$, i.e. $[(TeCl_3^+)(Cl^-)]_4$, also has an AX_3Y_3E geometry (108). The dimensions of the $TeCl_3^+$ cations in this $AlCl_4^-$ salt, however, are substantially different from those of the same cation in $TeCl_4$ (Table VII.2). There is a significant decrease in the Te--Cl bond length in going from $TeCl_4$ to the $AlCl_4^-$ salt, with a corresponding lengthening of the secondary Te...Cl contacts. This correlation between primary and secondary bond lengths is expected if the chlorine atoms in the anions donate electron density into antibonding σ^* orbitals associated with the Te--Cl bonds of the cation (see section III.9). Consistent with the weaker nature of the secondary bonds and the stronger primary Te--Cl bonds, there is also an increase in the mean intramolecular Cl-Te-Cl angle in the $AlCl_4^-$ salt over that in $TeCl_4$ (Table VII.2). The dimensions of the $TeCl_3^+$ cation in the triclinic $AlCl_4^-$ salt are very similar to those of the previously published monoclinic salt (104) (Table VII.2).

In the present structure the two $AlCl_4^-$ anions are both slightly flattened tetrahedra with some significant differences in bond lengths (Table VII.3). Notably, each anion contains a bond which is ca. 0.04 to 0.05 Å shorter than the remaining bonds and these two short bonds are to the two chlorine atoms of the anions that are not involved

Table VII.2 Mean Dimensions of MX_3^+ Cations.

MX_3^+	Bond Lengths (Å)		Bond Angles (deg)			Ref.
	M - X	M...Y	X-M-X	X-M...Y	Y...M...Y	
$\text{SF}_3(\text{BF}_4)$	1.492(2)	2.614(3)	97.5(1)			130
$\text{SeF}_3(\text{NbF}_6)$	1.73(4)	2.35(4)	94.9(3)	85(3)	96(3)	125
$\text{SeF}_3(\text{Nb}_2\text{F}_{11})$	1.66(2)	2.43(2)	94(2)	84(1)	99(1)	126
$\text{TeF}_3(\text{Sb}_2\text{F}_{11})$	1.84(4)	2.59(3) ^a	90(2)	75(1)	101(1)	46
$\text{SCl}_3(\text{ICl}_4)$	1.988(3)	3.115(3)	101.3(1)	159.5(1) ^b	77.1(1)	115
$\text{SCl}_3(\text{SbCl}_6)$	1.956(2)	3.220(3)	103.7(2)	88.31(7)	76.52(5)	116
$\text{SCl}_3(\text{UCl}_6)$	1.96(1)	3.25 ^c	102.3(7)			131
SeCl_4^{d}	2.166	2.837	96.0	89.6	84.0	132
$\text{SeCl}_3(\text{AlCl}_4)$	2.11	3.04	99.3	88.5	82.1	132
$\text{SeCl}_3(\text{MoOCl}_4)$	2.148(2)	2.878(2)				132
$\text{SeCl}_3(\text{SbCl}_6)$	2.10(1)	3.13(1)				116
TeCl_4^{e}	2.311(3)	2.929(3)	94.8(2)	89.9(3)	85.0(2)	108
$\text{TeCl}_3(\text{AlCl}_4)^{\text{f}}$	2.276(2)	3.061(2)	95.0(2)	85.6(2)	93.8(2)	104
$\text{TeCl}_3(\text{AlCl}_4)^{\text{g}}$	2.277(2)	3.075(2)	95.21(7)	86.81(6)	90.94(5)	h
$\text{TeCl}_3(\text{AsF}_6)$	2.264(2)	2.796(5) ^a	96.00(8)	80.9(1)	102.0(2)	h
$\text{TeCl}_3(\text{SbF}_6)$	2.258(2)	2.739(5) ^a	95.8(1)	81.2(1)	102.3(1)	h
SeBr_4^{i}	2.36(3)	2.98(3)	96(1)	90(1)	83(1)	133
$\text{SeBr}_3(\text{SbF}_6)$	2.269(8)	2.77(4)	100.9(3)	86.4(9)	86(1)	102
$\text{TeBr}_3(\text{AsF}_6)$	2.432(2)	2.84(1)	97.92(8)	84.4(3)	92.2(4)	102
$\text{TeI}_3(\text{AsF}_6)$	2.667(2)	2.98(1)	99.9(1)			134

(a) Mean of three face-capping contacts. (b) Trans- angle.

(c) Only two contacts reported. (d) i.e. $[(\text{SeCl}_3^+)(\text{Cl}^-)]_4$.

(e) i.e. $[(\text{TeCl}_3^+)(\text{Cl}^-)]_4$. (f) Monoclinic modification.

(g) Triclinic modification. (h) This work.

(i) i.e. $[(\text{SeBr}_3^+)(\text{Br}^-)]_4$.

Table VII.3 Bond Lengths (Å) and Bond Angles (deg).

a) $\text{TeCl}_3(\text{AlCl}_4)$

Bond Lengths			Bond Angles		
Te(1) - Cl(11)	2.279(2)		Cl(11)-Te(1)-Cl(12)	94.89(7)	
- Cl(12)	2.281(2)		-Cl(13)	94.41(8)	
- Cl(13)	2.277(2)		-Cl(14)	83.26(7)	
...Cl(14)	3.041(2)		-Cl(16)	173.11(5)	
...Cl(16)	3.086(2)		-Cl(17)	83.88(6)	
...Cl(17)	3.067(2)				
			Cl(12)-Te(1)-Cl(13)	94.97(7)	
			-Cl(14)	86.91(6)	
Al(1) - Cl(14)	2.145(2)		-Cl(16)	91.98(6)	
- Cl(15)	2.096(3)		-Cl(17)	177.41(6)	
- Cl(16)	2.138(3)				
- Cl(17)	2.151(2)		Cl(13)-Te(1)-Cl(14)	177.13(7)	
			-Cl(16)	85.53(6)	
			-Cl(17)	87.41(6)	
			Cl(14)-Te(1)-Cl(16)	96.58(5)	
			-Cl(17)	90.67(5)	
			Cl(16)-Te(1)-Cl(17)	89.23(4)	
Te(2) - Cl(21)	2.278(2)		Cl(21)-Te(2)-Cl(22)	96.04(7)	
- Cl(22)	2.273(2)		-Cl(23)	96.95(7)	
- Cl(23)	2.275(2)		-Cl(25)	90.83(6)	
...Cl(25)	3.065(2)		-Cl(24)	177.32(6)	
...Cl(24)	3.043(2)		-Cl(26)	92.44(6)	
...Cl(26)	3.150(2)				
			Cl(22)-Te(2)-Cl(23)	95.00(7)	
			-Cl(25)	86.61(6)	
			-Cl(24)	85.24(6)	
			-Cl(26)	171.13(6)	
Al(2) - Cl(24)	2.147(2)		Cl(23)-Te(2)-Cl(25)	172.83(6)	
- Cl(25)	2.153(3)		-Cl(24)	86.28(6)	
- Cl(26)	2.149(2)		-Cl(26)	81.53(7)	
- Cl(27)	2.087(2)				
			Cl(25)-Te(2)-Cl(24)	86.89(5)	
			-Cl(26)	95.86(5)	
			Cl(24)-Te(2)-Cl(26)	86.40(5)	

b) $\text{TeCl}_3(\text{AsF}_6)$

Bond Lengths

Te - Cl(1)	2.258(2)
- Cl(2)	2.266(2)
- Cl(3)	2.268(2)
...F(1)	2.738(5)
...F(2)	2.689(4)
...F(4)	2.962(6)
...F(6)	3.149(6)
...F(1')	3.259(5)
As - F(1)	1.727(4)
- F(2)	1.730(5)
- F(3)	1.663(5)
- F(4)	1.717(5)
- F(5)	1.690(5)
- F(6)	1.685(5)

Bond Angles

Cl(1) - Te - Cl(2)	95.65(9)
- Cl(3)	96.66(8)
...F(1)	84.6(1)
...F(2)	82.9(1)
...F(4)	169.5(1)
...F(6)	143.3(1)
...F(1')	144.0(1)
Cl(2) - Te - Cl(3)	95.69(8)
...F(1)	178.7(1)
...F(2)	80.9(1)
...F(4)	77.1(1)
...F(6)	88.7(2)
...F(1')	120.1(1)
Cl(3) - Te...F(1)	83.0(1)
...F(2)	176.4(1)
...F(4)	76.8(1)
...F(6)	119.2(1)
...F(1')	85.1(1)
F(1)...Te...F(2)	100.5(2)
...F(4)	102.5(2)
...F(6)	91.9(2)
...F(1')	59.8(2)
F(2)...Te...F(4)	103.1(2)
...F(6)	61.8(1)
...F(1')	97.3(2)
F(4)...Te...F(6)	45.2(2)
...F(1')	44.7(1)
F(6)...Te...F(1')	43.5(1)

c) $\text{TeCl}_3(\text{SbF}_6)$

Bond lengths			Bond Angles		
Te(1) - Cl(1)	2.261(2)		Cl(1) - Te(1) - Cl(2)	97.6(1)	
- Cl(2)	2.252(3)		- Cl(1)	92.3(1)	
...F(1)	2.660(6)		...F(1)	85.8(1)	
...F(3)	2.950(6)		...F(3)	133.8(1)	
...F(5)	2.778(4)		...F(5)	75.5(1)	
			...F(5')	167.6(1)	
Sb(1) - F(1)	1.879(5)		Cl(2) - Te(1) ...F(1)	175.0(2)	
- F(2)	1.842(7)		...F(3)	81.6(2)	
- F(3)	1.863(6)		...F(5)	82.3(1)	
- F(4)	1.843(7)		F(1) ...Te(1) ...F(3)	93.4(2)	
- F(5)	1.867(4)		...F(5)	95.1(1)	
			F(3) ...Te(1) ...F(5)	58.5(1)	
			F(5) ...Te(1) ...F(5')	116.6(2)	

d) $(\text{TeF}_3)_2\text{SO}_4$

Bond Lengths			Bond Angles		
Te(1)	- F(11)	1.860(8)	F(11)-Te(1)-F(12)	87.8(4)	
	- F(12)	1.900(8)	-F(13)	86.5(4)	
	- F(13)	1.837(8)	-O(1)	86.5(4)	
	- O(1)	2.213(9)	-O(3)	163.2(4)	
	- O(3)	2.321(11)			
	...O(2)	3.131(10)	F(12)-Te(1)-F(13)	86.5(4)	
	...F(21)	3.321(8)	-O(1)	166.4(4)	
	...F(23)	3.303(8)	-O(3)	82.8(4)	
...F(11')	3.079(8)				
Te(2)	- F(21)	1.850(9)	F(13)-Te(1)-O(1)	80.8(4)	
	- F(22)	1.857(10)	-O(3)	79.1(4)	
	- F(23)	1.845(8)			
	- O(2)	2.374(10)	O(1)-Te(1)-O(3)	99.5(4)	
	- O(4)	2.343(12)			
	...F(12)	2.667(9)	F(21)-Te(2)-F(22)	85.3(4)	
	...O(3)	3.155(11)	-F(23)	89.4(4)	
	...F(22')	3.274(10)	-O(2)	73.8(4)	
		-O(4)	164.8(4)		
S(1)	- O(1)	1.471(9)	F(22)-Te(2)-F(23)	89.1(4)	
	- O(2)	1.477(10)	-O(2)	156.8(4)	
	- O(3)	1.469(10)	-O(4)	81.8(4)	
	- O(4)	1.453(11)			
		F(23)-Te(2)-O(2)	80.7(4)		
		-O(4)	82.3(4)		
		O(2)-Te(2)-O(4)	117.0(4)		

in any significant Te...Cl interactions. In the monoclinic form of this compound the dimensions of the AlCl_4^- anion also illustrate this same trend (104).

$(\text{TeCl}_3^+)(\text{SbF}_6^-)$ and $(\text{TeCl}_3^+)(\text{AsF}_6^-)$: The hexafluoroantimonate salt of the TeCl_3^+ cation crystallizes in the orthorhombic space group Pnma. In this salt the cation has crystallographic mirror symmetry with Cl-Te-Cl angles of $97.6(1)$ (x2) and $92.3(1)^\circ$ (Fig. VII.3). Furthermore, the independent Te--Cl distances of $2.261(2)$ (x2) and $2.252(3)$ Å are significantly shorter than those for $(\text{TeCl}_3)(\text{AlCl}_4)$ or TeCl_4 (Table VII.2). These differences can be correlated with the strengths of the interionic contacts involving each TeCl_3^+ cation. As discussed above, the Te--Cl primary bond length decreases as the Te...Cl secondary bond in a direction approximately trans- to the primary bond increases in length.

In the present salt there are four Te...F contacts shorter than van der Waals distances, three of which may be considered to be capping the Cl-Cl-E faces of the TeCl_3E tetrahedron, with the fourth bridging a Cl...E edge of the same tetrahedron. This arrangement of primary and secondary bonds may be described as $\text{AX}_3\text{Y}'_3\text{E}$ and is related to a tricapped trigonal-prismatic arrangement of ligands $\text{AX}_3\text{Y}'_3\text{E}$ in which all three faces and all three edges of the AX_3E tetrahedron containing the lone pair E would be

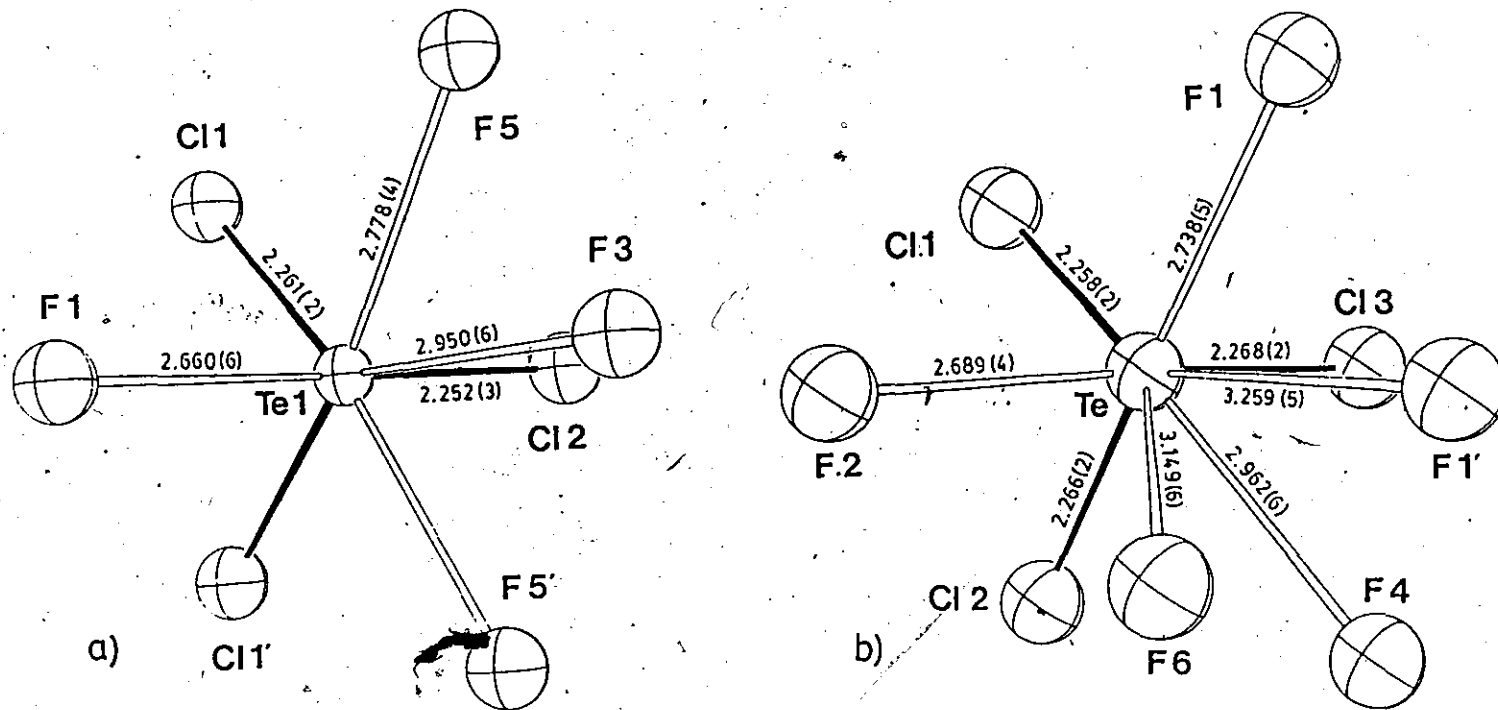


FIGURE VII.3 The TeCl_3^+ cation in a) $\text{TeCl}_3(\text{SbF}_6)$, an example of the $\text{AX}_3\text{Y}_3\text{E}$ geometry, and b) $\text{TeCl}_3(\text{AsF}_6)$, $\text{AX}_3\text{Y}_3\text{E}$. Both views are toward the assumed positions of the lone pairs of electrons.

involved in secondary bonds. In the present salt two of the generally longer Y' edge-bridging contacts are missing. A similar $AX_3Y_3Y'E$ geometry has been described above for the three-coordinate tellurium atom in $Te_{4.5}Se_{5.5}(AsF_6)_2$ (Fig. III.8). A good example of an $AX_3Y_3Y'_3E$ geometry in this class of compounds is available in the structure of $(TeF_3)(Sb_2F_{11})$ (Fig. III.7).

When the difference in van der Waals radii for fluorine and chlorine is taken into consideration, the three face-capping $Te...F$ contacts in $(TeCl_3)(SbF_6)$ are weak compared to the $Te...Cl$ contacts in other $TeCl_3^+$ salts (Table VII.2), but are consistent with the short $Te-Cl$ primary bond lengths observed. This difference in secondary bond strengths for fluorine and chlorine ligands is a function of size and polarizability ($Cl > F$). The effect of the additional edge-bridging contact to F(3) is to lengthen the two $Te-Cl$ bonds (to Cl(1) and Cl(1')) trans- to F(3) relative to $Te-Cl(2)$, which has only one opposing $Te...F$ bond (see Fig. VII.3). The contact to F(3) also serves to spread F(5) and F(5') apart so that $F(1)...Te-Cl(2)$ is closer to 180° ($175.2(2)^\circ$) than are $F(5)...Te-Cl(1')$ and $F(5')...Te-Cl(1)$ ($167.6(1)^\circ$).

The corresponding hexafluoroarsenate salt, $(TeCl_3)(AsF_6)$, is not isomorphous with $(TeCl_3)(SbF_6)$, but crystallizes in the monoclinic space group $P2_1/n$. This

situation was also observed (102) for the corresponding salts $(\text{SeBr}_3)(\text{SbF}_6)$ (orthorhombic, space group $P2_12_12_1$) and $(\text{SeBr}_3)(\text{AsF}_6)$ (monoclinic, space group $P2_1/c$), but this does not completely exclude the possibility that other polymorphic forms of these TeCl_3^+ and SeBr_3^+ salts isomorphous with the current structures might exist.

In $(\text{TeCl}_3)(\text{AsF}_6)$ the TeCl_3^+ cation has no crystallographic symmetry and the Cl-Te-Cl bond angles show that the cation is much less distorted from C_{3v} symmetry than that in the SbF_6^- salt, although the average Cl-Te-Cl angle in both salts is virtually the same (Tables VII.2 and VII.3). The Te-Cl bond lengths in the AsF_6^- salt are marginally longer than those observed for the SbF_6^- salt (Table VII.3). These differences are again related to the secondary bonds to the tellurium atom, and are consistent with AsF_6^- being a better Lewis base (F^- donor) than SbF_6^- .

In $(\text{TeCl}_3)(\text{AsF}_6)$ there are five Te...F interactions which are less than the sum of the van der Waals radii of 3.53 Å (39) and may be considered as secondary bonding interactions. Three of these interactions are approximately trans- to the Te-Cl primary bonds and cap the faces of the TeCl_3E tetrahedron, while two further longer interactions approximately bridge two Cl...E edges of the same tetrahedron (Fig. VII.3). Overall the environment of tellurium in this salt may be designated as $\text{AX}_3\text{Y}_3\text{Y}'_2\text{E}$.

The hexafluoroantimonate and hexafluoroarsenate an-

ions in these two structures are distorted octahedra with Sb--F and As--F bond lengths of 1.842(7) to 1.879(5) Å and 1.663(5) to 1.730(5) Å respectively. The primary bonds to fluorine atoms involved in the shortest Te...F contacts are slightly longer than those to atoms which do not form any contacts (Table VII.3).

(TeF₃)₂(SO₄): In this salt the distinction between an ionic formulation and a covalently linked sulfate adduct is not clear since some of the anion-cation Te...O distances are as short as 2.213(9) Å (Table VII.3). Similar I--O and Xe--O bond lengths of 2.26(1) and 2.22(2) Å respectively are found in I₂S₂O₆F₂ (109) and the [(XeF₂)₂SO₃F]⁺ cation (110). In fact, each tellurium atom of (TeF₃)₂(SO₄) forms two short Te--O bonds so that the primary geometry of these atoms can be considered to be distorted AX₅E with the lone pairs in the remaining octahedral position, trans- to the shorter Te(1)--F(13) and Te(2)--F(23) axial bonds (Fig. VII.4). The remaining Te--F bond lengths then appear to be a function of the strength of the trans- related Te--O distances (Table VII.3). The Te(1)--F(12) bond is particularly long since F(12) is also involved in a secondary bond to Te(2). The atoms F(11), F(12), O(1) and O(3) constitute an equatorial plane of the Te(1) octahedron and are all pushed slightly out of the plane of Te(1) and towards the apical F(13) atom. Valence-shell electron-pair repulsion theory predicts this

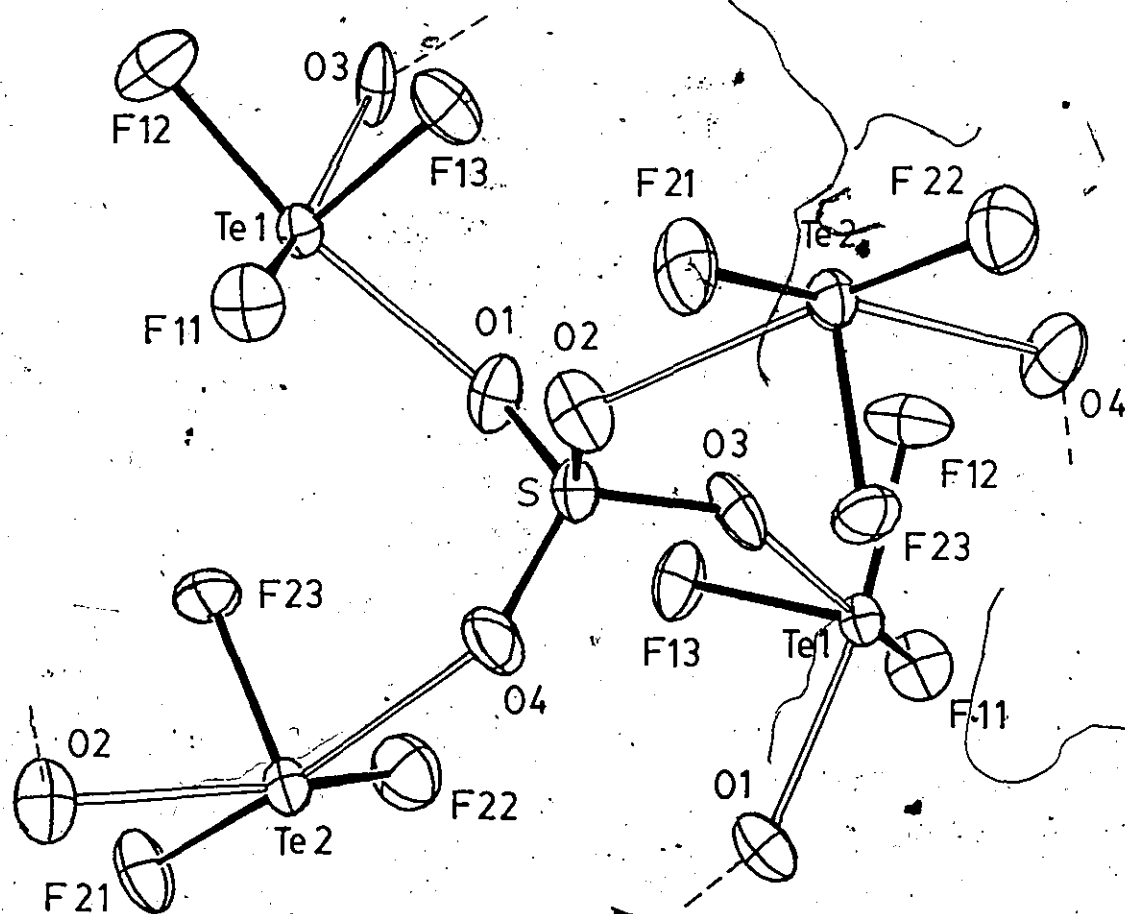


FIGURE VII.4 ORTEP drawing of the polymeric $(\text{TeF}_3)_2\text{SO}_4$ structure. Unfilled bonds between TeF_3 and SO_4 groups range from 2.21 to 2.37 Å in length (see Table VII.3). Dotted lines indicate primary bonds to next-nearest sulfur atoms.

distortion, resulting from the greater repulsive effect of the lone pair of electrons compared to the pair of electrons forming the Te(1)-F(13) bond (61). The AX_5E geometry observed here is rather different from that of the MX_3^+ salts described above, but is rather similar to that of TeF_4 (111).

Completing the overall coordination shell of each tellurium atom of $(TeF_3)_2(SO_4)$ out to the van der Waals limits are three further contacts at Te(2) and four contacts at Te(1) (Fig. VII.5). These remote atoms are arranged such that they are approximately capping three or four faces of the AX_5E octahedron describing the primary geometry. The overall geometry of Te(1) can be described as AX_5Y_4E and that of Te(2) as AX_5Y_3E . Remarkably similar AX_5Y_4E geometries are observed for the XeF_5^+ cation in $(XeF_5)(PtF_6)$ and for IF_5 in the $XeF_2(IF_5)$ adduct (112, 113). In TeF_4 there are three face-capping contacts, as for Te(2) above (111).

VII.7 The Geometry of MX_3^+ Cations.

It is interesting to note the close similarity of the geometry of the MX_3^+ cations to the isoelectronic Group V trihalide molecules. The bond lengths are in every case shorter and the bond angles slightly larger in the Group VI trihalide cations (see ref. (102), Table 6). The shorter bond lengths in the cations are consistent with the smaller covalent radii of the central atoms and the positive charge

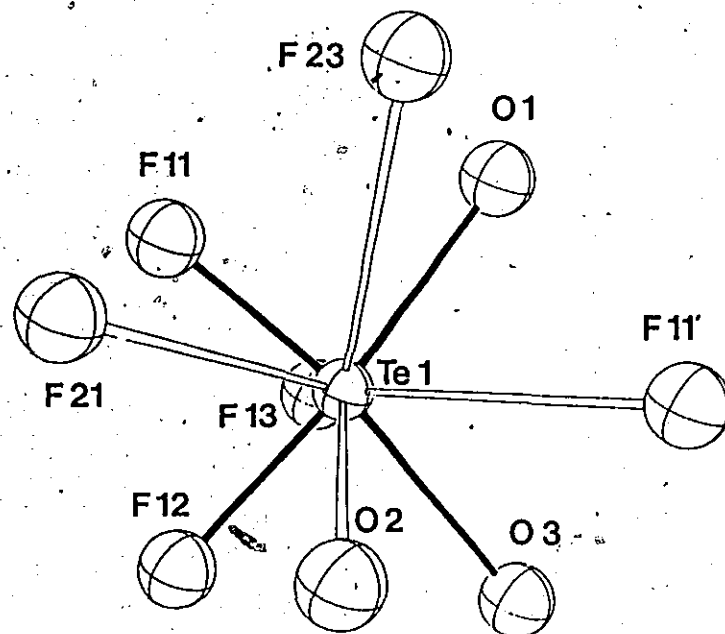
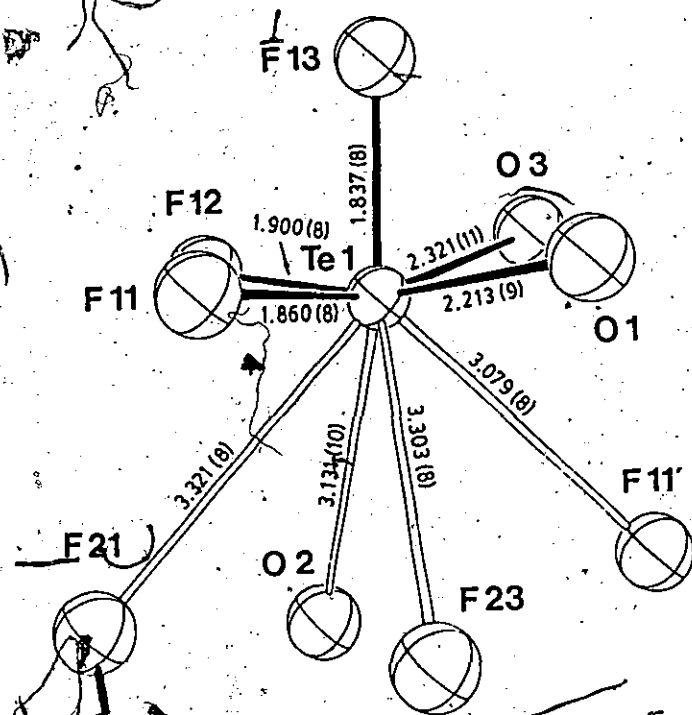


FIGURE VII.5 Two views of Te(1) in $(\text{TeF}_3)_2\text{SO}_4$ showing secondary bonds (unfilled bonds) capping X-X-E faces of the AX_5E polyhedron, giving an overall $\text{AX}_5\text{Y}_4\text{E}$ geometry. Right hand view is toward assumed direction of the lone pair of electrons.

may also have a small bond-shortening effect. The bonding electron pairs in the short bonds in the cations will be closer together and therefore repel each other more strongly than in the neutral molecules, leading to the larger observed bond angles. In addition, the electronegativity of a positively-charged chalcogen central atom is greater than that of a neutral group V atom and according to VSEPR theory the bonding pairs of electrons would then be relatively closer to the central atoms of the cations and take up more space in the valence shell of the central atom, contributing to the observed increase in the bond angle.

Secondary bonding is generally weaker in structures of the neutral molecules than the anion-cation interactions observed in the MX_3^+ structures. Since secondary bonds tend to weaken the M--X primary bonds (see section VI.12), bond pair - bond pair repulsions decrease with respect to lone pair - bond pair repulsions with increasing secondary bond strength, decreasing the X-M-X angles. The angle expansion in going from a neutral molecule to an MX_3^+ cation is therefore not as large as might be anticipated. For example, the mean Cl-P-Cl angle from the low temperature crystal structure of PCl_3 (114) is $100.09(9)^\circ$ and the inter-molecular contacts are all greater than the van der Waals distance. This angle is only marginally less than the mean Cl-S-Cl angles of $101.3(1)^\circ$ and $103.7(2)^\circ$ in $(\text{SCl}_2)_2$ and (ICl_4) and

(SbCl_3)(SbCl_6^-) respectively (115, 116). The larger angle in the SbCl_6^- salt is consistent with the weaker $\text{S}\cdots\text{Cl}$ bonds in this structure compared to the ICl_4^- salt (Table VII.2).

In the two series MF_3^+ and MCl_3^+ ($\text{M} = \text{S}, \text{Se}, \text{Te}$) the bonding electron pairs become further apart as M increases in size and the $\text{M}-\text{F}$ or $\text{M}-\text{Cl}$ bonds increase in length. These electron pairs therefore will repel each other less strongly and the lone pair of electrons will spread out over the surface of the central atom, reducing the angle between the bonding pairs of electrons. The $\text{X}-\text{M}-\text{X}$ bond angle steadily decreases from sulfur to selenium to tellurium in both of these series (Table VII.2). Similarly, $\text{X}-\text{M}-\text{X}$ is smaller in (TeBr_3)(AsF_6^-) than in (SeBr_3)(SbF_6^-). This trend can also be explained using a hybridization model and the inert pair effect. The increasing s-p energy separation down a group leads to the lone pair on tellurium having more s-character than for the other chalcogens. As a consequence, the $\text{M}-\text{X}$ primary bonds for tellurium have more p-character and therefore a correspondingly smaller bond angle. In the SnBr_3^- anion of CsSnBr_3 (117) the central tin atom is surrounded by a perfect octahedron of bromine atoms. The lone pair is stereoinactive and presumably resides in a spherical s-orbital. The same argument holds for the TeCl_6^{2-} anion (118).

In the series SX_3^+ , SeX_3^+ , and TeX_3^+ , $\text{X}-\text{M}-\text{X}$ increases in the order $\text{F} < \text{Cl} < \text{Br} < \text{I}$. A similar trend is noted for

the isoelectronic neutral molecules and is consistent with the changing electronegativity of X. The greater the electronegativity of X, the more X contracts the charge cloud of the bonding pair and attracts it to itself, reducing the repulsion between bond pairs and decreasing the X-M-X angle, despite shorter bond lengths. For example, X-Te-X is $90(2)^\circ$ in $(\text{TeF}_8)(\text{Sb}_2\text{F}_{11})$ compared to $96.0(1)^\circ$ and $95.8(1)^\circ$ in $(\text{TeCl}_3)(\text{AsF}_6)$ and $(\text{TeCl}_3)(\text{SbF}_6)$, $97.92(8)^\circ$ in $(\text{TeBr}_3)(\text{AsF}_6)$ and $99.9(1)^\circ$ in $(\text{TeI}_3)(\text{AsF}_6)$ (Table VII.2).

The geometry of the secondary bonds also changes in a regular manner. In general these interactions are formed in those directions which avoid the concentrations of electron density due to the primary bonds and the lone pair. They are therefore formed in directions between the unshared pair and the bond pairs. It is noted above that the bonding pairs are forced closer together as M increases in size in the series MF_3^+ , MCl_3^+ and MBr_3^+ as the lone pair spreads out on the surface of the larger central atom. The secondary bonds that form around this spreading lone pair are forced further and further apart and closer to the primary bonds in the same series. For example, the mean secondary secondary bond angle, Y...M...Y, increases from $76.52(5)$ to 82.1 to $90.94(5)^\circ$ in $(\text{SbCl}_3)(\text{SbCl}_6)$, $(\text{SeCl}_3)(\text{AlCl}_4)$ and $(\text{TeCl}_3)(\text{AlCl}_4)$ -triclinic respectively. The same trend is observed for SeF_3^+ and TeF_3^+ or SeBr_3^+ and TeBr_3^+ salts.

(Table VII.2).

VII.9 Anion-Cation Interactions in MX_3^+ Cations.

There are significant anion-cation contacts in all of the characterized examples of the MX_3^+ cations. The strength of these interactions at M, i.e. M...Y, increases in the series S < Se < Te, consistent with the increasing electropositive nature of the chalcogens in the same order. For example, M...Y is 3.220(3), 3.13(1) and 3.075(2) Å in the compounds $(\text{SbCl}_3)(\text{SbCl}_6)$, $(\text{SeCl}_3)(\text{SbCl}_6)$ and $(\text{TeCl}_3)(\text{AlCl}_4)$ -triclinic respectively (Table VII.2). These distances are 0.35, 0.52 and 0.73 Å respectively less than the van der Waals limiting distances (39). The stronger secondary bonds are probably partially responsible for the increase in the Y...M...Y angle down the group. The trend in this angle is described above in relation to the greater stereoactivity of the lone pair down the group.

Contacts to M similarly depend on the nature of Y. The degree of charge-transfer from the anion to the TeCl_3^+ cation is apparently greater in the AlCl_4^- salt than in the AsF_6^- and SbF_6^- salts, since the Te-Cl primary bonds are somewhat longer in the AlCl_4^- salt (Table VII.2). This is not too surprising since chlorine is larger and more polarizable than fluorine. The above comparison is conditional, however, on the overall environment of the central atom remaining essentially the same in the different salts. Most

of the cations have simple AX_3Y_3E geometries. The $TeCl_3^+$ cation has additional edge-bridging contacts in the AsF_6^- and $SbCl_6^-$ salts, but the degree of charge-transfer is still apparently somewhat less in these salts than in the $AlCl_4^-$ salt. There are variations in the $M...Y$ interaction for a given Y as well, depending on the Lewis basicity of the anion. The $M...Y$ distance in $(SbCl_3)(SbCl_6^-)$, for example, is somewhat longer than in $(SbCl_3)(ICl_4^-)$ (Table VII.2), consistent with $SbCl_5$ being a stronger Lewis acid than ICl_3 (116). Variations in the length of the $Te-Cl$ bond in $TeCl_3^+$ salts can be correlated with the positions of $TeCl_3^+$ stretches in their Raman spectra. The symmetric stretching vibration of the $TeCl_3^+$ cation occurs at successively higher frequencies in the Raman spectra of $TeCl_4$, $(TeCl_3)(AlCl_4^-)$ and $(TeCl_3)(AsF_6^-)$ (Fig. VII.1), consistent with a decrease in the primary $Te-Cl$ bond length in the same series (Table VII.2). This stretch occurs at a higher frequency in $(TeCl_3)(SbCl_6^-)$ than in $(TeCl_3)(AlCl_4^-)$, indicating that anion-cation interactions are weaker and the $Te-Cl$ primary bond somewhat shorter in the $SbCl_6^-$ salt than in the $AlCl_4^-$ salt. The $SbCl_6^-$ anion then is apparently a somewhat weaker Lewis base than $AlCl_4^-$, or in other words $SbCl_5$ is a stronger Lewis acid than $AlCl_3$.

For a given M the tendency for contacts to X , that is $X...Y$, to become significant increases in the order $F < Cl << Br < I$, corresponding to the increasing polarizability

and electropositive nature of X in the same series. In the structures reported here this type of contact is not prevalent, but they can be seen in structures of the compounds $(\text{SeBr}_3)(\text{SbF}_6)$, $(\text{TeBr}_3)(\text{AsF}_6)$ and $(\text{TeI}_3)(\text{AsF}_6)$ (102, 134). Consistent with the increase in the interactions at X appears to be a tendency for the contacts to M to simultaneously decrease in strength, that is the degree of charge-transfer to the cation via both the M and X contacts appears to be constant. The M...Y distance steadily increases from 2.59(3) to 2.738(5) to 2.84(1) to 2.98(1) Å in the compounds $(\text{TeF}_3)(\text{Sb}_2\text{F}_{11})$, $(\text{TeCl}_3)(\text{SbF}_6)$, $(\text{TeBr}_3)(\text{AsF}_6)$ and $(\text{TeI}_3)(\text{AsF}_6)$ respectively (Table VII.2).

VII.10 F-19, Se-77 and Te-125 NMR of SeF_3^+ and TeF_3^+ .

It is clear from the above discussion that the X-M-X bond angle decreases steadily in the series $\text{SX}_3^+ > \text{SeX}_3^+ > \text{TeX}_3^+$ for the crystal structures examined. It was also of interest to determine if the same angle dependence could be observed in solution. To this end, the ^{19}F , ^{77}Se and ^{125}Te NMR spectra of the SeF_3^+ and TeF_3^+ cations were obtained so that the ^{19}F - ^{77}Se and ^{19}F - ^{125}Te coupling constants could be used to compare the F-Se-F and F-Te-F bond angles in these cations in solution. The Fermi contact mechanism, which is concerned with the degree of s-character in a bond, generally dominates spin-spin coupling in high resolution NMR (12). Since the X-M-X bond angle is related to the amount

of s-character in the M--X bond, that is a large bond angle corresponds to a high degree of s-character, trends in the X-M-X bond angle can be related to changes in the spin-spin coupling constants.

Observed scalar coupling constants involving different nuclei cannot be compared directly, but useful comparisons can be made using reduced coupling constants, K_{MX} , which take into account the different magnetogyric ratios of the nuclides being compared (120). Reduced density coupling constants, L_{MX} , additionally correct for relativistic effects which become important for heavy nuclei (121-123).

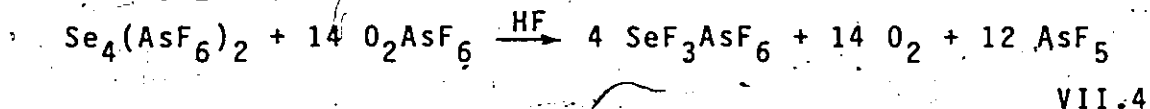
$$K_{MX} = (4\pi^2/h)J_{MX}(\gamma_M\gamma_X)^{-1} \quad \text{VII.2}$$

$$L_{MX} = (4\pi^2/c^2)K_{MX}(\nu(-1)_M\nu(-1)_X)^{-1} \quad \text{VII.3}$$

where h is Planck's constant, c is the speed of light, γ_M is the magnetogyric ratio of nucleus M (in nuclear magnetons) and $\nu(-1)_M$ is the hyperfine integral of nucleus M (a measure of the s-electron density of nucleus M). The hyperfine integrals of the main group elements have been tabulated in ref. (121): $F = -0.5272571$, $Se = -0.8300371$, $Te = -1.2585161$.

The TeF_3^+ cation was obtained by three routes (Table VII.4): 1) the reaction of TeF_4 with excess AsF_5 in SO_2 , 2) the reaction of $Te(O_2TeF_5)_4$ with excess AsF_5 in SO_2 and 3) the direct fluorination of elemental tellurium with SbF_5 in SO_2 . Excess AsF_5 was used in the first two reactions to help reduce line broadening by suppression of fluoride ex-

change in the presence of excess Lewis acid (124). Trifluoro-selenium hexafluoroarsenate was prepared by the reaction of $\text{Se}_4(\text{AsF}_6)_2$ with O_2AsF_6 (reaction VII.4).



An excess of $\text{Se}_4(\text{AsF}_6)_2$ was used since O_2^+ is paramagnetic and if present in even small amounts could cause significant line broadening in the NMR spectra. Anhydrous hydrogen fluoride was used as the solvent in the preparation since O_2^+ would be expected to oxidize SO_2 to SO_3 . Sulfur dioxide was the preferred solvent for the NMR samples and, with the exception of the Te/SbF_5 solution, low temperatures were employed to reduce line broadening resulting from fluoride exchange. The ^{125}Te NMR spectrum of a $\text{TeF}_4/\text{AsF}_5$ solution in SO_2 recorded at 200 K is given as Fig. VII.6.

The ^{19}F , ^{77}Se and ^{125}Te NMR parameters for the SeF_3^+ and TeF_3^+ cations are given in Table VII.4. The mean ^{19}F - ^{77}Se and ^{19}F - ^{125}Te coupling constants are 1202 and 2907 Hz respectively. The SeF_3^+ coupling compares well with the value of 1213 Hz reported for the ^{19}F NMR spectrum of a solution of $\text{SeF}_4(\text{BF}_3)$ in HF (124). The ^{19}F - ^{77}Se and ^{19}F - ^{125}Te couplings in SeF_3^+ and TeF_3^+ are compared with other Se-F and Te-F compounds in Table VII.5. The reduced density coupling constants for a given pair of Se(VI) and Te(VI) compounds should be approximately equal since the environments and bonding of the species are expected to be

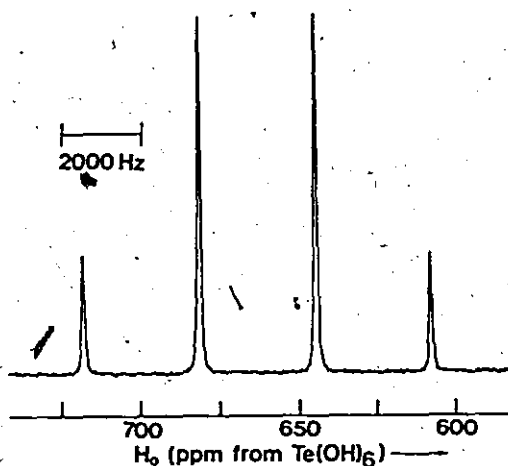


FIGURE VII.6 ^{125}Te NMR spectrum of the TeF_3^+ cation in SO_2 at 200 K (78.97 MHz; 0.47 m; 5800 scans; 6.1 Hz/pt).

Table VII.4 NMR Parameters^a for SeF_3^+ and TeF_3^+ .

Cation	δ (ppm)		J (Hz)			
	^{19}F	^{77}Se	^{125}Te	^{19}F - ^{77}Se	^{19}F - ^{125}Te	^{19}F - ^{125}Te
SeF_3^{+b}	11.2	-112.0		1201 ^c 1203 ^d		
TeF_3^+	-47.2 ^e		663.2 ^e 673.9 ^{e,f}		2430 ^{c,e}	2915 ^{c,e} 29149 ^e
	-45.1 ^h -43.1 ^{f,h}		688.9 ^{f,h}			2885 ^{c,h} 29189 ^{f,h}
			671.2 ⁱ			29059 ⁱ

(a) Spectra recorded at 200 K unless otherwise indicated. $\delta(^{19}\text{F})$, $\delta(^{77}\text{Se})$ and $\delta(^{125}\text{Te})$ referenced to external CFCl_3 , saturated aqueous H_2SeO_3 and saturated aqueous Te(OH)_6 at 295 K respectively.

(b) a 0.20 m solution of $\text{SeF}_3(\text{AsF}_6)$ in SO_2 . (c) From ^{19}F spectrum.

(d) From ^{77}Se spectrum. (e) TeF_4 (0.3862 g, 1.897 mmol) + AsF_5 (1.28 g, 7.51 mmol) + SO_2 (3 g) (see Fig. VII.6). (f) 295 K.


(g) From ^{125}Te spectrum. (h) Minor product of 0.2 g Te + 0.4 mL SbF_5 in 3 mL SO_2 , stirred and filtered after 48 h. (i) $\text{Te(OTeF}_5)_4$ (0.9287 g, 0.8583 mmol) + AsF_5 (0.729 g, 4.29 mmol) + 2.5 g SO_2 (Table VIII.1, Fig. VIII.3).

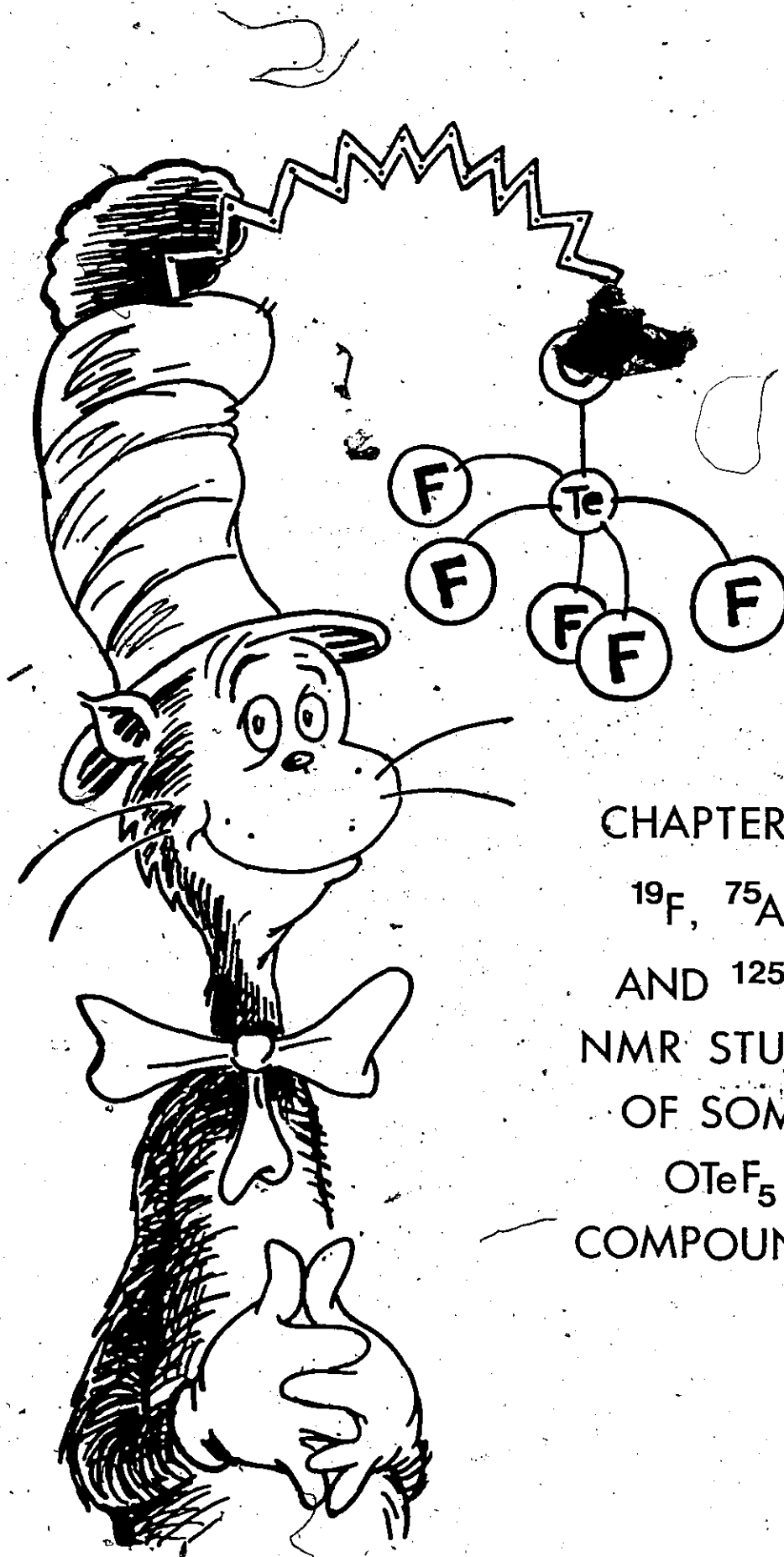
Table VII.5 Comparison of ^{19}F - ^{77}Se and ^{19}F - ^{125}Te Coupling Constants.

Solute	J_{MX}^{a} (Hz)	K_{MX}^{b} ($10^{21} \text{NA}^{-2} \text{m}^{-3}$)	L_{MX}^{c} ($10^{-43} \text{NA}^{-2} \text{m}^3$)	Ref.
SeF_3^+	1202 ^d	5.579	5.885	f
TeF_3	2907 ^d	8.142	5.664	f
SeF_6	1421	6.595	6.957	135
TeF_6	3736	10.463	7.279	136
HOSeF_5	1300 ^e	6.033	6.364	137
HOTeF_5	3577 ^e	10.018	6.970	138
$\text{Xe}(\text{OSeF}_5)_2$	1338 ^e	6.210	6.550	139
$\text{Xe}(\text{OTeF}_5)_2$	3600 ^e	10.082	7.014	139
$\text{F}_5\text{SeOSeF}_5$	1431 ^e	6.641	7.005	139
$\text{F}_5\text{TeOTeF}_5$	3830 ^e	10.727	7.463	139

(a) Scalar coupling constant. All couplings are absolute values. (b) Reduced coupling constant. (c) Reduced density coupling constant. (d) Mean value, see Table VII.4. (e) Coupling to equatorial F atoms. (f) This work.

nearly identical (i.e. octahedral, or pseudooctahedral for the OMF_5 species). These couplings are in fact very close in value, although L_{TeF} is generally somewhat larger than L_{SeF} (Table VII.5). The reduced density coupling constants for SeF_3^+ and TeF_3^+ are smaller than for the Se(VI) and Te(VI) species and in this case L_{SeF} is larger than L_{TeF} . This indicates that the M--F bonds have more s-character in SeF_3^+ than TeF_3^+ , or in other words the F-Se-F bond angle would be expected to be somewhat larger than the F-Te-F bond angle, which is consistent with X-ray crystallographic findings (46, 125, 126). This NMR result may be fortuitous, however, since other terms may also contribute to spin-spin coupling.

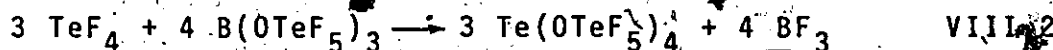




CHAPTER VIII
 ^{19}F , ^{75}As
AND ^{125}Te
NMR STUDY
OF SOME
 OTeF_5
COMPOUNDS

VIII.1 Introduction.

The discovery of pentafluoroorthotelluric acid, HOTeF_5 , by Engelbrecht and Stadky (140) opened the door to a new class of compounds. The OTeF_5 ligand is almost as electronegative as fluorine (136)-and OTeF_5 analogues of most of the known fluorides have been prepared (141, 142), including the noble gas compounds $\text{Xe}(\text{OTeF}_5)_2$ and $\text{Xe}(\text{OTeF}_5)_4$ (143, 144). The reaction of HOTeF_5 with boron trichloride, reaction VIII.1, leads to $\text{B}(\text{OTeF}_5)_3$ (145, 146), which is a very effective OTeF_5 -donor in substitution reactions such as VIII.2 (34).



The C_{4v} symmetry of the OTeF_5 group has been established by vibrational spectroscopic studies of OTeF_5^- salts (147) and by the characteristic AB_4 patterns in the ^{19}F NMR spectra of all of the compounds so far examined (142). X-ray crystallography has confirmed this geometry in a handful of compounds including $\text{Te}(\text{OTeF}_5)_6$ and $\text{B}(\text{OTeF}_5)_3$ (34, 146). An ORTEP drawing of $\text{B}(\text{OTeF}_5)_3$ is shown in Figure VIII.1.

A considerable portion of the main-group chemistry of simple binary fluorides is based upon the fluoride ion donor/acceptor properties of the parent compounds. In the present work we have extended the analogy to the OTeF_5^- anion and have studied its donor/acceptor properties in a series of mixed F/OTeF_5 compounds of $\text{Te}(\text{IV})$. Several examp-

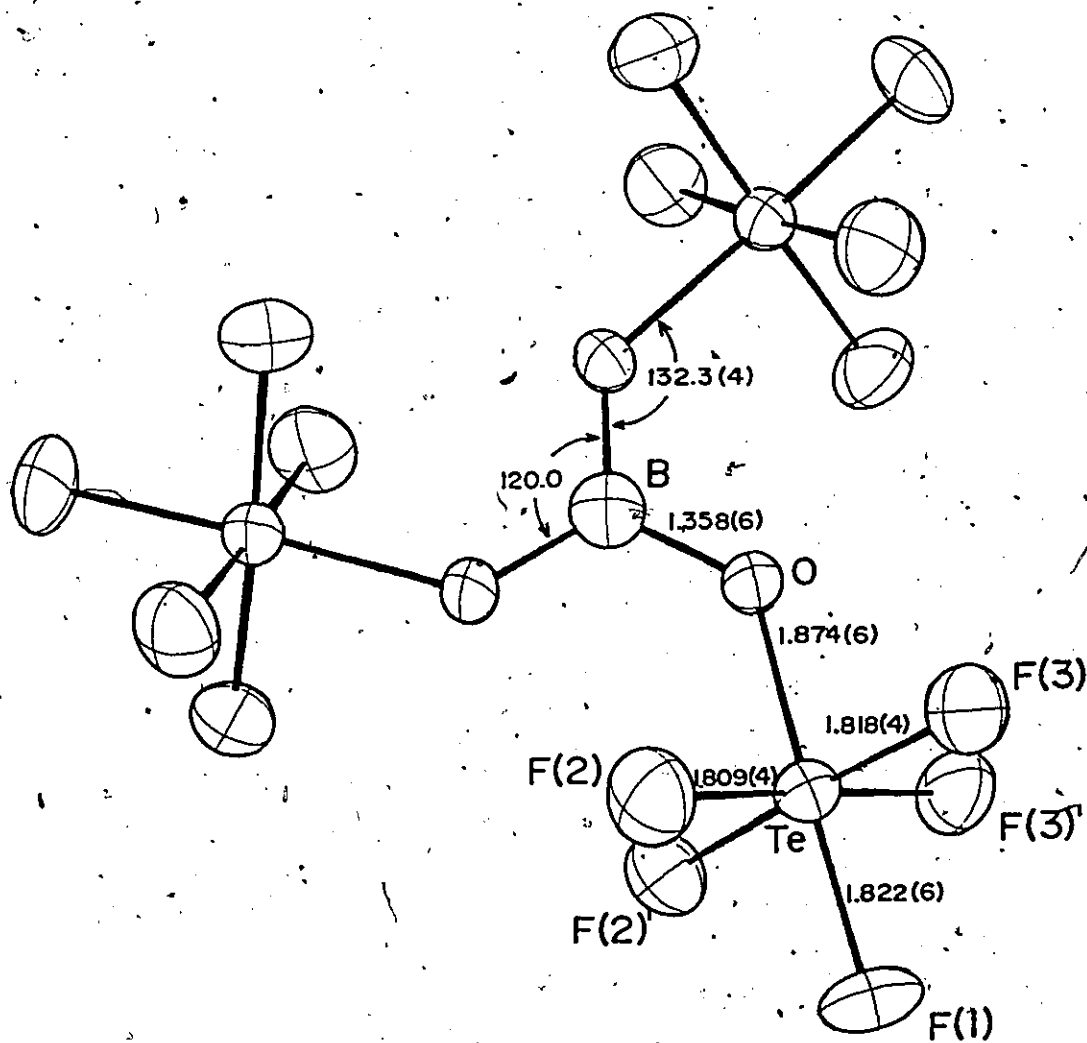


FIGURE VIII.1 ORTEP drawing of $B(OTeF_5)_3$ (reproduced from reference (146)).

les of OTeF_5/F ligand redistributions have been reported for derivatives of $\text{Xe}(\text{OTeF}_5)_2$, $\text{Xe}(\text{OTeF}_5)_4$ and $\text{OXe}(\text{OTeF}_5)_4$ (148). The OTeF_5 analogue of AsF_5 , $\text{As}(\text{OTeF}_5)_5$, has been prepared and employed as an acceptor species for OTeF_5^- in the course of the present investigations. Its preparation has also been described recently by Lentz and Seppelt (149). The precursor OTeF_5^- ion donor used in the present study, $\text{Te}(\text{OTeF}_5)_4$, had been prepared and studied earlier using room temperature ^{19}F NMR spectroscopy as the chief means of structural characterization (34). A subsequent low temperature ^{125}Te NMR study showed the structure of $\text{Te}(\text{OTeF}_5)_4$ to be consistent with a trigonal bipyramid undergoing rapid intramolecular exchange between the axial and equatorial ligand sites (136).

VIII.2 Preparation of $\text{TeF}_x(\text{OTeF}_5)_{4-x}$

Tellurium tetrakis(pentafluoroorthotellurate) was prepared by the stoichiometric reaction of TeF_4 with $\text{B}(\text{OTeF}_5)_3$ as reported previously (34). Mixed fluorides/pentafluoroorthotellurates were prepared using one half the amount of $\text{B}(\text{OTeF}_5)_3$ required for complete reaction with TeF_4 . In a typical reaction, TeF_4 (0.5906 g, 2.901 mmol) was weighed into a glass vessel equipped with a Rotaflo valve and $\text{B}(\text{OTeF}_5)_3$ (1.405 g, 1.934 mmol) was distilled onto the TeF_4 , the valve closed, and the mixture fused at ca. 400 K. Boron trifluoride was slowly liberated. When no

further gas evolution was observed the mixture was cooled to room temperature and the BF_3 removed by pumping under vacuum for several minutes, leaving a colorless crystalline solid.

VIII.3 Preparation of $[\text{TeF}_x(\text{OTeF}_5)_{3-x}]^+[\text{AsF}_y(\text{OTeF}_5)_{6-y}]^-$.

Mixed F/OTeF₅ derivatives of $(\text{TeF}_3)(\text{AsF}_6)$ were prepared directly in 10 mm NMR tubes by the addition of AsF_5 to $\text{Te}(\text{OTeF}_5)_4$ or $\text{TeF}_x(\text{OTeF}_5)_{4-x}$ in SO_2 solution. In a typical reaction AsF_5 (0.0692 g, 0.408 mmol) was distilled onto SO_2 (2 mL) and $\text{Te}(\text{OTeF}_5)_4$ (0.4433 g, 0.4097 mmol) in a 10 mm NMR tube and the end flame-sealed. Upon thawing the reaction mixture a colorless solution was produced with no residue.

VIII.4 Preparation of $\text{As}(\text{OTeF}_5)_5$.

The synthetic route employed here is analogous to that used for $\text{Te}(\text{OTeF}_5)_4$. In a typical reaction $\text{B}(\text{OTeF}_5)_3$ (5.7893 g, 7.968 mmol) was weighed into one bulb of a double-bulb reaction vessel equipped with a magnetic stirring bar and a glass frit separating the two bulbs. Arsenic pentafluoride (0.8217 g, 4.836 mmol) was added to a thin-walled glass weighing bulb prior to condensing, along with SO_2 (30 mL), into the reaction vessel containing $\text{B}(\text{OTeF}_5)_3$. The vessel was then flame-sealed, the resulting colorless solution stirred for 48 h and upon removal of the solvent by static distillation into the other bulb of the reaction vessel, colorless crystals of $\text{As}(\text{OTeF}_5)_5$ were deposited.

The low-melting crystals were washed several times with cold (ca. 250 K) SO_2 . Residual SO_2 was removed by freezing the other bulb of the vessel in liquid N_2 for 1 h before flame-sealing the bulb containing $\text{As}(\text{OTeF}_5)_5$. Raman spectrum of $\text{As}(\text{OTeF}_5)_5$ at 77 K (cm^{-1} , values in parentheses denote intensities): 760(6), 722(77), 690(85), 679(31), 670(100), 658(13), 554(31), 535(17), 519(56), 486(10), 331(16), 318(38), 283(6), 250(15), 215(5), 144(46), 134(13). This spectrum is significantly different from that reported by Lentz and Seppelt (149). Their ^{19}F NMR data, however, agrees well with ours, although a different sign convention was used. It is possible that their Raman sample, which was obtained via sublimation, was a different crystalline phase from that reported here.

VIII.5 Preparation of $\text{Cs}[\text{As}(\text{OTeF}_5)_6]$.

Cesium pentafluoroorthotellurate was prepared from CsCl and HOTeF_5 as previously described (147). Cesium chloride was dried at 430 K for 96 h and under vacuum at 450 K overnight. Stoichiometric portions of $\text{Cs}[\text{OTeF}_5]$ (0.1542 g, 0.4151 mmol), and $\text{As}(\text{OTeF}_5)_5$ (0.5247 g, 0.4138 mmol) were combined in an FEP tube fitted with a valve and melted and thoroughly mixed at ca. 350 K.

VIII.6 Tellurium-125 NMR of $\text{TeF}_x(\text{OTeF}_5)_{4-x}$.

When a mixture of the compounds $\text{TeF}_x(\text{OTeF}_5)_{4-x}$ was dissolved in SO_2ClF and the solution cooled to 200 K, fluor-

ine. exchange was slowed sufficiently on the NMR time scale for the individual compounds $\text{TeF}_x(\text{OTeF}_5)_{4-x}$ ($x = 0, 1$ or 2) to be identified (Fig. VIII.2). As previously reported (136), a $\text{Te}(\text{OTeF}_5)_4$ signal is observed at 602.4 ppm in the Te(IV) region of the spectrum. The monofluoro derivative, $\text{TeF}(\text{OTeF}_5)_3$, is identified by the doublet pattern resulting from a directly-bonded ^{19}F - $^{125}\text{Te}(\text{IV})$ coupling of 2810 Hz. The ^{19}F - ^{125}Te coupling in TeF_3^+ , which also has tellurium in its +4 oxidation state is 2914 Hz (section VII.8). The 1:2:1 triplet assigned to $\text{TeF}_2(\text{OTeF}_5)_2$ has a directly-bonded ^{19}F - $^{125}\text{Te}(\text{IV})$ coupling of 2850 Hz. There is a further coupling of Te(IV) to the equatorial fluorine atoms on Te(VI) of 40 Hz. This long-range coupling was not resolved for the other two $\text{TeF}_x(\text{OTeF}_5)_{4-x}$ compounds, but has been reported (136) to be 31.8 Hz for $\text{Te}(\text{OTeF}_5)_4$ in SO_2ClF . Long-range coupling of Te(IV) to the axial fluorine atom was not resolved for any of the compounds. The ^{129}Xe NMR spectra of XeOTeF_5^+ , $\text{XeF}_y(\text{OTeF}_5)_{2-y}$, $\text{OXeF}_x(\text{OTeF}_5)_{4-x}$, $\text{XeF}_x(\text{OTeF}_5)_{4-x}$ and $\text{O}_2\text{XeF}_y(\text{OTeF}_5)_{2-y}$ ($x = 0-4$ and $y = 0-2$) similarly display fine structure resulting from ^{129}Xe coupling to the equatorial fluorine atoms of the OTeF_5 groups only (138, 148). All of the peaks in Figure VIII.2 are broadened due to these small couplings and/or residual ligand exchange.

Satellite peaks resulting from $^{125}\text{Te}(\text{IV})$ - $^{125}\text{Te}(\text{VI})$ couplings are observed for $\text{TeF}(\text{OTeF}_5)_3$ and $\text{TeF}_2(\text{OTeF}_5)_2$ with

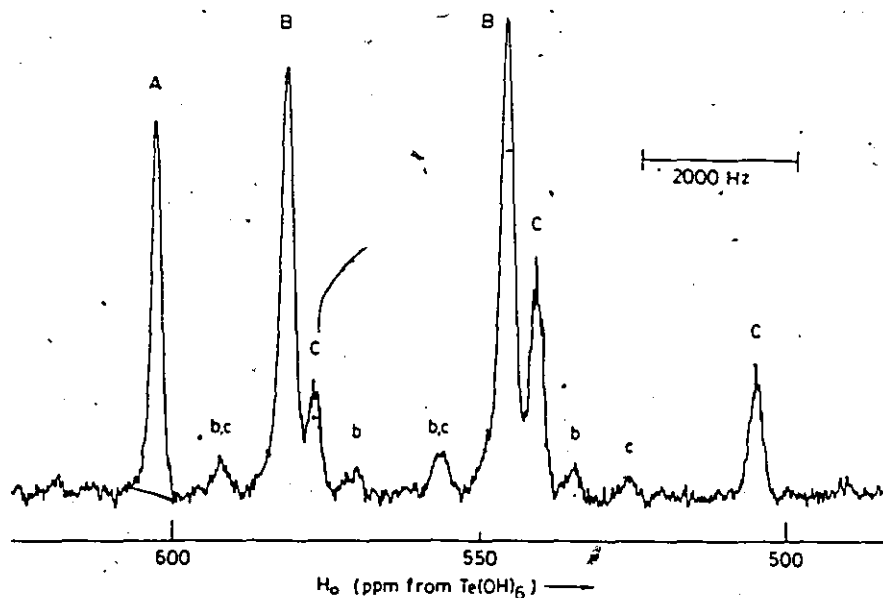


FIGURE VIII.2 ^{125}Te NMR spectrum of a 3:2 mixture of TeF_4 and $\text{B}(\text{OTeF}_5)_3$ in SO_2ClF at 200 K, Te(IV) region (0.77 m Te(IV)); 48,000 scans; 6.1 Hz/pt). (A) $\text{Te}(\text{OTeF}_5)_4$; (B) $\text{TeF}(\text{OTeF}_5)_3$; (C) $\text{TeF}_2(\text{OTeF}_5)_2$. (b) and (c) denote $^2\text{J}[^{125}\text{Te}(\text{IV})-^{125}\text{Te}(\text{VI})]$. $^3\text{J}[^{19}\text{F}-^{125}\text{Te}(\text{IV})]$ is resolved for $\text{TeF}_2(\text{OTeF}_5)_2$.

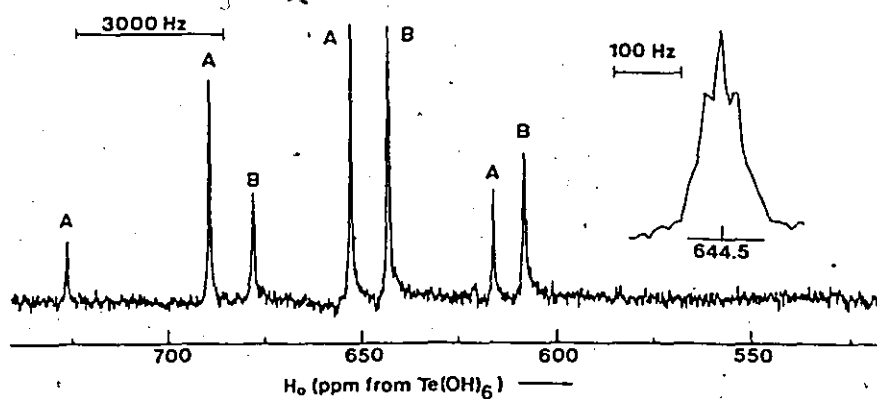


FIGURE VIII.3 ^{125}Te NMR spectrum for the reaction of $\text{Te}(\text{OTeF}_5)_4$ with excess AsF_5 in SO_2 , Te(IV) region at 200 K (0.34 m $\text{Te}(\text{OTeF}_5)_4$; 35,000 scans; 6.1 Hz/pt). (A) TeF_3^+ ; (B) $\text{TeF}_2(\text{OTeF}_5)^+$. Inset shows quintet resulting from coupling of Te(IV) to the equatorial fluorine atoms of the OTeF_5 group in $\text{TeF}_2(\text{OTeF}_5)^+$. Coupling to the axial fluorine atom is not resolved.

values of 1730 and 2440 Hz respectively (Table VIII.1). The analogous coupling for $\text{Te}(\text{OTeF}_5)_4$ is only 544 Hz in CH_3CN (136) and couplings to axial and equatorial OTeF_5 groups are 670 and 840 Hz respectively in SO_2ClF at 143 K (Table VIII.1). Analogous two-bond $^{129}\text{Xe}-^{125}\text{Te}$ couplings have been observed in the case of OTeF_5 derivatives of xenon and are similar in magnitude to those of the $\text{Te}(\text{IV})$ derivatives (148). This is not too surprising, since ^{129}Xe and ^{125}Te have similar magnetogyric ratios. The tetrakis derivative, $\text{Te}(\text{OTeF}_5)_4$, is the only member of the $\text{Te}(\text{IV})$ series for which individual axial and equatorial OTeF_5 groups have been distinguished. Intramolecular exchange cannot be slowed sufficiently for the other species above the freezing point of the solvent, SO_2ClF (see section VIII.10). The increase in the $^{125}\text{Te}(\text{IV})-^{125}\text{Te}(\text{VI})$ coupling constant as x increases in the compounds $\text{TeF}_x(\text{OTeF}_5)_{4-x}$ is consistent with an increase in the covalency of the $\text{Te}-\text{OTeF}_5$ bond. Since fluorine is more electronegative than OTeF_5 (136) and a $\text{Te}-\text{F}$ bond is more ionic than a $\text{Te}-\text{OTeF}_5$ bond, an increase in the number of $\text{Te}(\text{IV})-\text{F}$ bonds causes an increase in the covalency of the remaining $\text{Te}-\text{OTeF}_5$ bonds. As covalency increases, so does the magnitude of the coupling. This same effect is observed in the long-range $^{19}\text{F}-^{125}\text{Te}(\text{IV})$ couplings noted above. A decrease in the directly-bonded $^{19}\text{F}-^{125}\text{Te}(\text{IV})$ coupling from $\text{TeF}_2(\text{OTeF}_5)_2$ to $\text{TeF}(\text{OTeF}_5)_3$ (Table VIII.1) is also consistent with the above description, i.e. as more

TABLE VIII.1 ^{125}Te NMR Parameters for $\text{TeF}_x(\text{OTeF}_5)_{4-x}$ and $[\text{TeF}_x(\text{OTeF}_5)_{3-x}]^+$

Solute	$\delta_{^{125}\text{Te}}$ ^a	J(Hz)		Solvent	Temp. (K)	Concn. (molal)
		$^{19}\text{F}-^{125}\text{Te}$	$^{125}\text{Te}-^{125}\text{Te}$			
$\text{Te}(\text{OTe}'\text{F}_5)_4$ ^b	Te 633.3	31.8 ^c		SO_2ClF	297	0.18
	Te'-160.8	F(E)3665 ^d F(A)3555				
$\text{Te}(\text{OTe}'\text{F}_5)_4$	Te 581.6			SO_2ClF	143	0.18
	Te'(E)-156.0	F(E)3620 ^d F(A)3440	840			
	Te'(A)-167.7	F(E)3714 F(A)3602	670			
$\text{Te}(\text{OTe}'\text{F}_5)_4$	Te 600.4			SO_2ClF	200	0.18
	Te'-159.4					
$\text{Te}(\text{OTe}'\text{F}_5)_4$	Te 566.8			SO_2	200	0.03
	Te'-160.7					
$\text{TeF}(\text{OTe}'\text{F}_5)_3$	Te 563.0	2810	1730	SO_2ClF	200	0.45
$\text{TeF}(\text{OTe}'\text{F}_5)_3$	Te 535.3	2814		SO_2	200	0.03
$\text{TeF}_2(\text{OTe}'\text{F}_5)_2$	Te 540.7	40 ^c 2850	2440	SO_2ClF	200	0.17
TeF_4	606.6			SO_2	200	Sat'd
$[\text{Te}(\text{OTe}'\text{F}_5)_3]^+$	Te 646.0		311	SO_2	200	0.12
	Te'-162.5	F(E)3736 ^d F(A)3706				
$[\text{TeF}(\text{OTe}'\text{F}_5)_2]^+$	Te 637.2	15 ^c 2630		SO_2	200	0.12
	Te'-159.2	F(E)3724 ^d F(A)3681				
$[\text{TeF}_2(\text{OTe}'\text{F}_5)]^+$	Te 644.5	21 ^c 2736		SO_2	200	0.17
	Te'-151.3	F(E)3724 ^d F(A)3656				
$[\text{TeF}_3]^+$	671.2	2905		SO_2	200	0.17

^a Referenced with respect to saturated aqueous $\text{Te}(\text{OH})_6$ at 295 K.
^b Taken from reference 136.

^c $J(^{19}\text{F}-^{125}\text{Te})$.
^d A and E denote axial and equatorial, respectively.

relatively electropositive OTeF_5 groups are added, the remaining Te(IV)--F bonds become more ionic and $J(^{19}\text{F}-^{125}\text{Te(IV)})$ is reduced.

VIII.7 Tellurium-125 NMR of $[\text{TeF}_x(\text{OTeF}_5)_{3-x}]^+$ Cations.

Figure VIII.3 depicts the Te(IV) region of the ^{125}Te NMR spectrum resulting from the reaction of $\text{Te}(\text{OTeF}_5)_4$ with AsF_5 . In a procedure identical to that used for the accumulation of the TeF_3^+ spectra (section VII.10), an excess of AsF_5 was employed to help suppress fluoride/ OTeF_5 exchange. Two distinct species were observed in the Te(IV) region. The TeF_3^+ quartet appeared and was approximately equal in intensity to a triplet assigned to $\text{TeF}_2(\text{OTeF}_5)^+$. Clearly, AsF_5 behaves as a fluorinating agent as well as an OTeF_5 acceptor in this reaction. The directly-bonded $^{19}\text{F}-^{125}\text{Te(IV)}$ coupling in $\text{TeF}_2(\text{OTeF}_5)^+$, 2736 Hz, is somewhat less than that observed for TeF_3^+ (Table VIII.1). Each of the peaks of the $\text{TeF}_2(\text{OTeF}_5)^+$ triplet was further split into a quintet ($J = 21$ Hz) arising from coupling of Te(IV) to the equatorial-fluorine atoms of the OTeF_5 group.

When less AsF_5 was allowed to react with $\text{Te}(\text{OTeF}_5)_4$, the more OTeF_5 -rich $\text{TeF}(\text{OTeF}_5)_2^+$ cation was observed. The $^{19}\text{F}-^{125}\text{Te(IV)}$ coupling in $\text{TeF}(\text{OTeF}_5)_2^+$ is 2630 Hz (Table VIII.1). The steady decrease in $J(^{19}\text{F}-^{125}\text{Te(IV)})$ in the series TeF_3^+ , $\text{TeF}_2(\text{OTeF}_5)^+$, $\text{TeF}(\text{OTeF}_5)_2^+$ is consistent with the greater covalency of the Te--OTeF_5 bond in comparison to

the Te(IV)--F bond, as was noted above for the $\text{TeF}_x(\text{OTeF}_5)_{4-x}$ compounds. The coupling of Te(IV) to the fluorine atoms on Te(VI) in $\text{TeF}_2(\text{OTeF}_5)^+$ is larger than that observed for $\text{TeF}(\text{OTeF}_5)_2^+$ and this, again, is consistent with the increased covalency of the Te-- OTeF_5 bond in the presence of a larger number of relatively ionic Te(IV)--F bonds. The ^{19}F - ^{125}Te (VI) couplings reflect this same trend. Stronger (more covalent) Te-- OTeF_5 bonds are offset by weaker Te(VI)--F bonds and a smaller $J(^{19}\text{F}$ - ^{125}Te (VI)). Couplings of Te(VI) to both axial and equatorial fluorine atoms decrease steadily in the series $\text{Te}(\text{OTeF}_5)_3^+$, $\text{TeF}(\text{OTeF}_5)_2^+$, $\text{TeF}_2(\text{OTeF}_5)^+$ (Table VIII.1).

A significant concentration of $\text{Te}(\text{OTeF}_5)_3^+$ was not observed in reactions of $\text{Te}(\text{OTeF}_5)_4$ with AsF_5 , but was produced when $\text{As}(\text{OTeF}_5)_5$ was used as the OTeF_5 acceptor. The Raman spectrum of a solidified 1:1 melt of $\text{Te}(\text{OTeF}_5)_4$ and $\text{As}(\text{OTeF}_5)_5$ identified the starting materials only (Fig. VIII.4). When this melt was dissolved in SO_2 , however, it was clear from the NMR spectra that a reaction did take place in solution. The room temperature ^{125}Te NMR spectrum of this solution consisted of a single broad resonance at 601 ppm in the Te(IV) region. Upon cooling to 200 K, two distinct resonances were visible (Fig. VIII.5). The resonance at 570 ppm corresponds to that observed for $\text{Te}(\text{OTeF}_5)_4$ in SO_2 at this temperature (Table VIII.1). The remaining

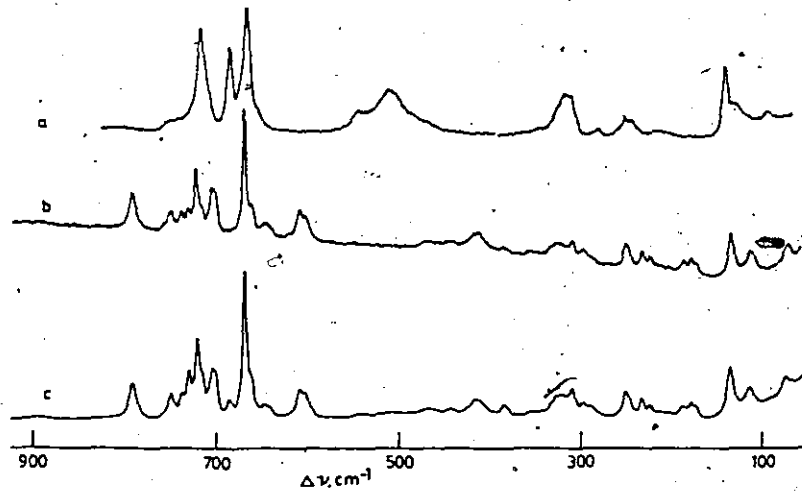


FIGURE VIII.4 Raman spectra (297 K, 5145 Å) of (a) $\text{As}(\text{OTeF}_5)_5$, (b) $\text{Te}(\text{OTeF}_5)_4$ and (c) a fused 1:1 mixture of $\text{As}(\text{OTeF}_5)_5$ and $\text{Te}(\text{OTeF}_5)_4$.

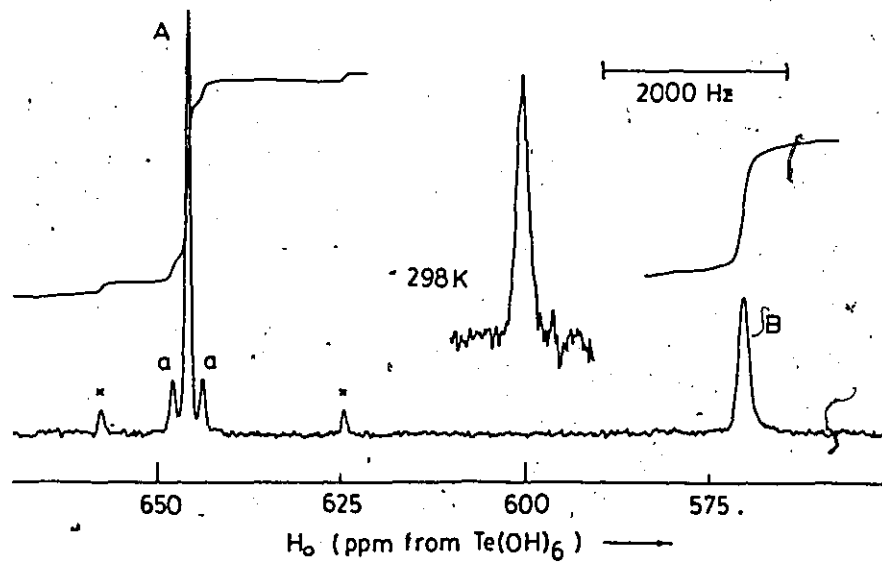
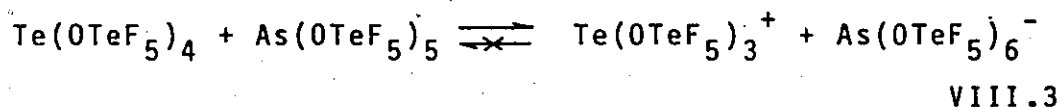


FIGURE VIII.5 ^{125}Te NMR spectrum of an SO_2 solution of a 1:1 $\text{Te}(\text{OTeF}_5)_4/\text{As}(\text{OTeF}_5)_5$ mixture at 200 K, $\text{Te}(\text{IV})$ region (the initial concentration was 0.24 M in $\text{Te}(\text{OTeF}_5)_4$; 78.97 MHz; 30,000 scans; 6.1 Hz/pt). (A) $\text{Te}(\text{OTeF}_5)_3^+$ with (a) satellites resulting from $^{125}\text{Te}(\text{IV})$ - $^{125}\text{Te}(\text{VI})$ coupling; (B) $\text{Te}(\text{OTeF}_5)_4$; (x) $\text{TeF}(\text{OTeF}_5)_2^+$ impurity. Inset shows exchange averaged resonance at 295 K.

resonance, at 646 ppm, was in the same region as Te(IV) in the $\text{TeF}_2(\text{OTeF}_5)^+$ and $\text{TeF}_2(\text{OTeF}_5)^+$ cations and the satellite peaks observed about the main resonance were consistent in intensity with coupling to three natural abundance tellurium atoms (see Table IV.4). These observations indicate that this second resonance results from the $\text{Te}(\text{OTeF}_5)_3^+$ cation. The Te(IV)-Te(VI) coupling of 311 Hz is considerably smaller than those observed in the neutral, $\text{TeF}_x(\text{OTeF}_5)_{4-x}$ compounds.

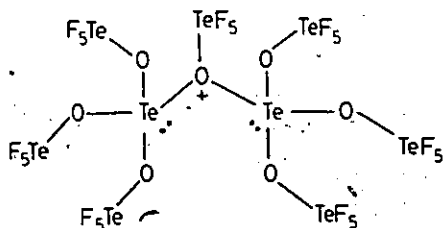
The averaged Te(IV) environment observed at 295 K for the above solution indicates OTeF_5 group exchange at this temperature. As described above, the chemical shift of this resonance lies between those of $\text{Te}(\text{OTeF}_5)_3^+$ and $\text{Te}(\text{OTeF}_5)_4$, indicating that the 295 K resonance may result from exchange averaging of the $\text{Te}(\text{OTeF}_5)_3^+$ and $\text{Te}(\text{OTeF}_5)_4$ resonances. The chemical shifts of these latter two species were necessarily recorded at 200 K, however, and since the chemical shift of Te(IV) in $\text{Te}(\text{OTeF}_5)_4$ is markedly temperature-dependent (see Table VIII.1), the position of the averaged resonance could be fortuitous. Three groups of resonances (doublets of quintets) were observed in the Te(VI) region of the spectrum. One of these, at -158 ppm, split into two sets of resonances at 200 K. The component at -160 ppm corresponds to $\text{Te}(\text{OTeF}_5)_4$, while the other component, at -162 ppm, was assigned to $\text{Te}(\text{OTeF}_5)_3^+$ based on the similar exchange behavior observed in the Te(IV) region of the spectrum. The $\text{Te}(\text{OTeF}_5)_4$ lines in the Te(VI) region are

very broad at 200 K owing to the slow Berry pseudorotation at this temperature. Of the two other groups of resonances in the Te(IV) region at 295 K, the group centered at -165 ppm corresponds to $\text{As}(\text{OTeF}_5)_5$, while the other, at -171 ppm, was assigned to $\text{As}(\text{OTeF}_5)_6^-$ (Table VIII.3). This anion was observed, along with ^{75}As - ^{125}Te coupling, in the ^{75}As NMR spectrum of the same solution at 295 K (see below). Clearly then, the OTeF_5 exchange is not between Te(IV) and As (equation VIII.3), which would result in equivalence of all of the OTeF_5 groups and a single set of resonances in the Te(VI) region.



Although a 1:1 stoichiometry of $\text{Te}(\text{OTeF}_5)_4$ and $\text{As}(\text{OTeF}_5)_5$ was used in the preparation, it was clear that a significant quantity of $\text{Te}(\text{OTeF}_5)_4$ remained unreacted and the observed facile exchange of OTeF_5 groups in solution was between $\text{Te}(\text{OTeF}_5)_4$ and $\text{Te}(\text{OTeF}_5)_3^+$. That is, the $\text{Te}(\text{OTeF}_5)_3^+$ initially formed in the reaction competes as a ligand acceptor towards unreacted $\text{Te}(\text{OTeF}_5)_4$, thus preventing complete reaction of $\text{Te}(\text{OTeF}_5)_4$ with $\text{As}(\text{OTeF}_5)_5$. Since $^{125}\text{Te}(\text{IV})$ - $^{125}\text{Te}(\text{VI})$ and ^{125}Te - ^{19}F couplings are retained for samples of $\text{Te}(\text{OTeF}_5)_4$ alone in solution at 297 K (136), it would appear that $\text{Te}(\text{OTeF}_5)_4$ does not dissociate to $\text{Te}(\text{OTeF}_5)_3^+$ and OTeF_5^- ions at this temperature. The observ-

ed facile exchange of OTeF_5 groups between $\text{Te}(\text{OTeF}_5)_3^+$ and $\text{Te}(\text{OTeF}_5)_4$ in the present sample then implies that OTeF_5 -bridged species such as structure VIII.I may act as intermediates for this exchange. Such proposed bridged intermediates would be of considerable interest since there are at present no known compounds with OTeF_5 bridges. The presumed lack of bridging in OTeF_5 compounds may be cited as a key difference between the donor-acceptor chemistry of OTeF_5 and that of fluorine.



VIII.I

Excess $\text{As}(\text{OTeF}_5)_5$ was observed in the Te(VI) region of the ^{125}Te NMR spectrum, but was not identified in the ^{75}As spectrum, presumably because the resonance was severely quadrupole relaxed and therefore severely broadened and collapsed into the spectral baseline. A sample of pure $\text{As}(\text{OTeF}_5)_5$ in SO_2 similarly did not produce an observable ^{75}As signal. The linewidths of ^{75}As resonances are discussed in more detail below.

VIII.8 Arsenic-75 NMR of the $\text{As}(\text{OTeF}_5)_6^-$ Anion.

The only solution NMR study of ^{75}As was reported by Balimann and Pregosin (150), although there have been applications of ^{75}As NMR in solid-state physics (151). Balimann

and Pregosin reported the ^{75}As chemical shifts for a series of tetrahedral arsonium ions in aqueous solution as well as those for the AsO_4^{3-} , AsF_6^- and AsH_4^+ ions.

Arsenic-75 has a spin of $3/2$, 100% natural abundance and a sensitivity of 2.51×10^{-2} relative to ^1H , which is similar to that of ^{125}Te . Despite a favorable natural abundance and sensitivity, ^{75}As NMR spectra are difficult to obtain as a result of the large quadrupole moment of the spin- $3/2$ ^{75}As nucleus ($Q = 0.3 \times 10^{-24} \text{ cm}^2$) which tends to produce very broad lines owing to quadrupolar relaxation. Under extreme narrowing conditions, linewidths, $\delta\nu_{1/2}$, are given by equation VIII.4.

$$\delta\nu_{1/2} = \frac{3\pi(2I+3)}{10 I^2(2I-1)} \left(\frac{e^2 q_{zz} Q}{h} \right)^2 \left(1 + \frac{1}{3} \eta^2 \right) \tau_c \quad \text{VIII.4}$$

where e is the charge on the electron, q is the electric field gradient at the nucleus, with q_{zz} as its largest component, η is the asymmetry parameter for q and τ_c is the isotropic tumbling correlation time (1-10 ps for non-viscous liquids). NMR spectra for quadrupolar nuclei can only be observed if the nucleus is in a highly symmetric environment, preferably a cubic environment, i.e. T_d or O_h . In such an environment q_{zz} and η are dramatically reduced and therefore so is $\delta\nu_{1/2}$ (equation VIII.4). Arsenic-75 has the additional disadvantage of having a spin of only $3/2$ so that the spin term of equation VIII.4 is relatively large and

$\delta\nu_{1/2}$ will even be large in a highly symmetric environment. In contrast, ^{209}Bi with $I = 9/2$ and $Q = -0.4 \times 10^{-24} \text{ cm}^2$ would have lines one tenth as wide as those of ^{75}As in the same environment, while ^{93}Nb with $I = 9/2$ and $Q = -0.2 \times 10^{-24} \text{ cm}^2$ would produce lines approximately 1/40 as broad.

The ^{75}As NMR spectrum of the $\text{As}(\text{OTeF}_5)_6^-$ anion in CH_3CN solution is presented in Figure VIII.6. The ^{75}As linewidth at 298 K is surprisingly narrow (165 Hz). It is clear that the local symmetry about the arsenic atom in this anion must be nearly octahedral for a signal to be observed at all. Balimann and Pregosin (150) have reported a value of 94 Hz for 0.1M aqueous KAsF_6 at 303K. An additional feature of the $\text{As}(\text{OTeF}_5)_6^-$ spectrum is the observation of long-range ^{75}As - ^{125}Te coupling which appears as shoulders about the central resonance. The magnitude of $^2J(^{75}\text{As}-^{125}\text{Te})$, as measured from the simulated spectrum, is 420 ± 42 Hz.

The $\text{As}(\text{OTeF}_5)_6^-$ spectrum was simulated using the two dimensionless parameters $x = (\omega_0 - \omega)2\pi J$ and $y = 2\pi J\tau$, where J is $^2J(^{75}\text{As}-^{125}\text{Te})$. The relaxation time of ^{75}As is represented by τ while the angular frequencies ω_0 and ω are taken at the center and any other point of the NMR multiplet respectively. This method has been successfully applied in the simulation of spectra of other quadrupolar nuclei coupled to spin-1/2 nuclei (152). A summation of several spec-

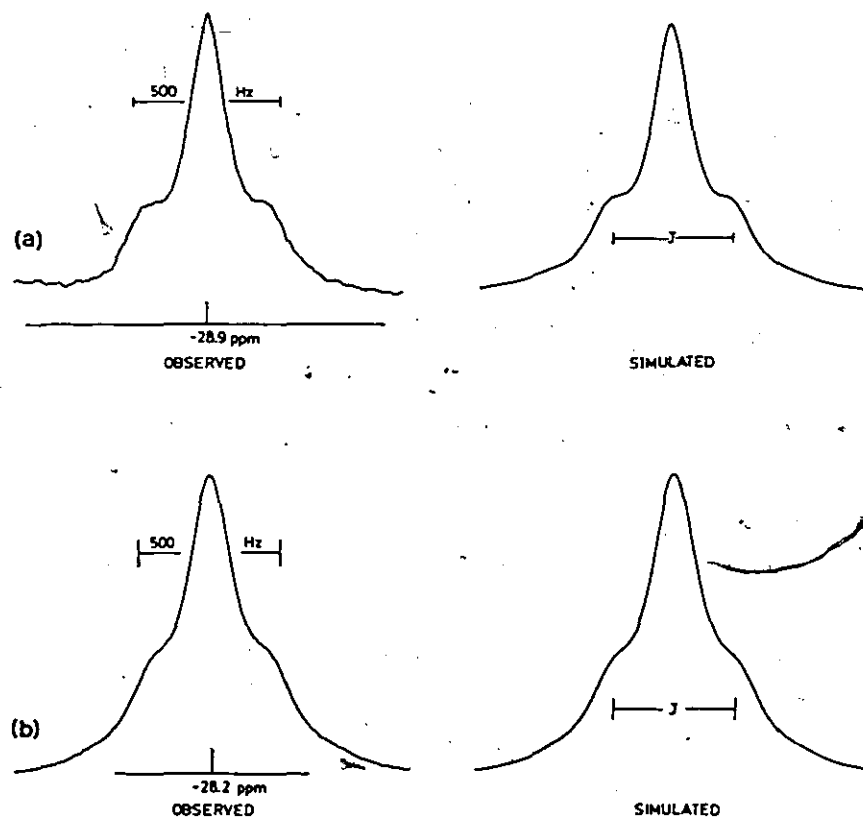


FIGURE VIII.6 Observed and simulated ^{75}As NMR spectra of (a) $\text{Cs}[\text{As}(\text{OTeF}_5)_6]$ in CH_3CN (42.82 MHz; 0.15 m; 60,000 scans; 12 Hz/pt) and (b) a 1:1 mixture of $\text{As}(\text{OTeF}_5)_5$ and $\text{Te}(\text{OTeF}_5)_4$ in SO_2 (42.82 MHz; 0.12 m; 340,000 scans; 6.1 Hz/pt), both at 298 K. Shoulders result from ^{75}As - ^{125}Te coupling.

tra for the most probable isotopic distributions of tellurium (^{125}Te , spin-1/2, 6.99% natural abundance) was included in the present simulation. The contribution of ^{123}Te (spin-1/2, 0.87% natural abundance) was considered insignificant and ignored. The probabilities for the possible isotopic isomers of $\text{As}(\text{OTeF}_5)_6^-$ are listed in Table VIII.2. The concentrations of only the first three isotopic isomers were considered to be high enough to be included in the simulation and the coupling constant, J , was assumed to be the same in all of the species. Simulations for a range of y values are presented in Figure VIII.7. Large values of y , which imply long τ values for a given J , indicate slow quadrupole relaxation rates and narrow lines. Small values of y indicate fast relaxation of ^{75}As and broad lines. At $y = 100.0$ the three individual spectra for the isotopic isomers considered are observed and at $y = 2.0$ all collapse to a single line. The simulated spectrum with a y value of 5.0 appeared to best match the shape of the observed spectrum. The uncertainty in J of $\pm 10\%$ is a measure of the uncertainty in the choice of y . The simulated spectrum for $y = 5.0$ was expanded to fit the observed spectrum and $2J(^{75}\text{As}-^{125}\text{Te})$ determined by comparing the known distance J on the simulated spectrum with the frequency scale of the observed spectrum. The $\text{As}(\text{OTeF}_5)_6^-$ resonance in the ^{75}As spectrum of an SO_2 solution of a 1:1 mixture of $\text{Te}(\text{OTeF}_5)_4$ and $\text{As}(\text{OTeF}_5)_5$ is considerably broader ($\delta\nu_{1/2} = 240$ Hz) than

Table VIII.2 Probabilities of the Natural Abundance
Te Isotopic Isomers of the $\text{As}(\text{OTeF}_5)_6^-$ Anion.

# of ^{125}Te nuclei	Probability	^{75}As resonance
0	0.6474	singlet
1	0.2919	doublet
2	0.0548	triplet
3	0.0055	quartet
4	0.0003	quintet
5	9×10^{-6}	sextet
6	1×10^{-7}	septet

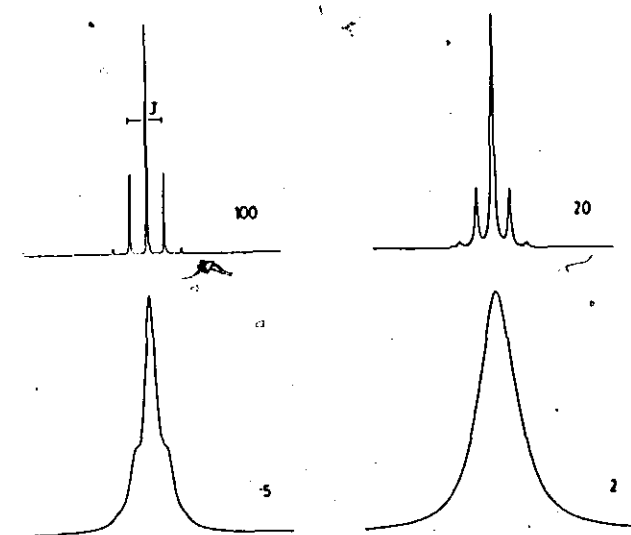


FIGURE VIII.7 Simulation of the ^{75}As NMR spectrum
of $\text{As}(\text{OTeF}_5)_6^-$ for a range of y values.

that observed for $\text{As}(\text{OTeF}_5)_6^-$ in CH_3CN (Fig. VIII.6). The best fit was obtained with $y = 4.2$ and in this instance $^2J(^{75}\text{As}-^{125}\text{Te})$ was found to be 432 Hz.

The narrow ^{75}As resonances in both solvent media are consistent with an octahedral arrangement of OTeF_5 ligands and the observed $^{75}\text{As}-^{125}\text{Te}$ coupling is consistent with the six tellurium atoms maintaining an octahedral disposition about the central arsenic atom, despite the presumed non-linear As-O-Te angle. Rapid rotation about the As-O bond would allow for the required high symmetry about arsenic, but this proposal seems rather unlikely in view of the large size of the OTeF_5 group. The central uranium and tellurium atoms in $\text{U}(\text{OTeF}_5)_6$ (153) and the two crystallographic forms of $\text{Te}(\text{OTeF}_5)_6$ (34) are octahedrally coordinated to the oxygen atoms of six OTeF_5 ligands and all three central atoms lie on inversion centers in their respective structures so that the tellurium atoms of the OTeF_5 groups are octahedrally arranged about the central atoms as well. It therefore seems reasonable to suppose that the same arrangement is found in $\text{As}(\text{OTeF}_5)_6^-$.

The reduced density coupling constant, $^1L_{\text{AsF}}$, of AsF_6^- calculated from the observed scalar coupling constant of 930 Hz (150) is $6.38 \times 10^{-43} \text{ NA}^{-2} \text{ m}^3$, in good agreement with the reduced density coupling constants of the isoelectronic SeF_6 and TeF_6 molecules (see Table VI.5). The two-

Table VIII.3 NMR Parameters for $\text{As}(\text{OTeF}_5)_5$ and $[\text{As}(\text{OTeF}_5)_6]^-$.

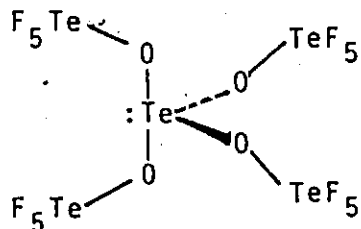
Solvent	$\text{As}(\text{OTeF}_5)_5$			$[\text{As}(\text{OTeF}_5)_6]^-$ $\text{Cs}^+ [\text{Te}(\text{OTeF}_5)_3]^+$	
	SO_2ClF	SO_2ClF	SO_2	CH_3CN	SO_2
Temp. (K)	295	190	295	295	295
Concn. (m)	0.31	0.24	0.05	0.15	0.12
$\delta(^{19}\text{F})$ (ppm) ^a	A: ^b -49.3 E: -39.6		-46.4 -37.2		
$\delta(^{75}\text{As})$ ^a				-28.9	-28.2
$\delta(^{125}\text{Te})$ ^a		-165.8	-165.8	-171.1	-170.3
$J(^{19}\text{F}-^{19}\text{F})$ (Hz)	178				
$J(^{19}\text{F}-^{123}\text{Te})$	A: 3030 ^c E: 3080		3082 ^c		
$J(^{19}\text{F}-^{125}\text{Te})$	A: 3650 ^c E: 3714	3650 ^d 3722	3714 ^c 3724	3408 ^d 3598	3396 ^d 3616
$J(^{75}\text{As}-^{125}\text{Te})$				420 ^e	432 ^e

(a) ^{19}F , ^{75}As and ^{125}Te spectra are referenced with respect to external neat CFCl_3 , a saturated CH_3CN solution of NaAsF_6 and saturated aqueous $\text{Te}(\text{OH})_6$ respectively at 295 K. (b) A and E denote axial and equatorial F atoms. (c) obtained from ^{19}F spectrum. (d) obtained from ^{125}Te spectrum. (e) obtained from ^{75}As spectrum.

bond $^{75}\text{As}-^{125}\text{Te}$ and $^{125}\text{Te}-^{125}\text{Te}$ scalar couplings of 432 and 1302 Hz in $\text{As}(\text{OTeF}_5)_6^-$ and $\text{Te}(\text{OTeF}_5)_6$ respectively (see Table VIII.3 and ref. (136)) give comparable reduced density coupling constants (3.69×10^{-43} and $3.16 \times 10^{-43} \text{ NA}^{-2} \text{ m}^3$ respectively). The $\text{Sb}(\text{OTeF}_5)_6^-$ anion (158) should have a scalar coupling constant, $^2J(^{121}\text{Sb}-^{125}\text{Te})$, of roughly 960 Hz if the reduced density coupling constant is considered to be approximately equal to that of $\text{As}(\text{OTeF}_5)_6^-$. Reduced density coupling constants have been discussed in some detail in section VII.10.

VIII.9 Berry Pseudorotation in $\text{Te}(\text{OTeF}_5)_4$ and $\text{As}(\text{OTeF}_5)_5$.

The Te(VI) region of the ^{125}Te NMR spectrum of $\text{Te}(\text{OTeF}_5)_4$ in SO_2ClF solution at 297 K consisted of two overlapping quintets resulting from coupling of ^{125}Te to one axial and four equatorial fluorine atoms. This pattern is characteristic of an OTeF_5 group and indicates that only one type of OTeF_5 is present. Valence-shell electron-pair repulsion (VSEPR) predictions (61) suggest that $\text{Te}(\text{OTeF}_5)_4$ should have a trigonal bipyramidal geometry with both axial and equatorial OTeF_5 groups (structure VIII.II).



VIII.II

Equivalence of these OTeF_5 groups with retention of ^{19}F - $^{125}\text{Te}(\text{IV})$ and $^{125}\text{Te}(\text{IV})$ - $^{125}\text{Te}(\text{VI})$ couplings indicate rapid intramolecular exchange in solution (136). Such exchange for five-coordinate molecules (the lone pair of electrons is considered part of the coordination sphere) is generally believed to take place via a square-pyramidal transition state (Berry pseudorotation (154)). If the activation energy for this pseudorotation is sufficiently high, cooling the sample can slow the exchange enough on the NMR time scale for separate axial and equatorial environments to be observed. Such was the case for $\text{Te}(\text{OTeF}_5)_4$ and two distinct $\text{Te}(\text{VI})$ environments were observed upon cooling to 146 K (Fig. VIII.8). The axial bonds in a trigonal bipyramid are generally somewhat longer than the equatorial bonds (61) so that the magnitude of the coupling from the central $\text{Te}(\text{IV})$ to $\text{Te}(\text{VI})$ in OTeF_5 should be smaller for the axial groups. A weaker (longer) $\text{Te}-\text{OTeF}_5$ bond should be complemented by stronger $\text{Te}(\text{VI})-\text{F}$ bonds and larger directly-bonded, $^{125}\text{Te}(\text{VI})$ - ^{19}F couplings. The axial and equatorial OTeF_5 groups are assigned in Figure VIII.8 using these assumptions (the observed couplings are listed in Table VIII.I).

The ^{19}F NMR spectrum of the same sample at 297 K (Fig. VIII.9) was an AB_4 spectrum as expected for a single OTeF_5 ligand environment. Upon cooling the solution, however, the signals broadened and eventually resonances for two separate environments emerged. The ^{19}F - $^{125}\text{Te}(\text{VI})$ satel-

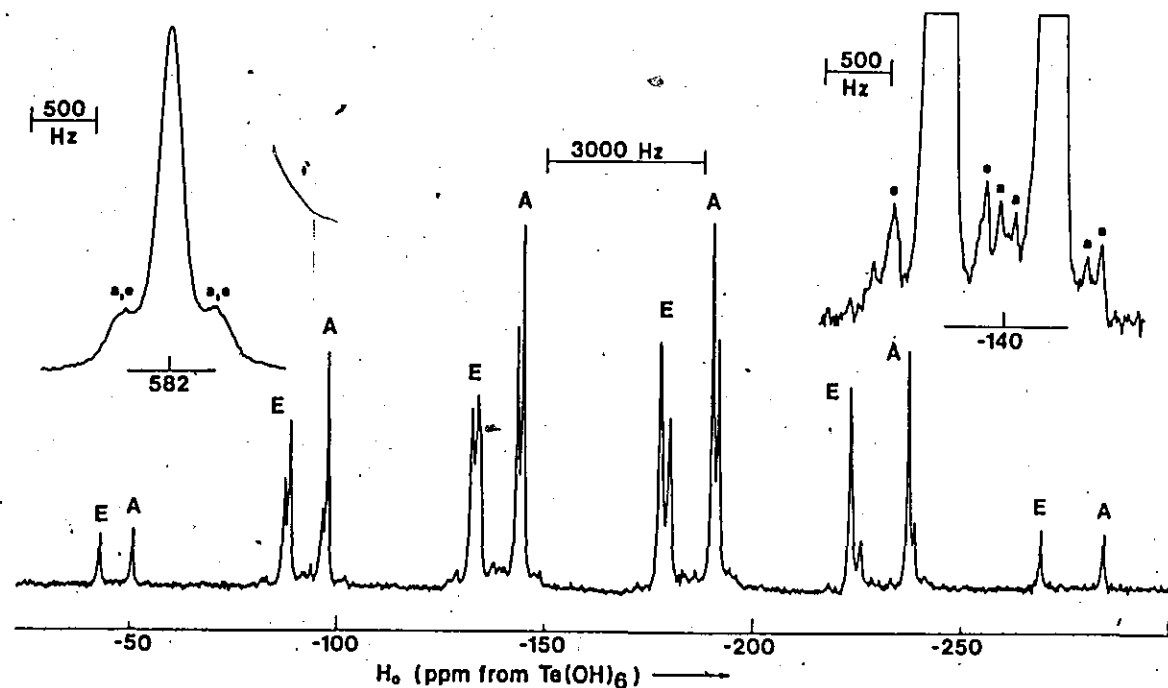


FIGURE VIII.8 ^{125}Te NMR spectrum of $\text{Te}(\text{OTeF}_5)_4$ in SO_2ClF solution at 146 K (0.18 m; 3500 scans; 3.0 Hz/pt). (A) and (E) denote axial and equatorial OTeF_5 groups respectively. Inset left shows $\text{Te}(\text{IV})$ (42,000 scans; 6.1 Hz/pt). Inset right shows $^2J[^{125}\text{Te}(\text{IV})-^{125}\text{Te}(\text{VI})]$ for axial (a) and equatorial (e) OTeF_5 groups (42,000 scans; 6.1 Hz/pt).

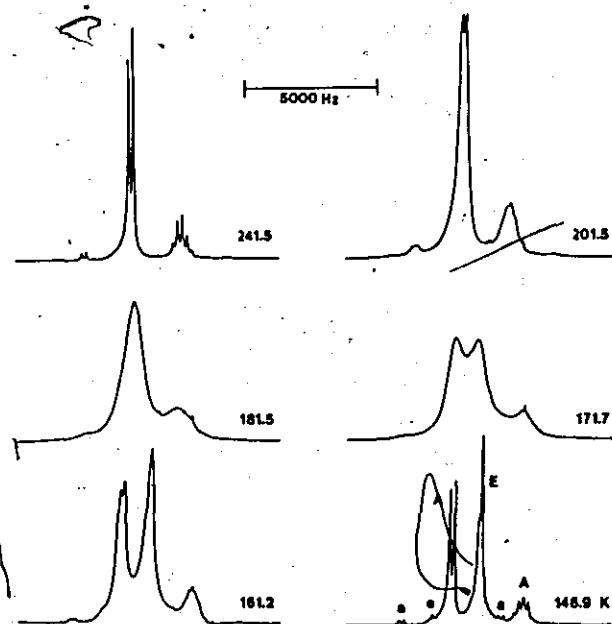


FIGURE VIII.9 Variable temperature ^{19}F NMR spectra of $\text{Te}(\text{OTeF}_5)_4$ in SO_2ClF solution (235.36 MHz; 0.18 m; 60 scans; 2.4 Hz/pt). (A) and (E) denote axial and equatorial OTeF_5 groups respectively, (a) and (e) denote $J(^{19}\text{F}-^{125}\text{Te}(\text{VI}))$.

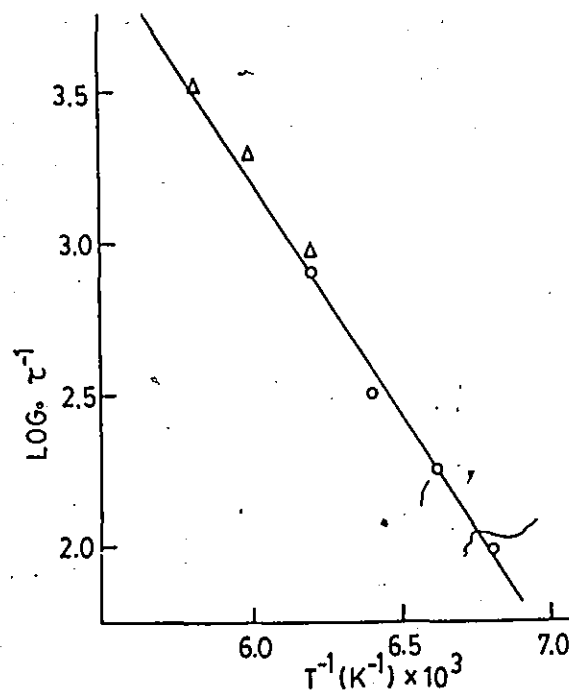


FIGURE VIII.10 Plot of $\log(\tau^{-1})$ as a function of T^{-1} ; (Δ) from $\delta\nu$; (o) from $\delta\nu_{\frac{1}{2}}$.

lite peaks. were of sufficient intensity to assign the two different OTeF_5 resonances by comparing these couplings with those observed in the ^{125}Te NMR spectrum. For the equatorial OTeF_5 groups, only a few of the lines of the second order AB_4 spectrum could be resolved ($J_{\text{FF}}/\delta\nu_{\text{AB}} \sim 1$). An AB_4 pattern was also observed for the axial OTeF_5 groups but the $J_{\text{FF}}/\delta\nu$ ratio was clearly much smaller ($J_{\text{FF}}/\delta\nu_{\text{AB}} = .066$) and this spectrum more closely approximates a first order spectrum.

The temperature dependence of the ^{19}F AB_4 spectrum of $\text{Te}(\text{OTeF}_5)_4$ can be separated into three distinct regions: (1) the range from room temperature down to where the resonances broaden and begin to be resolved into two sets of A and two B resonances (177 K); (2) the intermediate exchange region (156-177 K), where the resonances for four fluorine environments are resolved and the chemical shift differences between each pair of environments increase with decreasing temperature; (3) and finally, the range where there is no further change in the chemical shifts, but the linewidths continue to decrease (the slow exchange region). Rate data have been extracted for an equal population two-site exchange process from the temperature dependence of the chemical shift differences of the axial and equatorial environments in the intermediate exchange region using equation VIII.5 (55).

$$1/\tau = \sqrt{2\pi}[(\delta\nu_0)^2 - (\delta\nu)^2]^{1/2} \quad \text{VIII.5}$$

where $1/\tau$ is the exchange rate, $\delta\nu_0$ is the difference in chemical shift for the two exchanging sites in the slow exchange region and $\delta\nu$ is the separation of peaks in the intermediate exchange region (in Hz). The activation energy for the exchange process was determined from the temperature dependence of the exchange rate via the Arrhenius equation (VIII.6) (55).

$$\log(1/\tau) = \log A - E_a/(2.303 RT) \quad \text{VIII.6}$$

where A is a constant, E_a is the activation energy, R is the gas constant ($8.3143 \text{ JK}^{-1}\text{mol}^{-1}$) and T is the temperature (K).

In the slow and intermediate exchange regions the exchange rate was determined from line width measurements (equation VIII.7 (55)).

$$1/\tau = (\delta\nu_{1/2} - \delta\nu_{1/2}^0) \quad \text{VIII.7}$$

where $\delta\nu_{1/2}^0$ is the natural linewidth in the absence of exchange as measured at the fast or slow exchange limit, and $\delta\nu_{1/2}$ is the observed linewidth. An activation energy of $30.7 \pm 0.3 \text{ kJ mol}^{-1}$ ($7.34 \pm 0.06 \text{ kcal mol}^{-1}$) was determined from the ^{19}F NMR spectra using exchange rate data extracted from the temperature dependence of both $\delta\nu$ and $\delta\nu_{1/2}$ (see Fig. VIII.10 and Table VIII.4, correlation coefficient $R^2 = 0.994$).

Table VIII.4 Exchange Rate Data Extracted From Variable Temperature F-19 NMR Spectra of $\text{Te}(\text{OTeF}_5)_4$ in SO_2ClF .

$T(\text{K})$	$T^{-1}(\text{K}^{-1} \times 10^3)$	$\delta\nu(\text{Hz})^a$	$\delta\nu_{1/2}(\text{Hz})^b$	τ^{-1}	$\log(\tau^{-1})$
146.9	6.81		86	95 ^c	1.98 ^c
151.0	6.62		113	180 ^c	2.25 ^c
156.1	6.41	1121 ^d	157	319 ^c	2.50 ^c
161.2	6.20	1101	308	793 ^c , 937 ^e	2.90 ^a , 2.97 ^e
166.6	6.00	1032		1945 ^e	3.29 ^e
171.7	5.82	830		3348 ^e	3.52 ^e
294.5			56 ^f		

(a) separation of axial B resonance and largest resonance of equatorial AB_4 multiplet. (b) width at half-height of the high field component of the axial B doublet. (c) obtained from equation VIII.7. (d) $\delta\nu$. (e) obtained from equation VIII.5.

(f) $\delta\nu_{1/2}$.

The activation energy, E_a , can be determined from the coalescence temperature, T_c (the temperature at which the exchanging peaks just merge), according to equation VIII.8 (155).

$$E_a = 2.303 RT_c (10.319 - \log(\pi \delta \nu_0 / \sqrt{2}) + \log T_c) \quad \text{VIII.8}$$

This method is less reliable than the Arrhenius plot since only one data point is used, making it difficult to determine the coalescence temperature to a precision greater than ± 2 K. In the ^{19}F NMR spectra, $T_c = 177 \pm 2$ K and $\delta \nu_0 = 1121 \pm 3$ Hz. The activation energy, E_a , is 31.0 ± 0.4 kJ mol $^{-1}$ (7.4 ± 0.1 kcal mol $^{-1}$) according to equation VIII.8. In the ^{125}Te NMR spectra, coalescence of the two lowest frequency lines of the OTeF_5 resonances ($\delta \nu_0 = 1206 \pm 4$ Hz) was observed at 179 ± 2 K. The activation energy then is 31.3 ± 0.4 kJ mol $^{-1}$ (7.5 ± 0.1 kcal mol $^{-1}$). The mean activation energy from these three determinations is 31.0 ± 0.4 kJ mol $^{-1}$ (7.4 ± 0.1 kcal mol $^{-1}$). This value is very close to the value of 7.2 ± 0.5 kcal mol $^{-1}$ obtained for intramolecular exchange in both PF_3Cl_2 and PF_3Br_2 as followed by ^{19}F NMR (156).

The ^{19}F NMR spectrum of $\text{As}(\text{OTeF}_5)_5$ dissolved in SO_2ClF at 297 K also consisted of an AB_4 spectrum as expected for a single OTeF_5 environment (Fig. VIII.11). Directly-bonded ^{19}F - ^{123}Te and ^{19}F - ^{125}Te couplings were observed as satellite peaks about the main resonances. The ^{19}F - ^{125}Te

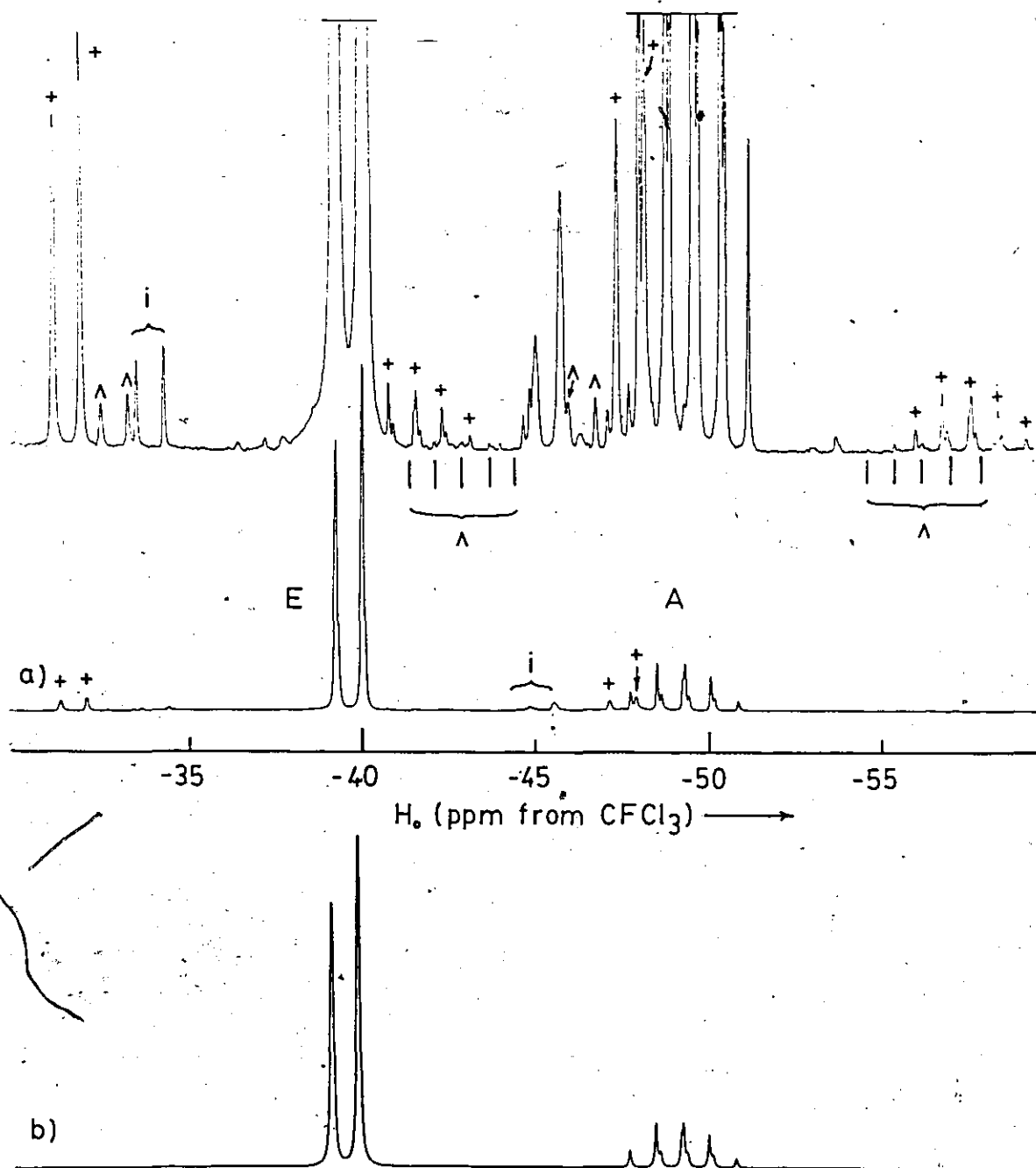


FIGURE VIII.11 The ^{19}F NMR spectrum of $\text{As}(\text{OTeF}_5)_5$ in SO_2ClF . (a) Observed spectrum, 235.36 MHz, 0.13 m, 1100 scans, 1.7 Hz/pt: (A) axial fluorine, (E) equatorial fluorine atoms, (+) ^{125}Te satellites, (Λ) ^{123}Te satellites, (i) impurity. (b) Simulated spectrum ignoring ^{19}F - ^{123}Te and ^{19}F - ^{125}Te coupling.

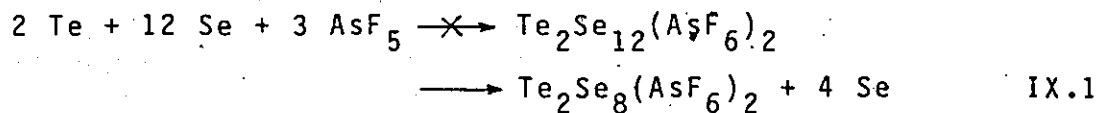
coupling constants agree well with those observed in the ^{125}Te NMR spectrum (Table VIII.3) and are typical for ^{19}F - $^{125}\text{Te(VI)}$ couplings (Table VIII.1). Since a single OTeF_5 environment is observed in both the ^{19}F and ^{125}Te NMR spectra, it would appear that this five-coordinate molecule also undergoes rapid Berry pseudorotation. Unlike $\text{Te}(\text{OTeF}_5)_4$, however, the exchange could not be slowed sufficiently on the NMR time scale to observe separate axial and equatorial OTeF_5 ligand environments. No significant broadening of the resonances in the ^{125}Te NMR spectrum was observed at temperatures as low as 155 K. It would appear that either the lone pair of electrons in $\text{Te}(\text{OTeF}_5)_4$ is more effective in obstructing pseudorotation than is the fifth OTeF_5 group in $\text{As}(\text{OTeF}_5)_5$ (giving a lower exchange barrier in the latter compound) or the chemical shift difference between the axial and equatorial OTeF_5 groups in $\text{As}(\text{OTeF}_5)_5$ is considerably smaller than in $\text{Te}(\text{OTeF}_5)_4$. If the latter were the case, coalescence could then occur at a substantially lower temperature in $\text{As}(\text{OTeF}_5)_5$ than in $\text{Te}(\text{OTeF}_5)_4$ even if the exchange barriers in the two compounds are similar (see equation VIII.8).

CHAPTER IX
CONCLUSIONS



IX.1 Summary and Conclusions.

The Te/Se/MF₅ (M = As or Sb) system has been extensively examined in SO₂ solution. Tellurium is more easily oxidized than selenium so that (Te₆)(Se₈)(AsF₆)₆(SO₂), with tellurium in the +2/3 oxidation state and selenium in the +1/4 oxidation state, was produced at high temperature in preference to mixed cations of intermediate oxidation state. Long (one week) reaction times lead to homopolyatomic cations and a very few mixed cations of particularly high stability, for example Te₂Se₄²⁺ and trans-Te₂Se₂²⁺. Cations such as Te₃Se₃²⁺ and Te₃Se²⁺ were obtained after only a few hours of reaction, but these were only isolated in compounds containing disordered mixtures of isostructural cations. Several of the published structures of the mixed polyatomic cations (17, 20) probably involve some disorder of this type. New, ordered forms of Te₂Se₄(SbF₆)₂ and Te₂Se₈(AsF₆)₂ were prepared. Attempts to prepare Te-Se cations of lower average oxidation state than +0.2, as in reaction IX.1, resulted only in Te₂Se₈²⁺ and unreacted chalcogen. There was no evidence for the formation of a Te₂Se_x²⁺ cation where x > 8.



The novel Te₂Se₆²⁺ cation was isolated in the compound (Te₂Se₆)(Te₂Se₈)(AsF₆)₄(SO₂)₂. This cube-like cation is very different in structure from that of the homopoly-

atomic cations of the same average oxidation state, S_8^{2+} and Se_8^{2+} , and is more closely related to the structure of the P_{11}^{3-} and As_{11}^{3-} anions (62, 63). Both of the $Te_2Se_6^{2+}$ and Se_8^{2+} structures can be derived, however, from their isostructural parent cations $Te_2Se_8^{2+}$ and Se_{10}^{2+} . The difference in the $Te_2Se_6^{2+}$ and Se_8^{2+} structures can be explained in terms of the preference of the more electropositive tellurium atoms for three-coordinate sites, where the positive charges are formally located. Selenium-77 and ^{125}Te NMR studies indicated that both the $Te_2Se_6^{2+}$ and the Se_8^{2+} cations retain their structures in solution.

The new $Te_2S_4^{2+}$ cation was prepared and characterized in the compound $(Te_{2.1}S_{3.9})(SbF_6)_2$, which includes a small percentage of the isostructural $Te_3S_3^{2+}$ cation in the same lattice. These are the only two Te-S cations to be isolated to date although numerous resonances were observed in the ^{125}Te NMR spectra of Te/S/MF₅ mixtures.

The mixed square cations $S_xSe_{4-x}^{2+}$ were identified in the ^{77}Se NMR spectra of S/Se/MF₅ solutions in SO₂. Spin-lattice relaxation times (T_1) were determined for Se_4^{2+} , S_3Se^{2+} , cis- $S_2Se_2^{2+}$ and SSe_3^{2+} , with a mean value of 0.38 s. The new compound $(S_{3.0}Se_{1.0})_2(Sb_4F_{17})(SbF_6)_3$ contains a disordered mixture of these cations and is the only compound with a mixed Se-S cation yet to be characterized by X-ray crystallography.

The compound $(S_{3.0}Se_{1.0})_2(Sb_4F_{17})(SbF_6)_3$ additionally provided the only example of the mixed-valence $Sb_4F_{17}^-$ anion. The Sb(III) atoms of this anion and $Sb_3F_{14}^-$ anions found in other fluoroantimonate salts of the polyatomic cations all have stereoactive lone pairs of electrons located in the equatorial plane of a trigonal bipyramid completed by short bonds to neighbouring fluorine atoms. There are numerous longer (secondary) bonds to fluorine atoms attached to other anions in the structures. These longer bonds form around the presumed position of the lone pair and in directions that can be described as capping faces or bridging edges of the trigonal bipyramid.

Anion-cation interactions are significant in all of the structures of the polyatomic cations. In the square cations the contacts to the anions either bridge edges or form along the diagonals of the squares. The $^{77}Se-^{77}Se$, $^{77}Se-^{125}Te$ and $^{125}Te-^{125}Te$ coupling constants varied markedly with different solvents in the ^{77}Se and ^{125}Te NMR spectra of these square cations. Charge transfer from the solvent to the cations is probably significant in these solutions just as anion-cation interactions are significant in the solid-state structures. The differences in the coupling constants probably result from the varying abilities of the solvents to donate electron density into antibonding orbitals of the cations. In crystal structures of the other polyatomic cations, interionic contacts were observed in

directions that can be described as bridging edges or capping faces of polyhedra comprised of the primary bonds and the lone pair(s).

Antimony pentafluoride oxidized elemental tellurium to produce TeF_3^+ as a minor product. Arsenic pentafluoride had previously been shown (22) to react with tellurium to produce TeF_3^+ in the presence of small amounts of Br_2 or I_2 . The SeF_3^+ cation resulted from the reaction of $\text{Se}_4(\text{AsF}_6)_2$ with O_2AsF_6 . The reduced density coupling constant, $^1L_{\text{SeF}}$, in SeF_3^+ is larger than that of TeF_3^+ , indicating that the F--Se bond has more s-character than the F--Te bond in these two cations. This is consistent with the observed increase in the F--Se--F bond angle over the F--Te--F bond angle in crystal structures of these cations (46, 126).

A number of MX_3^+ salts (M = S, Se, Te; X = F, Cl, Br, I) were prepared and characterized by X-ray crystallography. The geometries of these cations were compared with those of MX_3^+ cations in previously determined structures. The X--M--X bond angles in the cations are somewhat larger than in the isoelectronic neutral molecules owing to the shorter M--X bonds in the cations and greater repulsions between the bonding pairs of electrons. The greater electronegativity of the central atom in the cations serves to pull the bonding pairs of electrons closer to the central atom, increasing bond pair repulsions still further. The

bond angle differences between the cations and the neutral molecules are not as great as anticipated, however, probably as a result of the stronger secondary bonding in the structures of the cations. Bond angles decrease in the series $SX_3^+ > SeX_3^+ > TeX_3^+$, consistent with the longer M--X bonds and reduced bond pair - bond pair repulsions. Bond angles also decrease in the series $MI_3^+ > MBr_3^+ > MCl_3^+ > MF_3^+$. This is consistent with a more electronegative X atom contracting the charge cloud of the bonding electron pair and drawing it closer to itself and further away from the central atom, reducing repulsions between bonding pairs of electrons despite shorter bond lengths. Secondary bonds to the cation are also affected by the stereoactivity of the lone pair on the central atom. The Y...M...Y angle increases as X--M--X decreases in the above series. In most cases secondary bonds to the cation cap faces of the tetrahedron formed by the primary bonds and the lone pair, although in $(TeCl_3)(SbF_6)$ and $(TeCl_3)(AsF_6)$ additional edge-bridging contacts were observed. The geometries of these secondary bonds are very similar to those observed at three-coordinate positions in salts of the polyatomic cations. The strength of the secondary bonds is very much dependent upon the nature of the anion. The mean Te...X distance increases and the Te--Cl distance decreases significantly in the series $TeCl_4$ (i.e. $[(TeCl_3^+)(Cl^-)]_4$), $TeCl_3(AlCl_4)$, $TeCl_3(SbF_6)$. The increase in the strength of the Te--Cl bond is reflected

in an increase in the frequency of the symmetric TeCl_3^+ stretch in the Raman spectra of these compounds. Although the crystal structure of $(\text{TeCl}_3)(\text{SbCl}_6)$ could not be determined, the Raman spectrum indicates a Te--Cl bond length intermediate to the AlCl_4^- and SbF_6^- salts.

In $(\text{TeF}_3)_2\text{SO}_4$ the distinction between an ionic formulation and a covalently linked sulfate adduct is not clear. Each tellurium atom forms two short Te--O bonds so that the primary geometry of these atoms is AX_5E . Longer contacts to oxygen and fluorine atoms cap faces of the AX_5E pseudooctahedron, as previously observed in XeF_5^+ salts (112), the $\text{XeF}_2(\text{IF}_5)$ adduct (113) and in TeF_4 (111).

The chemistry of Te(IV) was extended in the preparation of new mixed F/OTeF₅ analogues of TeF_4 and TeF_3^+ . Trends in the ^{19}F - ^{125}Te and ^{125}Te - ^{125}Te couplings observed in the ^{125}Te NMR spectra can be explained in terms of the relative electronegativity of fluorine and the OTeF₅ group. As the number of OTeF₅ groups increases the remaining Te(IV)--F bonds become increasingly ionic and $J(^{19}\text{F}$ - $^{125}\text{Te}(\text{IV}))$ decreases. As the number of Te(IV)--F bonds increases the Te(IV)--OTeF₅ bond becomes increasingly covalent and long range ^{19}F - $^{125}\text{Te}(\text{IV})$ and $^{125}\text{Te}(\text{VI})$ - $^{125}\text{Te}(\text{IV})$ couplings increase. The $\text{As}(\text{OTeF}_5)_6^-$ anion was prepared as the counter anion of $\text{Te}(\text{OTeF}_5)_3^+$. This anion proved to be one of the few species of sufficiently high symmetry to

record an ^{75}As NMR spectrum. The two-bond reduced density coupling constant, $^2L(^{75}\text{As}-^{125}\text{Te})$, compared favorably with the analogous $^2L(^{125}\text{Te}-^{125}\text{Te})$ coupling in the $\text{Te}(\text{OTeF}_5)_6$ molecule. The intramolecular exchange of $\text{Te}(\text{OTeF}_5)_4$ in SO_2ClF solution was followed by variable temperature ^{19}F and ^{125}Te NMR spectroscopy and an exchange barrier of 7.4 ± 0.1 kcal/mol was determined for this presumed Berry pseudorotation.

IX.2 Discussion of Unit Cell Volumes.

The unit cell volumes of all of the known structures of the polyatomic cations of the chalcogens that have been characterized by X-ray crystallography are given in Table IX.1. When these volumes are divided by Z, the number of molecules in a unit cell, molecular volumes are obtained. Comparison of these molecular volumes allows the volumes of the individual atoms or ions in these structures to be determined. For example, the volume of a selenium atom can be obtained by taking one quarter of the difference in the molecular volumes of $(\text{Te}_2\text{Se}_8)(\text{AsF}_6)_2$ and $(\text{Te}_2\text{Se}_4)(\text{AsF}_6)_2$ (compounds 16 and 20 in Table IX.1) or $(\text{Te}_2\text{Se}_8)(\text{SbF}_6)_2$ and $(\text{Te}_2\text{Se}_4)(\text{SbF}_6)_2$ (compounds 17 and 21). The resulting volumes from these pairs of compounds are 27.5 and 29.2 \AA^3 respectively, or a mean of 28 \AA^3 . The volumes of the AsF_6^- and SbF_6^- anions can be determined by subtracting the volume of ten selenium atoms from the molecular volumes of

Table IX.1 Unit Cell and Molecular Volumes (\AA^3).

Compound	Unit Cell Volume	Z^a	Molec. Vol.		Ref
			obsd ^b	calc ^c	
1) $S_{19}(\text{AsF}_6)_2$	2744.9	4	686	648	14
2) $S_{19}(\text{SbF}_6)_2$	2847.7	4	712	674	15
3) $S_8(\text{AsF}_6)_2$	3154	8	394	390	18
4) $S_8(\text{Sb}_3\text{F}_{14})(\text{SbF}_6)$	4570.3	8	571	569	19
5) $S_4(\text{AsF}_6)_2(\text{SO}_2)_{0.62}^d$	1381	4	345	350	22
6) $\text{Se}_{10}(\text{AsF}_6)_2$	3839.5	8	480	482	16
7) $\text{Se}_{10}(\text{SbF}_6)_2$	4036.4	8	505	508	16
8) $\text{Se}_4(\text{Sb}_2\text{F}_4)(\text{Sb}_2\text{F}_5)(\text{SbF}_6)_5$	3617	4	904	-	23
9) $\text{Te}_4(\text{SbF}_6)_2$	706.2	2	353	380	23
10) $\text{Te}_6(\text{AsF}_6)_4(\text{AsF}_3)_2$	2760.7	4	690	-	26
11) $\text{Te}_6(\text{AsF}_6)_4(\text{SO}_2)_2$	1414.6	2	707	740	26
12) $(S_{3.0}\text{Se}_{1.0})_2(\text{Sb}_4\text{F}_{17})(\text{SbF}_6)_3$	3371.5	4	843	-	e
13) $\text{Te}_{2.1}\text{S}_{3.9}(\text{SbF}_6)_2$	6355	16	397	399	e
14) $\text{Te}_3\text{S}_3(\text{AsF}_6)_2$	1521.6	4	380	386	20
15) $\text{Te}_3\text{S}_3(\text{SbF}_6)_2$	1669	4	417	412	e
16) $\text{Te}_2\text{Se}_8(\text{AsF}_6)_2$	4000.6	8	500	502	e
17) $\text{Te}_2\text{Se}_8(\text{SbF}_6)_2$	4244	8	530	528	e
18) $\text{Te}_2\text{Se}_6(\text{Te}_2\text{Se}_8)(\text{AsF}_6)_4(\text{SO}_2)_2$	4543	4	1136	1056	e
19) $\text{Te}_{4.5}\text{Se}_{5.5}(\text{AsF}_6)_2$	2121.7	4	530	527	e
20) $\text{Te}_2\text{Se}_4(\text{AsF}_6)_2$	3124	8	390	390	21
21) $\text{Te}_2\text{Se}_4(\text{SbF}_6)_2$	6614	16	413	416	e
22) $\text{Te}_2\text{Se}_4(\text{Sb}_3\text{F}_{14})(\text{SbF}_6)$	4546	8	568	569	e
23) $\text{Te}_{2.7}\text{Se}_{3.3}(\text{SbF}_6)_2$	1691.2	4	423	423	e
24) $\text{Te}_{3.4}\text{Se}_{2.6}(\text{SbF}_6)_2$	1720.0	4	430	430	e
25) $\text{Te}_2\text{Se}_2(\text{Sb}_3\text{F}_{14})(\text{SbF}_6)$	2142.1	4	536	513	e
26) $\text{Te}_{3.0}\text{Se}_{1.0}(\text{Sb}_3\text{F}_{14})(\text{SbF}_6)$	2148.3	4	537	523	e
27) $\text{Te}_6(\text{Se}_8)(\text{AsF}_6)_6(\text{SO}_2)$	2158.7	2	1079	1112	e

(a) Number of molecules per unit cell. (b) Unit cell volume divided by Z . (c) Calculated volume using values listed in Table IX.2. (d) Treated as 1.0 sulfur dioxide molecule in this calculation. (e) This work.

$\text{Se}_{10}(\text{AsF}_6)_2$ and $\text{Se}_{10}(\text{SbF}_6)_2$ respectively. The volume of the tellurium atom can be obtained by adding one half of the volume difference between $(\text{Te}_2\text{Se}_8)(\text{AsF}_6)_2$ and $\text{Se}_{10}(\text{AsF}_6)_2$ to the established volume of selenium, or by comparison of the $(\text{Te}_{2.7}\text{Se}_{3.3})(\text{SbF}_6)_2$ and $(\text{Te}_{3.4}\text{Se}_{2.6})(\text{SbF}_6)_2$ volumes. Similarly, the volume of the sulfur atom can be calculated by subtracting the volumes of the appropriate number of SbF_6^- anions and tellurium atoms from the molecular volume of $(\text{Te}_{2.1}\text{S}_{3.9})(\text{SbF}_6)_2$ and the volume of the $\text{Sb}_3\text{F}_{14}^-$ anion can be obtained by comparison of $\text{Sb}_3\text{F}_{14}^-$ salts with SbF_6^- salts of the same cation. Mean values for all of these atoms and ions are given in Table IX.2. The component volumes in Table IX.2 accurately reproduce the molecular volumes of most of the compounds in Table IX.1 and can be useful in suggesting reasonable compositions for new compounds once the unit cell volume has been determined. The unknown compound $(\text{Te}_2\text{S}_8)(\text{SbF}_6)_2$, for example is predicted to have a molecular volume of 488 \AA^3 and $\text{Se}_8(\text{AsF}_6)_2$, if ever isolated in a crystalline form, would have a molecular volume of roughly 426 \AA^3 .

IX.3 Suggestions for Future Work.

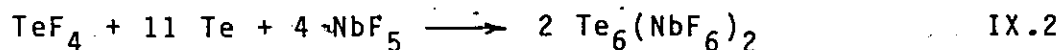
Investigations of the homopolyatomic cations of the chalcogens had been very extensive prior to the start of the present work. The isolation of new homopolyatomic cations will almost certainly require the use of different oxidants

Table IX.2 Component Volumes (\AA^3).

Species	Mean Volume	Reference Compounds ^a
AsF_6^-	101	6, 16, 19, 20
SbF_6^-	114	7, 17, 21, 23, 24
$\text{Sb}_3\text{F}_{14}^-$	267	2, 4, 21, 22
S	23.5	3, 4, 13
Se	28	16, 17, 20, 21
Te	38	6, 16, 23, 24,
SO_2	54	11, 27

(a) See Table IX.1.

and/or different methods of preparation. For example, reaction IX.2 may lead to crystalline samples of the long sought after Te_6^{2+} cation.



This reaction is analogous to the formation of $\text{Te}_6(\text{AlCl}_4)_2$ from a $\text{Te}/\text{TeCl}_4/\text{AlCl}_3$ melt (4). Arsenic trifluoride may prove to be a better solvent than SO_2 for this reaction since AsF_6^- and SbF_6^- salts of Te_6^{2+} have a very low solubility in SO_2 .

The Te-Se mixed cations have similarly been extensively studied using AsF_5 or SbF_5 as oxidants in SO_2 solution. Few, if any, new cations can be expected from this system other than cations isostructural with the presently known cations, but with different Te:Se ratios. It might be of interest, however, to compare the structure of $\text{Te}_x\text{Se}_{8-x}^{2+}$ cations, $x > 2$, with the unique structures of the $\text{Te}_2\text{Se}_6^{2+}$ and Se_8^{2+} cations. Experience dictates that attempted preparations of this cation, however, would lead instead to mixtures of $\text{Te}_x\text{Se}_{6-x}^{2+}$ and $\text{Te}_x\text{Se}_{10-x}^{2+}$ cations, which more readily crystallize with AsF_6^- and SbF_6^- anions. As in the search for new homopolyatomic cations, new anions are needed to isolate salts of new polyatomic Te-Se cations. Solutions of tellurium and selenium mixtures in oleum generate a large number of unidentified resonances in their ^{77}Se and ^{125}Te NMR spectra (Fig. IX.1). Salts of some of these unknown cations could perhaps be precipitated from oleum by the

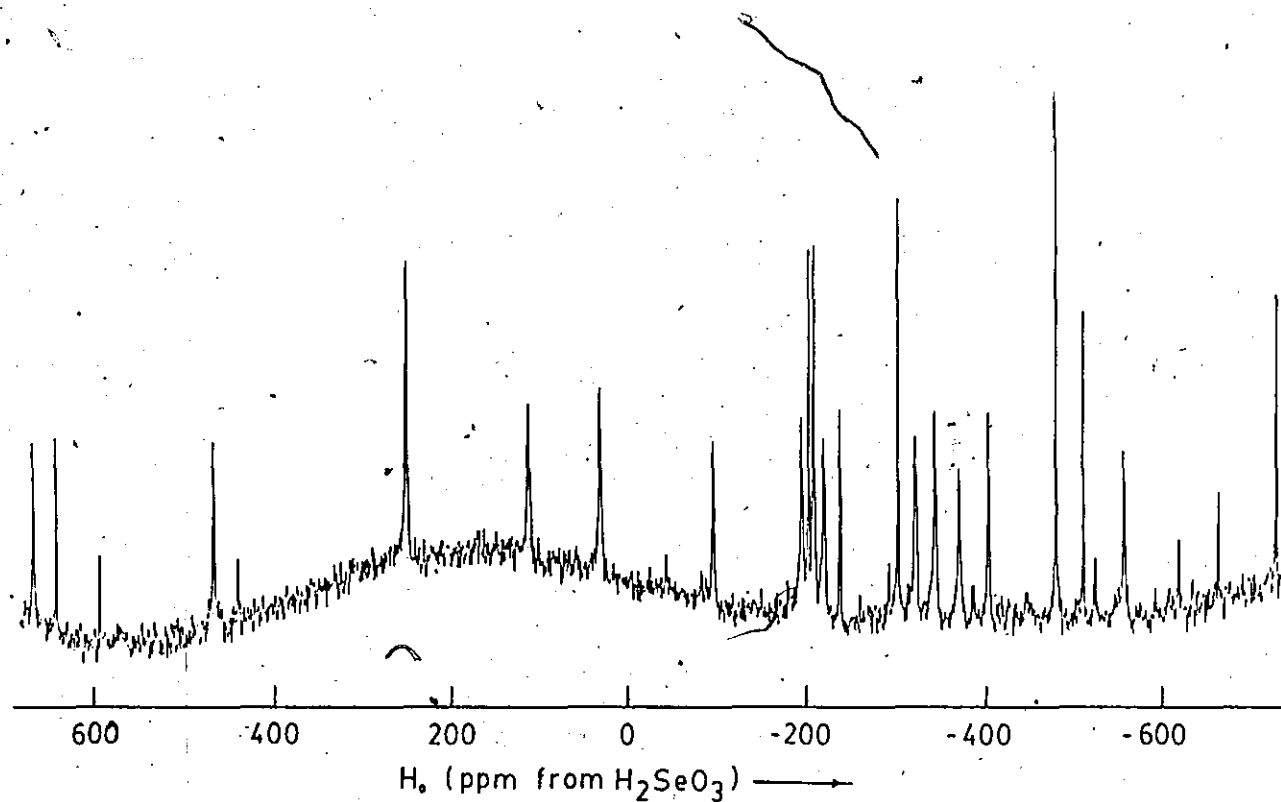
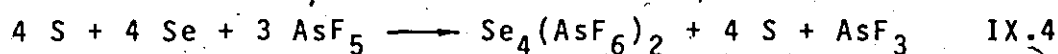
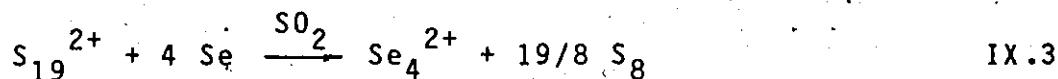


FIGURE IX.1 ⁷⁷Se NMR spectrum of a 1:2 Te-Se mixture in 30% oleum (1.3 g Te; 1.6 g Se; 3 mL oleum; 17.19 MHz; 51,000 scans; 6.1 Hz/pt).

addition of SO_2 . Decaselenium bis(fluorosulphate) was successfully crystallized during initial experiments with these mixtures (36).

The similar size and electronegativity of selenium and sulfur indicate that new mixed cations of these elements will almost certainly be disordered. Consider for example the compounds $(\text{S}_{3.0}\text{Se}_{1.0})_2(\text{Sb}_4\text{F}_{17})(\text{SbF}_6)_3$ (this work) and Se_3S_5 (157). The huge difference in the redox chemistries of sulfur and selenium also serves to limit the types of reactions that can be attempted. The reaction of S_{19}^{2+} with elemental selenium (reaction IX.3) somewhat surprisingly resulted in oxidation of selenium to Se_4^{2+} , which was identified by its ^{77}Se NMR spectrum. Mixed Se-S species or selenium cations of lower oxidation state were not observed. Reagent stoichiometries must be set so that there is more than enough oxidant to take all of the selenium present to Se_4^{2+} , otherwise the sulfur present will remain essentially unreacted (reaction IX.4).



Some mixed Se-S cations of unknown structure were observed in the ^{77}Se NMR spectra of Se/S/AsF₅ mixtures in SO_2 solvent (Fig. IV.7). These proved to be extremely soluble in SO_2 , but could perhaps be isolated from a $\text{SO}_2/\text{SO}_2\text{ClF}$ solvent mixture. The homopolyatomic sulfur cations are extremely

soluble in SO_2 , but are less soluble in SO_2ClF . The same was found to be the case for mixed Se/S and Te/S cations in the present work.

Perhaps the most lucrative area for the preparation of new polyatomic cations would be with Te-S mixtures. The preferential oxidation of tellurium over sulfur limits the possible products somewhat, but the preparation of salts of the $\text{Te}_2\text{S}_4^{2+}$ and $\text{Te}_3\text{S}_3^{2+}$ cations is a promising start. Cations with long chains of sulfur atoms attached to three-coordinate tellurium atoms can be envisaged. This fits the tendency of sulfur towards extensive catenation and the preference of electropositive tellurium atoms for three-coordinate positions. Reactions of tellurium and selenium in attempts to prepare $\text{Te}_2\text{Se}_x^{2+}$, $x > 8$, could be repeated with sulfur instead of selenium. Antimony pentafluoride is preferable over AsF_5 in most cases since the crystal quality of SbF_6^- salts is generally better than that of AsF_6^- salts. Some of the cations may only be obtained with larger Sb_xF_y^- anions.

Ternary reactions, that is reactions involving mixtures of sulfur, selenium and tellurium, may also be of interest. In the first such reaction investigated, a 1:1:1:1 mixture of S, Se, Te and AsF_5 led to the preparation of $(\text{Te}_2\text{Se}_6)(\text{Te}_2\text{Se}_8)(\text{AsF}_6)_4(\text{SO}_2)_2$ (see section IV.3).

The number of new salts of MX_3^+ cations that could

be prepared is practically limitless. The trends established for the presently known structures could be fleshed out with new examples. Orientations of secondary bonds about the central M(IV) atoms in these structures are limited to a very few different types at present, but new, less ionic examples could possibly have a whole range of geometries, as described for the isoelectronic Sb(III) atom in a recent review article (87). Comparison of the MX_3^+ cations with isoelectronic group IV anions may also be instructive. The NMR spectra of the SnF_3^- anion could be recorded and the coupling constant compared with those of the isoelectronic TeF_3^+ and SeF_3^+ cations reported here.

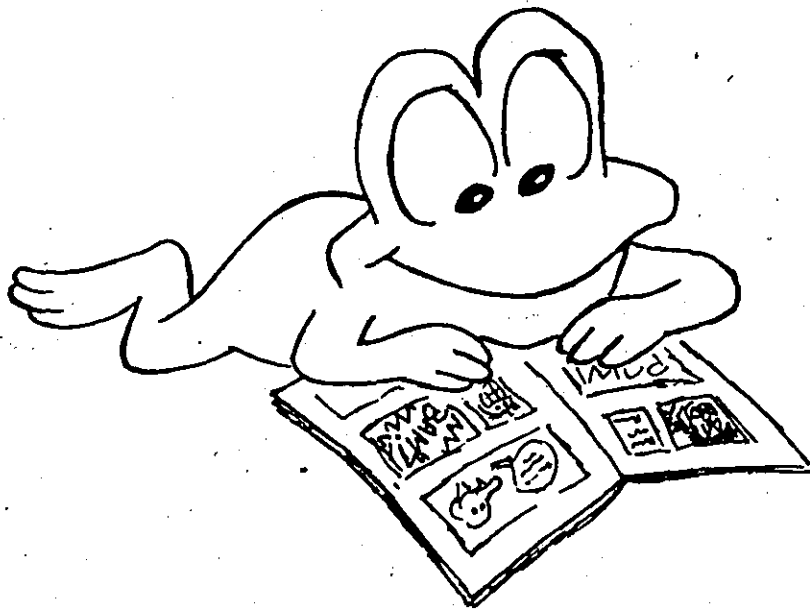
A crystal structure of a salt of the $\text{Te}(\text{OTeF}_5)_3^+$ cation would be of interest to compare the steric activity of the lone pair of electrons on Te(IV) with the bulky OTeF_5 ligands. The ^{121}Sb NMR spectrum of the recently reported $\text{Sb}(\text{OTeF}_5)_6^-$ anion (158) should be recorded and $^2J(^{125}\text{Te}-^{121}\text{Sb})$ compared with the analogous coupling in $\text{As}(\text{OTeF}_5)_6^-$. The reduced density coupling constant for $\text{As}(\text{OTeF}_5)_6^-$ is $3.69 \times 10^{-43} \text{ NA}^{-2} \text{ m}^3$, indicating that the two-bond scalar coupling in the antimony anion should be approximately 960 Hz since both cations are presumably octahedral in structure. The preparation of $\text{As}(\text{OTeF}_5)_5$ and the recent report of $\text{Sb}(\text{OTeF}_5)_5$ (158, 142) means that many of the reactions of MF_5 Lewis acids with simple fluorides can be repeated with OTeF_5 analogues. For example, the reaction of $\text{As}(\text{OTeF}_5)_5$

with $\text{Hg}(\text{OTeF}_5)_2$ and mercury could lead to new metallic compounds such as $\text{Hg}_3\text{As}(\text{OTeF}_5)_6$. Similar reactions involving mercury, HgF_2 and NbF_5 or TaF_5 have recently been reported (159). The large difference in size between the MF_6^- and $\text{M}(\text{OTeF}_5)_6^-$ anions separating the mercury chains or layers could lead to significantly different physical properties.

Bottom Line.

This thesis has presented a variety of perspectives on the reactions, structures and bonding of a number of simple compounds of sulfur, selenium and tellurium. It is hoped that these results and discussions have in some way helped to demonstrate that main-group chemistry remains a rich and exciting field.

BIBLIOGRAPHY



- 1) Klaproth, M.H. Phil. Mag. (1798), 1, 78.
- 2) Magnus, G. Ann. Phys. (Leipzig) (1827), 10, 491; (1828), 14, 328.
- 3) Bucholz, C.F. Gehlen's News. J. Chem. (1804), 3, 7.
- 4) Prince, D.J.; Corbett, J.D.; Garbisch, B. Inorg. Chem. (1970), 9, 2731.
- 5) Bjerrum, N.J.; Smith, G.P. J. Amer. Chem. Soc. (1968), 90, 4472.
- 6) Bjerrum, N.J. Inorg. Chem. (1970), 9, 1965.
- 7) Gillespie, R.J.; Passmore, J.; Acc. Chem. Res. (1971), 4, 413; Chem. Brit. (1972), 8, 475; Adv. Inorg. Chem. Radiochem. (1975), 17, 49.
- 8) Corbett, J.D. Prog. Inorg. Chem. (1976), 21, 129.
- 9) Gillespie, R.J. Chem. Soc. Rev. (1979), 8, 315.
- 10) Brown, I.D.; Crump, D.B.; Gillespie, R.J.; Santry, D.P. J. Chem. Soc. Chem. Commun. (1968), 853.
- 11) Brown, I.D.; Crump, D.B.; Gillespie, R.J. Inorg. Chem. (1971), 10, 2319.
- 12) McMullan, R.K.; Prince, D.J.; Corbett, J.D. J. Chem. Soc. Chem. Commun. (1969), 1438; Inorg. Chem. (1971), 10, 1749.
- 13) Couch, T.W.; Lokken, D.A.; Corbett, J.D. Inorg. Chem. (1972), 11, 357.
- 14) Burns, R.C.; Gillespie, R.J.; Sawyer, J.F. Inorg. Chem. (1980), 19, 1423.
- 15) Collins, M.J.; Faggiani, R.; Gillespie, R.J.; Sawyer, J.F.; Vekris, J.E. to be submitted.
- 16) Burns, R.C.; Chan, W.-L.; Gillespie, R.J.; Luk, W.-C.; Sawyer, J.F.; Slim, D.R. Inorg. Chem. (1980), 19, 1432.
- 17) Boldrini, P.; Brown, I.D.; Gillespie, R.J.; Ireland, P.R.; Luk, W.-C.; Slim, D.R.; Vekris, J.E. Inorg. Chem. (1976), 15, 765.
- 18) Davies, C.G.; Gillespie, R.J.; Park, J.J.; Passmore, J. Inorg. Chem. (1971), 10, 2781.

- 19) Gillespie, R.J.; Sawyer, J.F.; Vekris, J.E. to be submitted.
- 20) Gillespie, R.J.; Luk, W.-C.; Maharajh, E.; Slim, D.R. Inorg. Chem. (1977), 16, 892.
- 21) Burns, R.C.; Collins, M.J.; Eicher, S.M.; Gillespie, R.J.; Sawyer, J.F. to be submitted.
- 22) Passmore, J.; Sutherland, G.; White, P.S. Chem. Commun. (1980), 330.
- 23) Cardinal, G.; Gillespie, R.J.; Sawyer, J.F.; Vekris, J.E. J. Chem. Soc. Dalton (1982), 765.
- 24) Boldrini, P.; Brown, I.D.; Collins, M.J.; Gillespie, R.J.; Maharajh, E.; Sawyer, J.F.; Slim, D.R. to be submitted. The " $\text{Te}_3\text{Se}_7(2+)$ " cation refined to " $\text{Te}_{3.0}\text{Se}_{1.0}(2+)$ " in the present structure (see chapter VI).
- 25) Gillespie, R.J.; Luk, W.-C.; Slim, D.R. J. Chem. Soc. Chem. Commun. (1976), 791.
- 26) Burns, R.C.; Gillespie, R.J.; Luk, W.-C.; Slim, D.R. Inorg. Chem. (1979), 18, 3086.
- 27) Hoffman, C.F. Inorg. Synth. (1953), 4, 150.
- 28) Sladky, F.; Kropshofer, H.; Leitzke, O. J. Chem. Soc. Chem. Commun. (1973), 134.
- 29) Barr, J.; Ph.D. Thesis, McMaster University, 1959.
- 30) Weiss, J.; Pupp, M. Angew. Chem. Int. Ed. Engl. (1971), 9, 463.
- 31) Robinson, E.A.; Ph.D. Thesis, University College (London), 1958.
- 32) Schrobilgen, G.J.; Ph.D. Thesis, McMaster University, 1973.
- 33) Suttle, J.F.; Smith, C.R.F. Inorg. Synth. (1950), 3, 140.
- 34) Lentz, D.; Pritzkow, J.; Seppelt, K. Inorg. Chem. (1978), 17, 1926.
- 35) Durig, J.R.; Lau, K.K.; Nagarajan, G.; Walker, M.; Bragin, J. J. Chem. Phys. (1969), 50, 2130.
- 36) Collins, M.J.; Gillespie, R.J.; Sawyer, J.F.; Schrobilgen,

- G.J. submitted to Acta. Cryst.
- 37) Fehrmann, R.; Bjerrum, N.J. Inorg. Chem. (1977), 16, 2089.
- 38) Burns, R.C.; Gillespie, R.J.; Schrobilgen, G.J. unpublished results.
- 39) Bondi, A. J. Phys. Chem. (1964), 68, 441.
- 40) Alcock, N.W. Adv. Inorg. Chem. Radiochem. (1972), 15, 1.
- 41) Ziolo, R.F.; Troup, J.M. J. Am. Chem. Soc. (1983), 105, 229.
- 42) Chem. Eng. News, Jan. 31, 1983, p 17.
- 43) Rosenfield, R.E.; Parthasarathy, R.; Dunitz, J.D. J. Am. Chem. Soc. (1977), 99, 4860.
- 44) Gillespie, R.J.; Kent, J.P.; Sawyer, J.F. Inorg. Chem. (1981), 20, 3784.
- 45) Gillespie, R.J.; Kent, J.P.; Sawyer, J.F.; Slim, D.R.; Tyrer, J.D. Inorg. Chem. (1981), 20, 3799.
- 46) Edwards, A.J.; Taylor, P. J. Chem. Soc. Dalton (1973), 2150.
- 47) Nickless, G. "Inorganic Sulfur Chemistry", Elsevier, Amsterdam, 1968.
- 48) Sheldrick, G.M. SHELX Program for Crystal Structure Determination, University of Cambridge, England, 1976.
- 49a) Barr, J.; Gillespie, R.J.; Kapoor, R.; Malhotra, K.C. Can. J. Chem. (1968), 46, 149. b) Fehrmann, R.; Bjerrum, N.J.; Andreasen, H.A. Inorg. Chem. (1976), 15, 2187.
- 50) Schrobilgen, G.J.; Burns, R.C.; Granger, P. J. Chem. Soc. Chem. Commun. (1978), 957.
- 51) Burns, R.C.; Gillespie, R.J.; Barnes, J.A.; McGlinchey, M.J. Inorg. Chem. (1982), 21, 799.
- 52) Pople, J.A.; Schneider, W.G.; Bernstein, H.J. "High Resolution Nuclear Magnetic Resonance", McGraw-Hill, New York (1959).
- 53) Banwell, C.N. in "Nuclear Magnetic Resonance for Organic Chemists"; Mathieson, D.W. ed.; Academic Press, London (1967),

Chapter 6.

- 54) Abraham, R.J.; Bernstein, H.J. *Can. J. Chem.* (1961), 39, 216.
- 55) Emsley, J.W.; Feeney, J.; Sutcliffe, L.H. "High Resolution Nuclear Magnetic Resonance Spectroscopy", Vol. 1; Pergamon Press, Oxford (1965).
- 56) Harris, R.K.; Sheppard, N. *Trans. Faraday Soc.* (1963), 59, 606.
- 57) Allred, A.L.; Rochow, E.G. *J. Inorg. Nucl. Chem.* (1958), 5, 264.
- 58) Schmettow, W.; Lipka, A.; von Schnering, H.G. *Angew. Chem. Int. Ed. Engl.* (1974) 13, 345.
- 59) Barr, J.; Gillespie, R.J.; Pez, G.P.; Ummat, P.K.; Vaidya, O.C. *Inorg. Chem.* (1971), 10, 362.
- 60) Morrison, R.J.; Boyd, R.N. "Organic Chemistry", 3rd Ed., Allyn and Bacon, Boston, (1973), pp. 295-297.
- 61) Gillespie, R.J. "Molecular Geometry", Van Nostrand Reinhold Company (London), 1972.
- 62) Wichelhaus, W.; von Schnering, H.G. *Naturwissenschaften* (1973), 60, 104.
- 63) Belin, C.H.E. *J. Am. Chem. Soc.* (1980), 102, 6036.
- 64) von Schnering, H.G. *Angew. Chem. Int. Ed. Engl.* (1981), 20, 33.
- 65) Leung, Y.C.; Waser, J.; van Houten, S.; Vos, A.; Wiegers, G.A.; Wiebenga, F.H. *Acta Cryst.* (1957), 10, 574.
- 66) Christian, B.H.; Gillespie, R.J.; Sawyer, J.F. *Inorg. Chem.* (1981), 20, 3410.
- 67) Harris, R.K.; Mann, B.F. eds. "NMR and the Periodic Table", Academic Press, New York (1978).
- 68) Adolphson, D.G.; Corbett, J.D.; Merryman, D.J. *J. Am. Chem. Soc.* (1976), 98, 7234.
- 69) Luk, W.-C.; Ph.D. Thesis, McMaster University, 1975.
- 70) Bojes, J.; Chivers, T.; Laidlaw, W.G.; Trsic, M. *J. Am. Chem. Soc.* (1979), 101, 4517.

- 71) Chivers, T.; Coddington, P.W.; Laidlaw, W.G.; Liblong, S.W.; Oakley, R.T.; Trsic, M. J. Am. Chem. Soc. (1983), 105, 1186.
- 72) Jones, C.H.W. Can. J. Chem. (1977), 55, 3076.
- 73) Eatough, N.L.; Webb, A.W.; Hall, H.T. Inorg. Chem. (1969), 8, 2069.
- 74) Grdenić, D.; Scavnicar, S. Proc. Chem. Soc. (1960) 147. Scavnicar, S. Z. Krist. (1960), 114, 85. Hofmann W. Z. Krist. (1933), 86, 225.
- 75) Anderson, T.L.; Krause, H.B. Acta Cryst. B. (1974), 30, 1307.
- 76) Barr, J.; Gillespie, R.J.; Kapoor, R.; Pez, G.P. J. Am. Chem. Soc. (1968), 90, 6855.
- 77) Burns, R.C.; Gillespie, R.J. Inorg. Chem. (1982), 21, 3877.
- 78) Lassigne, C.R.; Wells, E.J. J. Chem. Soc. Chem. Commun. (1978), 956.
- 79) Mikulski, C.M.; Russo, P.J.; Saran, M.S.; MacDiarmid, A.G.; Garito, A.F.; Heeger, A.J. J. Am. Chem. Soc. (1975), 97, 6358.
- 80) Cisar, A.; Corbett, J.D. Inorg. Chem. (1977) 16, 2482.
- 81) Eisenmann, B.; Janzon, K.H.; Schafer, H.; Weiss, A. Z. Naturforsch. (1969), B24, 457.
- 82) Barr, J.; Gillespie, R.J.; Ummat, P.K. J. Chem. Soc. Chem. Commun. (1970), 264.
- 83) Gillespie, R.J.; Passmore, J.; Ummat, P.K.; Vaidya, O.C. Inorg. Chem. (1971), 10, 1327.
- 84) Koch, W.; Lutz, O.; Nolle, A. Z. Naturforsch. (1978), 33a, 1025.
- 85) Odom, J.D.; Dawson, W.H.; Ellis, P.D. J. Am. Chem. Soc. (1979), 101, 5815.
- 86) Eysel, H.H.; Sunder, S. Inorg. Chem. (1979), 18, 2626.
- 87) Sawyer, J.F.; Gillespie, R.J. submitted to Chem. Soc. Rev.
- 88) Eschande, P.; Tichit, D.; Ducourant, B.; Fourcade, R.;

- Mascherpa, G. *Ann. Chim. Fr.* (1978). 3, 117.
- 89) Collins, M.J.; Faggiani, R.; Gillespie, R.J.; Kapoor, R. unpublished results.
- 90) Golic, L.; Leban, J. *Acta Cryst.* (1977), B33, 232.
- 91) Vilminot, S.; Granier, W.; Al Oraibi, Z.; Cot, L. *Acta Cryst.* (1978), B34, 3306.
- 92) Alcock, N.W.; Harrison, W.D. *J. Chem. Soc. Dalton* (1982), 1421.
- 93) Alcock, N.W.; Moore, P.; Curzon, E.H.; Pierpoint, C. to be submitted to *J. Chem. Soc. Dalton*.
- 94) Edwards, A.J.; Taylor, P. *J. Chem. Soc. Dalton* (1975), 2174.
- 95) Nandana, W.A.S.; Passmore, J.; Swindells, D.C.N.; Taylor, P.; White, P.S.; Vekris, J.E. *J. Chem. Soc. Dalton* (1983), 619.
- 96) Edwards, A.J.; Slim, D.R. *J. Chem. Soc. Chem. Commun.* (1974), 178.
- 97) Nandana, W.A.S.; Passmore, J.; Swindells, D.C.N.; White, P.S.; Wong, M. reported at the 10th International Symposium on Fluorine Chemistry, Vancouver, Canada, Aug. 1-6, 1982.
- 98) McDonald, R.R.; Larson, A.C.; Cromer, D.T. *Acta Cryst.* (1964), 17, 1104.
- 99) Brown, I.D. *J. Solid State Chem.* (1974), 11, 214.
- 100) Rothman, J.J.; Bartell, L.S.; Ewig, C.S.; van Wazer, J.R. *J. Comput. Chem.* (1980), 1, 64.
- 101) Tanaka, K.; Yamabe, T.; Terama-E, H.; Fukui, K. *Inorg. Chem.* (1979), 18, 3591.
- 102) Passmore, J.; Richardson, E.K.; Whidden, T.K.; White, P.S. *Can. J. Chem.* (1980), 58, 851.
- 103) Weiss, J.; Pupp, M. *Angew. Chem. Int. Ed. Engl.* (1971), 9, 463.
- 104) Krebs, B.; Buss, B.; Altena, D. *Z. Anorg. Allg. Chem.* (1971), 386, 257.

- 105) Brooks, W.V.F.; Passmore, J.; Richardson, E.K.
Can. J. Chem. (1979), 57, 3230.
- 106) Sawodny, W.; Dehnicke, K. Z. Anorg. Allg. Chem. (1967),
349, 169.
- 107) Bartlett, N.; Robinson, P.L. J. Chem. Soc. (1961), 3417.
Evans, J.A.; Long, D.A. J. Chem. Soc. A (1968), 1688.
- 108) Buss, B.; Krebs, B. Inorg. Chem. (1971), 10, 2795.
- 109) Collins, M.J.; Denes, G.; Gillespie, R.J. unpublished
results.
- 110) Gillespie, R.J.; Schrobilgen, G.J.; Slim, D.R.
J. Chem. Soc. Dalton (1977), 1003.
- 111) Edwards, A.J.; Hewaidy, F.I. J. Chem. Soc. A (1968),
2977.
- 112) Bartlett, N.; Einstein, F.; Stewart, D.F.; Trotter, J.
J. Chem. Soc. A (1967), 1190.
- 113) Jones, G.R.; Burbank, R.D.; Bartlett, N. Inorg. Chem.
(1970), 9, 2264.
- 114) Hartl, H.; Rama, M.; Simon, A.; Deiseroth, H.-J.
Z. Naturforsch. (1979), 34b, 1035.
- 115) Edwards, A.J. J. Chem. Soc. Dalton (1978), 1723.
- 116) Christian, B.H. Ph.D. Thesis, McMaster University,
1982. Christian, B.H.; Collins, M.J.; Gillespie, R.J.;
Sawyer, J.F.; to be submitted.
- 117) Donaldson, J.D.; Silver, J.; Hadjiminolis, S.;
Ross, S.D. J. Chem. Soc. Dalton (1974), 1500.
- 118) Hazell, A.C. Acta Chem. Scand. (1966), 20, 165.
- 119) Webb, G.A. pp 62-75 of reference (67).
- 120) Harris, R.K. p 9 of reference (67).
- 121) Pyykko, P.; Weisenfeld, L. Mol. Phys. (1981), 43, 55.
- 122) Burns, R.C.; Devereux, L.A.; Granger, P.; Schrobilgen,
G.J. Inorg. Chem. submitted for publication.
- 123) Gillespie, R.J.; Granger, P.; Morgan, K.R.; Schrobilgen,
G.J. Inorg. Chem. accepted for publication.

- 124) Brownstein, M.; Gillespie, R.J. J. Chem. Soc. Dalton (1973), 67.
- 125) Edwards, A.J.; Jones, G.R. J. Chem. Soc. A (1970), 1891.
- 126) Edwards, A.J.; Jones, G.R. J. Chem. Soc. A (1970), 1491.
- 127) Ponsioen, R.; Stufkens, D.-J. Rec. Trav. Chim. (1971), 90, 521. Hayward, G.C.; Hendra, P.J. J. Chem. Soc. A (1967), 643.
- 128) Gerding, H.; Stufkens, D.-J. Rev. Chim. Miner. (1969), 6, 795. Brockner, W.; Deming, A.F. Z. Anorg. Allg. Chem. (1980), 469, 27.
- 129) Poulsen, F.W.; Bjerrum, N.J.; Nielsen, O.F. Inorg. Chem. (1974), 13, 2693.
- 130) Gibler, D.D.; Adams, C.J.; Fischer, M.; Zalkin, A.; Bartlett, N. Inorg. Chem. (1972), 11, 2325.
- 131) Sawodny, W.; Rediess, K.; Thewalt, U. Z. Anorg. Allg. Chem. (1983), 499, 81.
- 132) Kniep, R.; Korte, L.; Mootz, D. Z. Naturforsch. (1981), 36B, 1660. Stork-Blaisse, B.A.; Romers, C. Acta Cryst. (1971), B27, 386. Gleizes, A.; Galy, J.P. C. R. Acad. Sci. Paris, Ser. C (1978), 286, 29.
- 133) Born, P.; Kniep, R.; Mootz, D. Z. Anorg. Allg. Chem. (1979), 451, 12.
- 134) Passmore, J.; Sutherland, G.; White, P.S. Can. J. Chem. (1981), 59, 2876.
- 135) Birchall, T.; Gillespie, R.J.; Vekris, S.L. Can. J. Chem. (1965), 43, 1672.
- 136) Birchall, T.; Myers, R.D.; de Waard, H.; Schrobilgen, G.J. Inorg. Chem. (1982), 21, 1068.
- 137) Seppelt, K. Angew. Chem. Int. Ed. Engl. (1972), 11, 630.
- 138) Keller, N.; Schrobilgen, G.J. Inorg. Chem. (1981), 20, 2118.
- 139) Seppelt, K.; Nothe, D. Inorg. Chem. (1973), 12, 2727.
- 140) Engelbrecht, A.; Sladky, F. Angew. Chem. (1964), 76, 379; Angew. Chem. Int. Ed. Engl. (1964), 3, 383.

- 141) Engelbrecht, A.; Sladky, F. Adv. Inorg. Chem. Radiochem. (1981), 24, 189.
- 142) Seppelt, K. Angew. Chem. Int. Ed. Engl. (1982), 21, 877.
- 143) Sladky, F. Angew. Chem. (1969), 81, 536; Angew. Chem. Int. Ed. Engl. (1969), 8, 523.
- 144) Lentz, D.; Seppelt, K. Angew. Chem. (1978), 90, 391; Angew. Chem. Int. Ed. Engl. (1978), 17, 356.
- 145) Sladky, F.; Kropshofer, H.; Leitzke, O. J. Chem. Soc. Chem. Commun. (1973), 134.
- 146) Sawyer, J.F.; Schrobilgen, G.J. Acta Cryst. (1982), B38, 1561.
- 147) Mayer, E.; Sladky, F. Inorg. Chem. (1975), 14, 589.
- 148) Schümacher, G.A.; Schrobilgen, G.J. submitted to Inorg. Chem.
- 149) Lentz, D.; Seppelt, K. Z. Anorg. Allg. Chem. (1983), 502, 83.
- 150) Balimann, G.; Pregosin, P.S. J. Mag. Res. (1977), 26, 283.
- 151) see for example: Adriaenssens, G.J. Ferroelectrics (1976), 12, 269.
- 152) Gillespie, R.J.; Rao, U.R.K. J. Chem. Soc. Chem. Commun. (1983), 422 and references therein.
- 153) Templeton, L.K.; Templeton, D.H.; Bartlett, N.; Seppelt, K. Inorg. Chem. (1976), 15, 2720.
- 154) Berry, R.S. J. Chem. Phys. (1960), 32, 933.
- 155) Calder, I.C.; Garratt, P.J. J. Chem. Soc. B (1967), 660.
- 156) Mahler, W.; Meutterties, E.L. Inorg. Chem. (1965), 4, 1520.
- 157) Calvo, C.; Gillespie, R.J.; Vekris, J.E.; Ng, H.N. Acta Cryst. (1978), B34, 911.
- 158) Toetsch, W.; Bartlett, N. reported at the 10th International Symposium on Fluorine Chemistry, Vancouver, Canada, August 1-6, 1982.

159) Brown, I.D.; Gillespie, R.J.; Morgan, K.R.; Tun, Z.
submitted to Inorg. Chem.

160) Rytter, E.; Oye, H.A. J. Inorg. Nucl. Chem. (1973),
35, 4311.

161) Fung, K.W.; Begun, G.M.; Mamantov, G. Inorg. Chem.
(1973), 12, 53.

162) Begun, G.M.; Rutenberg, A.C. Inorg. Chem. (1967), 6,
2212.

163) Qureshi, A.M.; Aubke, F. Can. J. Chem. (1970), 48,
3117. Gillespie, R.J.; Whittle, A. ibid. (1970), 48, 657.

APPENDIX

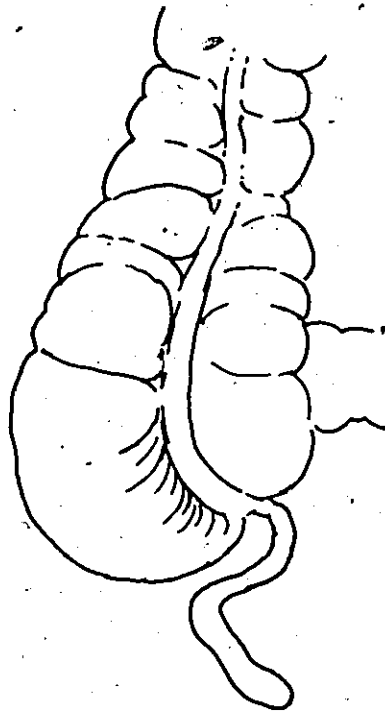


TABLE A.1 Unit Cell Dimensions and Space Groups for the Compounds Characterized by X-Ray Crystallography in this Thesis.

Compound	Space Group	a	b	c(Å)	α	β	γ (°)	V(Å ³)
Te ₂ Se ₈ (AsF ₆) ₂	Pbcn	16.118(3)	13.089(3)	18.951(4)	90	90	90	4001(1)
Te ₂ Se ₈ (SbF ₆) ₂	Pbcn	16.489(3)	13.251(4)	19.422(6)	90	90	90	4244(2)
Te _{4.5} Se _{5.5} (AsF ₆) ₂	Pbcn	14.790(3)	10.783(2)	13.304(2)	90	90	90	2121.7(7)
Te ₂ Se ₆ (Te ₂ Se ₈)(AsF ₆) ₄ (SO ₂) ₂	P2 ₁ /c	12.432(4)	15.956(6)	23.053(10)	90	96.61(3)	90	4542(3)
Te ₆ (Se ₈)(AsF ₆) ₆ (SO ₂)	P $\bar{1}$	12.407(4)	12.465(3)	14.109(5)	96.62(2)	90.49(3)	95.13(2)	2158(1)
Te ₂ Se ₄ (SbF ₆) ₂	Pbcn	12.124(4)	18.493(6)	29.503(7)	90	90	90	6614(3)
Te ₂ Se ₄ (Sb ₃ F ₁₄)(SbF ₆)	Pbca	15.288(5)	17.189(5)	17.300(5)	90	90	90	4546(2)
Te _{2.7} Se _{3.3} (SbF ₆) ₂	P2 ₁ 2 ₁ 2 ₁	12.192(2)	8.770(2)	15.817(3)	90	90	90	1691.1(6)
Te _{3.4} Se _{2.6} (SbF ₆) ₂	P2 ₁ 2 ₁ 2 ₁	12.266(3)	8.828(3)	15.884(4)	90	90	90	1720.0(9)
Te _{2.1} S _{3.9} (SbF ₆) ₂	Pbcn	11.988(3)	18.220(6)	29.096(8)	90	90	90	6355(3)
Te ₃ S ₃ (SbF ₆) ₂	P2 ₁ /n	8.689(8)	12.217(1)	15.732(1)	90	91.59(5)	90	1669(2)
Te ₂ Se ₂ (Sb ₃ F ₁₄)(SbF ₆)	Pbcm	8.293(2)	16.337(3)	15.811(4)	90	90	90	2142.2(8)
Te _{3.0} Se _{1.0} (Sb ₃ F ₁₄)(SbF ₆)	Pn2 ₁ a	16.594(8)	11.634(4)	11.128(3)	90	90	90	2148(1)
(S _{3.0} Se _{1.0}) ₂ (Sb ₄ F ₁₇)(SbF ₆) ₃	B2 ₁ /c	15.267(3)	13.440(4)	16.437(6)	90	91.59(2)	90	3372(2)
TeCl ₃ (AlCl ₄)	P $\bar{1}$	6.554(1)	19.691(4)	8.391(1)	92.79(1)	97.31(1)	96.11(1)	1065.8(3)
TeCl ₃ (SbCl ₆)	C2/c or Cc	22.137(4)	12.781(2)	19.308(3)	90	112.47(1)	90	5048(2)
TeCl ₃ (AsF ₆)	P2 ₁ /n	8.827(2)	10.009(3)	10.592(5)	90	108.27(3)	90	888.7
TeCl ₃ (SbF ₆)	Pnma	17.031(3)	8.460(1)	6.398(1)	90	90	90	921.8(4)
(TeF ₃) ₂ (SO ₄)	P2 ₁ 2 ₁ 2 ₁	8.758(1)	8.983(1)	9.946(2)	90	90	90	782.5(3)

TABLE A.2 Atomic Positional ($\times 10^4$) and Thermal ($\times 10^3$) Parameters.

(a) $\text{Te}_2\text{Se}_8(\text{AsF}_6)_2$.

ATOM	$x(\times 10^4)$	$y(\times 10^4)$	$z(\times 10^4)$	U(11)	U(22)	U(33)	U(12)	U(13)	U(23)
Te(1)	2462.6(8)	2197.4(9)	5335.2(5)	46.9(7)	37.4(7)	26.8(5)	- 3.9(6)	1.7(6)	1.6(5)
Te(2)	3612.4(8)	2814.5(9)	2987.3(6)	46.0(8)	39.4(7)	31.1(6)	1.6(6)	9.3(5)	3.8(6)
Se(1)	3552(1)	1187(1)	4639(1)	41.2(11)	34.1(10)	43.3(11)	7.0(9)	- 0.3(9)	10.0(9)
Se(2)	2986(1)	1189(1)	3528(1)	68.7(14)	30.4(10)	37.3(11)	- 6.6(10)	2.1(10)	- 2.5(9)
Se(3)	2218(1)	3657(1)	2646(1)	51.5(12)	40.3(11)	36.4(10)	- 0.6(9)	- 4.5(9)	10.5(8)
Se(4)	1207(1)	2484(1)	2910(1)	46.4(12)	45.8(11)	35.9(10)	- 7.8(9)	-10.7(9)	- 2.4(8)
Se(5)	737(1)	2959(1)	4037(1)	35.4(11)	40.0(11)	45.2(11)	3.3(9)	- 3.1(8)	- 0.4(9)
Se(6)	1121(1)	1595(1)	4721(1)	40.9(11)	39.0(10)	43.5(11)	- 9.0(9)	2.7(9)	5.4(9)
Se(7)	2628(1)	3866(1)	4630(1)	42.3(11)	27.5(10)	39.5(10)	1.8(8)	1.9(8)	- 1.7(8)
Se(8)	3927(1)	3716(1)	4158(1)	37.1(11)	40.7(11)	39.8(11)	-10.8(9)	- 2.4(8)	- 0.3(8)
As(1)	4177(1)	633(1)	1358(1)	39.7(11)	47.4(12)	32.7(11)	- 5.4(9)	- 9.2(9)	4.1(9)
As(2)	5962(1)	5226(1)	3538(1)	31.9(10)	34.7(10)	29.4(9)	4.6(8)	- 0.1(8)	0.4(8)
F(11)	4735(8)	1700(9)	1575(8)	73(9)	64(8)	118(12)	-25(7)	-12(8)	-32(8)
F(12)	3631(9)	432(10)	1146(7)	129(12)	90(10)	69(9)	-70(9)	8(8)	-10(7)
F(13)	4986(10)	64(11)	1118(15)	68(10)	65(10)	564(43)	-13(9)	132(18)	-114(18)
F(14)	4131(17)	275(20)	2170(8)	269(28)	277(27)	48(10)	-168(24)	- 7(13)	5(13)
F(15)	3986(19)	1149(13)	592(10)	390(34)	107(14)	107(15)	- 92(18)	-150(19)	70(12)
F(16)	3305(11)	1266(20)	1639(18)	82(14)	220(25)	348(36)	0(15)	39(18)	-145(24)
F(21)	5536(6)	5301(8)	4376(5)	58(7)	73(8)	25(5)	12(6)	5(5)	- 1(5)
F(22)	5500(8)	4071(8)	3417(7)	81(9)	50(7)	78(9)	- 13(6)	19(7)	- 20(7)
F(23)	6803(7)	4600(9)	3884(6)	54(8)	76(8)	69(8)	25(6)	- 4(6)	37(7)
F(24)	6397(7)	5097(8)	2699(5)	68(8)	67(7)	40(6)	14(6)	-12(6)	3(6)
F(25)	6437(7)	6372(8)	3669(6)	78(9)	50(7)	70(9)	- 19(6)	- 12(7)	5(6)
F(26)	5135(7)	5820(9)	3199(5)	52(8)	92(8)	39(7)	29(7)	- 6(5)	- 7(6)

(b) $\text{Te}_{4.5}\text{Se}_{5.5}(\text{AsF}_6)_2$

ATOM	X(x10 ⁴)	Y(x10 ⁴)	Z(x10 ⁴)	U11	U22	U33	U12	U13	U23
Te(1)*	1678.4(3)	3944.9(5)	2304.6(4)	31.8(3)	41.8(4)	38.6(3)	2.6(2)	-3.4(2)	2.7(3)
Te(2)*	683.7(5)	2707.0(7)	3654.2(5)	43.3(4)	44.9(5)	50.1(5)	-1.2(3)	-4.1(3)	12.7(4)
Se(1)*	377.3(6)	4363.9(9)	1032.9(6)	41.6(5)	52.9(6)	39.9(5)	-2.4(4)	-7.1(4)	8.3(4)
Se(2)*	4260.4(5)	2386.2(7)	2040.8(6)	82.6(6)	41.0(5)	57.5(5)	11.0(4)	2.1(4)	4.6(4)
Se(3)*	3343.9(5)	1124.0(8)	3164.4(6)	44.9(5)	44.2(6)	43.3(5)	8.4(4)	5.3(4)	-0.7(4)
As	1690.6(6)	1859.7(9)	176.8(7)	38.3(5)	58.5(6)	40.8(5)	5.9(4)	4.2(4)	1.4(4)
F(1)	658(3)	1414(7)	147(4)	41(3)	99(5)	87(4)	23(3)	-6(3)	-4(4)
F(2)	1435(5)	1011(8)	1400(5)	120(6)	173(9)	51(4)	42(5)	4(4)	1(5)
F(3)	1306(6)	573(6)	178(7)	117(6)	46(4)	231(10)	-20(5)	-22(6)	-5(6)
F(4)	2109(5)	2313(7)	212(8)	81(5)	53(4)	238(10)	-12(4)	-6(6)	13(5)
F(5)	2750(4)	334(6)	484(4)	56(4)	82(5)	77(4)	28(3)	-8(3)	7(3)
F(6)	1996(4)	795(8)	1027(4)	91(5)	227(10)	41(3)	79(6)	15(3)	9(5)

*Population Parameters: Te(1), 0.1998(4); Te(2), 0.843(3); Se(1), 1.065(4);
Se(2), 1.229(5); Se(3), 1.069(5).

(c) $\text{Te}_2\text{Se}_6(\text{Te}_2\text{Se}_8)(\text{AsF}_6)_4(\text{SO}_2)_2$

ATOM	X($\times 10^4$)	Y($\times 10^4$)	Z($\times 10^4$)	U ₁₁	U ₂₂	U ₃₃	U ₁₂	U ₁₃	U ₂₃
Te(1)	5153(3)	1755(2)	2984(2)	60(2)	40(2)	74(3)	- 4(2)	21(2)	- 8(2)
Te(2)	4362(3)	3929(2)	4324(2)	56(2)	58(2)	70(3)	- 7(2)	21(2)	-14(2)
Te(3)	- 154(3)	847(2)	1964(2)	86(3)	48(2)	72(3)	- 3(2)	24(3)	- 7(2)
Te(4)	- 298(3)	3429(2)	1232(2)	68(3)	47(2)	91(4)	4(2)	15(3)	4(2)
Se(3)	6632(6)	2727(4)	2724(3)	96(5)	74(4)	96(6)	-21(4)	45(5)	-13(4)
Se(4)	7770(5)	2898(4)	3584(3)	61(4)	86(4)	93(6)	- 4(3)	24(4)	- 4(4)
Se(5)	7236(5)	4235(4)	3904(3)	56(4)	77(4)	89(6)	-21(3)	25(4)	-14(4)
Se(6)	6383(5)	3898(4)	4698(3)	71(4)	91(4)	76(6)	- 5(3)	10(4)	- 2(4)
Se(7)	3912(4)	2348(3)	4346(3)	66(4)	59(4)	67(5)	- 9(3)	32(4)	- 2(3)
Se(8)	5525(5)	1796(3)	4109(3)	77(4)	58(4)	68(5)	3(3)	22(4)	8(3)
Se(9)	3609(4)	2836(3)	2877(3)	57(4)	62(4)	80(5)	3(3)	- 7(4)	-18(4)
Se(10)	4526(4)	4043(3)	3212(3)	67(4)	45(3)	57(5)	- 7(3)	9(3)	- 4(3)
Se(11)	- 671(5)	3128(3)	2285(3)	69(4)	64(4)	100(6)	11(3)	29(4)	-15(4)
Se(12)	560(5)	2124(3)	2584(3)	83(5)	67(4)	75(5)	12(3)	7(4)	-18(4)
Se(13)	- 1992(4)	1536(4)	1556(3)	45(4)	75(4)	113(6)	-12(3)	20(4)	- 6(4)
Se(14)	- 1537(5)	2244(4)	752(3)	74(5)	91(5)	92(6)	- 6(4)	-12(4)	- 7(4)
Se(15)	1510(4)	2554(3)	1282(3)	38(3)	55(3)	103(6)	- 4(3)	28(4)	- 8(3)
Se(16)	796(4)	1205(3)	1042(3)	57(4)	52(3)	74(5)	7(3)	28(4)	-10(3)
As(1)	4605(5)	1567(3)	1170(3)	58(4)	66(4)	50(4)	2(3)	9(4)	- 1(3)
As(2)	10996(5)	1151(3)	795(3)	53(4)	69(4)	59(5)	- 8(3)	11(4)	- 5(3)
As(3)	- 2240(5)	64(3)	3177(3)	76(5)	53(4)	109(7)	19(3)	32(5)	15(4)
As(4)	7362(4)	5104(3)	1989(3)	55(4)	55(4)	103(6)	14(3)	20(4)	2(4)

continued.

$\text{Te}_2\text{Se}_6(\text{Te}_2\text{Se}_8)(\text{AsF}_6)_4(\text{SO}_2)_2$ continued.

ATOM	X(x10 ³)	Y(x10 ³)	Z(x10 ³)	U	ATOM	X(x10 ³)	Y(x10 ³)	Z(x10 ³)	U
F(11)	387(5)	116(4)	161(3)	213(25)	F(34)	- 179(5)	- 46(4)	378(3)	220(26)
F(12)	542(4)	189(3)	68(2)	163(18)	F(35)	- 103(6)	42(4)	322(3)	258(30)
F(13)	522(5)	67(3)	116(3)	200(22)	F(36)	654(7)	- 46(5)	307(4)	345(41)
F(14)	558(5)	180(4)	164(3)	208(24)	F(41)	730(3)	607(2)	229(2)	92(10)
F(15)	407(5)	241(4)	112(3)	228(26)	F(42)	745(3)	415(2)	169(2)	109(12)
F(16)	369(5)	122(4)	63(3)	225(25)	F(43)	861(3)	530(2)	180(2)	122(13)
F(21)	1004(4)	68(3)	- 129(2)	168(18)	F(44)	681(3)	555(2)	137(2)	128(14)
F(22)	1091(6)	212(4)	- 122(3)	265(33)	F(45)	791(3)	469(2)	263(2)	107(12)
F(23)	1006(4)	143(3)	- 39(2)	176(19)	F(46)	612(3)	486(2)	220(2)	130(14)
F(24)	1192(4)	81(3)	- 119(2)	152(17)	S(1)	510(3)	408(2)	73(2)	214(13)
F(25)	1120(5)	24(4)	- 51(3)	227(25)	S(2)	38(4)	122(3)	447(2)	267(18)
F(26)	1196(4)	163(3)	- 29(2)	157(17)	O(11)	365(9)	425(7)	36(5)	402(58)
F(31)	- 281(4)	79(3)	362(2)	150(16)	O(12)	626(12)	385(9)	22(7)	494(79)
F(32)	- 278(4)	52(3)	254(2)	155(17)	O(21)	- 74(6)	136(5)	458(3)	231(30)
F(33)	179(4)	- 67(3)	272(2)	161(18)	O(22)	155(7)	85(5)	475(4)	269(35)

(d) $\text{Te}_6(\text{Se}_8)(\text{AsF}_6)_6(\text{SO}_2)_6$

ATOM	X	Y	Z	U_{11}	U_{22}	U_{33}	U_{12}	U_{13}	U_{23}
Te(1)	2432(1)	4198(1)	304(1)	48.9(9)	25.8(7)	50.0(9)	2.6(6)	1.8(7)	5.2(6)
Te(2)	831(1)	2603(1)	282(1)	30.0(7)	47.5(8)	54.4(9)	4.5(6)	9.5(6)	5.1(7)
Te(3)	1616(1)	3189(1)	-1381(1)	50.0(9)	51.2(9)	35.9(8)	13.0(7)	-10.6(7)	13.6(7)
Te(4)	3280(1)	1530(1)	-1422(1)	49.1(9)	41.9(8)	35.4(8)	10.0(6)	10.8(6)	6.2(6)
Te(5)	2568(1)	880(1)	243(1)	45.8(8)	31.2(7)	50.7(9)	4.7(6)	1.8(7)	15.7(6)
Te(6)	4165(1)	2477(1)	256(1)	29.3(7)	47.0(8)	50.7(9)	2.3(6)	-9.8(6)	5.7(7)
Se(1)	5869(2)	2105(2)	5369(2)	38.7(12)	58.8(14)	48.5(14)	-1.9(10)	-4.8(10)	10.8(11)
Se(2)	6995(2)	2770(2)	6638(2)	65.9(16)	64.7(15)	37.4(13)	5.8(12)	-0.8(11)	5.3(11)
Se(3)	7968(2)	1288(2)	6527(2)	78.0(19)	71.7(17)	69.5(19)	11.0(14)	-25.5(15)	23.1(14)
Se(4)	8954(2)	1950(2)	-5303(2)	37.3(14)	87.5(19)	87.5(21)	6.4(13)	-6.2(13)	3.3(16)
Se(5)	7625(2)	1428(2)	4158(2)	57.7(15)	46.4(13)	49.1(14)	6.5(11)	1.1(11)	10.3(11)
Se(6)	7719(3)	2887(2)	3281(2)	119.2(25)	70.8(18)	46.3(16)	0.3(17)	27.7(16)	8.8(14)
Se(7)	7455(2)	4250(2)	4492(2)	87.0(19)	42.1(13)	63.6(17)	-4.9(13)	6.0(14)	5.5(12)
Se(8)	5654(2)	3649(2)	4629(2)	62.8(16)	64.0(16)	67.4(17)	26.1(13)	-1.7(13)	14.4(13)
As(1)	4719(2)	4645(2)	-2035(1)	36.4(11)	34.0(11)	30.7(11)	-4.3(9)	-0.2(9)	3.3(9)
As(2)	7505(2)	2507(2)	82(2)	33.5(11)	33.8(11)	47.6(13)	4.1(9)	-0.5(10)	6.0(10)
As(3)	167(2)	196(2)	2033(1)	34.2(11)	36.8(11)	32.2(11)	-2.8(9)	4.5(9)	5.3(9)
As(4)	4766(2)	543(2)	2462(2)	33.5(11)	36.0(11)	48.1(13)	9.7(9)	-9.6(10)	0.6(10)
As(5)	2333(2)	1947(2)	-4287(2)	49.3(13)	51.9(13)	32.9(12)	-2.0(11)	-4.3(10)	11.5(10)
As(6)	288(2)	5062(2)	2528(2)	35.5(12)	35.3(11)	57.2(15)	8.4(9)	-3.3(10)	1.1(10)
S	2469(6)	2974(6)	3141(4)	100(6)	89(5)	37(4)	5(4)	3(4)	20(4)
O(1)	2575(12)	2818(13)	2141(10)	63(10)	87(12)	38(9)	27(9)	-4(7)	9(8)
O(2)	3086(15)	3847(16)	3655(12)	103(15)	108(15)	56(12)	-24(12)	-19(11)	29(11)
F(11)	6065(10)	4647(13)	-1855(12)	33(8)	124(13)	116(13)	-7(8)	-4(8)	22(10)
F(12)	4601(12)	3251(10)	-2178(11)	99(11)	37(7)	101(12)	-5(7)	8(9)	12(7)
F(13)	4523(12)	4583(13)	-828(9)	106(12)	119(13)	31(8)	-6(10)	-4(7)	10(8)
F(14)	3344(10)	4612(11)	-2161(10)	41(8)	96(11)	86(11)	10(7)	-8(7)	23(8)
F(15)	4870(11)	4674(11)	-3223(9)	92(10)	88(10)	32(7)	-16(8)	15(7)	10(7)
F(16)	4852(12)	6011(9)	-1832(11)	104(12)	32(7)	109(13)	-14(7)	5(9)	6(8)
F(21)	6581(15)	3407(15)	9(14)	121(6)					
F(22)	8451(16)	1607(16)	-131(15)	134(7)					

continued.

Te₆(S₆)(AsF₆)₆(SO₂) continued.

ATOM	X	Y	Z	U ₁₁	U ₂₂	U ₃₃	U ₁₂	U ₁₃	U ₂₃
F(231) ^b	8500(27)	3468(26)	- 414(26)	93(10)					
F(241) ^b	6518(26)	1528(26)	249(26)	89(10)					
F(251) ^b	7810(37)	2791(35)	1098(32)	135(15)					
F(261) ^b	7246(34)	2079(35)	- 1220(30)	124(13)					
F(232) ^b	7774(39)	2988(39)	- 1109(35)	147(16)					
F(242) ^b	6931(43)	2161(41)	911(38)	163(18)					
F(252) ^b	6630(30)	1569(29)	- 614(30)	108(11)					
F(262) ^b	8371(31)	3470(30)	443(30)	114(12)					
F(31)	- 1498(10)	145(12)	2249(9)	42(8)	124(12)	59(9)	15(8)	8(6)	- 6(8)
F(32)	134(11)	440(13)	3188(9)	-81(10)	117(12)	39(8)	- 30(9)	0(7)	- 9(8)
F(33)	- 469(11)	- 117(13)	829(9)	69(9)	125(12)	37(8)	- 3(9)	8(7)	20(8)
F(34)	1169(10)	223(13)	1763(10)	39(8)	128(13)	83(11)	4(8)	5(7)	26(10)
F(35)	- 216(13)	- 1161(10)	2082(12)	111(13)	41(8)	110(13)	1(8)	- 12(10)	22(8)
F(36)	- 135(14)	1516(11)	1877(13)	127(14)	47(8)	139(16)	0(9)	- 8(12)	34(9)
F(41)	6164(9)	626(10)	2538(10)	36(7)	67(8)	89(10)	3(6)	- 12(7)	- 2(8)
F(42)	4881(11)	185(12)	1236(9)	75(10)	107(11)	42(8)	6(8)	9(7)	21(8)
F(43)	4729(10)	- 796(10)	2584(11)	61(9)	51(8)	103(12)	4(7)	- 5(8)	38(8)
F(44)	4712(13)	892(16)	3640(10)	91(12)	181(18)	41(9)	21(12)	- 5(8)	- 40(10)
F(45)	3404(9)	464(11)	2342(10)	36(7)	93(10)	86(11)	19(7)	1(7)	- 2(8)
F(46)	4825(12)	1869(10)	2250(14)	73(10)	44(8)	177(18)	24(7)	- 28(11)	9(10)
F(51)	1507(14)	2656(14)	- 4859(13)	107(6)					
F(52)	3105(18)	1295(18)	- 3595(17)	148(8)					
F(53)	1345(17)	954(16)	- 4241(15)	134(7)					
F(54)	3390(15)	2818(15)	- 4432(14)	121(6)					
F(55)	2002(22)	2562(21)	- 3258(20)	188(11)					
F(56)	2645(23)	1310(24)	- 5273(22)	206(12)					
F(61)	- 1075(9)	4999(11)	2630(10)	39(7)	74(9)	95(11)	11(7)	19(7)	11(8)
F(62)	102(12)	5090(11)	1318(10)	85(10)	80(10)	61(9)	6(8)	3(8)	0(8)
F(63)	1660(10)	5129(11)	2329(11)	46(8)	76(10)	115(13)	5(7)	- 8(8)	15(9)
F(64)	336(10)	6451(9)	2668(11)	61(9)	37(7)	102(11)	13(6)	- 7(8)	- 19(7)
F(65)	251(11)	3698(10)	2313(12)	70(10)	40(7)	129(14)	18(7)	- 1(9)	14(8)
F(66)	484(16)	5015(15)	3693(12)	163(18)	120(14)	64(11)	47(13)	- 9(11)	28(10)

^bRefined as 1/2 a fluorine atom.

(e) $\text{Te}_2\text{Se}_4(\text{SbF}_6)_2$

Atom	X	Y	Z	U ₁₁	U ₂₂	U ₃₃	U ₁₂	U ₁₃	U ₂₃
Te(11)	2710(2)	1181(1)	4364(1)	56(2)	34(1)	52(2)	4(1)	- 8(1)	- 7(1)
Te(12)	1526(2)	- 117(1)	4315(1)	34(1)	93(1)	60(2)	- 6(1)	4(1)	9(1)
Se(13)	3177(4)	- 947(2)	4452(2)	62(3)	40(2)	79(3)	6(2)	- 2(2)	4(2)
Se(14)	4417(4)	- 337(2)	3999(2)	40(3)	56(3)	111(4)	- 5(2)	20(3)	20(2)
Se(15)	5350(4)	- 661(2)	5535(2)	34(2)	58(2)	103(4)	- 5(2)	- 17(2)	- 16(2)
Se(16)	2182(4)	529(2)	3630(1)	71(3)	69(3)	33(2)	- 12(2)	- 13(2)	7(2)
Te(21)	2328(2)	1453(1)	1722(1)	51(2)	89(1)	75(2)	0(1)	1(1)	- 2(1)
Te(22)	3508(2)	2717(1)	1930(1)	36(2)	63(2)	67(2)	- 3(1)	- 14(1)	- 19(1)
Se(23)	1831(4)	3512(2)	2084(2)	71(3)	50(2)	79(3)	12(2)	- 8(3)	- 20(2)
Se(24)	769(4)	3102(2)	1493(1)	57(3)	59(2)	67(3)	13(2)	- 15(2)	15(2)
Se(25)	392(4)	1982(2)	1799(2)	31(2)	62(3)	110(4)	- 7(2)	5(2)	7(3)
Se(26)	3117(4)	2303(3)	1138(1)	61(3)	99(3)	37(2)	3(3)	10(2)	1(2)
Sb(1)	0(0)	- 139(2)	2500(0)	41(2)	33(2)	46(2)	0(0)	2(2)	0(0)
Sb(2)	5000(0)	546(2)	2500(0)	43(2)	50(2)	58(2)	0(0)	- 14(2)	0(0)
Sb(3)	359(2)	2138(1)	106(1)	39(1)	36(1)	41(1)	1(1)	4(1)	0(1)
Sb(4)	1992(2)	- 246(1)	795(1)	34(1)	49(1)	38(1)	1(1)	- 4(1)	3(1)
Sb(5)	3000(2)	2808(1)	3365(1)	38(1)	49(1)	45(1)	- 3(1)	9(1)	8(1)

Atom	X	Y	Z	U	Atom	X	Y	Z	U
F(11)	809(26)	563(15)	2212(10)	102(9)	F(41)	3028(24)	- 295(14)	1260(9)	94(9)
F(12)	- 845(23)	- 829(13)	2785(8)	85(8)	F(42)	1005(23)	- 160(13)	325(9)	84(8)
F(13)	- 952(34)	- 115(19)	2022(12)	139(13)	F(43)	1285(24)	- 1075(13)	1005(9)	90(8)
F(21)	5000(0)	1574(20)	2500(0)	92(12)	F(44)	1098(24)	372(14)	1146(9)	91(8)
F(22)	3511(27)	599(16)	2632(10)	107(10)	F(45)	2777(27)	570(16)	596(10)	110(10)
F(23)	5000(0)	- 463(32)	2500(0)	177(24)	F(46)	2863(28)	- 851(16)	419(10)	115(10)
F(24)	4607(31)	596(19)	1908(12)	138(13)	F(51)	2131(23)	2181(13)	3008(8)	84(8)
F(31)	- 21(31)	2906(18)	460(12)	129(12)	F(52)	3839(20)	2993(11)	2863(7)	66(6)
F(32)	805(23)	1351(13)	- 229(8)	83(8)	F(53)	2080(24)	3561(13)	3229(8)	86(8)
F(33)	1615(47)	2012(26)	433(17)	216(21)	F(54)	2119(21)	2555(12)	3856(8)	75(7)
F(34)	863(37)	2720(21)	- 345(14)	164(15)	F(55)	3876(25)	2049(14)	3519(9)	94(9)
F(35)	- 1065(37)	2151(19)	- 134(13)	152(14)	F(56)	3879(25)	3401(14)	3697(9)	96(9)
F(36)	- 287(38)	1524(22)	541(14)	171(16)					

(f) $\text{Te}_2\text{Se}_4(\text{Sb}_3\text{F}_{14})(\text{SbF}_6)$.

Atom	X	Y	Z	U_{11}	U_{22}	U_{33}	U_{12}	U_{13}	U_{23}
Te(1)	-51(2)	1235(1)	2525(2)	61(1)	35(1)	59(2)	4(1)	-14(1)	2(2)
Te(2)	-90(2)	2280(2)	1306(2)	56(2)	87(2)	31(1)	-21(1)	5(1)	-4(2)
Se(3)	654(3)	3386(2)	1966(3)	65(3)	52(3)	60(3)	-15(2)	17(2)	2(2)
Se(4)	21(3)	3240(2)	3151(3)	89(3)	41(2)	49(3)	-7(2)	17(2)	-20(2)
Se(5)	733(3)	2123(3)	3456(3)	98(4)	84(4)	54(3)	-4(3)	-53(3)	-1(3)
Se(6)	-1323(2)	2045(2)	2194(2)	28(2)	70(3)	44(3)	-3(2)	4(2)	15(2)
Sb(1)	2280(1)	-324(1)	2972(1)	37(1)	32(1)	23(1)	-2(1)	-1(1)	2(1)
Sb(2)	2435(1)	499(1)	824(1)	31(1)	25(1)	22(1)	1(1)	-1(1)	-5(1)
Sb(3)	2626(1)	2752(1)	297(1)	32(1)	26(1)	31(1)	0(1)	2(1)	-1(1)
Sb(4)	5000(0)	0(0)	5000(0)	34(1)	28(2)	27(2)	-8(1)	6(1)	-2(2)
Sb(5)	0(0)	5000(0)	0(0)	28(1)	47(2)	40(2)	-11(1)	7(1)	-22(2)

Atom	X	Y	Z	U	Atom	X	Y	Z	U
F(11)	225(1)	-34(1)	404(2)	69(7)	F(33)	257(1)	280(1)	-76(2)	64(6)
F(12)	231(1)	-29(1)	182(1)	50(5)	F(34)	267(1)	264(1)	136(2)	68(7)
F(13)	248(2)	-136(2)	291(2)	77(7)	F(35)	384(2)	268(1)	26(2)	71(7)
F(14)	348(1)	-12(1)	295(2)	64(7)	F(36)	140(1)	272(1)	37(1)	58(6)
F(15)	111(1)	-50(1)	280(2)	70(7)	F(41)	55(2)	-68(2)	-66(2)	80(8)
F(16)	206(1)	73(1)	296(2)	62(6)	F(42)	-86(1)	-73(1)	20(2)	71(7)
F(21)	332(1)	93(1)	144(1)	39(5)	F(43)	-68(1)	35(1)	-82(1)	54(6)
F(22)	157(1)	107(1)	138(1)	42(5)	F(51)	-102(2)	-30(1)	450(2)	74(7)
F(31)	263(1)	381(1)	40(2)	65(6)	F(52)	36(2)	39(1)	405(2)	75(7)
F(32)	259(1)	163(1)	20(1)	37(4)	F(53)	-48(2)	99(1)	527(2)	69(7)

(g) $\text{Te}_{2.7}\text{Se}_{3.3}(\text{SbF}_6)_2$

Atom	X	Y	Z	U_{11}	U_{22}	U_{33}	U_{12}	U_{13}	U_{23}
Te(1)	2563(1)	3833(3)	4365(1)	56.3(11)	82.3(15)	59.6(11)	4.9(11)	4.2(8)	-21.9(10)
Te(2)	1396(1)	2837(2)	2949(1)	47.3(10)	67.8(13)	62.2(11)	1.9(9)	-11.4(8)	7.1(10)
Te(4)	4193(2)	1124(3)	3035(2)	61.8(14)	64.2(16)	79(2)	16.4(13)	7.6(12)	-0.7(14)
Se(3)	1809(2)	1114(4)	4214(2)	70(2)	77(2)	84(2)	-1(2)	16.6(14)	33(2)
Se(5)	4502(2)	3439(4)	3809(2)	37(2)	84(3)	82(2)	-6.7(14)	0.7(13)	-14(2)
Se(6)	3055(3)	2328(4)	2006(2)	88(2)	80(2)	46.6(15)	7(2)	5.4(14)	-0.4(15)
Sb(1)	2058(1)	7347(2)	1962(1)	48.2(9)	41.5(11)	68.3(10)	0.6(8)	3.9(8)	-1.6(9)
Sb(2)	4676(1)	7903(2)	5186(1)	44.8(9)	47.7(11)	48.3(8)	-1.5(9)	3.3(7)	4.5(8)
F(1)	1301(27)	7747(39)	978(13)	249(37)	164(28)	81(14)	44(31)	-11(17)	4(17)
	919(17)	5995(29)	2195(19)	70(12)	92(16)	240(27)	-35(12)	14(16)	11(19)
	1305(15)	8944(24)	2477(12)	87(13)	76(12)	110(14)	10(12)	28(10)	-28(11)
	2790(19)	5819(24)	1377(17)	123(17)	64(13)	183(22)	48(13)	9(16)	-40(14)
F(5)	2595(23)	6637(36)	2968(16)	186(25)	188(29)	113(18)	21(26)	-48(17)	45(19)
F(6)	3108(23)	8605(27)	1672(31)	134(21)	65(16)	534(72)	-35(16)	203(34)	-18(28)
F(7)	3359(17)	8942(31)	5140(16)	77(12)	126(20)	170(21)	42(14)	12(13)	22(18)
F(8)	4389(22)	7505(57)	6268(11)	148(20)	471(64)	53(10)	50(32)	55(13)	94(24)
F(9)	3943(28)	6241(38)	4868(26)	150(24)	133(25)	344(48)	-65(22)	-4(30)	-89(29)
F(10)	4973(30)	8430(45)	4078(19)	245(33)	243(42)	146(22)	140(32)	110(22)	108(25)
F(11)	5953(24)	6820(43)	5206(23)	122(21)	201(36)	255(33)	104(25)	43(23)	71(29)
F(12)	6395(21)	9620(36)	5492(32)	94(18)	106(22)	479(66)	-28(18)	-50(28)	-48(35)

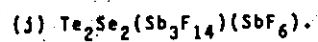
(h) $\text{Te}_{3.4}\text{Se}_{2.6}(\text{SbF}_6)_2$

Atom	X	Y	Z	U ₁₁	U ₂₂	U ₃₃	U ₁₂	U ₁₃	U ₂₃
Te(1)	2564(1)	3847(2)	4368(1)	56.0(9)	73.5(12)	57.8(9)	3.1(8)	4.6(6)	-22.1(8)
Te(2)	1414(1)	2903(2)	2938(1)	47.7(8)	58.1(9)	65.8(9)	3.7(7)	-12.7(6)	7.1(7)
Te(3)	1792(2)	1061(3)	4219(1)	65.7(13)	70.2(14)	94.3(15)	-9.9(10)	17.0(10)	33.5(11)
Te(4)	4234(1)	1116(2)	3029(1)	59.2(10)	54.4(10)	80.5(11)	17.4(8)	4.9(8)	-1.9(8)
Se(5)	4518(2)	3486(3)	3824(2)	44.6(14)	78.2(20)	77.8(17)	-10.5(12)	0.3(10)	-17.0(13)
Se(6)	3085(2)	2401(3)	1993(1)	84(2)	72(2)	47.4(12)	6.0(13)	1.9(10)	0.7(11)
Sb(1)	2054(1)	7395(2)	1967(1)	47.2(7)	38.6(8)	70.2(9)	3.9(6)	4.0(6)	-1.4(6)
Sb(2)	4674(1)	7926(2)	5199(1)	45.1(7)	43.3(8)	49.8(7)	2.2(6)	3.7(5)	4.2(6)
F(1)	1289(12)	8988(20)	2472(12)	66(9)	74(10)	145(15)	-7(9)	31(9)	-48(10)
F(2)	3166(20)	8663(24)	1768(25)	102(16)	57(11)	423(50)	-9(12)	117(25)	-39(21)
F(3)	1385(27)	7863(37)	1003(14)	242(34)	165(25)	108(14)	66(28)	-31(18)	45(16)
F(4)	857(15)	5998(24)	2168(16)	76(11)	84(13)	190(20)	-36(11)	-8(12)	0(14)
F(5)	2800(17)	5927(20)	1370(12)	124(15)	65(10)	110(12)	38(11)	-1(11)	-22(9)
F(6)	2587(21)	6619(32)	3000(14)	160(20)	164(24)	106(14)	39(20)	-25(13)	46(15)
F(7)	3815(52)	6157(81)	5163(37)	332(31)					
F(8)	4867(19)	8105(56)	4078(10)	135(16)	452(63)	46(8)	112(30)	26(9)	13(17)
F(9)	4489(21)	7727(71)	6258(15)	122(20)	599(96)	107(15)	134(38)	-14(14)	56(36)
F(10)	3346(13)	8998(29)	5143(14)	49(8)	128(18)	168(18)	39(10)	-4(9)	2(14)
F(11)	5990(23)	6912(41)	5175(16)	153(21)	244(36)	158(20)	164(25)	38(16)	63(21)
F(12)	5295(19)	9589(37)	5415(45)	51(13)	107(22)	1048(144)	-10(14)	24(36)	-135(53)

(1) $Te_2I_3(SbF_6)_2$

Atom	X	Y	Z	U ₁₁	U ₂₂	U ₃₃	U ₁₂	U ₁₃	U ₂₅
Te(11)	1567(1)	-157(1)	4298(1)	41.4(40)	42.0(10)	73.3(14)	-7.3(7)	6.4(8)	5.8(8)
Te(12)	2732(1)	1156(1)	4372(1)	63.2(12)	31.6(9)	62.5(12)	0.3(7)	-10.5(9)	-5.7(7)
Te(21)	3522(1)	2776(1)	1909(1)	44.9(10)	52.8(11)	69.8(13)	-5.9(8)	-12.6(8)	-12.5(8)
Te(22)	2227(1)	1496(1)	1739(1)	48.6(11)	37.0(9)	96.8(16)	-5.1(8)	1.6(9)	-3.3(9)
S(13)	2237(6)	563(3)	3655(2)	88(5)	68(4)	56(4)	-15(3)	-14(3)	12(3)
S(14)	4322(6)	-311(5)	4052(3)	54(5)	83(6)	133(9)	10(4)	16(4)	-30(5)
S(15)	3230(6)	-901(3)	4430(3)	81(6)	37(4)	102(7)	12(3)	-8(4)	-4(4)
S(16)	4552(6)	584(5)	4466(3)	42(4)	72(6)	115(8)	-7(4)	-17(4)	-18(5)
S(23)	3089(5)	2320(4)	1151(2)	67(4)	98(5)	58(4)	-1(3)	6(3)	-5(3)
S(24)	869(6)	3078(4)	1543(3)	56(4)	56(4)	93(6)	11(3)	-20(4)	12(4)
S(25)	1859(6)	3510(4)	2040(3)	81(5)	58(4)	97(6)	14(4)	-9(4)	-27(4)
S(26)	509(5)	2086(4)	1812(3)	39(4)	70(5)	140(8)	-4(3)	3(4)	13(5)
Sb(1)	5000	4917(1)	2500	46.6(12)	23.9(10)	52.8(14)	0.0	-3.6(10)	0.0
Sb(2)	5000	582(1)	2500	49.8(14)	48.1(14)	68.8(18)	0.0	-7.3(13)	0.0
Sb(3)	360(1)	785(1)	5113(1)	41.9(8)	31.7(7)	55.7(10)	1.4(7)	1.9(7)	3.0(7)
Sb(4)	2985(1)	4770(1)	799(1)	40.2(8)	44.9(9)	50.0(10)	1.5(7)	7.5(7)	7.7(7)
Sb(5)	2947(1)	2812(1)	3359(1)	44.1(8)	44.4(9)	52.2(10)	-1.5(7)	8.2(7)	7.1(7)

Atom	X	Y	Z	U	Atom	X	Y	Z	U
F(11)	4168(15)	4195(10)	2210(6)	86(5)	F(41)	3728(15)	3973(10)	1050(6)	94(5)
F(12)	5817(18)	5646(11)	2795(7)	112(6)	F(42)	2239(18)	5553(13)	568(7)	125(7)
F(13)	4046(23)	4904(15)	2988(9)	160(9)	F(43)	2160(16)	4142(12)	423(7)	108(6)
F(21)	5000	1649(16)	2500	103(8)	F(44)	4020(16)	4829(10)	327(6)	100(6)
F(22)	3485(15)	632(11)	2627(6)	103(6)	F(45)	1925(18)	4756(12)	1262(7)	124(7)
F(23)	5000	-449(26)	2500	202(19)	F(46)	3856(17)	5395(11)	1157(7)	108(6)
F(24)	4672(19)	631(13)	1886(8)	136(8)	F(51)	2170(14)	2132(10)	2998(6)	91(5)
F(31)	861(14)	8628(9)	4763(6)	89(5)	F(52)	3830(13)	3047(8)	2850(5)	75(4)
F(32)	-35(21)	7055(13)	5473(8)	137(8)	F(53)	1955(16)	3567(10)	3219(6)	95(5)
F(33)	-267(22)	8535(15)	5512(9)	158(10)	F(54)	2055(14)	2529(10)	3858(6)	93(5)
F(34)	1642(28)	7936(18)	5404(11)	206(14)	F(55)	3934(15)	2071(10)	3523(6)	96(6)
F(35)	-987(25)	7836(15)	4863(10)	176(11)	F(56)	3755(14)	3487(9)	3710(6)	86(5)
F(36)	958(27)	7230(17)	4722(11)	192(12)					

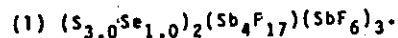


Atom	x	y	z	u ₁₁	u ₂₂	u ₃₃	u ₁₂	u ₁₃	u ₂₃
Sb(1)	10992(2)	2341(1)	2500	34.4(9)	42.7(11)	55.0(12)	0.4(8)	0	0
Sb(2)	6344(2)	3156(1)	2500	31.4(8)	24.8(8)	40.2(9)	-2.6(7)	0	0
Sb(3)	6074(3)	272(1)	2500	37.5(10)	26.6(9)	99.9(18)	-2.5(8)	0	0
Sb(4)	4864(4)	2500	0000	53.6(14)	171.4(38)	40.6(11)	0	0	25.5(17)
Te(1)	1655(3)	163(1)	671(2)	86.1(14)	49.8(10)	104.8(16)	1.3(9)	-56.3(12)	1.6(10)
Se(1)	-108(4)	1036(2)	-210(2)	82.6(18)	35.2(11)	101.2(22)	-1.6(13)	-42.5(17)	13.0(14)
F(11)	13146(29)	2201(23)	2500	41 (12)	126 (26)	174 (33)	19 (15)	0	0
F(12)	8731(26)	2513(17)	2500	34 (10)	55 (13)	275 (48)	13 (11)	0	0
F(13)	11194(70)	3375(28)	2500	152 (43)	77 (27)	825 (222)	-93 (31)	0	0
F(14)	10499(51)	1254(26)	2500	94 (26)	69 (22)	550 (127)	10 (22)	0	0
F(15)	10820(49)	2267(36)	1389(24)	174 (32)	319 (62)	129 (25)	-47 (39)	-23 (25)	-39 (32)
F(21)	7390(18)	3832(9)	1672(10)	72 (9)	57 (8)	62 (8)	-18 (8)	17 (7)	12 (7)
F(31)	6479(48)	1375(16)	2500	113 (25)	29 (12)	342 (66)	9 (15)	0	0
F(32)	4509(24)	4100(11)	2500	51 (10)	37 (9)	76 (13)	0 (8)	0	0
F(33)	4558(55)	407(14)	1717(31)	285 (44)	57 (13)	349 (51)	-46 (20)	-226 (42)	51 (20)
F(34)	7592(39)	51(13)	1695(21)	178 (25)	63 (11)	188 (26)	-29 (14)	110 (23)	-19 (14)
F(41)	3213(35)	1777(18)	296(19)	120 (8)					
F(42)	6206(91)	1749(46)	279(49)	279 (30)					
F(43)	4926(50)	2811(24)	1115(24)	168 (13)					

(k) $\text{Te}_{3.0}\text{Se}_{1.0}(\text{Sb}_3\text{F}_{14})(\text{SbF}_6)$.

Atom	x	y	z	U_{11}	U_{22}	U_{33}	U_{12}	U_{13}	U_{23}
Sb(1)	548.5(4)	0(0)	2570.9(7)	225.3(3)	40.5(4)	38.7(4)	1.9(3)	-1.0(3)	4.1(4)
Sb(2)	-1787.5(4)	-876.2(10)	2368.0(6)	28.6(3)	29.5(4)	29.7(3)	3.0(3)	1.1(3)	-3.2(3)
Sb(3)	-2904.7(6)	-3336.0(12)	515.3(8)	41.9(5)	46.1(5)	44.1(5)	6.1(4)	-8.1(4)	-21.7(4)
Sb(4)	-2126.5(5)	2261.6(11)	581.5(7)	41.1(4)	30.5(4)	35.7(4)	0.8(4)	-1.4(3)	2.8(3)
Te(1) ^a	-873.0(8)	5340.9(14)	3430.0(11)	56.9(7)	62.9(8)	48.0(7)	21.0(6)	17.5(5)	11.7(5)
Te(2) ^a	-163.3(7)	5916.4(13)	1478.2(9)	54.4(6)	61.3(7)	50.8(6)	11.6(5)	7.4(5)	25.6(5)
Te(3) ^a	37.7(12)	3650.4(15)	3659.7(13)	124.5(15)	56.1(8)	64.8(9)	40.4(9)	38.7(9)	24.8(7)
Te(4) ^a	792.9(9)	4125.4(16)	1718.2(10)	84.0(9)	78.5(9)	50.6(6)	32.2(7)	27.5(6)	9.7(6)
F(11)	1646 (5)	131 (10)	2277 (9)	26 (4)	88 (7)	84 (6)	1 (4)	13 (4)	2 (6)
F(12)	-592 (4)	-131 (8)	2915 (8)	26 (3)	74 (6)	64 (5)	-4 (4)	13 (3)	-21 (5)
F(13)	731 (7)	-787 (11)	3978 (9)	91 (7)	111 (9)	51 (5)	39 (7)	14 (5)	33 (6)
F(14)	289 (7)	895 (15)	1291 (11)	72 (8)	208 (17)	83 (8)	33 (9)	18 (6)	103 (10)
F(15)	541 (7)	1300 (10)	3581 (13)	64 (6)	72 (7)	151 (12)	3 (5)	-6 (7)	-57 (7)
F(16)	480 (7)	-1336 (12)	1714 (13)	73 (7)	119 (10)	146 (12)	-19 (7)	42 (7)	-103 (9)
F(21)	-1348 (6)	-811 (9)	805 (6)	79 (6)	73 (6)	31 (4)	-3 (5)	15 (4)	-8 (4)
F(22)	-1203 (5)	-2257 (7)	2603 (8)	46 (4)	43 (4)	67 (5)	14 (3)	1 (4)	1 (4)
F(31)	-3125 (7)	-4629 (10)	-391 (10)	82 (7)	73 (7)	88 (8)	7 (5)	-21 (5)	-53 (6)
F(32)	-2703 (5)	-2004 (7)	1508 (8)	44 (4)	50 (5)	64 (5)	-1 (4)	3 (4)	-29 (4)
F(33)	-3939 (7)	-3337 (11)	1082 (12)	76 (7)	84 (8)	122 (10)	-22 (6)	19 (7)	-54 (8)
F(34)	-1833 (7)	-3282 (16)	49 (17)	52 (7)	170 (15)	179 (15)	-9 (8)	43 (8)	-110 (13)
F(35)	-2596 (11)	-4212 (11)	1839 (12)	199 (16)	50 (7)	96 (9)	33 (9)	-52 (11)	-8 (7)
F(36)	-3226 (10)	-2324 (11)	-664 (11)	164 (13)	75 (8)	71 (7)	3 (8)	-29 (8)	2 (6)
F(41)	-1505 (6)	3460 (10)	1038 (12)	120 (11)	70 (7)	102 (8)	-44 (7)	-25 (8)	-7 (7)
F(42)	-1285 (6)	1622 (10)	-316 (9)	78 (7)	82 (7)	71 (6)	11 (6)	35 (5)	1 (5)
F(43)	-1766 (7)	1430 (8)	-1935 (8)	80 (9)	57 (6)	37 (4)	27 (6)	4 (5)	10 (4)
F(44)	-2993 (7)	2648 (11)	1420 (13)	78 (8)	82 (8)	119 (10)	23 (6)	43 (7)	-4 (7)
F(45)	-2761 (7)	967 (11)	173 (13)	78 (7)	83 (8)	111 (9)	-31 (6)	9 (7)	-37 (7)
F(46)	-2490 (10)	3040 (14)	-776 (11)	191 (17)	125 (12)	57 (6)	51 (12)	-37 (8)	29 (7)

^a All four "Te" sites are partially occupied by Se.



ATOM	X	Y	Z	U11	U22	U33	U12	U13	U23
Se(1)*	6551(1)	344(2)	2356(1)	25.6(11)	46.0(13)	26.4(11)	7.3(8)	1.2(7)	-4.0(8)
Se(2)*	7473(2)	314(2)	3380(2)	35.0(15)	51.8(18)	23.1(14)	6.0(12)	1.1(10)	-5.1(11)
Se(3)*	3202(2)	784(2)	2432(1)	38.3(14)	45.9(15)	31.7(13)	-15.9(10)	-8.8(9)	7.5(10)
Se(4)*	2712(2)	113(2)	3382(2)	43.2(17)	47.4(18)	26.8(15)	-13.8(13)	-3.9(11)	5.5(12)
Sb(1)	147.1(6)	2002.0(7)	2345.7(5)	34.8(5)	28.9(5)	16.4(4)	2.6(4)	2.5(3)	-1.3(3)
Sb(2)	33.6(5)	3556.1(6)	4498.6(4)	25.0(4)	27.6(4)	13.2(4)	0.2(3)	0.7(3)	2.0(3)
Sb(3)	2597.3(6)	2387.8(7)	5127.3(5)	24.0(5)	33.9(5)	24.8(5)	-1.3(4)	1.7(3)	0.6(3)
Sb(4)	5000.0(0)	0.0(0)	0.0(0)	24.2(6)	23.0(6)	20.8(6)	0.1(4)	-1.7(4)	1.5(4)
F(11)	227(8)	1650(8)	1254(6)	100(9)	64(7)	23(4)	-2(6)	3(5)	-4(5)
F(12)	63(8)	2360(7)	3473(5)	93(8)	42(5)	21(4)	-5(5)	18(5)	-9(4)
F(13)	45(7)	3333(7)	2095(6)	59(6)	40(5)	48(6)	-12(5)	1(5)	9(5)
F(14)	1356(6)	2154(8)	2454(7)	37(5)	71(7)	66(7)	13(5)	4(5)	17(6)
F(15)	1089(6)	1874(8)	2312(7)	34(5)	71(7)	67(7)	4(5)	-1(5)	23(6)
F(16)	251(7)	673(6)	2627(6)	72(6)	16(4)	57(6)	14(4)	7(5)	6(4)
F(21)	825(6)	4163(8)	3768(5)	38(5)	67(6)	28(4)	-19(4)	8(4)	9(4)
F(22)	921(5)	4048(6)	3811(5)	33(4)	45(5)	35(5)	11(4)	-2(4)	14(4)
F(222)	0(0)	5000(0)	5000(0)	103(12)	25(6)	32(7)	-22(7)	5(7)	-8(5)
F(31)	1913(8)	1760(9)	5949(8)	76(8)	80(8)	62(7)	-23(7)	26(6)	21(7)
F(32)	3321(8)	3012(10)	4451(7)	69(7)	96(9)	45(6)	-40(7)	19(5)	-3(6)
F(33)	3491(8)	1418(9)	5368(7)	81(8)	82(8)	41(6)	32(7)	13(6)	3(6)
F(34)	1768(9)	3396(10)	5056(7)	94(10)	100(10)	52(7)	58(8)	-8(6)	12(7)
F(35)	2099(8)	1650(12)	4351(8)	53(7)	127(12)	71(8)	-24(7)	-10(6)	-43(9)
F(36)	3060(8)	3155(8)	6049(6)	87(8)	58(7)	41(5)	-8(6)	-24(5)	-18(5)
F(41)	5839(7)	79(7)	877(6)	51(5)	44(5)	40(5)	10(4)	-18(4)	-2(4)
F(42)	5094(6)	1386(6)	23(6)	56(6)	25(4)	48(5)	-1(4)	-16(4)	-2(4)
F(43)	4082(6)	90(8)	729(6)	33(5)	63(6)	40(5)	5(4)	13(4)	2(4)

* Population Parameters: Se(1), 0.684(6); Se(2), 0.552(7);
Se(3), 0.641(7); Se(4), 0.539(7)

(m) $\text{TeCl}_3(\text{AlCl}_4)$.

Atom	X	Y	Z	U_{11}	U_{22}	U_{33}	U_{12}	U_{13}	U_{23}
Te(1)	2473.6(5)	6186.3(2)	2607.4(4)	33.5(2)	42.6(2)	33.4(2)	8.5(2)	4.4(2)	0.4(2)
Te(2)	7183.6(5)	1075.4(2)	2871.0(4)	32.6(2)	37.2(2)	35.2(2)	6.2(2)	9.0(2)	4.9(2)
Al(1)	3146(3)	3972(1)	1185(2)	36.2(9)	36.1(9)	35.1(9)	6.9(7)	5.3(7)	0.2(7)
Al(2)	2778(3)	1242(1)	6727(2)	33.8(9)	40.5(9)	36.6(9)	8.5(7)	7.6(7)	4.5(7)
Cl(11)	1016(3)	6015(1)	4901(2)	65.7(12)	108.4(16)	42.3(9)	19.2(11)	21.9(8)	7.7(9)
Cl(12)	5668(3)	6595(1)	3913(2)	43.0(9)	63.3(11)	66.2(11)	3.0(8)	-10.3(8)	-1.3(8)
Cl(13)	1385(3)	7238(1)	2291(2)	72.8(12)	53.6(10)	77.0(12)	30.2(9)	-1.5(10)	-1.5(9)
Cl(14)	3727(3)	4760(1)	3095(2)	94.8(15)	44.5(9)	44.8(9)	17.0(9)	-2.7(9)	-7.1(7)
Cl(15)	1260(3)	3141(1)	1884(2)	55.3(10)	58.6(10)	63.7(10)	-7.1(8)	17.2(8)	10.1(8)
Cl(16)	6053(2)	3661(1)	720(2)	43.0(9)	67.9(11)	54.5(9)	19.8(8)	15.0(7)	13.3(8)
Cl(17)	1802(3)	4425(1)	9077(2)	50.2(9)	60.8(10)	50.3(9)	5.9(8)	-5.4(7)	15.6(8)
Cl(21)	4049(3)	579(1)	1630(2)	45.5(9)	59.8(11)	71.0(11)	-3.1(8)	-6.1(8)	5.5(9)
Cl(22)	6317(3)	2162(1)	2971(2)	61.0(10)	39.7(9)	72.1(11)	12.7(8)	8.0(9)	8.1(8)
Cl(23)	8692(3)	1179(1)	585(2)	68.3(12)	84.4(13)	46.8(9)	12.0(10)	27.1(9)	12.1(9)
Cl(24)	1343(2)	1698(1)	4662(2)	43.5(9)	64.3(10)	53.6(9)	5.4(8)	-7.7(7)	18.1(8)
Cl(25)	5703(3)	956(1)	6178(2)	45.1(9)	83.7(12)	52.5(9)	28.5(9)	18.8(7)	20.8(9)
Cl(26)	901(3)	325(1)	7166(2)	52.1(10)	42.5(9)	87.2(13)	3.1(7)	21.2(9)	7.6(8)
Cl(27)	3174(3)	1929(1)	8724(2)	74.6(12)	54.0(10)	47.6(9)	11.4(9)	6.6(8)	-8.1(8)

(n) $\text{TeCl}_3(\text{AsF}_6)$.

Atom	X	Y	Z	U_{11}	U_{22}	U_{33}	U_{12}	U_{13}	U_{23}
Te	659.5(5)	1440.9(4)	3194.4(4)	33.7(2)	33.0(2)	34.4(2)	0.2(2)	10.2(1)	4.1(2)
As	6091.6(9)	2908.7(7)	2246.6(7)	41.5(3)	35.4(3)	40.2(3)	7.5(3)	13.2(3)	3.3(3)
Cl(1)	1140(3)	3635(2)	3638(2)	68(1)	34(1)	75(1)	-5(1)	27(1)	-1(1)
Cl(2)	906(3)	1520(2)	1130(2)	68(1)	72(1)	42(1)	9(1)	26(7)	9(1)
Cl(3)	3182(2)	723(2)	4226(2)	42(1)	69(1)	63(2)	17(6)	2(1)	0(1)
F(1)	5432(6)	3678(5)	711(5)	74(3)	72(3)	49(2)	28(2)	23(2)	19(2)
F(2)	7725(5)	2329(5)	1839(5)	46(2)	69(3)	69(3)	20(2)	21(2)	9(2)
F(3)	5061(7)	1551(5)	1586(7)	69(3)	48(3)	124(4)	-15(2)	31(3)	-12(3)
F(4)	4463(6)	3586(6)	2568(5)	70(2)	83(4)	91(3)	26(2)	50(2)	7(3)
F(5)	6770(9)	2152(7)	3745(6)	146(5)	119(4)	55(3)	56(4)	38(3)	38(3)
F(6)	7086(7)	4323(6)	2860(7)	75(4)	59(3)	127(5)	-7(3)	-2(3)	-34(3)

(o) $\text{TeCl}_3(\text{SbF}_6)$.

Atom	X	Y	Z	U_{11}	U_{22}	U_{33}	U_{12}	U_{13}	U_{23}
Sb(1)	4242.5(5)	2500	8497(1)	58.6(4)	24.4(3)	34.5(3)	0.0	-3.2(4)	0.0
Te(1)	1049.8(4)	2500	1295(1)	43.1(3)	29.4(3)	37.0(3)	0.0	4.7(3)	0.0
Cl(1)	3562(2)	-575(3)	4075(4)	119(2)	40(1)	66(1)	12(1)	-34(1)	6(1)
Cl(2)	7120(2)	2500	1648(7)	48(2)	85(2)	101(3)	0.0	18(2)	0.0
F(1)	4715(4)	2500	5840(10)	63(4)	70(4)	39(2)	0.0	7(3)	0.0
F(2)	3260(4)	2500	7320(20)	53(4)	60(4)	101(6)	0.0	-9(5)	0.0
F(3)	5245(5)	2500	9610(10)	92(5)	42(4)	88(5)	0.0	-43(4)	0.0
F(4)	3823(8)	2500	11170(10)	230(10)	97(7)	52(4)	0.0	52(6)	0.0
F(5)	4268(3)	297(5)	8416(8)	109(4)	29(2)	72(3)	-4(3)	-31(3)	6(2)

(p) $(\text{TeF}_3)_2\text{SO}_4$

Atom	X	Y	Z	U_{11}	U_{22}	U_{33}	U_{12}	U_{13}	U_{23}
Te(1)	407.8(9)	1427.2(9)	411.8(8)	20.1(4)	23.4(4)	16.94(4)	-0.6(3)	-2.0(3)	0.1(3)
Te(2)	538.6(10)	6654.4(9)	-844.1(8)	23.6(4)	26.1(4)	17.4(4)	1.7(3)	-1.1(3)	0.5(3)
S(1)	1700(3)	4503(4)	2073(3)	22(2)	31(2)	18(1)	-1(1)	-4(1)	-3(1)
F(11)	2240(9)	2090(10)	-320(10)	24(4)	44(5)	37(5)	-6(3)	6(4)	1(4)
F(12)	735(12)	-408(10)	-493(10)	49(6)	29(4)	57(6)	-3(4)	10(5)	-15(4)
F(13)	1559(9)	649(11)	1786(9)	30(4)	50(5)	33(5)	5(4)	-15(4)	12(4)
F(21)	-841(10)	7188(11)	-2167(8)	36(5)	61(6)	23(4)	13(4)	-8(4)	8(4)
F(22)	-1094(11)	6867(11)	332(10)	44(5)	50(5)	36(5)	-1(4)	9(4)	3(4)
F(23)	3(9)	4686(9)	-1084(9)	35(5)	21(4)	32(4)	-9(3)	-4(3)	2(3)
O(1)	514(10)	3406(11)	1734(9)	20(4)	44(5)	25(5)	-6(5)	6(4)	-11(4)
O(2)	3224(11)	3798(14)	2072(10)	21(5)	52(6)	28(5)	8(4)	-4(4)	-5(5)
O(3)	1419(12)	5052(13)	3442(10)	33(5)	54(7)	15(4)	9(5)	-7(4)	-12(5)
O(4)	1709(15)	5699(13)	1090(11)	60(8)	45(6)	27(6)	-18(6)	-23(6)	12(5)